DOKUZ EYLÜL UNIVERSITY

GRADUATE SCHOOL OF NATURAL AND APPLIED SCIENCES

DEVELOPING THERMALLY CONDUCTIVE AND RESISTIVE SOIL MIXTURES FOR ENERGY GEO-STRUCTURES

by

Cihat AŞÇI

March, 2023

İZMİR

DEVELOPING THERMALLY CONDUCTIVE AND RESISTIVE SOIL MIXTURES FOR ENERGY GEO-STRUCTURES

A Thesis Submitted to the
Graduate School of Natural and Applied Sciences of Dokuz Eylül University
In Partial Fulfillment of the Requirements for the Degree of Master of Science
in Civil Engineering, Geotecnical Engineering Program

by

Cihat AŞÇI

March, 2023
İZMİR

M.Sc THESIS EXAMINATION RESULT FORM

We have read the thesis entitled "**DEVELOPING THERMALLY CONDUCTIVE AND RESISTIVE SOIL MIXTURES FOR ENERGY GEO-STRUCTURES**" completed by **CİHAT AŞÇI** under supervision of **PROF.DR. YELİZ YÜKSELEN AKSOY** and we certify that in our opinion it is fully adequate, in scope and in quality, as a thesis for the degree of Master of Science.

Prof. Dr. Yeliz YÜKSELEN AKSOY

Supervisor

Prof. Dr. Gürkan ÖZDEN

(Jury Member)

Dr. Öğr. Üyesi Ender BAŞARI

(Jury Member)

Prof. Dr. Okan FISTIKOĞLU

Director

Graduate School of Natural and Applied Sciences

ACKNOWLEDGEMENTS

First of all, I would like to thank Prof. Dr. Yeliz YÜKSELEN AKSOY for her advice and support in this thesis. I would like to thank Prof. Dr. Gürkan ÖZDEN and Prof. Dr. Okan ÖNAL for their help in the continuation of my thesis.

I would like to thank Şükran Gizem ALPAYDIN, Dr. Esra GÜNERİ, Yusuf BATUGE, Emir OKUCU and İsa ÇİRKİN for their help during my laboratory works. I would also like to thank my family for supporting me during this process.

I would like to thank TÜBİTAK for their financial support as funding me a scholarship and supplying test equipment in order to conduct the study within the scope of the project title ‘’Enerji Geo-Yapıları İçin Tampon Malzeme Bentonitin Kısa ve Uzun Vadeli Mühendislik Performansı ile Termal İletkenlik Özelliklerinin İyileştirilmesi’’ and the project no 120M470.

Cihat AŞÇI

DEVELOPING THERMALLY CONDUCTIVE AND RESISTIVE SOIL MIXTURES FOR ENERGY GEO-STRUCTURES

ABSTRACT

Investigation of thermal properties of soils has come to the fore in recent years. Thermal properties of soils are very important in energy geo-structures where nuclear waste disposal areas, buried power cables and heat exchangers are directly affected by temperature changes. Recent studies have focused on the use of bentonite as an engineering filler in nuclear waste disposal areas. Sand-bentonite mixtures are required for strength-requiring energy piles and power cables.

In this study, the effects of boron minerals, glass fiber and slags as additives on the thermal properties of the soils were investigated. Colemanite mineral is used in nuclear power plants because it neutralizes radionuclides. It is known that boron minerals generally increase resistance to temperature. Glass fiber, on the other hand, is an important additive that has been researched in recent years due to its light weight and high strength. It can be benefited from the non-electrically conductive and non-combustible properties of glass fiber. Slags are waste materials with high strength. The use of slags in various fields for recycling and sustainability should be examined.

In this study, bentonite and different ratios of sand-bentonite mixtures were used. The change of thermal properties was also investigated by adding 10 percent and 20 percent additives to each mixture. The variation of the thermal properties of these mixtures according to the compaction curve, the variation of the thermal properties according to the degree of saturation and the variation of the thermal conductivity depending on the temperature were investigated. The effect of additives on the thermal properties of bentonite mixtures were generally negligible. While boron additives affected the thermal properties negatively in sand-bentonite mixtures, negligible changes occurred in sand-bentonite mixtures with glass fiber additives. While ferrochrome slag positively affected the thermal properties of sand-bentonite mixtures, the effect of copper slag on sand-bentonite mixtures was either negligible or in negative direction.

Keywords: Boron, slag, glass fiber, thermal conductivity, energy geo-structure, bentonite, sand-bentonite

ENERJİ GEO-YAPILARI İÇİN TERMAL İLETKEN VE YALITKAN ZEMİN KARIŞIMLARININ GELİŞTİRİLMESİ

ÖZ

Zeminlerin termal özelliklerinin araştırılması son yıllarda öne çıkmıştır. Sıcaklık değişimlerinden doğrudan etkilenen nükleer atık sahaları, gömülü yüksek gerilimli güç kabloları ve ısı eşanjörlerinin uygulandığı mühendislik yapılarında zeminlerin termal özellikleri oldukça önemlidir. Son zamanlarda yapılan çalışmalar bentonitin mühendislik dolgusu olarak nükleer atık sahalarında kullanılmasına yoğunlaşmıştır. Kum-bentonit karışımları ise mukavemet gerektiren ısı kazıkları ve yüksek gerilimli güç kabloları için gereklidir.

Ayrıcı bu çalışmada bor mineralleri, cam elyaf ve cüruflar katkı malzemesi olarak zeminlerin termal özelliklerine etkisi araştırılmıştır. Kolemanit minerali nükleer enerji santrallerinde radyonüklidleri nötrlediği için kullanılmaktadır. Bor minerallerinin genel olarak sıcaklığa karşı dayanıklılığı artırdığı bilinmektedir. Cam elyaf ise hafif ve yüksek mukavemet göstermesinden dolayı son yıllarda araştırılan önemli bir katkıdır. Cam elyafın elektriği iletmeme ve yanmama özelliklerinden faydalanılabilir. Cüruflar ise yüksek dayanıma sahip atık malzemelerdir. Cürufların geri dönüşümü ve sürdürülebilirliği için çeşitli alanlarda kullanılması incelenmelidir.

Bu çalışma, bentonit ve farklı oranlar kum-bentonit karışımları kullanılmıştır. Her karışıma yüzde 10 ve yüzde 20 katkı eklenerek termal özelliklerinin değişimi de incelenmiştir. Bu karışımların kompaksiyon eğrisine göre termal özelliklerinin değişimi, doygunluk derecesine göre termal özelliklerinin değişimi ve sıcaklığa bağlı termal iletkenliklerinin değişimi incelenmiştir. Katkıların bentonit karışımlarının termal özelliklerine etkisi genellikle ihmal edilebilir düzeydeder. Bor katkıları kum-bentonit karışımlarında termal özellikler negatif etkilerken, cam elyaf katkılı kum-bentonit karışımlarında genellikle ihmal edilebilir düzeyde değişimler meydana gelmiştir. Ferrokrom cürufu kum-bentonit karışımlarının termal özelliklerini pozitif etkilerken, bakır cürufunun kum-bentonit karışımlarına etkisi ya ihmal edilebilir düzeyde ya da negatif etkilemiştir.

Anahtar kelimeler: Bor, cüruf, cam elyaf, termal iletkenlik, enerji geo-yapıları, bentonit, kum-bentonit

CONTENTS

Page

M.Sc THESIS EXAMINATION RESULT FORM ii
ACKNOWLEDGEMENTS iii
ABSTRACT iv
ÖZ vi
CONTENTS viii
LIST OF FIGURES ii
LIST OF TABLES x
LIST OF SYMBOLS xii
ABBREVIATIONS xvi

CHAPTER 1 - INTRODUCTION 1

1.1 Statement of the problem 1
1.2 Objective and Scope 3
1.3 Organization of the thesis 4

CHAPTER 2 – LITERATURE REVIEW 6

2.1 Energy Geo-Structures 6
2.1.1 Energy Piles – Heat Exchangers 6
2.1.2 Nuclear Waste Storage Repositories 9
2.1.3 High Power Buried Cables 10
2.2 Thermal Properties of Soils 13
2.2.1 Theoretical models 16
2.2.2 Empirical Models 18
2.3 Factors Effecting on Thermal Properties of Soils 21

2.3.1 Saturation Degree/Water Content 21
2.3.2 Dry Density 26
2.3.3 Porosity 29
2.3.4 Fine Content 31
2.3.5 Mineralogy 36
2.3.6 Temperature 38
2.3.7 Other Parameters 42
2.3.7.1 Effect of Salts 42
2.3.7.2 Coefficient of Uniformity 47
2.3.7.3 Specific Surface Area 47
2.4 Boron Minerals, Ferrochrome and Copper Slags and Fiber Glass 48
2.4.1 Boron Minerals 48
2.4.2 Ferrochrome Slag and Copper Slag 50
2.4.3 Fiber Glass 53

CHAPTER 3 – MATERIALS AND METHODS 56

3.1 Materials 56
3.2 Methods 58
3.2.1 Compaction 58
3.2.2 Soil Classification Tests 58
3.2.3 Measurement of Thermal Properties of Soils 60

CHAPTER 4 – COMPACTION RESULTS 71

4.1 Compaction Test Results of Bentonite Mixtures 71
4.2 Compaction Test Results of SB10 Mixtures 75

CHAPTER 5 – THERMAL PROPERTIES DEPENDING ON PROCOR CURVE 80

5.1 Thermal Properties of Bentonite Depending on Proctor Curve 80

5.1.1 Thermal Properties of Bentonite Depending on Proctor Curve in their Presence of Boron Minerals 82

5.1.2 Thermal Properties of Bentonite Depending on Proctor Curve in their Presence of Slags 89

5.1.3 Thermal Properties of Bentonite Depending on Proctor Curve in their Presence of Fiber Glass 94

5.2 Thermal Properties of Sand-Bentonite Mixtures Depending on Proctor Curve 96

5.2.1 Thermal Properties of SB10 Depending on Proctor Curve in their Presence of Boron Minerals 98

5.2.2 Thermal Properties of SB10 Depending on Proctor Curve in their Presence of Slags 105

5.2.3 Thermal Properties of SB10 Depending on Proctor Curve in their Presence of Fiber Glass 111

CHAPTER 6 – THERMAL CONDUCTIVITY DEPENDING ON TEMPERATURE 113

6.1 Thermal Conductivity of Bentonite Depending on Temperatures 113

6.1.1 Thermal Conductivity of Bentonite-Boron Mixtures Depending on Temperatures 113

6.1.2 Thermal Conductivity of Bentonite-Slag Mixtures Depending on Temperatures 114

6.2 Thermal Conductivity of Sand-Bentonite Mixtures Depending on Temperatures 115

6.2.1 Thermal Conductivity of Sand-Bentonite-Boron Mixtures Depending on Temperatures 116

6.2.2 Thermal Conductivity of Sand-Bentonite-Slag Mixtures Depending on Temperatures 119

6.2.3 Thermal Conductivity of Sand-Bentonite-Fiber Glass Mixtures Depending on Temperatures 121

CHAPTER 7 - THERMAL PROPERTIES DEPENDING ON SATURATION 123

7.1 Thermal Properties of Bentonite Depending on Saturations 123

7.1.1 Thermal Properties of Bentonite-Boron Mixtures Depending on Saturations 124

7.1.2 Thermal Properties of Bentonite-Slag Mixtures Depending on Saturations 125

7.1.3 Thermal Properties of Bentonite-Fiber Glass Mixture Depending on Saturations 128

7.2 Thermal Properties of Sand-Bentonite Mixtures Depending on Saturations 128

7.2.1 Thermal Properties of Sand-Bentonite-Boron Mixtures Depending on Saturations 131

7.2.2 Thermal Properties of Sand-Bentonite-Slag Mixtures Depending on Saturations 136

7.2.3 Thermal Properties of Sand-Bentonite-Fiber Glass Mixtures Depending on Saturations 141

CHAPTER 8 - CONCLUSIONS AND FUTURE RECOMMENDATIONS 145

8.1 Results of Thermal Properties-Compaction Curve of Bentonite..... 145

8.2 Results of Thermal Properties – Compaction Curve of SB10 147

8.3 Results of Bentonite and Additive Mixtures Depending on Temperature and Saturation 149

8.4 Results of Sand-Bentonite and Additive Mixtures Depending on Temperature 151

8.5 Results of Sand-Bentonite and Additive Mixtures Depending on Saturation 154

8.6 General Conclusions and Future Recommendations 159

REFERENCES 163

LIST OF FIGURES

Page

Figure 2.1 Concept of geotechnical energy structure..... 7
Figure 2.2 Heat transfer mechanism in energy piles..... 7
Figure 2.3 Schematic plans of heat exchangers a) Drilling method b) Pipes laid horizontally c) Pipes laid both horizontally and vertically 8
Figure 2.4 Schematic plans for ventilation control a) Winter b) Summer..... 9
Figure 2.5 Concept of Deep Geological Disposal a) Genel design method b) Detailed design chart 10
Figure 2.6 Schematic implementation of underground cable a) Cables inside directly backfill b) Cables inside casing pipe..... 11
Figure 2.7 Schematic of Wiener model a) Series flow (lower bound) b) Parallel flow (upper bound) 17
Figure 2.8 a) Dry State b) Low Water Content c) Partially saturated d) Fully Saturated e) Heat flow at dry state f) Heat flow at low water content g) Heat flow at partially saturated state h) Heat flow at fully saturated state 22
Figure 2.9 Change of thermal conductivity various water content at constant dry unit weight a) Bentonite b) Aeolin Sand 23
Figure 2.10 a) Variation of specific heat of soils with dry unit weight b) Variation of specific heat of soils with the moisture content 24
Figure 2.11 Moisture content versus volumetric heat capacity relationships a) Volumetric heat capacity as a function of moisture content for a clay soil b) Volumetric heat capacity as a function of moisture content for a sandy soil. 24
Figure 2.12 a) Variation of thermal diffusivity of soil with the dry unit weight b) Variation of thermal diffusivity of soils with the moister content c) Thermal diffusivity of different soils related to moisture content. 25
Figure 2.13 Soil structure change with dry density..... 26
Figure 2.14 Particle-level conduction mechanism 27
Figure 2.15 Thermal conductivity changes according to dry density a) Clay from Xianyang, China b) Aeolin sand from Tibetan Plateau c) Sand from Melbourne region, Australia d) Clayey sand from Melbourne region, Australia..... 28

Figure 2.16 Thermal conductivity changes according to porosity a) sample A b) sample B c) sample C d) sample D 30
Figure 2.17 Thermal conductivity versus saturation and porosity at constant volume fraction of sand 30% 30
Figure 2.18 The variances in thermal conductivity with respect to porosity a) Dry quartz sand specimens; b) Saturated quartz sand specimens 31
Figure 2.19 Pure quartzitic sand and silica flour (a) Dry mass density versus fine content; and (b) Thermal conductivity versus fine content 32
Figure 2.20 Heat transfer mechanism of grain-grain contact a) Monosized soils b) Fine and coarse grains in soils 33
Figure 2.21 Effect of particle size on heat flow path in dry sand a) Pure and b) Mixed 34
Figure 2.22 Experiment results of different sand mixtures a) Particle size distribution of quartz sands b) Silica 12/20–Ottawa 20/30 sand, c) Silica 12/20-ASTM graded sand, and d) Ottawa 20/30-ASTM graded sand 35
Figure 2.23 Thermal conductivity with montmorillonite content 37
Figure 2.24 Thermal Conductivity variation with quartz content for soils 38
Figure 2.25 Temperature effect on the thermal conductivity a) Compaction curve of Genhe silty clay b) Negative temperature effect at dry side of compaction curve c) Negative temperature effect at wet side of compaction curve 40
Figure 2.26 The variation of thermal conductivity with temperature 41
Figure 2.27 Change in thermal conductivity for each temperature with saturation for lateritic: (a) Guilin lateritic clay; (b) Liuzhou lateritic clay, (c) Ando soil (Clay loam) (d) Red Yellow soil (Light Clay) 42
Figure 2.28 Thermal conductivity measurements at different temperature and salinity 43
Figure 2.29 Variations in thermal conductivity with salt concentration with 22% water content 44
Figure 2.30 Structure diagram of soil particles in different NaCl concentrations (Lyu et al., 2020) a) Soil samples with no NaCl, b) Soil samples with 2% NaCl, c) Soil samples with 5% NaCl 45

Figure 2.31 Test results that relationships between water content and a) Thermal conductivity, b) Thermal diffusivity and c) Specific heat 46
Figure 2.32 Variations of thermal conductivity of carbonate sands with the uniformity coefficient and void ratio 47
Figure 2.33 Relation between specific surface area and the thermal conductivity of solids 48
Figure 2.34 Some colemanite crystals from different provinces of Türkiye 49
Figure 2.35 Ferrochrome a) Fine aggregate b) Coarse aggregate 51
Figure 3.1 Microscope images of the materials a) Sand b) Bentonite c) Ulexite d) Colemanite e) Etibor-48 f) Glass Fiber g) Copper Slag h) Ferrochrome Slag 57
Figure 3.2 Sieve analysis results a) Bentonite and Sand b) Borons (Etibor-48, Colemanite, Uleksite) c) Slags (Copper and Ferrochrome) 59
Figure 3.3 pH measurement device 60
Figure 3.4 Instruments used in thermal properties measurements 61
Figure 3.5 Thermal conductivity values of sand, bentonite and additives 64
Figure 3.6 Measurement method of bentonite samples in standard proctor mold 66
Figure 3.7 Measurement method of sand-bentonite samples 66
Figure 3.8 a) Modified Oven for Temperature Measurements b) Sample Wrapped with Stretch Film and Aluminum Foil c) Placement of the TR-3 Sensor d) Re-coating the Top Surface with Aluminum Foil e) Measurement of the Thermal Conductivity of the Sample f) Closing the 68
Figure 4.1 Compaction curve of bentonite…… 71
Figure 4.2 Compaction curve of bentonite-ulexite mixtures…….. 71
Figure 4.3 Compaction curve of bentonite-colemanite mixtures……72
Figure 4.4 Compaction curve of bentonite-etibor-48 mixtures…….. 73
Figure 4.5 Compaction curve of bentonite-fiber glass mixture……..73
Figure 4.6 Compaction curve of bentonite-copper slag mixtures……...74
Figure 4.7 Compaction curve of bentonite-ferrochrome slag mixtures……..74
Figure 4.8 Compaction curve of SB10……... 75
Figure 4.9 Compaction curves of SB10-ulexite mixtures……...76
Figure 4.10 Compaction curves of SB10-colemanite mixtures……..76

Figure 4.11 Compaction curves of SB10-etibor48 mixtures…….. 77
Figure 4.12 Compaction curves of SB10-glass fiber mixture…….77
Figure 4.13 Compaction curves of SB10-copper slag mixtures……. 78
Figure 4.14 Compaction curves of SB10-ferrochrome slag mixtures…… 78
Figure 5.1 Variation of thermal properties of bentonite according to the compaction curve a) Thermal conductivity b) Volumetric heat capacity c) Diffusivity… 81
Figure 5.2 Variation of thermal properties of B10U according to the compaction curve a) Thermal conductivity b) Volumetric heat capacity c) Diffusivity……..83
Figure 5.3 Variation of thermal properties of B20U according to the compaction curve a) Thermal conductivity b) Volumetric heat capacity c) Diffusivity……..84
Figure 5.4 Variation of thermal properties of B10C according to the compaction curve a) Thermal conductivity b) Volumetric heat capacity c) Diffusivity……..85
Figure 5.5 Variation of thermal properties of B20C according to the compaction curve a) Thermal conductivity b) Volumetric heat capacity c) Diffusivity……..86
Figure 5.6 Variation of thermal properties of B10E48 according to the compaction curve a) Thermal conductivity b) Volumetric heat capacity c) Diffusivity… 87
Figure 5.7 Variation of thermal properties of B20E48 according to the compaction curve a) Thermal conductivity b) Volumetric heat capacity c) Diffusivity… 88
Figure 5.8 Variation of thermal properties of B10CS according to the compaction curve a) Thermal conductivity b) Volumetric heat capacity c) Diffusivity… 90
Figure 5.9 Variation of thermal properties of B20CS according to the compaction curve a) Thermal conductivity b) Volumetric heat capacity c) Diffusivity… 91
Figure 5.10 Variation of thermal properties of B10FS according to the compaction curve a) Thermal conductivity b) Volumetric heat capacity c) Diffusivity…92
Figure 5.11 Variation of thermal properties of B20FS according to the compaction curve a) Thermal conductivity b) Volumetric heat capacity c) Diffusivity…93
Figure 5.12 Variation of thermal properties of BGF according to the compaction curve a) Thermal conductivity b) Volumetric heat capacity c) Diffusivity……..95
Figure 5.13 Variation of thermal properties of SB10 according to the compaction curve a) Thermal conductivity b) Volumetric heat capacity c) Diffusivity……..97
Figure 5.14 Variation of thermal properties of SB10U10 according to the compaction curve a) Thermal conductivity b) Volumetric heat capacity c) Diffusivity…99

Figure 5.15 Variation of thermal properties of SB10U20 according to the compaction curve a) Thermal conductivity b) Volumetric heat capacity c) Diffusivity..100
Figure 5.16 Variation of thermal properties of SB10C10 according to the compaction curve a) Thermal conductivity b) Volumetric heat capacity c) Diffusivity..101
Figure 5.17 Variation of thermal properties of SB10C20 according to the compaction curve a) Thermal conductivity b) Volumetric heat capacity c) Diffusivity..102
Figure 5.18 Variation of thermal properties of SB10E4810 according to the compaction curve a) Thermal conductivity b) Volumetric heat capacity c) Diffusivity……103
Figure 5.19 Variation of thermal properties of SB10E4820 according to the compaction curve a) Thermal conductivity b) Volumetric heat capacity c) Diffusivity……104
Figure 5.20 Variation of thermal properties of SB10CS10 according to the compaction curve a) Thermal conductivity b) Volumetric heat capacity c) Diffusivity..106
Figure 5.21 Variation of thermal properties of SB10CS20 according to the compaction curve a) Thermal conductivity b) Volumetric heat capacity c) Diffusivity..107
Figure 5.22 Variation of thermal properties of SB10FS10 according to the compaction curve a) Thermal conductivity b) Volumetric heat capacity c) Diffusivity..108
Figure 5.23 Variation of thermal properties of SB10FS20 according to the compaction curve a) Thermal conductivity b) Volumetric heat capacity c) Diffusivity..109
Figure 5.24 Variation of thermal properties of SB10GF according to the compaction curve a) Thermal conductivity b) Volumetric heat capacity c) Diffusivity..112
Figure 6.1 Variation of thermal conductivity of bentonite at different temperatures (S = 0.658 and e =1.769)..... 113
Figure 6.2 Variation of thermal conductivity of bentonite-boron mixtures at different temperatures (S = 0.658 and e =1.769) 114
Figure 6.3 Variation of thermal conductivity of bentonite-slag mixtures at different temperatures (S = 0.658 and e =1.769) 114
Figure 6.4 Variation of thermal conductivity of bentonite-glass fiber mixture at different temperatures (S = 0.658 and e =1.769)..... 115

Figure 6.5 Variation of thermal conductivity of SB10 (S = 0.606 and e =0.564), SB20 (S = 0.602 and e =0.632) and SB30 (S = 0.617 and e =0.735) mixtures at different temperatures 116
Figure 6.6 Variation of thermal conductivity of SB10-boron mixtures at different temperatures (S = 0.606 and e =0.564) 117
Figure 6.7 Variation of thermal conductivity of SB20-Boron mixtures at different temperatures (S = 0.602 and e =0.632) 117
Figure 6.8 Variation of thermal conductivity of SB30-Boron mixtures at different temperatures (S = 0.617 and e =0.735) 118
Figure 6.9 Variation of thermal conductivity of SB10-Slag mixtures at different temperatures (S = 0.606 and e =0.564) 119
Figure 6.10 Variation of thermal conductivity of SB20-Slag mixtures at different temperatures (S = 0.602 and e =0.632) 120
Figure 6.11 Variation of thermal conductivity of SB30-Slag mixtures at different temperatures (S = 0.617 and e =0.735) 121
Figure 6.12 Variation of thermal conductivity of SB10-Glass Fiber mixture at different temperatures (S = 0.606 and e =0.564) 122
Figure 6.13 Variation of thermal conductivity of SB20-Glass Fiber mixture at different temperatures (S = 0.602 and e =0.632) 122
Figure 6.14 Variation of thermal conductivity of SB30-Glass Fiber mixture at different temperatures (S = 0.617 and e =0.735) 122
Figure 7.1 Variation of thermal properties of bentonite at different degrees of saturation (e = 1.769) a) Thermal conductivity b) Volumetric heat capacity c) Diffusivity 124
Figure 7.2 Variation of thermal properties of bentonite-boron mixtures at different degrees of saturation (e = 1.769) a) Thermal conductivity b) Volumetric heat capacity c) Diffusivity 126
Figure 7.3 Variation of thermal properties of bentonite-slag mixtures at different degrees of saturation (e = 1.769) a) Thermal conductivity b) Volumetric heat capacity c) Diffusivity 127

Figure 7.4 Variation of thermal properties of bentonite-glass fiber mixture at different degrees of saturation (e = 1.769) a) Thermal conductivity b) Volumetric heat capacity c) Diffusivity 129
Figure 7.5 Variation of thermal properties of SB10 (e = 0.564), SB20 (e = 0.632) and SB30 (e = 0735) at different degrees of saturation (e = 0.564) a) Thermal conductivity b) Volumetric heat capacity c) Diffusivity..... 130
Figure 7.6 Variation of thermal properties of SB10-Boron mixtures at different degrees of saturation (e = 0.564) a) Thermal conductivity b) Volumetric heat capacity c) Diffusivity 132
Figure 7.7 Variation of thermal properties of SB20-Boron mixtures at different degrees of saturation (e = 0.632) a) Thermal conductivity b) Volumetric heat capacity c) Diffusivity 133
Figure 7.8 Variation of thermal properties of SB30-Boron mixtures at different degrees of saturation (e = 0.735) a) Thermal conductivity b) Volumetric heat capacity c) Diffusivity 135
Figure 7.9 Variation of thermal properties of SB10-Slag mixtures at different degrees of saturation (e = 0.564) a) Thermal conductivity b) Volumetric heat capacity c) Diffusivity 137
Figure 7.10 Variation of thermal properties of SB20-Slag mixtures at different degrees of saturation (e = 0.632) a) Thermal conductivity b) Volumetric heat capacity c) Diffusivity 138
Figure 7.11 Variation of thermal properties of SB30-Slag mixtures at different degrees of saturation (e = 0.735) a) Thermal conductivity b) Volumetric heat capacity c) Diffusivity 140
Figure 7.12 Variation of thermal properties of SB10-Glass Fiber mixture at different degrees of saturation (e = 0.564) a) Thermal conductivity b) Volumetric heat capacity c) Diffusivity 142
Figure 7.13 Variation of thermal properties of SB20-Slag mixture at different degrees of saturation (e = 0.632) a) Thermal conductivity b) Volumetric heat capacity c) Diffusivity 143

Figure 7.14 Variation of thermal properties of SB30-Glass Fiber mixture at different degrees of saturation (e = 0.735) a) Thermal conductivity b) Volumetric heat capacity c) Diffusivity 144

LIST OF TABLES

Page

Table 2.1 The thermal properties of thermal backfill according to some countries .. 12
Table 2.2 The materials which effect on thermal conductivity of soils 14
Table 2.3 Thermal conductivity of materials which found in soil and used energy geo-structures 15
Table 2.4 Thermal conductivity of some minerals 36
Table 2.5 Composition of bentonite 37
Table 2.6 The content of boron minerals and the countries where they are found 50
Table 2.7 Classification of glass fiber 54
Table 3.1 Content of Ferrochrome Slag 56
Table 3.2 The Physcio – Chemical Properties of Materials 58
Table 3.3 Bentonite Samples 69
Table 3.4 SB10 Samples 69
Table 3.5 SB20 Samples 70
Table 4.1 Compaction results of bentonite mixtures 75
Table 4. 2 Compaction results of sand-bentonite mixtures 79
Table 8.1 Highest thermal conductivity values of bentonite and additive mixtures measured by TR-3 sensor 145
Table 8.2 Best thermal properties of bentonite and additive mixtures measured by SH-3 sensor 146
Table 8.3 Highest thermal conductivity values of SB10 and additive mixtures measured by TR-3 sensor 147
Table 8.4 Best thermal properties of SB10 and additive mixtures measured by SH-3 sensor 148
Table 8.5 Variation of thermal conductivity of bentonite and additive mixtures at different temperatures (at constant S=0.658 and e=1.769) 150
Table 8.6 Variation of thermal properties of bentonite and additive mixtures according to saturation degree (at constant e =1.769) 150
Table 8.7 Variation of thermal conductivity of SB10 and additive mixtures at different temperatures (at constant S = 0.606 and e =0.564) 152

Table 8.8 Variation of thermal conductivity of SB20 and additive mixtures at different temperatures (at constant S = 0.602 and e =0.632) 153
Table 8.9 Variation of thermal conductivity of SB30 and additive mixtures at different temperatures (at constant S = 0.617 and e =0.735) 154
Table 8.10 Variation of thermal properties of SB10 and additive mixtures according to saturation degree (at constant e =0.564) 154
Table 8.11 Variation of thermal properties of SB10 and additive mixtures according to saturation degree (at constant e =0.632) 156
Table 8.12 Variation of thermal properties of SB30 and additive mixtures according to saturation degree (at constant e =0.735) 158

LIST OF SYMBOLS

%	: Percent
℃	: Celsius Degree
Econv	: Heat convection
Econd	: Heat conduction
D	: Thermal diffusivity (mm^2/s)
k	: Thermal conductivity (W/mK)
Cp	: Specific heat (kJ/kgK)
C	: Volumetric heat capacity (MJ/m^3K)
$\emptyset_\alpha$	: Volume fraction and
k_α	: Thermal conductivity of phase
$k_w^\perp$	: Lower Wiener bounds
k_w^U	: Upper Wiener bounds
x	: Volume fraction
K	: Average thermal gradient
g	: Grain shape coefficient
n	: Porosity
S_r	: Saturation Degree
ζ	: Coefficient of thickness of water film
χ	: Degree of Saturation
α_w	: The ratio of thermal conductivity of water to thermal conductivity of solids
α_a	: The ratio of thermal conductivity of air to thermal conductivity of solids
β	: Width of water film
w	: Water content
ρ_d	: Dry density
q	: Quartz content

ρ_b	: Bulk density
κ	: Soil texture dependent parameter
χ	: Parameter for particle shape effect
η	: Parameter for particle shape effect
a	: Parameter depending on soil texture
a	: Coefficient related dry soil
b	: Coefficient related dry soil
c	: Empirical coefficient for quartz sand
d	: Empirical coefficient for quartz sand
D_{50}	: Mean particle size
λ	: Thermal conductivity (W/mK)
F_{cr}	: Critical fine content
d_f	: Mean ratio of fine sand grain size
d_c	: Mean ratio of coarse sand grain size
Na	: Sodium
Ca	: Calcium
NaCl	: Sodium Chloride
$CaCl_2$	: Calcium Chloride
c_u	: Uniformity Coefficients
B	: Boron
CaO	: Calcium Oxide
B_2O_3	: Boric oxide
H_2O	: Water
$2CaO.3B_2O_3.5H_2O$	: Colemanite
HCl	: Hydrochloric Acid
$Na_2B_4O_7$	: Borax
$Na_2B_4O_7.5H_2O$	: Etibor48
$Na_2B_4O_7.10H_2O$	: Tincal

Na_2O : Sodium Oxide

CaO : Calcium Oxide

$Na_2O.2CaO.5B_2O_3.16H_2O$: Ulexite

H_3BO_3 : Sassolite

$Na_2B_4O_7.10H_2O$: Tincal

$Na_2B4O7.4H_2O$: Kernite

$Ca_2B_6O_{11}.5H_2O$: Colemanite

$NaCaB_5O_9.5H_2O$: Ulexite

$Ca_2B_6O_{11}.13H_2O$: Probertite

$CaMgB_6O_{11}.6H_2O$: Inyoite

CaMgB6O11.6H2O : Hydroboracite

$Mg_3B_7O_{13}Cl$: Boracite

$MgBO_7(OH)$: Szaibelyite

$Ca_2B_2Si_2O_9.H_2O$: Datolit

SiO_2 : Silicon dioxide, also known as silica

Al_2O_3 : Aluminum Oxide

FeO : Pure ferrous

Fe_2O_3 : ferric

Cr_2O_3 : Chromium(III) oxide (or chromia)

MgO : Magnesium oxide (or magnesia)

Fe : Iron

Cu : Copper

Co : Cobalt

Zn : Cobalt

Ni : Nickel

Mn : Manganese

ΔT : Temperature change

q : Heat input (W/m)

r	: the distance from the heated needle to the measuring needle
t	: time (s),
t_h	: the heating time (s)
Ei	: the exponential integral
e	: void raito
Υ_d	: Dry unit weight
Υ	: Unit weight
R	: Thermal Resistivity (°Ccm/W)

ABBREVIATIONS

IEC	: International Electrotechnical Commission
FC	: Fine content
BC	: Basaltic Clay
CIS	: Coode Island
FBS	: Fishermens Bend Silt
RS	: Residual Siltstone
BGCS	: Brighton Group clayey sand
BGS	: Brighton Group sand
USA	: The United States of America
ASTM	: American Society for Testing and Materials
B	: Bentonite
B10E48	: %10 Etibor48 added bentonite
B20E48	: %20 Etibor48 added bentonite
B10U	: %10 Ulixte added bentonite
B20U	: %20 Ulixte added bentonite
B10C	: %10 Colemanite added bentonite
B20C	: %20 Colemanite added bentonite
BFG	: %1 Glass fiber added bentonite
B10CS	: %10 Copper slag added bentonite
B20CS	: %20 Copper slag added bentonite
B10FS	: %10 Ferrochrome slag added bentonite
B20FS	: %20 Ferrochrome slag added bentonite
SB10	: %90 Sand - %10 Bentonite mixture
SB10E4810	: %10 Etibor48 added SB10
SB10E4820	: %20 Etibor48 added SB10
SB10U10	: %10 Ulexite added SB10

SB10U20	: %20 Ulexite added SB10
SB10C10	: %10 Colemanite added SB10
SB10C20	: %20 Colemanite added SB10
SB10GF	: %1 Glass fiber added SB10
SB10CS10	: %10 Copper slag added SB10
SB10CS20	: %20 Copper slag added SB10
SB10FS10	: %10 Ferrochrome slag added SB10
SB10FS20	: %20 Ferrochrome slag added SB10
SB20	: %80 Sand - %20 Bentonite mixture
SB20E4810	: %10 Etibor48 added SB20
SB20E4820	: %20 Etibor48 added SB20
SB20U10	: %10 Ulexite added SB20
SB20U20	: %20 Ulexite added SB20
SB20C10	: %10 Colemanite added SB20
SB20C20	: %20 Colemanite added SB20
SB20GF	: %1 Glass fiber added SB20
SB20CS10	: %10 Copper slag added SB20
SB20CS20	: %20 Copper slag added SB20
SB20FS10	: %10 Ferrochrome slag added SB20
SB20FS20	: %20 Ferrochrome slag added SB20
SB30	: %70 Sand - %30 Bentonite mixture
SB30E4820	: %20 Etibor48 added SB30
SB30U20	: %20 Ulexite added SB30
SB30C20	: %20 Colemanite added SB30
SB30GF	: %1 Glass fiber added SB30
SB30CS20	: %20 Copper slag added SB30
SB30FS20	: %20 Ferrochrome slag added SB30

CHAPTER 1
INTRODUCTION

1.1 Statement of the problem

Increase in the world population, the rapid depletion of fossil fuels and increase in the world's energy demand have brought the development of energy structures to the fore. In particular, nuclear energy has an important place as a clean energy source in the fight against climate change and having less carbon emissions compared to other sources. However, the use of nuclear energy produces radioactive effects and high-level waste. It is very important that these wastes can be stored without harming the environment. For this reason, the concept of deep geological disposal is being developed.

It is important to use high power buried cables to distribute electricity. With the increase in population and the development of technology, the use of power cables has increased. It is possible for these cables to reach high temperatures during energy transmission and to damage the cable itself. For this reason, the soil where the cable is buried is required to distribute the heat quickly to the environment.

Heat exchangers come to the prominent in the heating and cooling of buildings due to the increase in energy prices, the prevention of energy crisis and the efficient use of energy. By taking advantage of the constant temperature of the ground, it consumes less energy to provide heating and cooling of buildings.

All of these energy structures are directly connected to their surroundings and the most influential factor is the soil. Therefore, it is necessary to investigate the thermal properties of soils. Particularly in the areas where nuclear disposal area and high power buried cables are located, rapid conduction of heat is desired. Heat exchangers also give more efficient results on soils with high thermal conductive.

In this thesis, the behavior of bentonite material for nuclear waste storage repositories is investigated. Bentonite is known to have high swelling pressure, sealing property and low hydraulic conductivity. By examining the behavior of the thermal

properties of bentonite, it is aimed to extract data that can be used for nuclear waste disposal areas. For this purpose, how the thermal properties change in the compaction curve of bentonite was investigated. In addition, the variation of thermal properties was investigated by using additives. Since the heat dissipation in nuclear waste storage repositories can take up to 100 years, the temperature of the soil is an important parameter. Therefore, thermal conductivity behavior depending on temperature was investigated in bentonite and additive mixtures. Bentonite becomes dry in places where it is found due to temperature differences and becomes saturated in the parts where it is fed from groundwater. For this reason, the variation of the thermal properties of bentonite and additive mixtures according to the degree of saturation was also investigated.

Coarse grained soils are generally preferred for heat exchanger and high power buried cable systems. Sand-bentonite mixture was investigated for these structures. For energy piles where high strength is required, a mixture of 90% sand-10% bentonite was prepared and its thermal properties were investigated according to the compaction curve. In addition, 80% sand - 20% bentonite and 70% sand - 30% bentonite ratios were also investigated. The soils where high power cables are embedded can be dry and wet according to the season of the region. Therefore, the thermal properties of these mixtures should be investigated at different saturation levels. Temperatures in the core of the cable can reach up to 90 °C, so the thermal conductivity behavior of sand-bentonite mixtures at different temperatures is important. In addition, the effect of all additives were investigated in the sand-bentonite mixtures.

Boron minerals (colemanite, ulexite and etibor48) and glass fiber are known to be materials with low thermal conductivity. Single and double barrier systems can be used for the storage of nuclear waste. In the double barrier system, the inner engineering buffer is thermally conductive, while the outer engineering buffer is thermally resistive. Thus, the bedrock is less exposed to the effects of high temperature. It is known that colemanite is used in nuclear power plants due to its radionuclide absorption feature. The reason for the investigation of etibor48 and ulexite is the commercially common boron minerals in Türkiye. Ferrochrome slag and copper slag were chosen as slag. The recycling of these slags is used in some areas. Since the slags

are made of metal oxides, it is expected to show high thermal conductivity. In addition, studies have shown that slags have higher strengths than soil grains. In this thesis, the effect of slag as an additive was investigated due to its low cost.

1.2 Objective and Scope

In this thesis, the behavior of bentonite and sand-bentonite materials for nuclear waste storage repositories is investigated. For this purpose, how the thermal properties change in the compaction curve of bentonite was investigated. In addition, the variation of thermal properties was investigated by using additives. Since the heat dissipation in nuclear waste storage repositories can take up to 100 years, the temperature of the soil is an important parameter. Therefore, thermal conductivity behavior depending on temperature was investigated in bentonite and additive mixtures. Bentonite becomes dry in places where it is found due to temperature differences and becomes saturated in the parts where it is fed from groundwater. For this reason, the variation of the thermal properties of bentonite and additive mixtures according to the degree of saturation was also investigated.

Coarse grained soils are generally preferred for heat exchanger and high power buried cable systems. Sand-bentonite mixture was investigated for these structures. For energy piles where high strength is required, a mixture of 90% sand-10% bentonite was prepared and its thermal properties were investigated according to the compaction curve. In addition, 80% sand - 20% bentonite and 70% sand - 30% bentonite ratios were also investigated. The soils where high power cables are embedded can be dry and wet according to the season of the region. Therefore, the thermal properties of these mixtures should be investigated at different saturation levels. Temperatures in the core of the cable can reach up to 90 ℃, so the thermal conductivity behavior of sand-bentonite mixtures at different temperatures is important. In addition, all additives were investigated with sand-bentonite mixtures.

Boron minerals (colemanite, ulexite and etibor48) and glass fiber are known to be materials with low thermal conductivity. Single and double barrier systems can be used for the storage of nuclear waste. In the double barrier system, the inner engineering

buffer is thermally conductive, while the outer engineering buffer is thermally resistive. Thus, the bedrock is less exposed to the effects of high temperature. It is known that colemanite is used in nuclear power plants due to its radionuclide absorption feature. The reason for the investigation of etibor48 and ulexite is the commercially common boron minerals in Türkiye. Ferrochrome slag and copper slag were chosen as slag. The recycling of these slags is used in some areas. Since the slags are made of metal oxides, it is expected to show high thermal conductivity. In addition, studies have shown that slags have higher strengths than soil grains. In this thesis, the effect of slag as an additive was investigated due to its low cost.

1.3 Organization of the thesis

Within the scope of the master thesis, eight chapters were created. The content of each chapter in this thesis as follows:

In Chapter 1, the problem statement, objective, and scope of the thesis are given.

Chapter 2 presents an information about the energy geo-structures. And a literature review on the termal properties of soils and effecting factors like water content, dry density, temperature, porosity etc. are given in this chapter. This chapter also includes information on the used additive materials.

Chapter 3 presents the material characterization and the experimental techniques.

Chapter 4 shows the Proctor test results of bentonite, sand-bentonite, and additive-added bentonite and sand-bentonite mixtures.

Chapter 5 presents change of thermal properties of bentonite, %90 sand - %10 bentonite and additive-added mixtures depending on compaction curve.

Chapter 6 shows the thermal conductivity change according to temperature. In this chapter bentonite, %90 sand - %10 bentonite, %80 sand - %20 bentonite and %70 sand - %30 bentonite and addive-added mixtures investigated.

Chapter 7 presents the effects of saturation degree on the thermal properties. The materials in Chapter 6 are also investigated here.

In Chapter 8, all results are shown in the tables. According to these tables, summary information of the results and recommendations for future studies are given.

CHAPTER 2
LITERATURE REVIEW

2.1 Energy Geo-Structures

2.1.1 Energy Piles – Heat Exchangers

With the increase in population, the world's energy needs have increased, the use of fossil fuels has created a greenhouse effect and, renewable and sustainable energy sources are needed because of fossil fuels are non-renewable (Abdelaziz et al., 2011; Abuel-Naga et al., 2015; Hakhamaneshi & Black, 2016; Peron et al., 2011). Among the renewable energy systems, the heat pump system, which can be used for heating and cooling of buildings, has come to the fore recently. Although heat pump systems use electricity, they are not used for direct heating with electricity, their purpose is to transfer heat using electricity. So it is more efficient, less costly and reduces the greenhouse effect (Abuel-Naga et al., 2015).

The use of ground source heat pump systems is claimed to be one of the important innovations in terms of both sustainability and energy efficiency (López-Acosta et al., 2021). After about 5 meters of depth, the temperature of the ground remains constant between 10-18 degrees and the temperature increases by 1 degree every 33 meters (Abdelaziz et al., 2011; Abuel-Naga et al., 2015; Desenerji 2019). Energy piles are designed by taking advantage of the fact that the ground is not affected by seasonal differences and remains approximately stable. While energy piles are used for heating and cooling of buildings, they also support the bearing capacity (Abuel-Naga et al., 2015; Abdelaziz et al., 2011). Figure 2.1 shows the working principle of energy piles according to the seasons. While it can be used to heat the building by absorbing heat from the ground in winter, it can be used to cool the building by using the ground as a heat sink in summer. And the pipes may contain water, brine water and antifreeze (Abdelaziz et al., 2011).

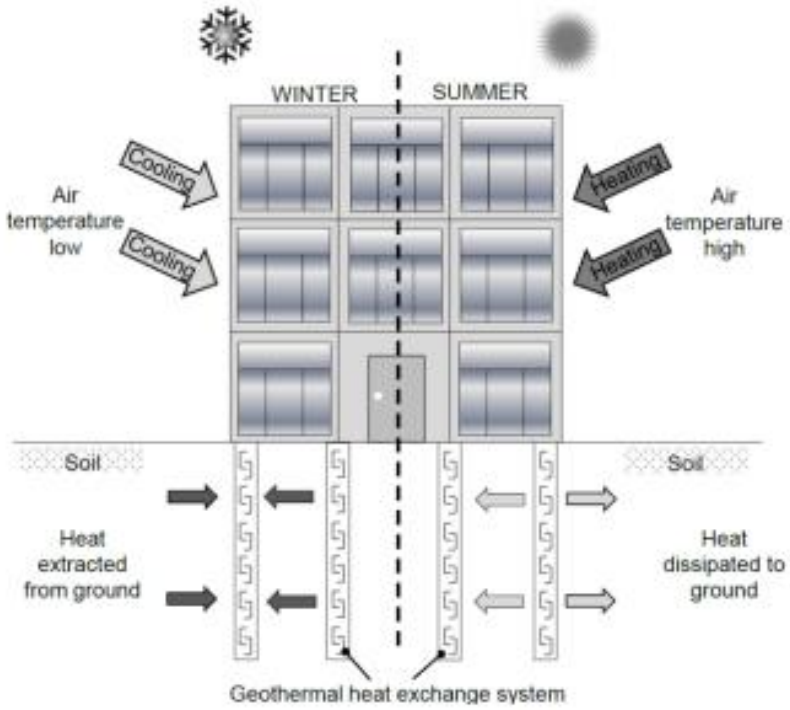


Figure 2.1 Concept of geotechnical energy structure (Hakhamaneshi & Black, 2016)

Abdelaziz et al. (2011) explained how heat transfer takes place in energy piles. The energy pile transfers heat with the ground around it, and this heat transfer comes to the pipes buried inside the pile and is used for heating and cooling of the building with fluid. Figure 2.2 shows the heat transfer schematically.

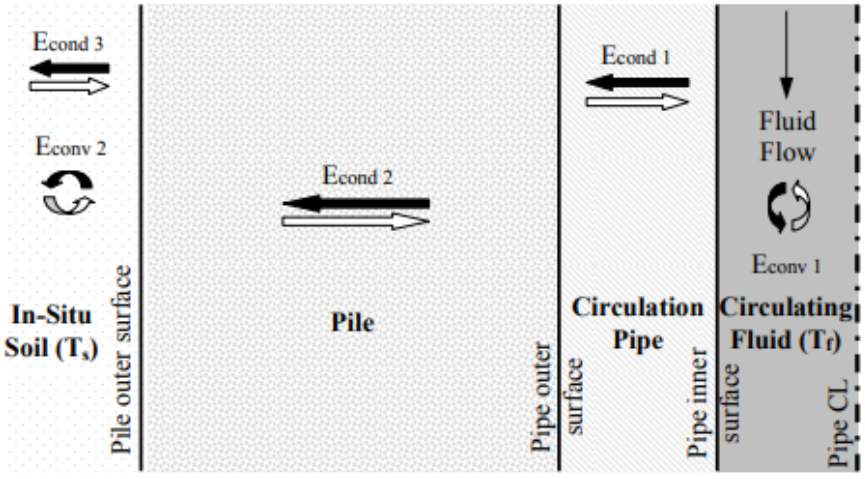


Figure 2.2 Heat transfer mechanism in energy piles (Abdelaziz et al., 2011)

E_{conv1} and E_{conv2} are heat convection between the inner surface of the pipe and circulating fluid, and heat convection through ground water flow, respectively. E_{cond1}, E_{cond2} and E_{cond3} are heat conduction through the pipe wall, heat conduction through the pipe wall and heat conduction within the in-situ soil, respectively. Black arrows indicate the cooling state, while the white arrows indicate the heating state. The heat transfers mechanism indicates the importance of thermal conducutivity of the surrounding soils.

Heat exchanger systems can also be made by directly burying the pipes in the ground. The drilling method (Figure 2.3a), pipes laid horizontally (Figure 2.3b) and pipes laid both horizontally and vertically without going too deep (Figure 2.3c) are examples of this.

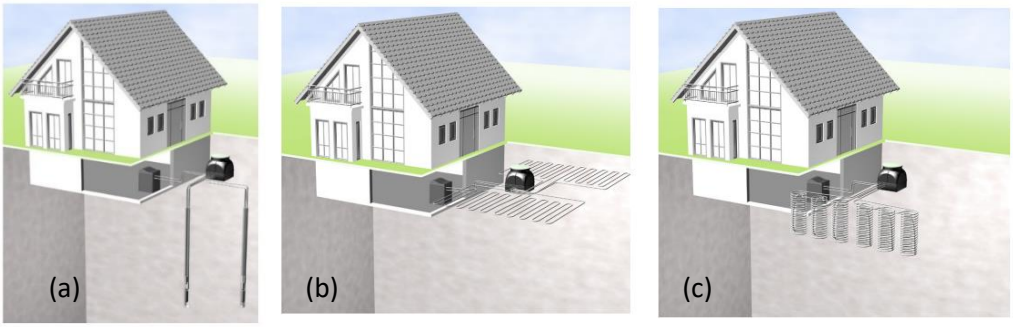


Figure 2.3 Schematic plans of heat exchangers (Desenerji, 2019) a) Drilling method b) Pipes laid horizontally c) Pipes laid both horizontally and vertically

In addition, the heat of the ground can be used in the ventilation control for the winter and summer seasons. There is a schematic drawing in Figure 2.4.

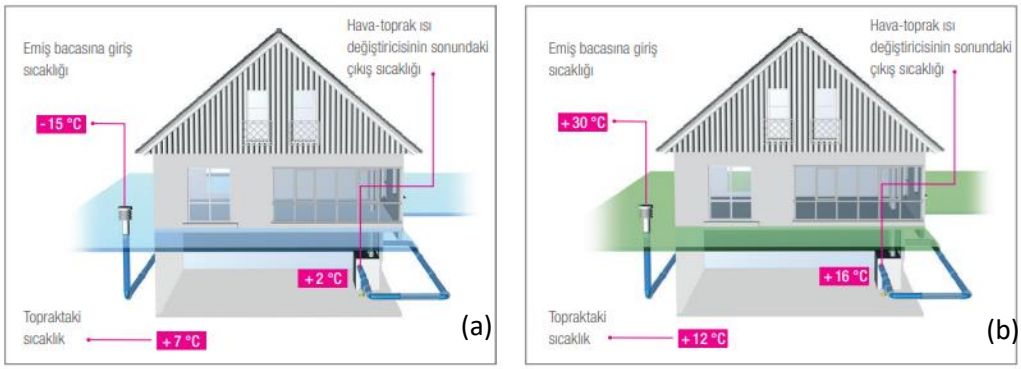


Figure 2.4 Schematic plans for ventilation (Desenerji, 2019) control a) Winter b) Summer

2.1.2 Nuclear Waste Storage Repositories

Increasing oil prices, energy needs and global warming have increased research on the use of nuclear energy. Disposal of fuels used in nuclear energy is important for human and environmental health and sustainability of nuclear energy. (Cho et al., 2010; Yoon et al., 2018). For the disposal of these wastes, studies have focused on the concept of deep geological disposal (Cho et al., 2010; Yoon et al., 2018; Yoon et al., 2022; Chen et al., 2018; Man et al., 2011).

Nuclear wastes are aimed to be buried between 500 and 1500 m below the ground (Yoon et al., 2018; Chen et al., 2018). Deep geological repositories consist of multi-barrier system and this geological repository is composed of canister, backfill, buffer and near field rock seen in Figure 2.5 (Yoon et al., 2018; Chen et al., 2018; Cho et al., 2010). Spend fuel is aimed to store inside the metal canister (steel and copper) that can withstand corrosion and physical effects, then canisters are planned to be embedded in preholled bedrock to be stored inside (Yoon et al., 2018; Cho et al., 2010). It is aimed to be used as engineering buffer with bentonite, bentonite-sand and with various additives (Man et al., 2011). One of the main purposes of engineering buffer is to inhibit or delay the propagation of radionucleoids into the biosphere (Chen et al., 2018; Cho et al., 2010). Afterwards, it is aimed to be completely sealed with a backfill and to isolate the nuclear waste from the ecosystem (Yoon et al., 2018).

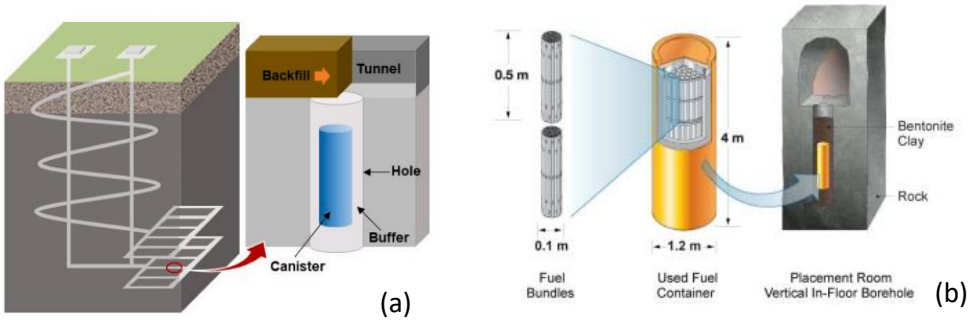


Figure 2.5 Concept of Deep Geological Disposal a) Genel design method (Yoon et al., 2022) b) Detailed design chart (Man et al., 2011)

Long-term performance of engineered and natural barriers is necessary for a geological deposit to be safe (Cho et al., 2010). It is desired that the engineer barrier has swelling and sealing, low hydraulic conductivity and high retention capability of radionuclides, therefore bentonite is generally preferred as the engineering barrier (Cho et al., 2010; Man et al., 2011; Chen et al., 2018).

In designs, many countries limit the temperature that bentonite can reach to a maximum of 90-100 °C (Cho et al., 2010; Chen et al., 2018; Yoon et al., 2022). The fact that the temperature is above 100 °C for a long time changes the structure of bentonite and negatively affects the engineering parameters and performance (for example swelling and hydraulic conductivity) of bentonite (Chen et al., 2018; Yoon et al., 2022). It is aimed that the material of the buffer dissipates the heat quickly and transfers it to the bedrock (Man et al., 2011). For this reason, it is aimed to use bentonite material with high thermal conductivity and temperature not exceeding 100 °C (Yoon et al., 2018). At the same time, it is aimed to be able to store in smaller areas by reducing the distance between two containers by using materials with high thermal conductivity.

2.1.3 High Power Buried Cables

The installation of underground cable lines has a century-old history and significant developments have been made in high voltage cables in this century (Ocłoń et al., 2016). The increase in population and the need for electrical energy have increased the application of power cable (Metwally et al., 2013). Cable lines also considerably minimize electromagnetic field emissions and are resistant to weather. When

comparing the probability of a cable line failing, underground power cables are more reliable than overhead transmission lines (Ocłoń et al., 2016).

Figure 2.6 shows the schematic implementation of the underground high voltage cable. Sundberg (2016) summarized the factors affecting the temperature of the cable; thermal properties of natural ground, ground temperature and temperature changes, thermal properties of cable at different temperatures, cable type, cable dimensions, cable number, cable depth, distance between cables and, dimensioning electric power and its duration.

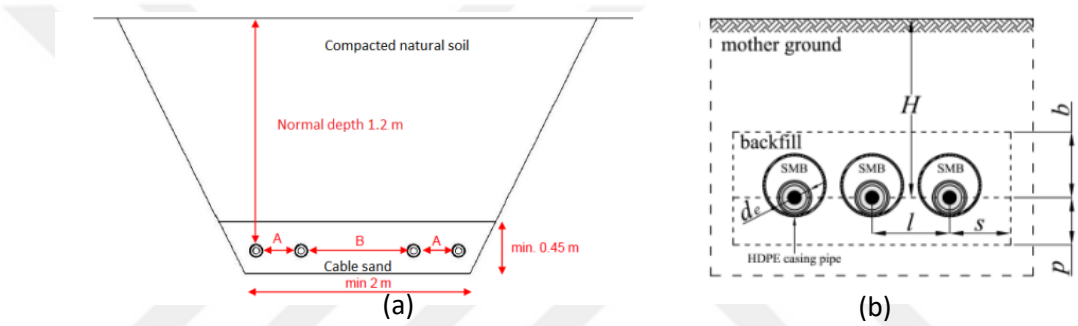


Figure 2.6 Schematic implementation of underground cable a) Cables inside directly backfill (Sundberg, 2016) b) Cables inside casing pipe (Ocłoń et al., 2016)

High-voltage cables produce heat while carrying currents. While Georgiev et al. (2020) calculated the cable core temperature at 90 ℃, Ocłoń et al. (2016) calculated 65 ℃ in their studies. The cable line is expected to have an average life of 30 years and more. Therefore, long-term analyzes and observation of temperature changes are important in the design of underground cables (Georgiev et al., 2020). The temperature of the cable and the magnitude of the potential electric power transmission are controlled by the thermal processes around buried power lines (Sundberg, 2016).

Cable sands (also known as thermal backfill) (Figure 2.6a) cover the cable and provide a cooling effect on its surface by extending its thermal surface. The cable's temperature can be considerably impacted by the quality, quantity, and geometry of the cable sand, which can also counteract the effects of the natural ground's high thermal resistivity (Sundberg, 2016**)**. Also Figure 2.6b shows that cables can be

situated in casing pipes filled with sand-bentonite mixtures for protecting cable from external loads (Ocłoń et al., 2016).

Table 2.1 The thermal properties of thermal backfill according to some countries (IEC 60287-3-1, 2017)

Country	Thermal characteristics of the soil	
Australia	Thermal conductivity	Nominal 0.833 W/K·m
	Soil ambient temperature	Summer 25 °C Winter 18 °C
Austria	Thermal conductivity	nominal, (wet) 1,0 W/K·m dry zone, (dry) 0.4 W/K·m
	Temperature	20 °C
Canada	Thermal conductivity	Nominal 0,5 to 0.333 W/K·m
	Temperature	Summer 25 °C Winter -5 °C
China	Thermal conductivity	0.833 to 1.0 W/K·m
	Temperature	Summer 30 °C Winter 5 °C
Egypt	Thermal conductivity	0.833 W/K·m
	Temperature	Summer 35 °C Winter 0 °C
Finland	Thermal conductivity	Average value 1.0 W/K·m For submarine 2.5 W/K·m
	Temperature	Max. 15 °C Min. 0 °C (average value 5 °C to 10 °C, exceptional maximum 20 °C)
France	Thermal conductivity	nominal, summer 0.833 W/K·m nominal, winter 1.177 W/K·m dry zone[a], summer 0.4 W/K·m dry zone[a], winter 0.4 W/K·m
	Temperature, summer	20 kV cables 20 °C 63 kV, 90 kV, 225 kV, and 400 kV cables hot area 25 °C intermediate area 22 °C cold area 20 °C
	Temperature, winter	20 kV cables 10 °C 63 kV, 90 kV, 225 kV and 400 kV cables hot region 17 °C intermediate region 15 °C cold region 13 °C
Germany	Thermal conductivity	average 1.0 W/K·m dry zone 0.4 W/K·m dry zone near the cable 0.4 W/K·m
	Temperature	Max 20 °C Min 0 °C Average 10 °C

The cable could be destroyed or suffer severe damage as a result of the temperature increase (Sundberg, 2016). For this reason, it is desired that the thermal properties of the backfill are good. While the backfill is being designed, the water level of the ground changes due to seasonal changes and the backfill can be dry, unsaturated and saturated depending on the seasons (Ocłoń 2016 and Sundberg 2016). The thermal properties of the backfill required in the designs of some countries in IEC 60287-3-1 are given in Table 2.1.

2.2 Thermal Properties of Soils

Thermal properties of soils have become an important research topic due to increasing energy demands, engineering practices and environmental factors (Bi et al., 2018). Especially in recent years, the increasing energy structures and the need for nuclear waste storage areas have intensified the studies on this subject. Thermal conductivity, it is the physical property that determines the heat transfer capacity of the material. It is a measure of how well heat energy can be transferred from one material to another. Its unit is watts per meter-kelvin (W/mK).

U.S. Army Corps of Engineers (1988) explained volumetric heat capacity which refers to a substance's potential to store heat while enduring a particular temperature change without transitioning into a different phase. It is the quantity of energy in the form of heat that must be added to a material's volume in order to raise its temperature by one unit. The volumetric heat capacity is measured in joules per kelvin per cubic meters, or $J \cdot K^{-1} \cdot m^{-3}$. The specific heat capacity (heat capacity per unit of mass, in $J \cdot K^{-1} \cdot kg^{-1}$) multiplied by the substance's density (in kg/m^3 or g/mL) yields the volumetric heat capacity. The volumetric heat capacity differentiates from specific heat capacity in that it is based on the material's volume, whereas specific heat is based on the material's mass.

Thermal diffusivity, which is used in heat transfer analysis, is calculated by dividing the thermal conductivity by the density and specific heat capacity at constant pressure. (Lide, 2009). It determines how quickly heat is transferred from a material's hot end to its cold end. Its unit is m^2/s. The equation is:

$$D = \frac{k}{\rho C_p} \quad (1)$$

where, D is diffusivity, k is thermal conductivity (W/mK), C_p is specific heat capacity (J/kgK) and ρ is density (kg/m^3). The total value of ρC_p is referred to as the volumetric heat capacity (C, J/(m^{3}K)). Table 2.2 shows thermal properties of some materials which effect on thermal conductivity of soils. Table 2.3 shows some soils and materials thermal properties which using in energy geo-structures.

Table 2.2 The materials which effect on thermal conductivity of soils (Bejan & Kraus, 2003)

Materials	Density (kg/m^3)	Heat Capacity (kJ/kgK)	Thermal Conductivity (W/mK)	Thermal Diffusivity (m^2/s) x 10^{-7}
Air (10 ℃)	1.25	1.00	0.026	0.21
Water (25 ℃)	999.87	4.20	0.59	1.43
Water Vapor (1 atm, 127 ℃)	-	1.90	0.016	233.8
Ice (0 ℃)	917	2.04	2.25	12

The thermal properties of soils are affected by many factors: mineralogical structure, particle diameter and distribution of grains, dry unit weight, porosity, water content, temperature, pore size, soil skeleton and texture, etc. (Bi et al., 2018; Fricke et al., 1992; Xu et al., 2020)

According to Zhang and Wang (2017), the factors which affecting thermal conductivity can be divided into three groups: compositional factors, environmental factors and other factors. Examples of compositional factors are mineral composition, shape, gradation, particle size, interparticle physical contact area. Water content, unit volume weight, temperature, etc. can be said as environmental factors. Other factors are salts, ions, additives, etc.

Table 2.3 Thermal conductivity of materials which found in soil and used energy geo-structures (Pahud, 2003)

	Thermal Conductivity (W/m°C)		Volumetric Heat Capacity (MJ/m^3°C)	
	Dry	Saturated	Dry	Saturated
Clay	0.4-1.0	0.9-2.3	1.5-.16	1.6-3.4
Silt	0.4-1.0	0.9-2.3	1.5-1.6	1.6-3.4
Sand	0.3-0.8	1.7-5.0	1.3-1.6	2.2-2.9
Gravel	0.4-0.5	1.8	1.4-1.6	2.4
Steel	14-60		3.12	
Concrete	0.9-2.0		1.8-2.0	
Granite	2.1-4.1		2.1-3.0	
Basalt	1.3-2.3		2.3-2.6	
Gabbro	1.7-2.5		2.6	
Metaquartzite	5.8		2.1	
Limestone	2.5-4.0		2.1-2.4	
Peat	0.2-0.7		0.5-3.8	
Claystone/siltstone	1.1-3.5		2.1-2.4	
Sandstone	1.3-5.1		1.6-2.8	
Quartzite	3.6-6.6		2.1-2.2	

Different methods have been tried for years in thermal conductivity measurements. These methods can be divided into three main groups: steady state, unsteady state and transient state. In the thermal conductivity of soils, methods such as measurement with needle, hot-ball method (Kubičár et al., 2010), measurement with disc-shaped probe (Song et al., 2020) have been applied, and there are still tested and developing measurement methods. Mitchell and Kao (1978) investigated the thermal conductivity of soils using different measurement methods and said that the transient state method (especially thermal needle probe) is more suitable than other methods due to its short measurement time and simplicity. Jackson and Taylor (1986) stated that the advantage of the transient state method is that water migration is minimized by temperature change and no need to wait a very long time for the thermal gradients to equalize. However, in this method, since the needle has to be immersed in the soil, contact gaps may occur between the needle and the soil on hard soils or rocks. These soils should be pre-holled and inserted in the soil with thermal conductive grease (Barry-Macaulay et al., 2013).

Due to the growing need for energy-related geo-structures, such as underground heat pumps and underground electric power cable tunnels, which are some of the most promising renewable energy sources or sustainable urban designs, the determination of the thermal conductivity of soils has attracted a lot of attention (Lee et al., 2016; Johnston et al., 2011; Go et al., 2014). As a result of the studies, theoretical and empirical models have been discovered and continue to be discovered in order to calculate the thermal conductivity of various soils without directly measuring them.

2.2.1 Theoretical models

Wiener (1912) demonstrated soil thermal conductivity which be formed solid, liquid and gas. If all components are assignment in series (Figure 2.7a), it has the lowest thermal conductivity values. And the highest thermal conductivity value obtained when all components are arranged in parallel (Figure 2.7b). And the effective thermal conductivities can be expressed as in Equation 2 and 3:

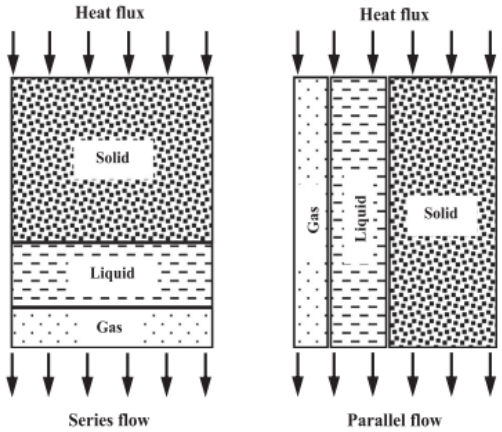
$$k = k_w^{\perp} = \left[\sum \frac{\emptyset_\alpha}{k_\alpha}\right]^{-1} \ (Series) \tag{2}$$

$$k = k_w^{U} = \sum \emptyset_\alpha k_\alpha \ (Series) \tag{3}$$

Where $\emptyset_\alpha$ is volume fraction and k_α is thermal conductivity of phase. The pore structure of a porous media has no influence on these two bounding limits, which are also known as Wiener bounds. $k_w^{\perp}$ and k_w^{U} are the lower and upper Wiener bounds respectively.

De Vries (1963) proposed a theoretical model for soil thermal conductivity based on the Maxwell equation, assuming that soil solid particles were equally dispersed in continuous pore fluid in soils. This model is provided below:

$$k = \frac{\sum_{i=0}^{N} K_i x_i k_i}{\sum_{i=0}^{N} K_i x_i} \tag{4}$$



(a) (b)

Figure 2.7 Schematic of Wiener (1912) model a) Series flow (lower bound) b) Parallel flow (upper bound)

Where k_i, x_i and K_i are the thermal conductivity of each soil component, volume fraction of each component and ratio of average thermal gradient of each component to that of continuous medium in soils, respectively.

$$K_i = \frac{(dT/dz)_1}{(dT/dz)_0} \tag{5}$$

Some factors such as particle size, relative position, shape and ratio of thermal conductivity of one soil component to that of continuous medium in soils (k_1/k_0) effected K_i. So De Vries (1963) proposed the equation for calculating K_i:

$$K_i = \frac{1}{3}\sum_{a,b,c}\left[1 + (\frac{k_i}{k_0} - 1)g_a\right]^{-1} \tag{6}$$

Where g_a, g_b and g_c are the grain shape coefficients and generally taken as 1/3 spherical soil particles.

To forecast soil thermal conductivity, Johansen (1977) proposed a geometric mean method. The mathematical expression for saturated soils is as follows,

$$k = k_s^{1-n} k_f^n \tag{7}$$

Where k_s is the thermal conductivity of solid phase and k_f is the thermal conductivity of fluid. n is the porosity of soils. While soil occurs soil particle, water and air, the geotmetric mean model can be expressed as:

$$k = k_s^{1-n} k_w^n k_a^{(1-S_r)n} \quad (8)$$

Where k_a and k_w are the thermal conductivities of air and water, respectively, and S_r is soil saturation degree.

2.2.2 Empirical Models

Kersten (1949) measured the thermal conductivities of 19 different soils using single thermal probe method and proposed empirical equation for unfrozen clay and silt (Equation 1) and for unfrozen sandy soil (Equation 2).

$$k = \left((0.9 \log w - 0.2) \times 10^{0.6242\rho_d - 3.4628}\right) \times 418.6 \ \ for\ silt\ and\ clay \quad (9)$$

$$k = \left((0.7 \log w + 0.4) \times 10^{0.6242\rho_d - 3.4628}\right) \times 418.6 \ \ for\ sand \quad (10)$$

Where k is thermal conductivity of the soil (W/mK), w is water content (%) and ρ_d is dry density (g/cm^3).

Johansen (1977) developed an empirical equation using some dates from Karsten (1949). Johansen proposed the concept of normalized thermal conductivity, k_e and proposed a relationship between soil thermal conductivity, k for unsaturated soils:

$$k = (k_{sat} - k_{dry})k_e + k_{dry} \quad (11)$$

Where k_{sat} and k_{dry} are the thermal conductivity (W/mK) of saturated and dry soils, respectively. Volumetric water content, S_r (or soil porosity, n) related to normalized thermal conductivity, k_e:

$$k_e = 0.7 \log S_r + 1.0 \ (S_r > 0.05)\ for\ coarse - textured\ soils, and \quad (12)$$

$$k_e = \log S_r + 1.0 \ (S_r > 0.1)\ for\ fine - textured\ soils \quad (13)$$

The value of k_{sat} was estimated according to effective thermal conductivity of oil solids k_s and thermal conductivity of water (k_w = 0.594 W/mK at 20 °C) using a geometric mean equation.

$$k_{sat} = k_s^{1-n} k_w^n \tag{14}$$

Thermal conductivity of solids, k_s was determined using another geometric mean equation from quart content (q):

$$k_s = k_q^q k_o^{1-q} \tag{15}$$

where k_q is the thermal conductivity of quartz (7.7 W/mK) and k_o is the other minerals. K_o was determined according to quartz content, 2.0 W/mK for soils with q > 0.2 and 3.0 W/mK for soils with q ≤ 02.

And Johansen (1977) used semiempirical relationship for k_{dry}:

$$k_{dry} = \frac{0.135\rho_b + +64.7}{2700 - 0.947\rho_b} \tag{16}$$

Where ρ_b is bulk density of soils (kg/m^3) and 2700 is the density of soil solids.

Cote and Konrad (2005) conducted new k_e-S_r relationship using Johansen (1977) equation according to soil type.

$$k_e = \frac{\kappa S_r}{1 + (\kappa - 1) S_r} \tag{17}$$

where κ is soil texture dependent parameter and 0.60, 1.90, 3.55 and 4.60 for organic fibrous soils, silty and clayey soils, medium and fine sand, and gravel and coarse sand, respectively.

Also Cote and Konrad (2005) proposed new empirical equation for k_{dry}.

$$k_{dry} = \chi 10^{-n\eta} \tag{18}$$

where χ (W/mK) and η are parameters for particle shape effects. For crushed rocks, χ is 1.70 W/mK and η is 1.80. χ is 0.75 W/mK and η is 1.20 for mineral soils. χ and η are 0.30 W/mK and 0.87 for organic fibrous soils, respectively. According to these equations Cote and Konrad (2005) model can be expressed as:

$$k = (k_w^n k_s^{1-n} - \chi 10^{-n\eta}) \left[\frac{\kappa S_r}{1+(\kappa-1)S_r}\right] + \chi 10^{-n\eta} \quad (19)$$

Lu et al. (2007) changed the k_e and k_{dry} and proposed new equation.

$$k_e = exp\left(\alpha\left[1 - {S_r}^{\alpha-1.33}\right]\right) \quad (20)$$

$$k_{dry} = -an + b \quad (21)$$

Where α is a parameter depending on soil texture which is 0.96 for coarse soils and 0.27 for fine soils. And 1.33 is the shape parameter. Where a and b are the coefficients related dry soils which are 0.56 and 0.51 for coarse and fine soils respectively. Lu et al. (2007) did not measure the quartz percent and assumed quartz percent equal the sand content (Nikoosokhan, 2016). And the final equation is:

$$k = k_w^n k_s^{1-n} - (b - an))exp\left(\alpha\left[1 - {S_r}^{\alpha-1.33}\right]\right) + (b - an) \quad (22)$$

Chen (2008) investigated quartz sands thermal conductivity using thermal probe method. He discovered that the porosity of the test sands had a linear relationship with the logarithm of thermal conductivity measurements. Also, degree of saturation affected the slope off the linear trend. Chen (2008) proposed the equation using exponential function to fit the experiment data:

$$k = k_w^n k_s^{1-n}[(1-b)S_r + b]^{cn} \quad (23)$$

where b and c are empirical coefficients and 0.0022 and 0.78 for quartz sands respectively.

2.3 Factors Effecting on Thermal Properties of Soils

The thermal properties of the soils vary according to the conditions of the region and the structure of the ground. For this reason, the minerals that make up the soil, the skeleton and bonds of the soil affect the thermal properties. Depending on the seasonal changes, the soils become dry and wet. Thus, the amount of water in the ground changes, and causing a change in thermal properties. It is very important to examine dry unit weight, water content, void ratio, temperature, mineralogy, grain distribution, etc.

2.3.1 Saturation Degree/Water Content

Previous researches have shown that degree of saturation is one of the most important parameter for thermal conductivity. When soil is divided into three phases, it consists of grains, water and air. The structure of the soil is porous and these porous are filled with air and/or water. Since the thermal conductivity of water (0.56 W/mK) is approximately 25 times greater than that of air (0.026 W/mK), an increase in the degree of saturation causes an increase in thermal conductivity (Barry-Macaulay et al., 2013).

According to the findings of Song et al. (2020), Fricke et al. (1992), and Xu et al. (2019), the increase in water between soil grains creates alternative pathways for heat conduction. When this change is examined in four stages (Figure 2.8); a) when the soil is dry, the conduction of heat consists of the contact points of the grains; b) with a little increase in the water in the soil, bridges are formed in the heat transmission between the parts where the water is present and the contact points of the grains expand. At the contact area, water fills interstices and produces a meniscus around contacts in grains, which greatly enhances heat conduction in the interstitial space (Cho & Santamarina 2001; Yun & Santamarina, 2008; Tang et al., 2008). Consequently, grain-to-grain heat transfer is significantly affected by even minimal water saturation in the pendular regime. (Wallen et al., 2016); c) when the soil particles are completely covered with water film, the thermal conductivity value increases rapidly. The grains are completely covered with water. Heat conduction can be provided by grain-grain, water-grain and water-water; d) in the case where the soils are close to full saturation with water, the

increase in thermal conductivity decreases and stabilizes. Increasing the amount of water does not affect the thermal conductivity.

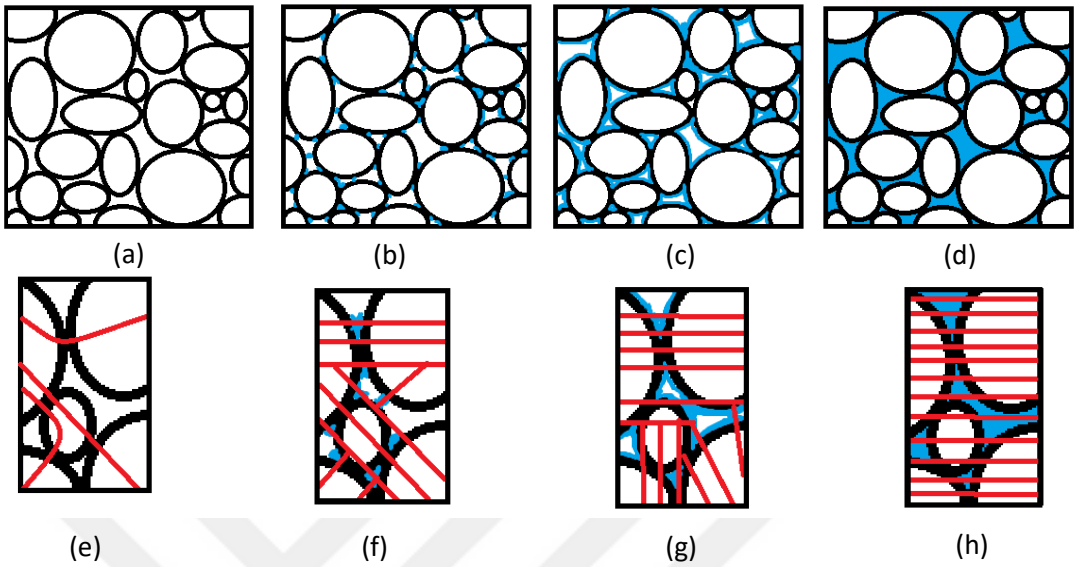
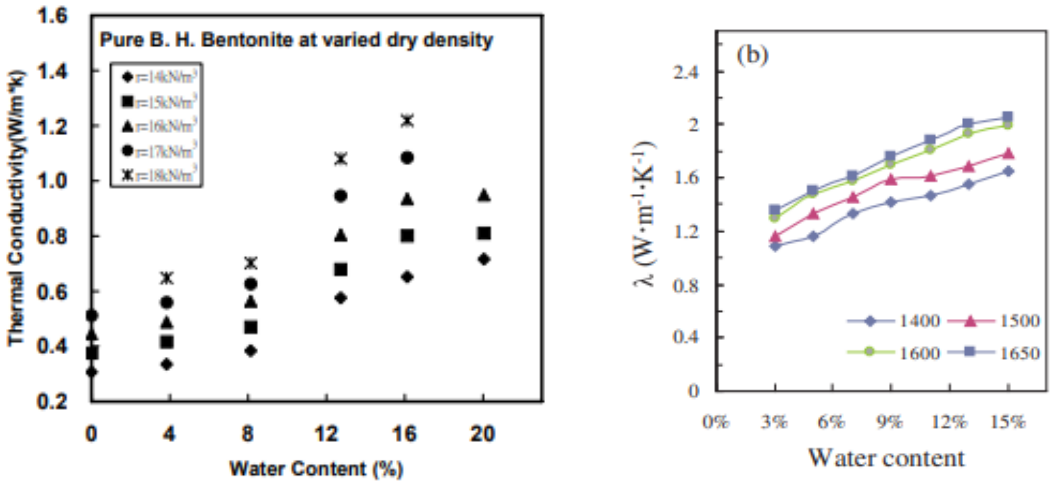


Figure 2.8 a) Dry State b) Low Water Content c) Partially saturated d) Fully Saturated e) Heat flow at dry state f) Heat flow at low water content g) Heat flow at partially saturated state h) Heat flow at fully saturated state

In Figure 2.8e, heat flow occurs between the grains. In Figure 2.8f, when a small amount of water enters the soil, a path can be formed between the particles and the contact area between the grains may be greater due to the water present. In Figure 2.8g the grains are fully covered with water and heat can be reach directly other grains with using the water. In Figure 2.8h, voids are fully filled with water and heat can be spread easily every direction.

Tien et al. (2005) prepared samples with constant dry unit weight and different water content in bentonite (Figure 2.9a), while Lu et al. (2018) used aeolian sand from the Honglianghe (Figure 2.9b). Both test results show that the thermal conductivity increases as the water content increases.



(a) (b)

Figure 2.9 Change of thermal conductivity various water content at constant dry unit weight a) Bentonite (Tien et al., 2005) b) Aeolin Sand (Lu et al., 2018)

Krishnaiah and Singh (2003), Abu-Hamdeh (2003) and Alnefaie and Abu-Hamdeh (2013) studied the thermal properties of soils. They observed that the volumetric heat capacity increased as the water content increased. It was known from the studies of Yadav and Saxena (1973) and Ghuman and Lal (1985) that the specific heat of clay soils is higher than sandy soils. Studies on this subject have also been compatible with each other. While volumetric heat capacity increases linearly in clayey soils (Figure 2.11a), specific heat increases linearly up to high water contents and then increases rapidly (Figure 2.10b). The reason for this rapid increase is thought to be the adsorption water layer around the clay particles (Ghuman and Lal, 1985). In sandy soils, the increase in volumetric heat capacity is close to linear with the increase in water content, while the specific heat progresses linearly at first, the rate of increase decreases at high water contents (Figure 2.11b).

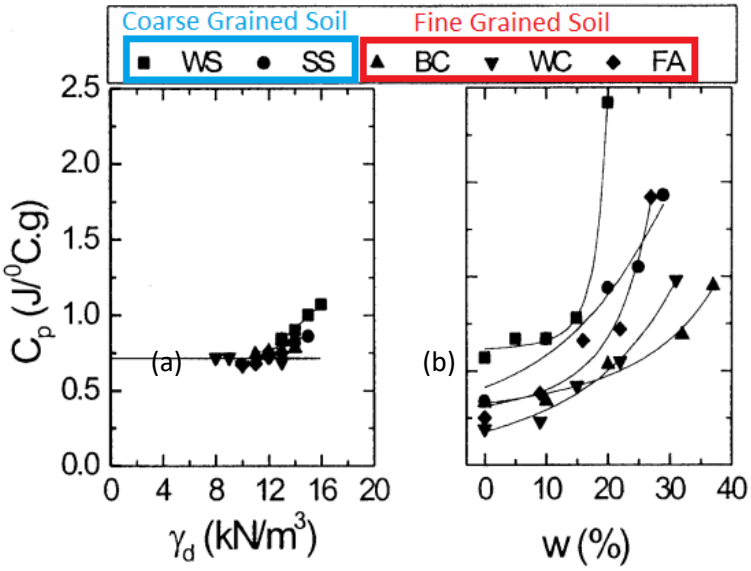


Figure 2.10 a) Variation of specific heat of soils with dry unit weight b) Variation of specific heat of soils with the moisture content (Krishnaiah & Singh, 2003)

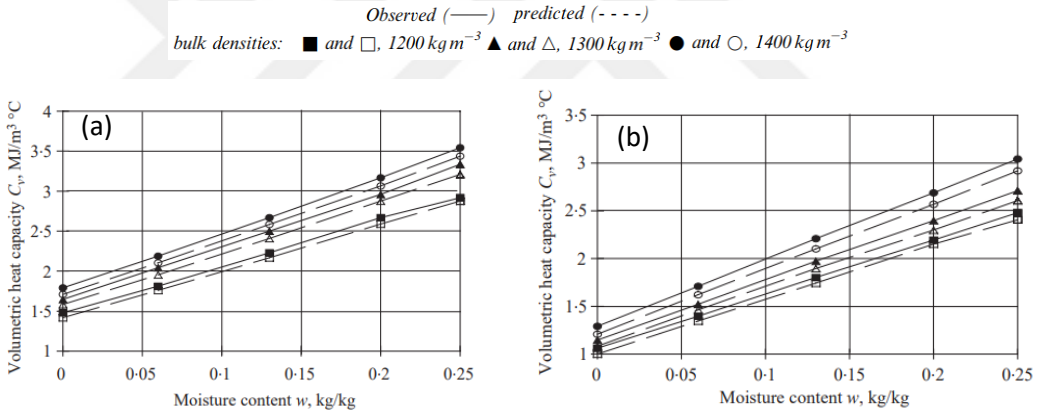


Figure 2.11 Moisture content versus volumetric heat capacity relationships a) Volumetric heat capacity as a function of moisture content for a clay soil b) Volumetric heat capacity as a function of moisture content for a sandy soil (Abu-Hamdeh, 2003)

The diffusivity value of sands is generally higher than clay soils. Sand has minerals with higher thermal conductivity, clay contains minerals with lower thermal conductivity, and volumetric heat capacity is less affected by the minerals contained in soils (Boukelia et al., 2017; Abu-Hamdeh, 2003). While diffusivity values may be close for sandy and clayey soils at low water contents, sandy soils show higher diffusivity value with increasing water content (Krishnaiah & Signh, 2003). The diffusivity value of sandy soils reaches a peak value and decreases at a certain water

content (Figure 2.12b). The reason for this is that while the thermal conductivity of sandy soils increases rapidly at first, the increase in thermal conductivity decreases with the increase of water content and the rate of increase in volumetric heat capacity is less than thermal conductivity (Figure 2.12 c) (Al Nakshabandi & Kohnke, 1965). On the other hand, in clayey soils, thermal conductivity and volumetric heat capacity increase at about the same rate, which causes the diffusivity in clayey soils to increase continuously without showing a peak value (Figure 2.12c) (Al Nakshabandi & Kohnke, 1965).

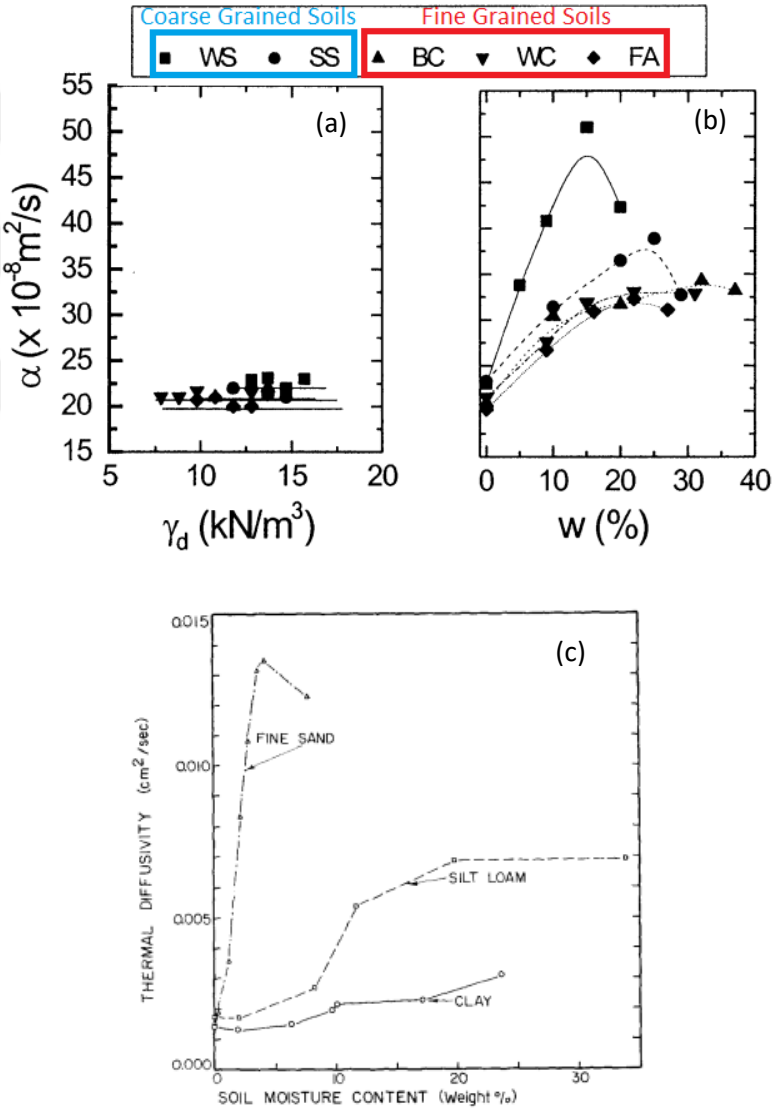


Figure 2.12 a) Variation of thermal diffusivity of soil with the dry unit weight (Krishnaiah & Signh, 2003) b) Variation of thermal diffusivity of soils with the moister content (Krishnaiah & Signh, 2003) c) Thermal diffusivity of different soils related to moisture content (Al Nakshabandi & Kohnke, 1965).

2.3.2 Dry Density

Song et al. (2020) explained how the thermal conductivity changes when the dry density changes. For example, if there are two different dry unit weight soils in a constant volume, the soil with a high dry unit weight will have a low porosity and a larger contact surface between the grains. As the water inside the soil fills the gaps more, it will increase the contact surface. Since the thermal conductivity value of the grains is higher than water and air, it will also cause an increase in thermal conductivity. Figure 2.13 shows how the soil structure will change as the dry unit weight increases.

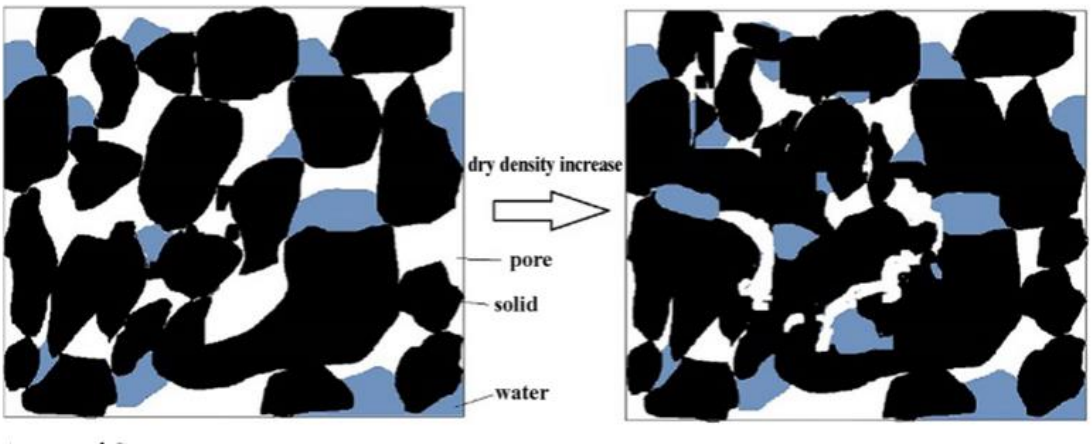


Figure 2.13 Soil structure change with dry density (Song et al., 2020)

Yun and Santamarina (2008) were mentioned particle-level conduction mechanism.

- Conduction in the Solid Particle: The mineral that forms the solid particle conducts heat.
- Conduction from one solid to another inside the contact area.
- Heat is transferred from a particle into a fluid and then back into nearby particles in a process known as solid-fluid-solid conduction. This conduction channel is particularly important in soils containing pendular water that are partially saturated.
- Heat is transferred through the fluid in the pores of the porous network by conduction.

- Convection: Currents of natural convection are started by the warming of the fluid around the particles. When $D_{50} \geq 6$ mm, this heat transfer mode is proper.
- Radiation at interparticle contacts: Heat is transmitted across the space between contacting particles by radiation.
- Radiation into the surrounding medium from the particle surface. The material density has an inverse relationship with the penetration depth (for instance, a few millimeters in water and several meters in the air). Figure 2.14 shows particle-level conduction mechanism.

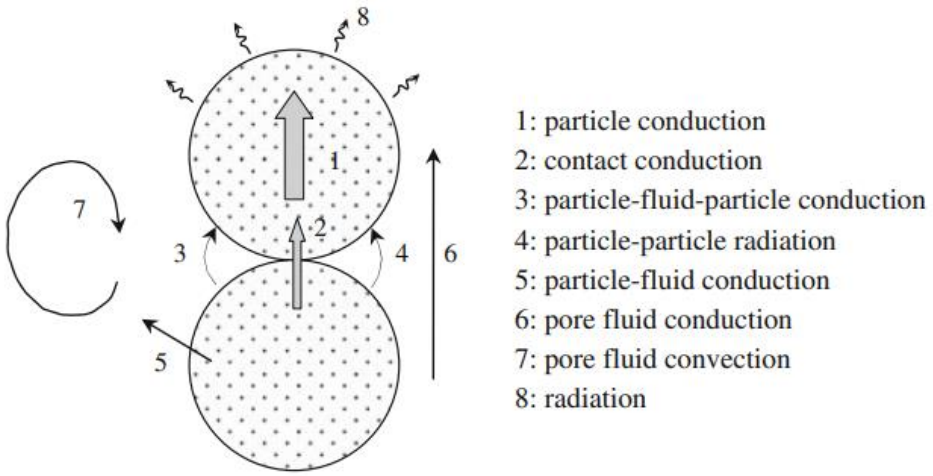


Figure 2.14 Particle-level conduction mechanism (Yun & Santamarina, 2008)

Song et al. (2020), Lu et al. (2018) and Barry-Macaulay et al. (2013) investigated how thermal conductivity changes when dry density changes. Song et al. (2020) used clay from Xianyang, China. Lu et al. (2018) used aeolian sand from Tibetan Plateau. And Barry-Macaulay et al. (2013) used sand and clayey sand from the Melbourne region, Australia. According to results, thermal conductivity increased with increasing dry density (Figure 2.15).

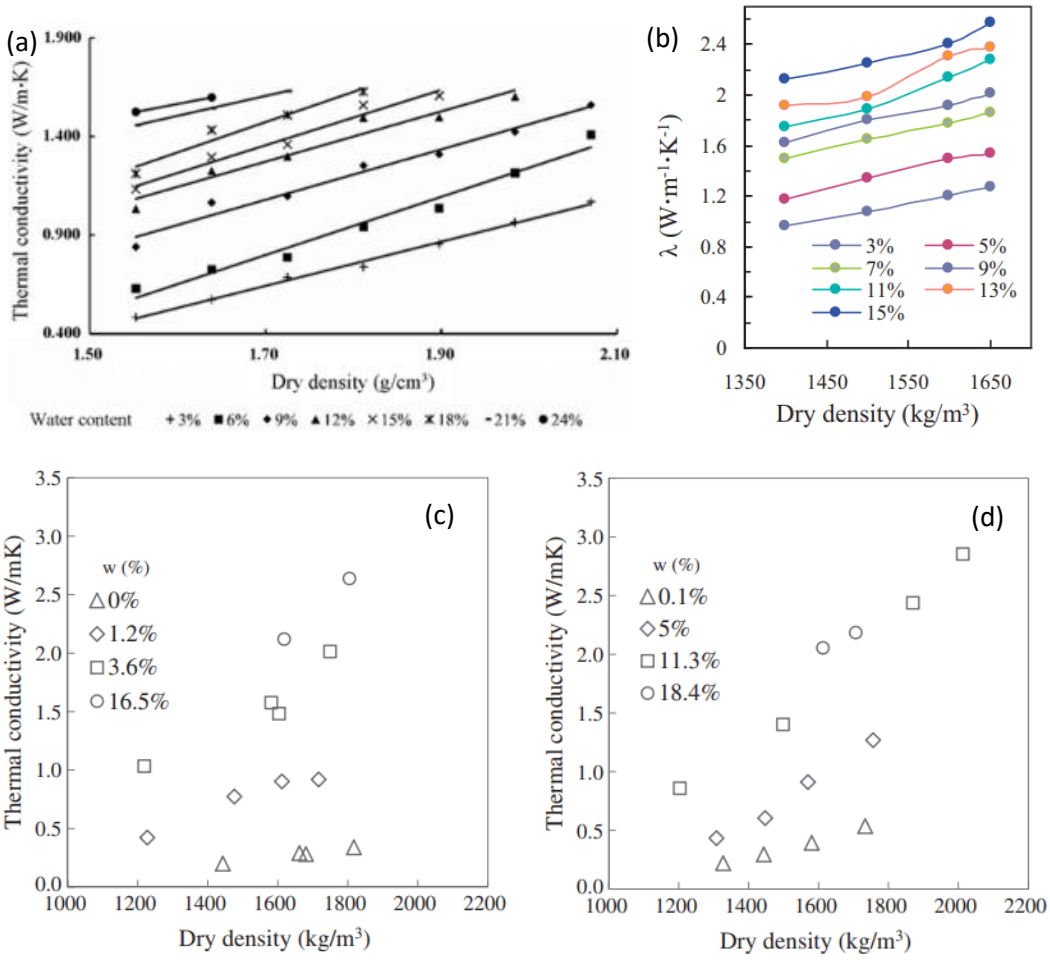


Figure 2.15 Thermal conductivity changes according to dry density a) Clay from Xianyang, China (Song et al., 2020) b) Aeolin sand from Tibetan Plateau (Lu et al., 2018) c) Sand from Melbourne region, Australia (Barry-Macaulay et al., 2013) d) Clayey sand from Melbourne region, Australia (Barry-Macaulay et al., 2013)

The volumetric heat capacity increases as the bulk density of the soil increases (Al Nakshabandi & Kohnke, 1965). It has been suggested that the reason for this is that the contact area of the grains increases as the porosity decreases (Abu-Hamdeh, 2003). Krishnaiah and Singh (2003) stated that the specific heat capacity increases with dry unit weight, but the effect of this increase is much less than that of water (Figure 2.10a).

Krishnaiah and Signh (2003) suggested that the diffusivity value is independent of dry unit weight for coarse and fine-grained soils (Figure 2.12a).

2.3.3 Porosity

The increase in porosity is the increase in the void volume in the soil. The void inside the soil is filled with air and since the thermal conductivity of the air is very low, it causes a decrease in thermal conductivity (Wang et al., 2015). At the same time, it causes a decrease in the inter-granular contact surfaces, thus extending the necessary path for heat dissipation. When the porosity decreases, a denser soil is obtained. The grains are in contact with each other more and there are more paths for the heat to dissipate (Ahn & Jung, 2017). Also, the soil can become saturated with a small amount of water, and thus the heat can spread more easily.

Chen (2008) investigated four different sand soil for thermal conductivity. And the soils have high quartz content. Figure 2.16 shows porosity versus thermal conductivity at different saturation, and the sands have different grain distribution: sample A to be a uniform medium sand, sample B to be a uniform coarse sand, sample C to be a uniform silty sand, and sample D to be a well-graded medium sand.

Wang et al. (2015) worked on MX-80 bentonite-sand mixtures. Figure 2.17 shows that thermal conductivity versus saturation and porosity at constant volume fraction of sand 30%. Figure 2.17 shows that as the porosity increases, the effective thermal conductivity decreases at any given saturation level. When the porosity is low (for example porosity = 5%), the bentonite matrix dominates thermal conductivity and water content has a weak effect on thermal conductivity. Whereas at high porosity values (for example porosity = 90%), the thermal conductivity is primarily influenced by the thermal conductivities of water and gas, with the lowest values determined by the thermal conductivity of gas when the water content decreases to zero.

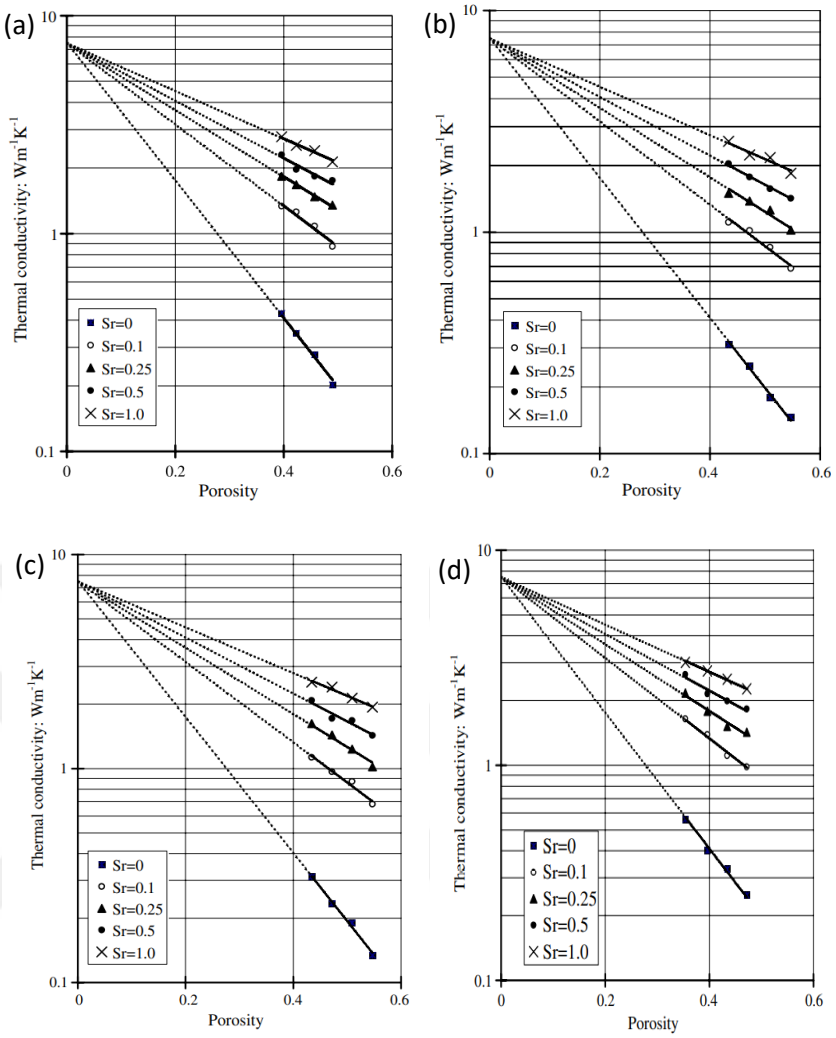


Figure 2.16 Thermal conductivity changes according to porosity (Chen, 2008) a) sample A b) sample B c) sample C d) sample D

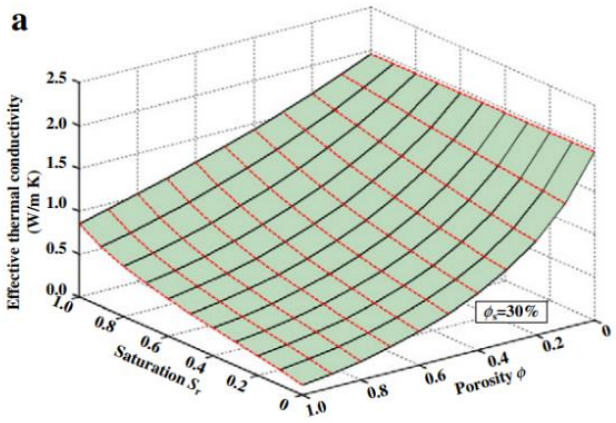


Figure 2.17 Thermal conductivity versus saturation and porosity at constant volume fraction of sand 30% (Wang et al., 2015)

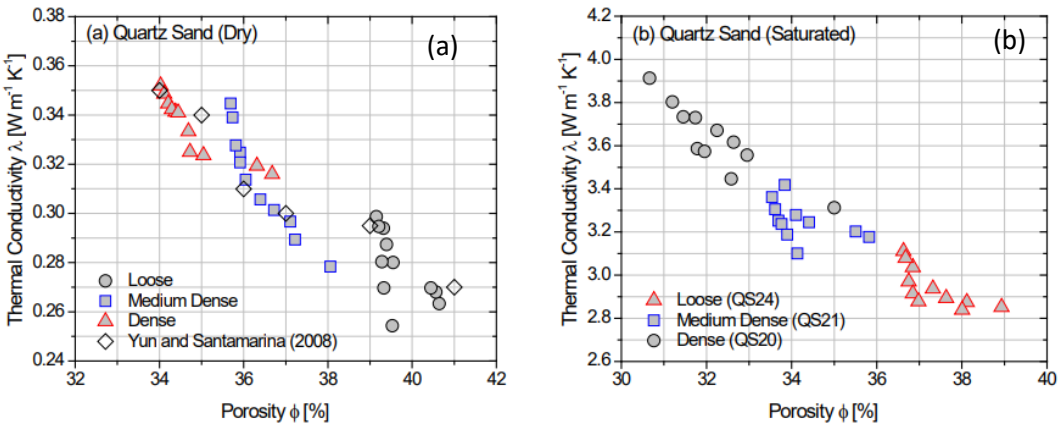


Figure 2.18 The variances in thermal conductivity with respect to porosity a) Dry quartz sand specimens; b) Saturated quartz sand specimens (Lee et al, 2016)

Lee et al. (2016) studied on quartz sands with different state. Soils in different compaction states are shown in Figure 2.18. When the soil is dense, which means lower porosity value, the thermal conductivity of the soil increases. Both dry and saturated quartz sands show the same trend.

Łydżba et al. (2014) investigated thermal conductivity and porosity and dry bulk density relationships for saturated and dry clayey soils. Thermal conductivity readings for soil samples in both saturated and dry stages exhibit a notable decline in relation to porosity. The slope of the drop is influenced by the nature of the medium that fills the soil's pores because the solid portion of the soil has a higher thermal conductivity value than water or air. However, the increase in porosity creates a noticeable downward trend.

2.3.4 Fine Content

Roshankhak et al. (2021) prepared sand-silt mixtures with different degrees of saturation, effective stress and fine content in their study. In Figure 2.19, it is seen that the effect of saturation on thermal conductivity is more than the effective stress and fine content. As seen in Figure 2.19b, the thermal conductivity continues to increase as long as the fines fill the voids. However, when the fine ratio exceeds 40%, the behavior and skeleton of the soil begin to be governed by the fines. With the increase

of fine grains, the resistance in heat transfer between grains becomes greater. The presence of more fine particles in the structure of the soil lengthens the path to be followed for the heat to be dissipated, which delays the dissipation of the heat.

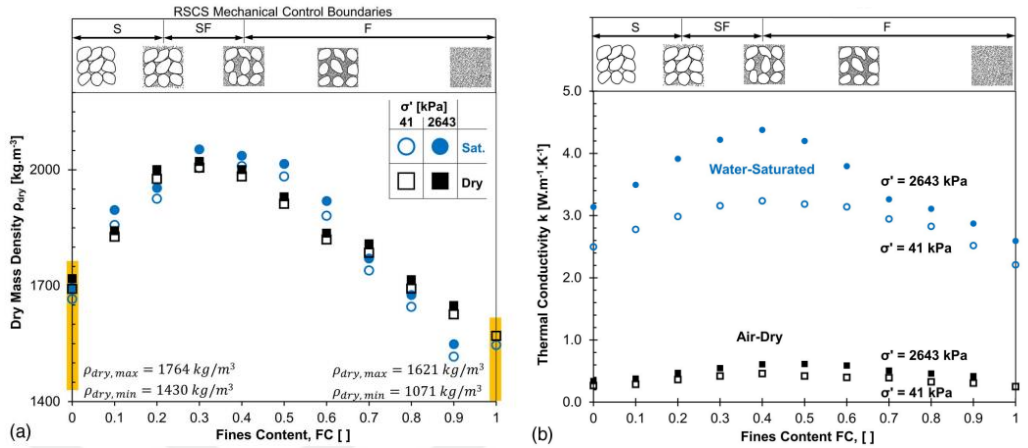


Figure 2.19 Pure quartzitic sand and silica flour (a) Dry mass density versus fine content; and (b) Thermal conductivity versus fine content (Roshankhah et al., 2021)

The increase in the fines ratio in the soil skeleton causes the formation of new heat flow paths due to the increase in the coordination number and packing density. The fine content, the relative grain sizes, and the individual packing densities of the coarse and fine components all affect the packing density in binary mixes. When fines are significantly smaller than the coarse percentage, the theoretical maximum packing density forms at fine content = 0.32 for simple cubic packing and fine content = 0.21 for tetrahedral packing. On the contrary, when soils solely contain fines (fine content 1) or coarse (fine content = 0), the minimum packing densities happen. In a manner similar to packing density, the mean coordination number changes with fine content and exhibits minima in both the pure coarse and pure fines situations, as well as a maximum soon after the fines have completely filled the pores of the coarse grains (Pinson et al., 1998). The revised soil categorization system's borders are represented in Figure 2.19a and Figure 2.19b, where the threshold fine contents represent transitions in the mechanical behavior of soil mixtures (Park & Santamarina 2017). For both the air-dry and saturated mixes, the density and thermal conductivity peaks are close to fine content 0.3-0.4. The heat flow through a few contacts in monosized soils are shown in Figure 2.20a. Also sands have better thermal conductivity and less total thermal contact resistance than silts. Also sands have better thermal conductivity

and less total thermal contact resistance than silts. Heat is transported through both fine and coarse grains in mixtures, as seen in Figure 2.20b.

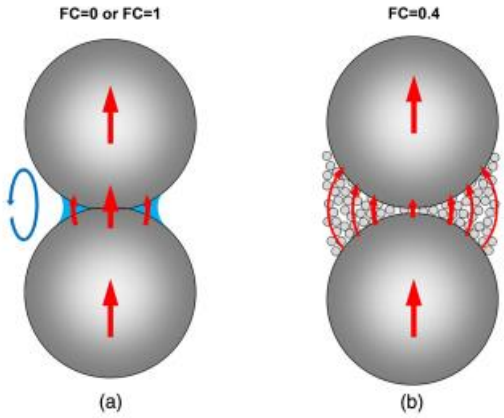


Figure 2.20 Heat transfer mechanism of grain-grain contact a) Monosized soils b) Fine and coarse grains in soils (Roshankhah et al., 2021)

Zhang et al. (2015) studied sand mixtures of different grain sizes. According to results, if coarse and fine sand are blended, there will be more physical contact surfaces and less thermal conductivity due to higher thermal resistance. However, in dry conditions, the thermal resistance at the grain-grain interface (i.e., the new physical contact locations) is lower than at the initial grain-air interface, which could lead to an improvement in the thermal conductivity of mixed sands. In other words, newly generated physical contact points offer some fresh pathways for heat to travel between sand grains, hence reducing thermal resistance and raising thermal conductivity.

The influence of particle size on the heat transfer process in dry sand is shown in Figure 2.21. Figure 2.21a displays the two horizontal heat transfer pathways between sand particles with just one point of physical contact in the direction of heat flow. Then, when particle size reduces and heat resistance would increase because the contact area at contact points is so small, the total number of physical contacts increases steadily. Figure 2.21b demonstrates that if one small particle is placed in the original pore, the number of horizontal heat flow pathways increases to four; two additional inclined heat flow paths going via this particle may also boost thermal conductivity as a whole. If the small particle is swapped out for four even smaller particles, it is expected that these four horizontal flow channels remain unaltered. But

because more physical contact sites are created in this process, more inclined flow routes are developed, and thermal conductivity should rise even further. As a result, the thermal conductivity of sands can be represented as either decreasing with decreasing particle size for homogenous sands or increasing due to the filling of fine particles in sand pores for nonuniform sands.

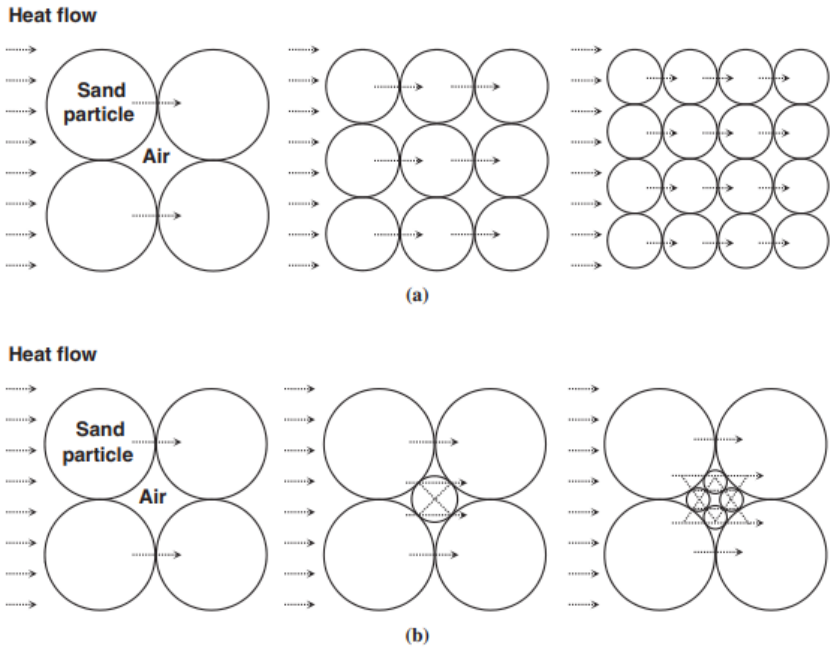


Figure 2.21 Effect of particle size on heat flow path in dry sand a) Pure and b) Mixed (Zhang et al., 2015)

Figure 2.22 shows the correlation between thermal conductivity and fines content for three mixed sands at various water content. The critical fines content (F_{cr}) increased as the mean ratio of fine sand grain size to coarse sand grain size (d_f /d_c) reduced. The highest thermal conductivity was at the same fine content for all water content and the optimum mixing ratio for the highest thermal conductivity is special for each mixed sand. When soils with different grain sizes are mixed (Figure 2.22a), the maximum thermal conductivity value is reached at a certain mixing ratio (Figure 2.22b and Figure 2.22c). When coarse and fine sands are mixed, some of the coarse sand's initial pores must be filled by fine sand particles, which may result in a slight reduction in the mixture's porosity. Additionally, when the environment becomes moister, more contact areas, water bridges, and heat transmission pathways through the sand particles are developed. As a result, the critical fines content, which is influenced by various

variables like grain shape and d_f/d_c, should be where the thermal conductivity of mixed sands should improve with fines content and reach its maximum value. For instance, at Figures 2.22b and Figure 2.23c, the mixing ratio that corresponded to the maximum thermal conductivity changed from 50% to 70%. To get the highest thermal conductivity, more fine sand is required to fill sand pores because ASTM graded sand has a higher fines content than Ottawa 20/30 sand. However, if the grain size distribution is uniform in the soil mixtures, the thermal conductivity change may not be affected by the fine grain ratio (Figure 2.22d). The fact that both sands are exceedingly fine and have a very high roundness of 0.9+ accounts for the remarkably similar measured thermal conductivity at Figure 2.22d.

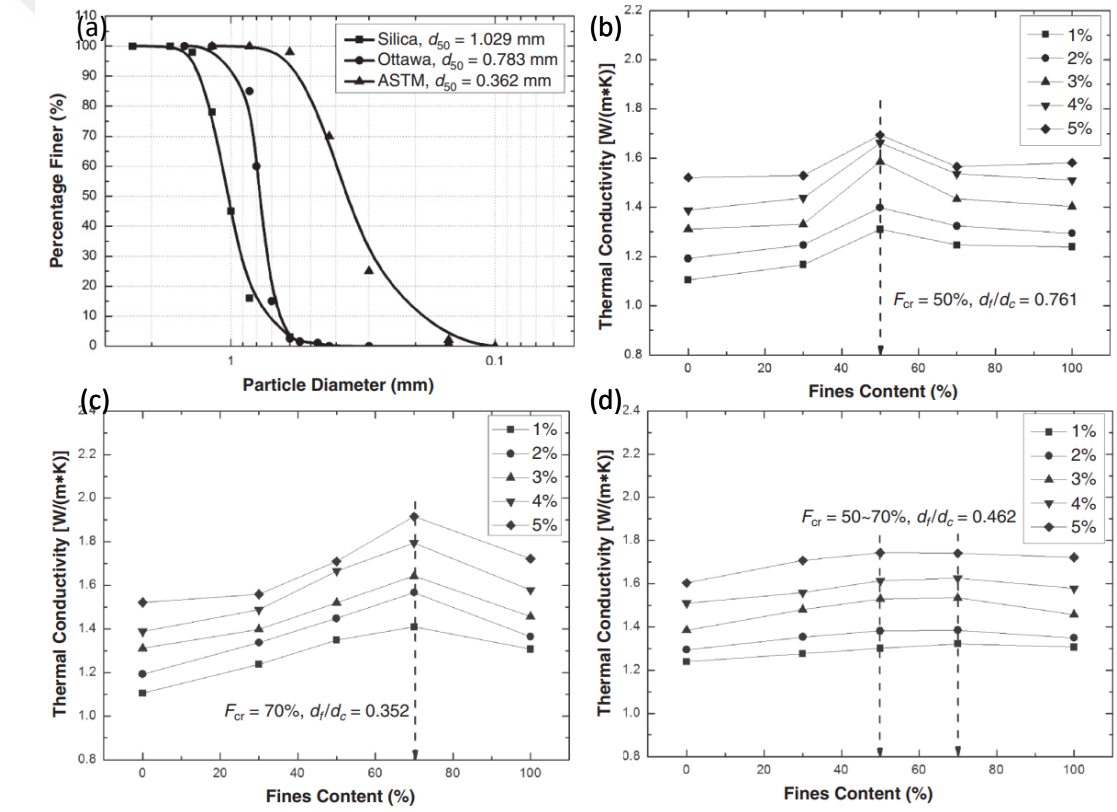


Figure 2.22 Experiment results of different sand mixtures (Zhang et al., 2015) a) Particle size distribution of quartz sands b) Silica 12/20–Ottawa 20/30 sand, c) Silica 12/20-ASTM graded sand, and d) Ottawa 20/30-ASTM graded sand

2.3.5 Mineralogy

The soil is formed by the coexistence of uncemented or weakly cemented minerals in a hollow structure, which is formed by the weathering of any type of rock. Clay minerals are formed by crystalline particles, usually in colloidal structure, by chemical weathering.

There are many types of soils that are formed by different rocks and changed by chemical effects. Soils are generally classified as rocks, gravel, sand, silt and clay. However, the minerals that make up the soil, the arrangement and proportions of the minerals are different. For example, while sands are generally composed of quartz minerals, clays are composed of montmorillonite, kaolinite, illite minerals. Thermal conductivity values of some minerals are given in Table 2.4.

Table 2.4 Thermal conductivity of some minerals

Mineral	k (W/mK)	Mineral	K (W/mK)
Quartz[1]	7.7	Dolostone[2]	3.8
Illite[1]	1.85	Gabbro[2]	2.2
Smectite[1]	1.88	Gneiss[2]	2.6
Anorthosite[2]	1.8	Granite[2]	2.5
Basalt[2]	1.7	Feldispar[1,2]	2.3
Diabase[2]	2.3	Limestone[2]	2.5
Marble[2]	3.2	Sandstone[2]	3
Schist[2]	1.5	Shale[2]	2
Syenite[2]	2	Trap rock[2]	2
Kaolinite[1,2]	2.6	Calcite[1,2]	3.5
Salt rock[2]	5.6	Dolomite[1,2]	5
Chlorite[1]	3.26	Amphibole[1]	2.81
Albite[1]	2.14	Geothite[1]	2.91
Hematite[1]	12.42		

[1] Song, X., Fan, H., Liu, J., & Yang, X. (2020) [2] Tarnawski, V. R., & Leong, W. H. (2016)

Lee et al. (2021) examined Ca-bnetonite and Na-bentonite in terms of thermal conductivity. According to the results, Ca-bentonite has better thermal conductivity than Na bentonite. The reason for this is explained by the fact that the thermal conductivity value of the pore water is higher with the ion exchanges in the diffuse double layers. When we look at the mineralogical structures, it is seen that FEBEX bentonite has the highest thermal conductivity value although it contains montmorillonite at a high rate. Although GMZ07 bentonite contains the highest

amount of quartz and cristobalite, its thermal conductivity value was lower than FEBEX bentonite. Lee et al. (2021) explained this situation with the hardness of the minerals and how they came into contact. Due to the exceedingly soft phyllosilicate minerals found in montmorillonite and the somewhat less hard tectosilicate minerals found in feldspars, the particles of these minerals may be in close proximity to one another, resulting in better heat conduction. Contrarily, the contact between quartz particles, which are hard crystalline silicon dioxide minerals, and cristobalite, that is also a hard mineral polymorph of silicon dioxide, may form more loosely, leading to poor heat conduction. As a result, compared to quartz and cristobalite, montmorillonite and feldspars significantly contribute more to the overall thermal conductivity of bentonite. The mineral structure of the investigated bentonites is shown in Table 2.5.

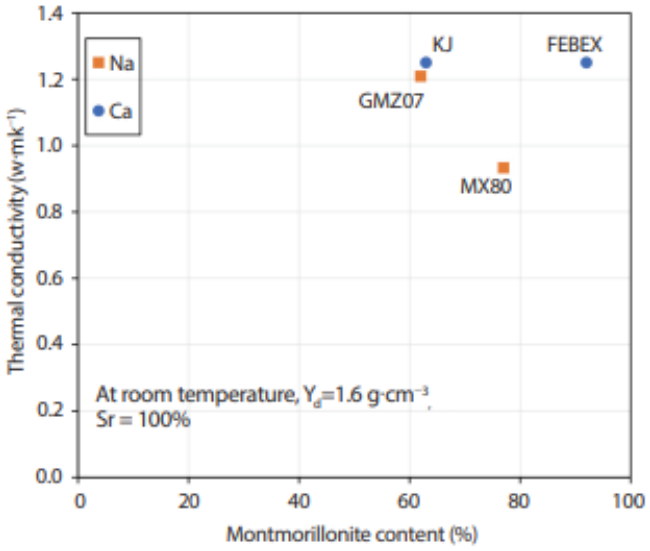


Figure 2.23 Thermal conductivity with montmorillonite content (Lee et al., 2021)

Table 2.5 Composition of bentonite (Lee et al., 2021)

Mineral	Composition (%)			
	GMZ07 (Na^+) (Xu et al. 2019)	MX80 (Na^+) (Xu et al. 2019)	KJ (Ca^{+2}) (Yoon et al. 2018)	FEBEX (Ca^{+2}) (Villar, 2004)
Montmorillonite	62	77	63	92
Quartz	10	7	4.9	2
Cristobalite	6	5	3	2 (Cristobalite
Feldspar	11	6	25.6	+Feldspar)

Barry-Macaulay et al. (2013) worked on the soils which have a significant amount of quartz. Quartz content in fine-grained soils is lower than in coarse-grained soils. However, silt or clay-sized particles formed the majority of the quartz in the fine grain soils. For all types of soil with the same density of approximately 1600 kg/m^3 and the same water content of roughly 20%, the change of thermal conductivity versus quartz content is shown in Figure 2.24. It should be noted that soils with more quartz have higher thermal conductivities. Because of their low quartz content, fine grain soils (RS, BC, FBS, and CIS) had much lower thermal conductivities than coarse grain soils (BGS and BGCS).

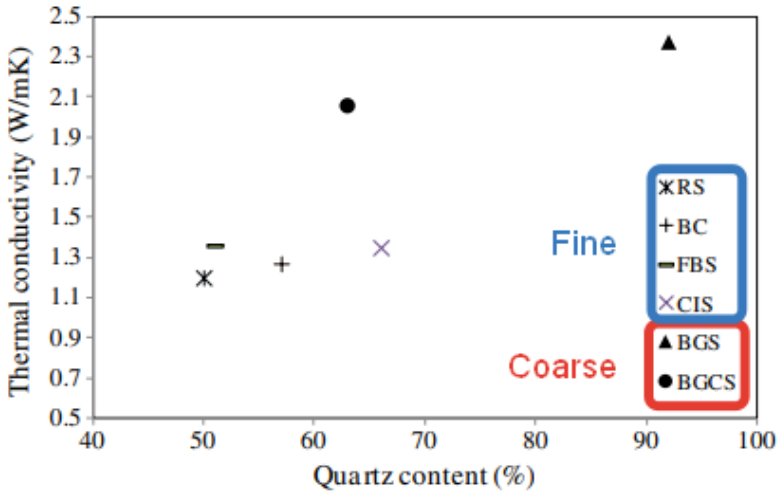


Figure 2.24 Thermal Conductivity variation with quartz content for soils (Barry-Macaulay et al. 2013)

Lydzba et al. (2014) argued that the mineral composition did not have a significant effect in their study on soils taken from various depths. Although the soil particles are composed of minerals, the mineral structure may not have a significant effect on the thermal conductivity due to the structure of the soil, the arrangement of the minerals, the porous structure of the soil, etc. However, it is said that the main reasons for the thermal conductivity value of sands being higher than silt and clays are the higher amount of quartz mineral in the sands and the difference in grain sizes.

2.3.6 Temperature

The effect of temperature on thermal conductivity has been mentioned by many researchers. It is known that the seasonal temperature differences of the regions and the change of water content (Li et al., 2019) affect the heat conduction of the soils.

Especially at negative degrees and high positive temperatures (60 ℃ to 100 ℃), this effect is more (Xu et al., 2020; Xu et al., 2019; Lu et al., 2020; Hiraiwa & Kasubuchi, 2000).

At negative temperatures, water turns into ice. Xu et al. (2020) studied the thermal conductivity behavior of Genhe silty clay at negative degrees. It has been said that since the thermal conductivity of ice (2.21–2.326 W/(mK)) is higher than the thermal conductivity of water (0.56–0.6 W/(mK)) (Xu et al., 2001; Sharqawy, 2013), there is an increase in thermal conductivity, and it also increases the thermal conductivity value since ice formation will increase the contact surface between the particles. The increase in negative temperatures increases exponentially because the conversion of water to ice occurs rapidly at first, reaching its maximum value. Figure 2.25 shows the thermal conductivity change at negative temperatures and Figure 2.25a shows the points on the compaction curve.

At positive temperatures, it is seen that the temperature does not have a significant effect up to 60 ℃, and after 60 ℃, significant increases in thermal conductivity occur (Campbell et al., 1994; Xu et al., 2019; Lu et al., 2020; Hiraiwa & Kasubuchi, 2000). However, it has been observed in Ogacho et al. (2003) and Yoon et al. (2018) studies that it can have a negative effect on thermal conductivity at temperatures higher than 100 ℃. At temperatures higher than 100 ℃, a decrease in thermal conductivity is expected as the water in the soil voids will evaporate (Yoon et al., 2018). Also, Ogacho et al. (2003) stated that there may be an increase in thermal conductivity at temperatures of 500 – 600 ℃, as radial heat transfer will be more effective than conduction heat transfer. Figure 2.26 shows the variation of thermal conductivity at very high temperatures.

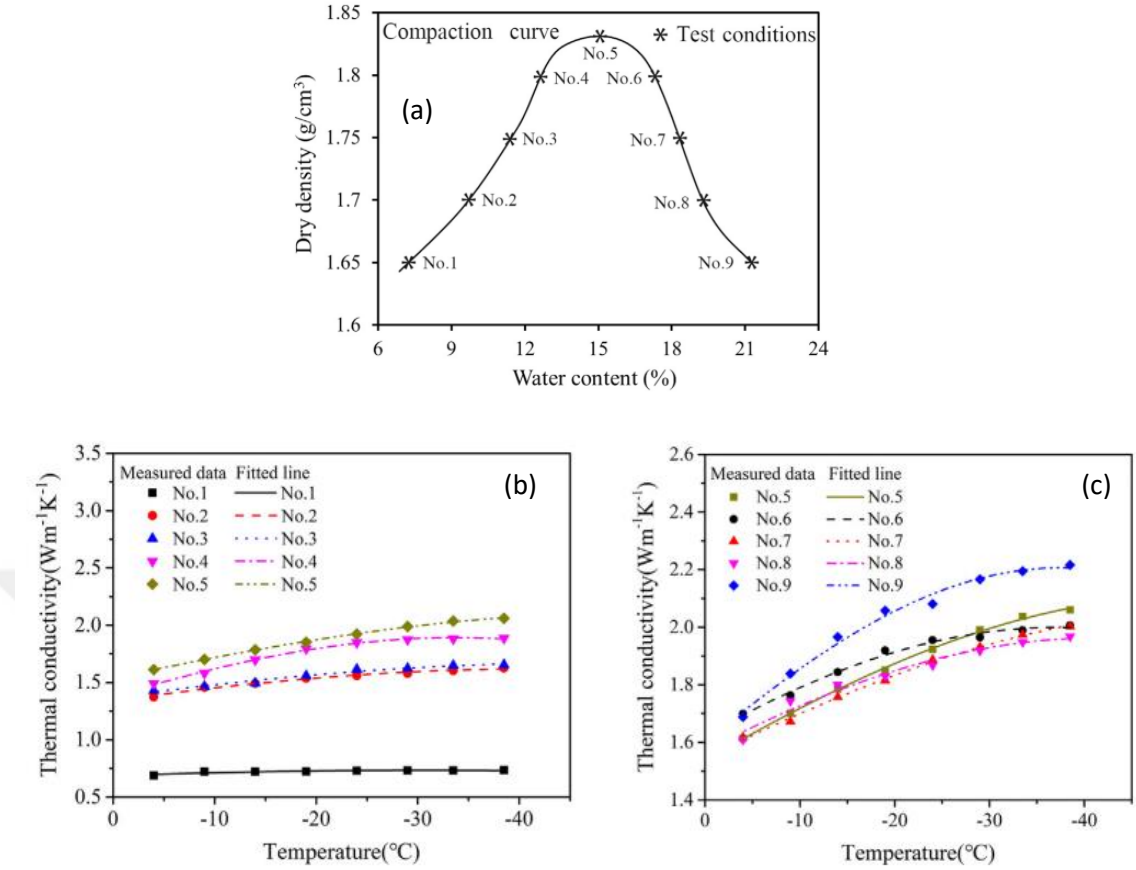


Figure 2.25 Temperature effect on the thermal conductivity (Xu et al., 2020) a) Compaction curve of Genhe silty clay b) Negative temperature effect at dry side of compaction curve c) Negative temperature effect at wet side of compaction curve

Although the thermal conductivity effect of temperature is important, it should be evaluated together with the structure, content, and saturation of the soil (Xu et al. 2019). It has been seen in the studies of the researchers Campbell et al. (1994), Xu et al. (2019), Lu et al. (2020), Hiraiwa and Kasubuchi (2000) that the effect of temperature is low at low and high saturation degrees, and the effect of temperature is more at medium saturation degrees. Due to the absence of water at low saturation degrees or the small amount of water, heat conduction takes place from the contact surface of the grains. As the temperature increases, the grains expand and the contact surfaces increase, which causes an increase in the thermal conductivity value, but this increase is generally negligible. (Xu et al., 2020; Yoon et al., 2018).

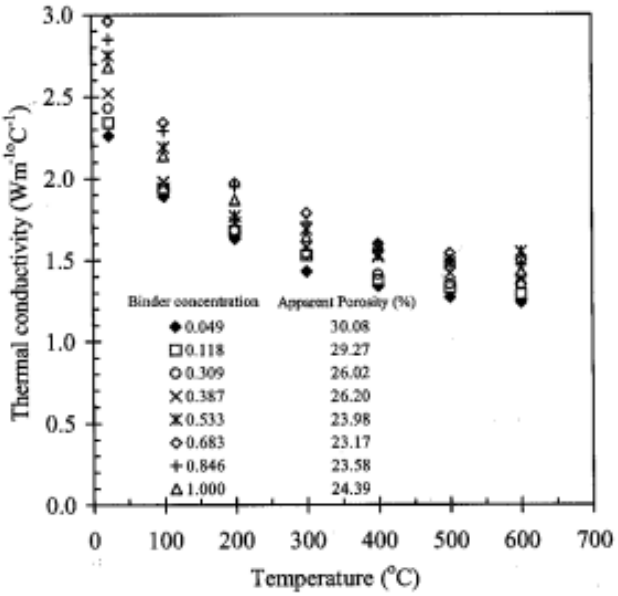


Figure 2.26 The variation of thermal conductivity with temperature (Ogacho et al., 2003)

At medium saturation degrees, there is water and air between the soil particles. With the increase in temperature, the latent heat transfer mechanism takes place (Xu et al., 2019; Campbell et al., 1994; Lu et al. 2020; Hiraiwa & Kasubuchi, 2000). Since the thermal conductivity value of water vapor is higher than the thermal conductivity value of air, with the increase in temperature, the voids are filled with water vapor and an increase in thermal conductivity occurs. At the same time, with the increase in temperature, the thermal conductivity value of water will increase, the volume of water and particles will expand and the contact surfaces will increase, which will increase the thermal conductivity (Xu et al., 2020).

At high saturation degrees, the thermal conductivity value will increase with the increase in temperature, but this increase will be lower than the soil at medium saturation degrees (Xu et al. 2019; Campbell et al. 1994; Lu et al. 2020; Hiraiwa & Kasubuchi, 2000). Because most of the void volume will be filled with water and the volume occupied by the water vapor will be significantly reduced. Excess water volume will significantly suppress the effect of water vapor (Xu et al., 2019).

Xu et al. (2019), Campbell et al. (1994), Lu et al. (2020), and Hiraiwa and Kasubuchi (200) have studied on different soils and explained the behavior of thermal conductivity under the influence of temperature in similar ways. The studies of

Hiraiwas and Kasubuchi (2000) on Ando soil (Clay loam) and Red Yellow soil (Light Clay) are shown in Figure 2.27.

Boukelia et al. (2019) in their research at high temperatures and on the compaction curve, stated that while the thermal conductivity and thermal diffusivity values increased rapidly on the dry side of the proctor curve (due to water vapor movements), the volumetric heat capacity did not change significantly.

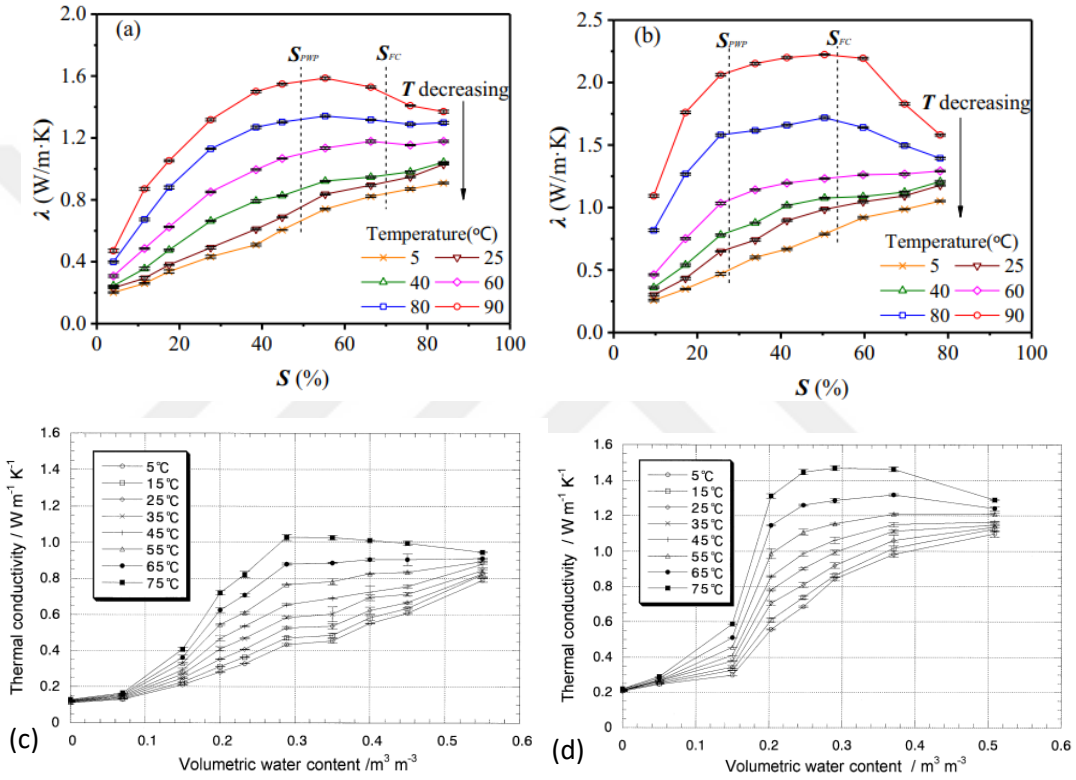


Figure 2.27 Change in thermal conductivity for each temperature with saturation for lateritic clays (Xu et al., 2019): (a) Guilin lateritic clay; (b) Liuzhou lateritic clay, changes in thermal conductivity for each temperature with volumetric water content (Hiraiwas & Kasubuchi, 2000) (c) Ando soil (Clay loam) (d) Red Yellow soil (Light Clay)

2.3.7 Other Parameters

2.3.7.1 Effect of Salts

Sharqawy (2013) measured the thermal conductivity values of water and seawater at different temperatures and different salt solution. The uncertainty bars of these measurements are shown in Figure 2.28, and they reveal a maximum level of certainty

that is not greater than 2.4%. This graph shows that the thermal conductivity significantly increases with temperature and slightly decreases with salinity.

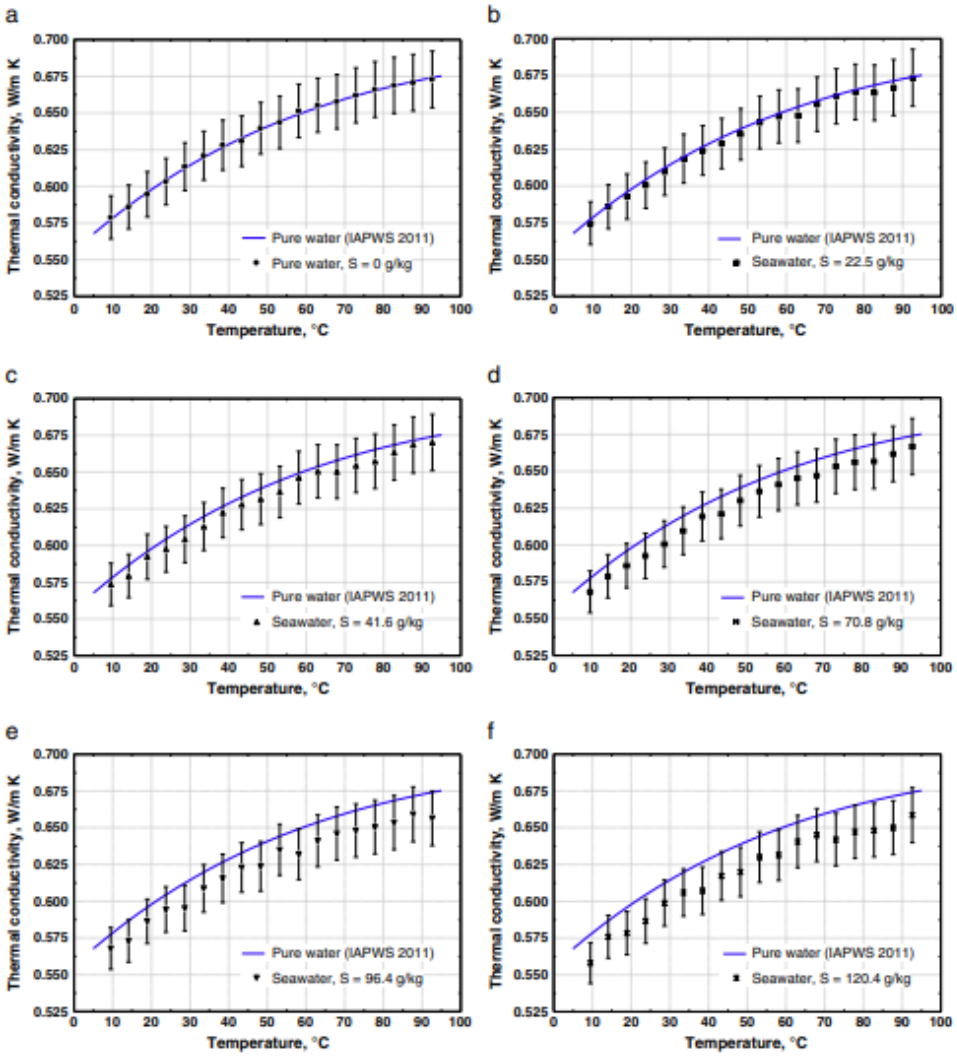


Figure 2.28 Thermal conductivity measurements at different temperature and salinity (Sharqawy, 2013)

Lyu et al. (2020) studied the effect of NaCl solutions on the thermal conductivity of clay at different temperatures. Figure 2.29 shows the relationship between the salt concentration in the electrolyte solution and the thermal conductivity of clay soils.

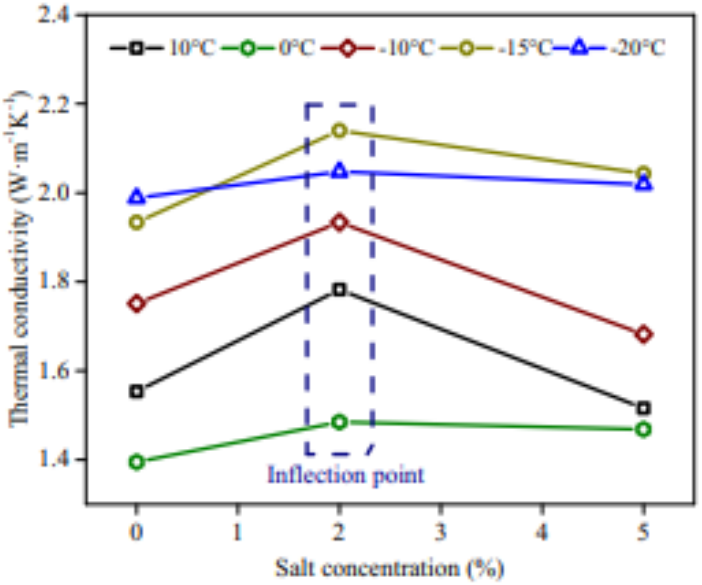


Figure 2.29 Variations in thermal conductivity with salt concentration with 22% water content (Lyu et al., 2020)

Figure 2.30a shows the diffuse double layer between the clay particles. Na^+ is adsorbed on the surface of clay particles when salt concentration rises, balancing the negative potential of soil particles. As a result, the concentration of electrolyte in the solution would rise, compressing the electrical double layer as shown in Figure 2.30b (Van Olphen, 1977). The soil particles become more electrically attracted to one another, increasing the amount of contact between their surfaces. As a result, larger salt concentrations lead to a higher thermal conductivity. In Figure 2.30c, flocculation between clay particles occurs when the salinity is raised to 5% (Palomino & Santamarina, 2005). As a result, voids between soil particles are increased. Thus, free water separates soil particles, and the forces that hold soil particles together weaken. (Sun & Lü, 2019).

As the salt concentration increases, the freezing point of water decreases. As the salt concentration increases at negative temperature, the thermal conductivity will decrease because the thermal conductivity value of ice is higher than that of water.

In general, water has a higher thermal conductivity than a solution of NaCl (Mogomedov, 1998; Sharqawy, 2013). However, because of the higher salt content, the electrical double layer is thinner. As a result, higher salt concentration causes an increase in thermal conductivity followed by a reduction.

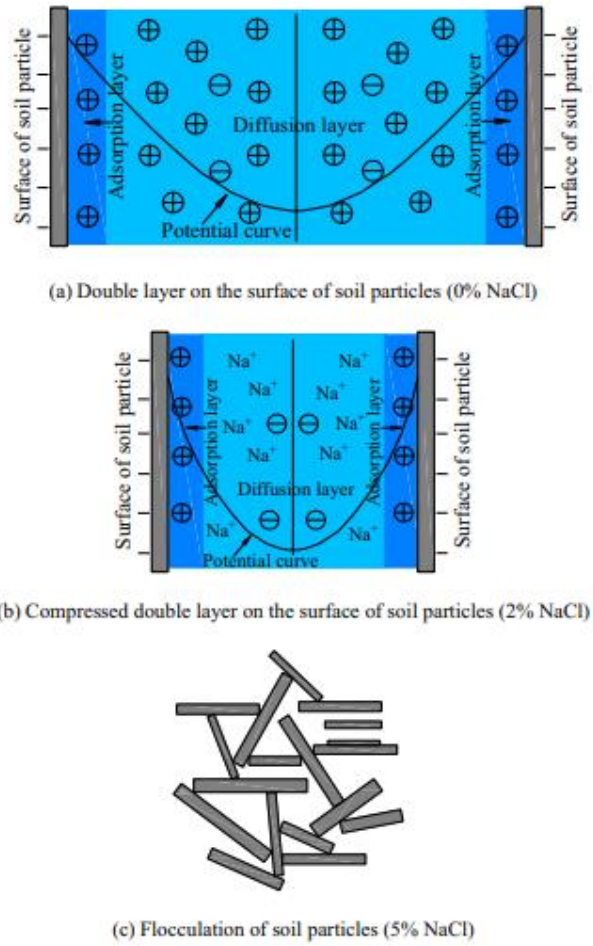


Figure 2.30 Structure diagram of soil particles in different NaCl concentrations (Lyu et al., 2020) a) Soil samples with no NaCl, b) Soil samples with 2% NaCl, c) Soil samples with 5% NaCl

Yan et al. (2021) investigated the variation of thermal properties of silty clay in different water content and salt solutions. The samples were prepared in 1.7 g/cm^3 dry unit weight, water content increasing from 8% to 18%, pure and salt ratios of 2-4-6 %. The correlations between soil thermal conductivity, thermal diffusivity, and a specific heat under distilled water and various salt solutions are shown in Figure 2.31. Generally, the thermal conductivity rises with water content for a given salt concentration. The thermal conductivity gradually drops when the water content of the soil surpasses the plastic limit (16.10%). Thermal diffusivity and specific heat both exhibit this shift in trend, which happens when the water content is getting close to the plastic limit. The thermal diffusivity of soil fluctuates at about 0.625 mm^2/s as water content rises from 8 to 16%. When the water content reaches the plastic limit, the soil's

thermal diffusivity value drops quickly at all four salt contents, and the more salt present, the more noticeably the thermal diffusivity value is affected. The specific heat of the soil increases slowly until a water content close to the plastic limit. Th all samples in this process displayed comparable trends in specific heat with increases in water content. The four soils' specific heat increased quickly, though to various degrees, as the water content went beyond the plastic limit, being ranked 6%>4%>2%>0% for soil, respectively.

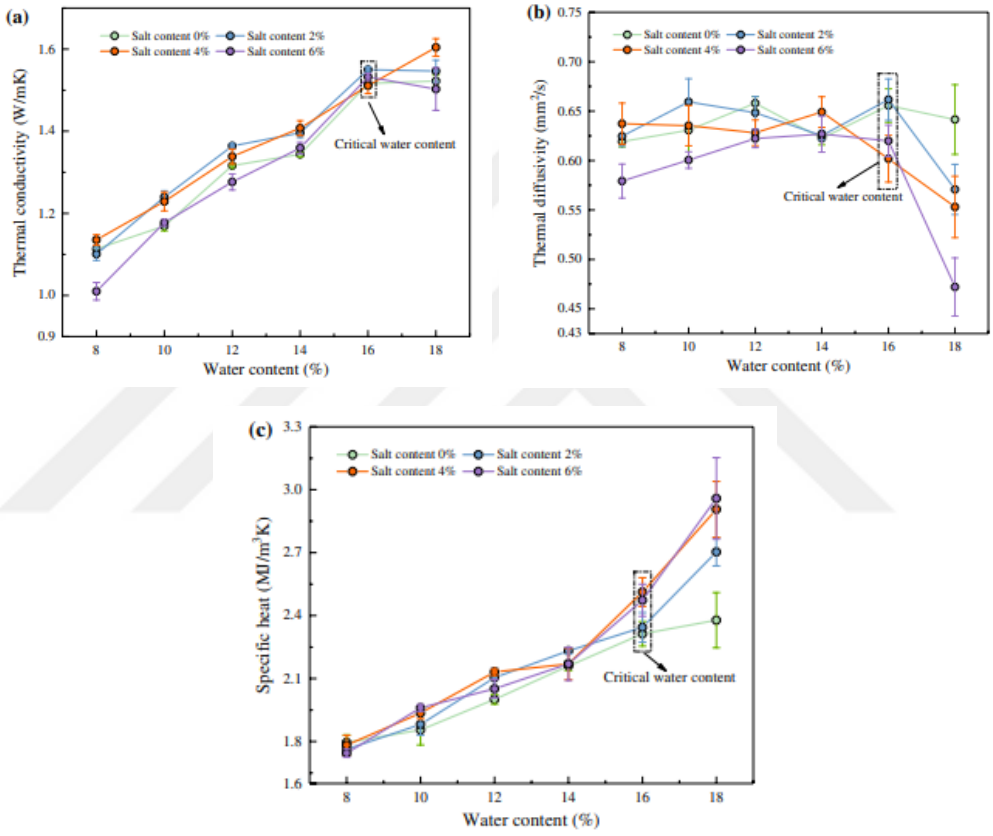


Figure 2.31 Test results that relationships between water content and a) Thermal conductivity, b) Thermal diffusivity and c) Specific heat (Yan et al., 2021)

Abu-Hemdah and Reeder (2000) measured the thermal conductivity change of sand using NaCl and $CaCl_2$ solutions. It was determined that the thermal conductivity of the sand decreases as the salt concentration increases.

2.3.7.2 Coefficient of Uniformity

Xiao et al. (2018) studied the grain distribution of carbonate sands. They have prepared samples at three different void ratios and uniformity coefficients ranging from 2 to 20. It is seen in Figure 2.32 that as the void ratio increases, the thermal conductivity decreases. It was observed that as the c_u value increased, the thermal conductivity value increased. As the c_u value increased, fine particles filled between the coarse grains of the soil, reducing the void ratio and increasing the grain-grain contact surfaces, which led to an increase in thermal conductivity.

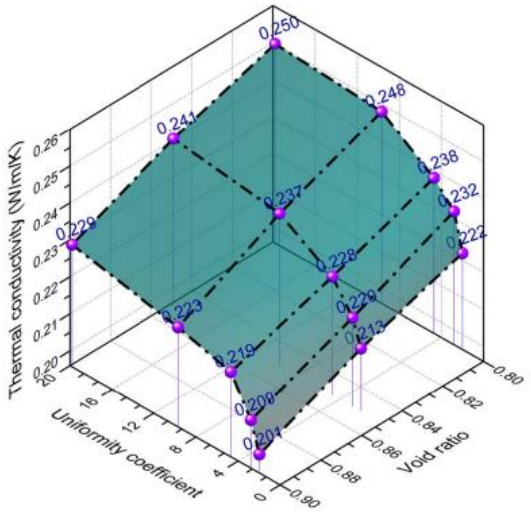


Figure 2.32 Variations of thermal conductivity of carbonate sands with the uniformity coefficient and void ratio (Xiao et al., 2018)

2.3.7.3 Specific Surface Area

Làyzdba et al. (2014) observed that the thermal conductivity value decreases with the increase of the specific surface area in soils with high clay and silt content (Figure 2.33). Xu et al. (2019) found similar findings with their studies on clays. As the specific surface area will increase with the increase of the clay content, the water absorption capacity of the soil will increase. So soils will need more water to fill the voids. Also, since the particle size will be small, more particles will have to fill the voids, thus heat flow resistance will be greater.

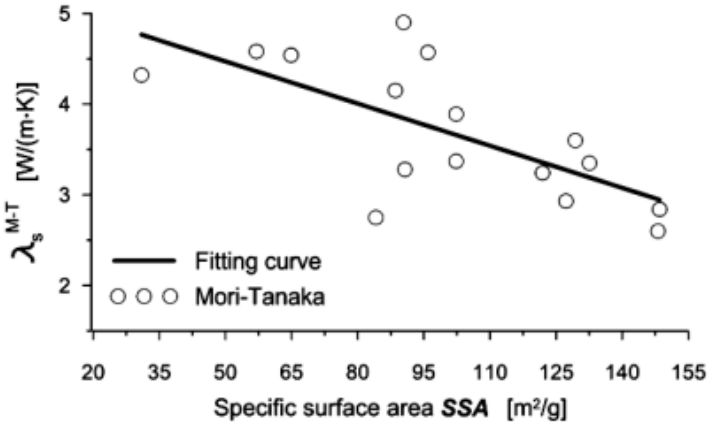


Figure 2.33 Relation between specific surface area and the thermal conductivity of solids (Làyzdba et al., 2014)

2.4 Boron Minerals, Ferrochrome and Copper Slags and Fiber Glass

2.4.1 Boron Minerals

Boron is the element with atomic number 5, symbolized by B. Boron is found in nature as B10 and B11 isotopes (Etimaden, 2023). The 10B isotope shows very high thermal neutron retention. Thus, it can be used in nuclear materials and nuclear power plants (Tenmak, 2023). It is found in nature in the form of compounds with metal and nonmetal elements. Since it is not found in pure form in nature, it can be used in many different industries. Boron behaves like non-metal compounds in its compounds (Tenmak, 2023). Pure boron, on the other hand, is an electrical conductor like carbon (Tenmak, 2023). Crystallized boron is similar to diamond in appearance and optical properties and is almost as hard as diamond.

Boron is found in nature as boron oxides in different proportions and in different compounds. There are more than 230 boron minerals in nature. Tinkal, colemanite and ulexite are the main boron minerals mined in Türkiye.

Boron processed by Eti Maden in Türkiye is enriched with various mining methods and converted into concentrated boron products. These products are used in various fields such as glass, ceramics, agriculture, construction, nuclear power plant, cleaning and insulation (Etimaden, 2023).

Colemanite ($2CaO.3B_2O_3.5H_2O$) is the most common boron compound that crystallizes in the monoclinic system (Etimaden, 2023). According to Mohs hardness classification, its hardness is 4-4.5 and its specific gravity is 2.42 gr/cm^3 (Yigitbasoglu, 2004). It is found as large, shiny, transparent crystals in ore spaces in clays. Pure Colemanite dissolves slowly in water and quickly in HCl (Yigitbasoglu, 2004). It is found in Emet, Bigadiç and Kestelek in Türkiye and is also found in the USA. Colemanite crystals taken from different regions of Türkiye are shown in Figure 2.34.



Figure 2.34 Some colemanite crystals from different provinces of Türkiye (Arslan & Drelich, 2022)

Etibor48 ($Na_2B_4O_7.5H_2O$) was obtained from Tincal ($Na_2B_4O_7.10H_2O$) by Eti Maden studies (Etimaden, 2023). Etibor48 is very rich in tincal. Tinkal stands out in the fact that glasses are resistant to physical impacts, while etibor48 is used alone or as a compound fertilizer. Tincal is usually transparent and colorless, but can be found in pink, yellow and gray colors due to various impurities. Its hardness is 2-2.5 Mohs, its specific gravity is 1.7 gr/ cm^3 (Yigitbasoglu, 2004). Tincal could turn into tincalconite as decomposing quickly and losing its water (Etimaden, 2023). It is found together with ulexite and intercalated tincalconite with clay (Yigitbasoglu, 2004). It is located in Eskişehir-Kırka deposit in Türkiye.

Ulexite ($Na_2O.2CaO.5B_2O_3.16H_2O$) is rich in minerals. It plays an important role in the glass, ceramics, heat and sound insulation and fertilizer industries (Etimaden, 2023). Ulexite; It takes place in nature with its massive, cauliflower, fiber, cone, rosette, cotton ball and stick appearance (Etimaden, 2023). According to Mohs hardness classification, its hardness is 2.5 and its specific gravity is 1.95-2 gr/cm^3 (Yigitbasoglu, 2004). Ulexite, which is found at three different levels in boron deposits in Kütahya/Emet, is associated with colemanite and hydroboracite in these deposits. In Kırka, it is found in borate deposits together with borax, colemanite and inionite. The ulexite mineral is also found in Argentina.

The countries where boron minerals are found and their chemical formulas are shown in Table 2.6. It is used in the construction and cement industry for strength enhancing and is used in insulation industry for isolation purposes. Insulation materials containing boron and boron products, which make the structures more durable and heat resistant, are used in the construction of light and low-cost products (Etimaden, 2023).

Table 2.6 The content of boron minerals and the countries where they are found (Kavak & Kaya, 2022)

Minerals	Chemical Formula	% B_2O_3	Province
Sassolite (natural boric acid)	H_3BO_3	56.4	Volcanic waters in Italy
Tincal (Borax)	$Na_2B_4O_7.10H_2O$	36.5	Türkiye, USA, South America
Kernite	$Na_2B_4O_7.4H_2O$	51.0	USA, South America
Colemanite	$Ca_2B_6O_{11}.5H_2O$	50.8	Türkiye, USA, South America
Ulexite	$NaCaB_5O_9.8H_2O$	43.0	Türkiye, USA, South America
Probertite	$NaCaB_5O_9.5H_2O$	49.6	USA, Türkiye
Inyoite	$Ca_2B_6O_{11}.13H_2O$	37.6	USA, Türkiye
Hydroboracite	$CaMgB_6O_{11}.6H_2O$	50.5	Russia
Boracite	$Mg_3B_7O_{13}Cl$	62.2	By-product in potash deposits
Szaibelyite	$MgBO_7(OH)$	41.4	Kazakhistan, China
Datolite	$Ca_2B_2Si_2O_9.H_2O$	26.7	Kazakhistan, Russia

In nuclear applications; In atomic reactors, boron steels, boron carbides and titanium boron alloys are used extensively. Boron steel, which is highly resistant to corrosion, is preferred as a neutron absorber. Approximately each boron atom absorbs one neutron (Yigitbasoglu, 2004). Boron and boron products are also used in the control systems of atomic reactors, in cooling pools and in closing the reactor with alarm (Etimaden, 2023). In addition, colemanite is used in the storage of nuclear waste.

2.4.2 Ferrochrome Slag and Copper Slag

With the increase of industrialization, large amounts of industrial waste and by-products have emerged (Mahamaya & Das, 2020). Failure to properly store and use these wastes can lead to pollution of natural resources (Al-Jabri, 2018; Mahamaya & Das, 2020). In the last 2 decades, the use of wastes such as copper slag, steel slag, ferrochrome slag, fly ash, spent catalyst etc. has been investigated in terms of sustainability and cost efficiency (Al-Jabri, 2018; Patel et al., 2012).

Ferrochrome is used to increase the physical properties of steel (for example; corrosion, oxidation and to improve hardness, tensile strength at high temperatures,

wear and abrasion resistance) (Yılmaz & Sütaş, 2008; Sangamitra & Reddy, 2017). Ferrochrome slag is the waste material obtained as a result of ferrochrome production.

During ferrochrome production, non-reducing oxides and some SiO_2 form a liquid slag layer on the metal surface (Yılmaz & Sütaş, 2008). The structure and properties of the slag change according to the cooling method. When cooled slowly in air, it usually has stable and dense crystalline structure and is formed large sizes (8 to 20 mm), as shown in Figure 2.35b (Yılmaz & Sütaş, 2008; Fares et al., 2021; Al-Jabri, 2018). Slags cooled slowly in air generally have high mechanical properties and can be used instead of aggregates (Yılmaz, 2008; Islam et al., 2021). If the slag is cooled rapidly, it will have a metastable glassy crystal structure in smaller sizes (5 mm), as shown in Figure 2.35a (Yılmaz & Sütaş ,2008; Fares et al., 2021). Rapidly cooled slags can be used in cement and concrete production (Yılmaz & Sütaş, 2008).



Figure 2.35 Ferrochrome (Fares, et al., 2021) a) Fine aggregate b) Coarse aggregate

About 1.1 to 1.6 tons of ferrochrome slag are produced for every ton of ferrochromium alloy (Al-Jabri, 2018; Islam et al., 2021). Ferrochrome has a more irregular and rougher surface than aggregates (Fares et al., 2021; Islam et al., 2021). Also, ferrochrome slag has higher fire resistance than aggregate (Islam et al., 2021). Compared to aggregate, Ferrochrome slag has a comparatively higher specific gravity. Ferrochrome slag has a specific gravity between 2.63 to 3.22 (Islam et al., 2021). Because Ferrochrome slag contains various metals, including iron and magnesium, it has a relatively high specific gravity (Al-Jabri 2018, Islam 2021). Ferrochrome slag contains high amounts of metal oxides (SiO_2, Al_2O_3, FeO/ Fe_2O_3 Cr_2O_3, MgO, CaO, Cr_2O_3) (Lind et al., 2001; Sangamitra & Reddy, 2017; Mahamaya & Das, 2020).

In the leaching tests of Lin et al. (2001) and Yılmaz and Yıldız (2015), it was revealed that many elements remained below the limit values. However, it has been suggested that since some exceeding values will not reflect the field conditions, it will be on the reliable side in field conditions.

Copper is a soft and ductile metal and has high thermal and electrical conductivity. It is widely utilized in the transportation, construction, and electrical industries. Pure copper is not usually found in nature, but it is generally united with other elements in the form of copper ores. Depending on the type of ore and the desired level of purity in the finished product, different extraction techniques are used to extract copper from copper ore. Each procedure entails a number of phases where waste materials are either physically or chemically eliminated and the concentration of copper is gradually raised (Yadav et al., 2018; Chandrshekhar et al., 2015; Lavanya et al., 2011).

Copper slag is the waste material produced by the melting of copper. Depending on the kind of ore and the degree of purity of the finished product, different extraction techniques are used for copper slag. Yadav et al. (2018) and Patel et al. (2012) have summarized the formation of copper slag. To get the proper concentration of slag, the undesirable materials are physically or chemically removed. In a blast furnace, copper ore, coke powder, and sand are combined and heated to high temperature. Steel plates with fire clay bricks within make up the furnace. The furnace's tuyerenearthe base is where hot air is first injected. At the base of the furnace, hot air at a temperature of 800°C is introduced, creating two molten separated layers. The copper slag is in the upper layer. Based on the amount of copper it contains, there are primarily two types of copper slag. Copper slag that includes more than 1% copper is processed again for the purpose of producing copper. Copper slag that contains less than 1% copper is cooled and disposed of as waste.

About two to three tonnes of copper are produced from one ton of copper (Yadav et al., 2018; Chandrshekhar et al., 2015; Patel et al., 2012). Because copper slag contains significant amounts of Fe_2O_3, SiO_2, CaO, and other compounds, it can be chemically stabilized (Havanagi et al., 1989). Also, production of copper slag does not produce any hazardous gases (Patel et al., 2012). Copper slag is a type of industrial

waste that has a marketable value and can be used to enhance the engineering properties of soil, including its strength, workability, texture, and plasticity (Yadav et al., 2018).

Past studies have proven that copper and ferrochrome slags are suitable for use in road construction (Tandel & Patel, 2009). These slags are used in sub-grade, sub-base, and bitumen mixes and are also suitable for use in soil improvement and fillings embankment construction, land reclamation (Tandel & Patel, 2009; Lavanya et al., 2011; Patel et al., 2012; Chandrshekhar et al., 2015; Dhanesh et al., 2019; Havanagi et al., 2007; Sanghamitra & Reddy, 2017; Yılmaz & Karaşahin, 2010; Al-Jabri, 2018; Vapur et al., 2013) Moreover, it could be used in-stead of sand used in backfill for retaining walls and shallow foundations as a construction material (Tandel & Patel, 2009; Lavanya et al., 2011; Chandrshekhar et al., 2015). The grain size of the slag used by the researchers generally corresponds to aggregate or sand (Tandel & Patel, 2009; Lavanya et al., 2011; Patel et al., 2012; Chandrshekhar et al., 2015; Havanagi et al., 2007; Sanghamitra & Reddy, 2017; Vapur et al., 2013). Ferrochrome slag could be used in stone columns due to its high strength, hardness, and resistance to abrasion (Sanghamitra & Reddy, 2017). Copper slag could be used in place of sand in sand piles and sand drains, also it could obtain good results when mixing with expanding soils (Tandel & Patel, 2009). Copper slag increases the bearing capacity and stability due to angularity and high internal friction angle, it is also frost resistant and has high permeability (Chandrshekhar et al., 2015; Havanagi et al., 2007; Vapur et al., 2013). Ferrochrome slag is also known to be resistant to freezing (Yılmaz & Karaşahin, 2010).

2.4.3 Fiber Glass

The use of fibers in the construction industry has started to broaden as sustainability has taken center stage nowadays. Fibers have become a recent research trend due to reasons such as locally available materials, adaptability, cost effectiveness and reproducibility (Ateş, 2016; Gul & Mir 2022). Fibers are divided into natural and synthetic according to their production source and method. For example, natural fibers are coir, bagasse, sisal, jute and palm, while synthetic fibers are polyethylene, polypropylene, polyester, nylon, glass, carbon and steel (Rabab'ah et al., 2021;

Valipour et al., 2021). Although natural fibers are cheaper and more sustainable, they have less durability, but synthetic fibers are highly resistant, biodegradable, plentiful renewable resources with little health risks, cause less damage to processing equipment, and increase the surface smoothness of composite molded products. (Ateş. 2016; Valipour et al., 2021). Recently, the use of recycled and waste fibers has been investigated (for example recycled aste caret fiber) (Valipour et al., 2021).

Shrinkage potential, swell potential, compressibility, workability and cracks were reduced by mixing the fibers with the soils (Valipour et al., 2021; Chen et al., 2022; Gul & Mir, 2022; Miller & Rifai, 2004). Also, it has been observed that the peak strength of the soils, the ductility of the soil, the hydraulic conductivity, and the undrained shear strength have increased (Rabab'ah et al., 2021; Gul & Mir 2022; Baruah, 2015, Puppala & Musenda, 2007).

Another method used in soil improvements is the use of cementitious material. When we compare fibers and cementitious materials in soil improvements, cementitious materials significantly increase strength, while fibers significantly improve deformation behavior (Gul & Mir, 2022).

Glass fiber is used in this thesis. Glass fiber is a substance made of multiple, incredibly fine fibers of glass. Glass is extruded into multiple fibers with small diameters from thin silica-based or other glass formulation strands.

Glass fibers can be divided into two groups: expensive special-purpose fibers and inexpensive general-purpose fibers. The majority of glass fibers are used for general purposes. These fibers are referred to as E-glass. Many of them, like E-glass, have letter designations that suggest they have unique features, as seen in Table 2.7.

Table 2.7 Classification of glass fiber (Wallenberger et al., 2001)

Letter Designation	Property or Characteristic
E, electrical	Low electrical conductivity
S, strength	High strength
C, chemical	High chemical durability
M, modulus	High stiffness
A, alkali	High alkali or soda lime glass
D, dielectric	Low dielectric constant

Wallenberger et al. (2001) have explained the production of glass fiber. Glass fibers are used to make printed circuit boards, structural composites, and a variety of other goods with unique uses. Processes for forming fiber: By combining (co-melting) silica with minerals that have the oxides required to create a specific composition, glass melts are created. In a procedure called as fiberization, the molten mass is quickly cooled to prevent crystallization and shaped into glass fibers. The majority of continuous glass fibers are produced using the direct draw method, which involves forcing molten glass through a platinum alloy bushing with up to thousands of 0.793 to 3.175 mm diameter orifices. The resultant fibers are quickly pulled to a small diameter and harden while they are still quite viscous.

CHAPTER 3
MATERIALS AND METHODS

3.1 Materials

Sand, bentonite, borons, glass fiber and slags were used in this study. The sand was taken from the Izmir region. Bentonite, a calcium bentonite activated with sodium bicarbonate, was obtained from Ünye Madencilik. The boron minerals ulexite, colemanite and etibor48 were used and were supplied from Eti Maden AŞ. Glass fiber was purchased from Dost Kimya. Copper slag and ferrochrome slag were used as slag. Copper slag was supplied from Radöksan Metalurji ve Maden San. Tic. Ltd. Şti. Ferro chrome slag was supplied from Eti Krom A.Ş. The materials used in this thesis are shown in Figure 3.1. The content of ferrochrome slag is given in Table 3.1 by Eti Krom AŞ.

Table 3.1 Content of ferrochrome slag

	Al_2O_3	Cr_2O_3	SiO_2	CaO	Fe_2O_3	MgO	Others	Cr/Fe
					(%)			
Ferrochrome slag	24.34	3.63	31.94	0.69	1.23	37.68	0.49	2.88

A typical copper slag consists of 30-40% Fe, 35-40% SiO_2, ≤ 10% CaO, ≤ 10% Al_2O_3, 0.5-2% Cu and others (Co, Zn, Ni, Mn) (Uysal & Bahar, 2018). Since slags are waste and by-products, it is seen that their pure state is quite low and generally consists of metal oxides.

The average length of the glass fiber is 3 mm and the diameter is 16-17 microns. Slags and Boron minerals were sieved through No.40 (0.425 mm) sieve. All materials in the thesis were used with natural water content. The physico-chemical properties of the materials used in the thesis are given in Table 3.2.

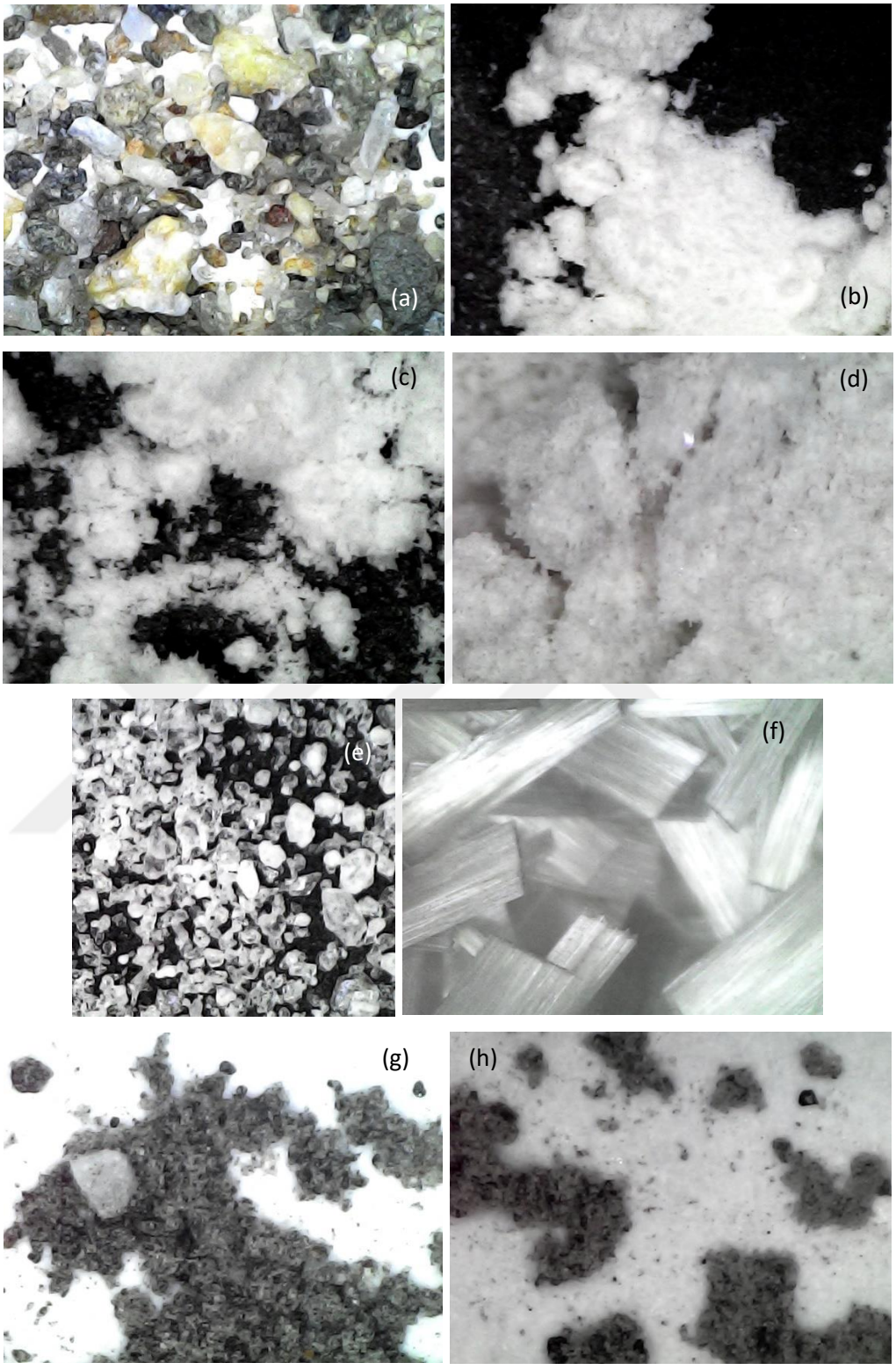


Figure 3.1 Microscope images of the materials a) Sand b) Bentonite c) Ulexite d) Colemanite e) Etibor48 f) Glass Fiber g) Copper Slag h) Ferrochrome Slag (Personal archive, 2023)

Table 3.2 The Physcio – chemical Properties of Materials

	Sand	Bentonite	Colemanite	Ulexite	Etibor48	Fiber Glass	Copper Slag	Ferrochrome Slag
Specific Gravity	2.63	2.60	2.48	2.44	1.80	2.60	3.43	3.22
Liquid Limit	-	270	28.5	33.4*	-	-	-	-
Plastic Limit	-	63	19.70	25.12*	-	-	-	-
pH	8.62	9.13	9.26*	9.13*	9.25	7.81	10.01	9.80
Natural Water Content (%)	0.8	6.5 ∓1	1	7.5	10	-	1	0.8
Passing Sieve	-No 6	-No 200	-No 40	-No 40	-No 40	-	-No 40	-No 40

*Alpaydın, Ş. G. (2019). *An investigation of effects of boron additives on the permeability and shear strength behavior of sand bentonite mixtures under high temperatures* [Master dissertation, Dokuz Eylül University]. YOK Ulusal Tez Merkezi

3.2 Methods

3.2.1 Compaction

The compaction test was performed in accordance with ASTM: D698-(2012e2). Preparation of compaction samples: (1) The materials in natural water were mixed in the desired proportions. (2) By adding water, the mixture was brought to the desired water content and mixed again. (3) The mixtures were kept in plastic bags for one day to allow homogeneous distribution of water. (4) Samples were compressed in 3 layers of 25 blows in a standard proctor mold. (5) The samples were taken out of the mold and put in an oven for water content and waited for drying. (6) Necessary calculations were made and the compaction curve was drawn.

3.2.2 Soil Classification Tests

Sieve analysis was performed according to ASTM: D422-63 (2007). Dry sieve analysis of sand and Etibor48 was performed. Wet sieve analysis could not be performed because etibor48 solidified immediately upon contact with water. Wet sieve analysis of other materials was made. Since the structure of bentonite and boron minerals may change at high temperatures, sieve analysis was performed on the natural water content. The sieve analysis results are shown in Figure 3.2. Bentonite (100%), ulexite (95.6%) and colemanite (99.99%) have passed through No. 200 (0.075 mm) in

high proportion. Due to the high proportion of materials passing through No. 200, hydrometer analyzes of these materials were made. Hydrometer analysis was performed in accordance with ASTM: D422-63 (2007). Glass fiber is not suitable for sieve analysis and hydrometer analysis.

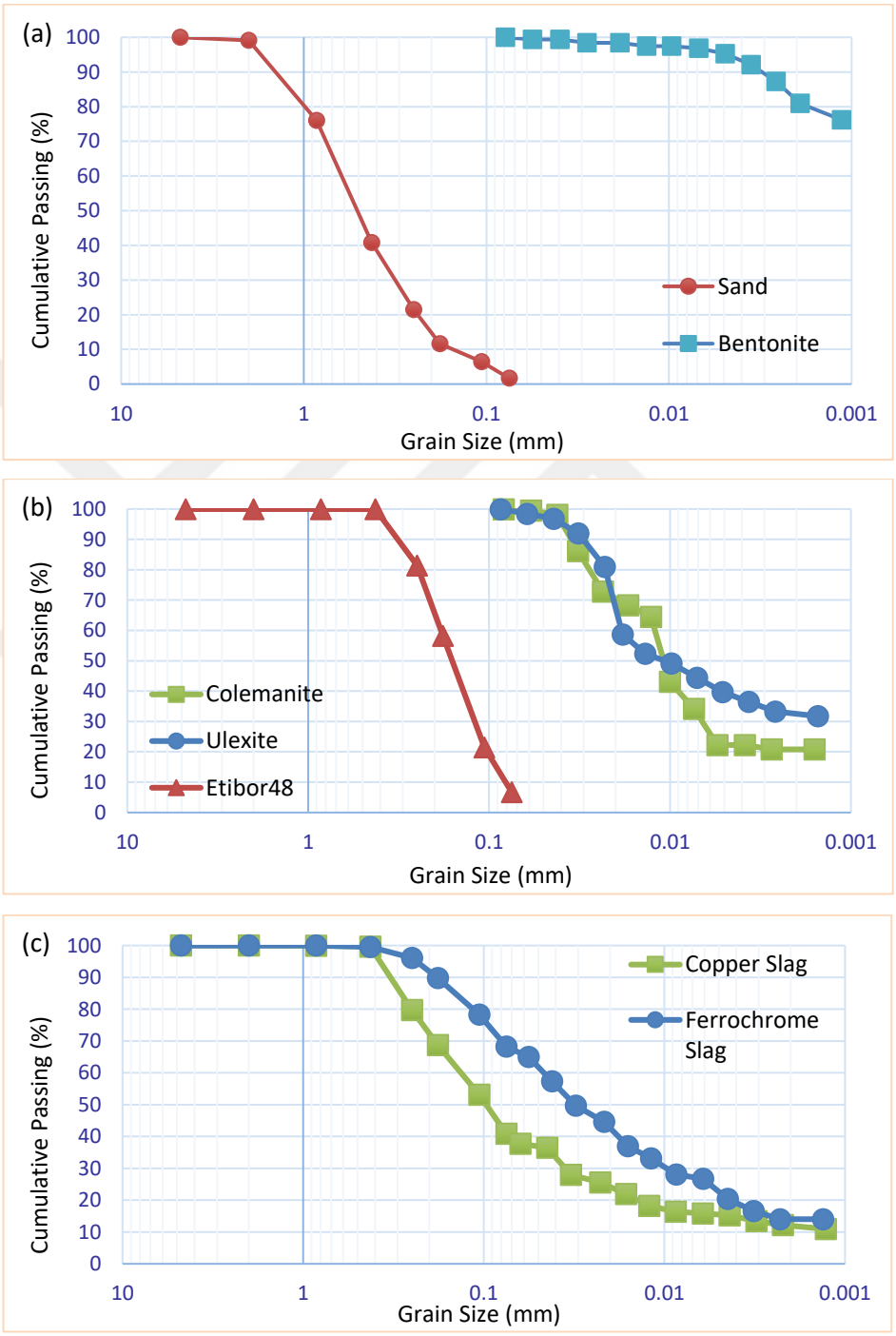


Figure 3.2 Sieve analysis results a) Bentonite and Sand b) Borons (Etibor48, Colemanite, Uleksite) c) Slags (Copper and Ferrochrome)

Materials' specific gravities were determined in accordance with ASTM D854-14 (2014). Using ASTM: D4318-17e1 (2017), the consistency limits of the materials were established. The liquid limit of bentonite was determined using the Casagrande method; colemanite and ulexite were determined using the fall cone method.

The pH values of the materials were determined according to ASTM: D4972-19 (2019). For boron minerals, glass fiber and slags, 1:1 water-material mixtures were prepared and shaken for 1 hour. For bentonite, a mixture of 1:5 was prepared. The pH measurement was measured with the device in Figure 3.3.

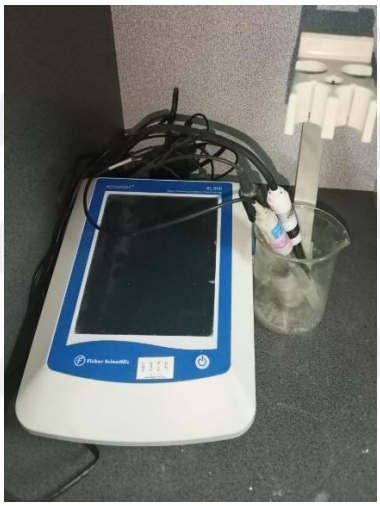


Figure 3.3 pH measurement device (Personal archive, 2023)

3.2.3 Measurement of Thermal Properties of Soils

The SH-3 and TR-3 sensors of the Tempos device were used to measure the thermal properties of the materials. The TR-3 sensor has a 10 cm long and 2.4 mm wide needle. The TR-3 probe measurement range is 0.1-4.0W/mK, and the accuracy is ± 10% from 0.2 to 4.0 W/mK (METER Group, 2018). The SH-3 sensor has two needles, the needles are 3 cm long and 1.3 mm wide. The SH-3 probe measurement range is 0.02–2.00 W/mK and accuracy is ±10% from 0.02–2.0 W/mK for thermal conductivity, diffusivity range is 0.1–1.0 mm^2/s and accuracy is ±10% at conductivity above 0.2 W/mK and ±0.02 W/mK from 0.10–0.20 W/mK, volumetric specific heat capacity range is 0.5–4.2 MJ/m^3K and accuracy is ±10% at conductivities above 0.1 W/mK (METER Group, 2018). While the TR-3 sensor was used to determine the thermal

conductivity and thermal resistivity values, the SH-3 sensor was used to determine the thermal conductivity, volumetric heat capacity and diffusivity values. The thermal conductivity values of the TR-3 sensor and the SH-3 sensor were taken for each sample and their measurement accuracy was checked. Holes were drilled in the samples with guides to place the sensors. Since there may be gaps between the soil particle and the probe, the thermal paste with high thermal conductivity to ensure contact is slightly squeezed into the hole. The instruments used in thermal properties measurements are shown in Figure 3.4.



Figure 3.4 Instruments used in thermal properties measurements (Personal archive, 2023)

Thermal conductivity of porous materials has been measured using transient line heat source techniques for more than 60 years. The probe has temperature sensor and heater inside the needle for measuring thermal conductivity. The system tracks the temperature of the sensor over time while a current flows through the heater. Thermal conductivity is calculated by analyzing the sensor temperature's time dependence when the probe is inserted into the test material. When the heater and temperature sensors placed in separate needles, also diffusivity and heat capacity could be calculated by using temperature versus time relationship for separated probes.

To reduce thermally induced water movement and shorten measurement times, the TEMPOS keeps heating durations as short as possible. To reduce water movement and free convection, the heat input is also restricted. High resolution temperature readings and specialized algorithms are needed to measure thermal characteristics while using very brief heating durations and low heating rates. The TEMPOS measures temperature with a sensitivity of 0.001 °C and calculates the rate of temperature drift before the measurement to account for drift.

For SH-3 sensor, heat is given to the heated needle for the predetermined amount of time, th, and temperature is recorded in the monitoring needle at a distance of 6 mm both during heating and during the cooling phase that follows heating. The readings are then processed by subtracting the ambient temperature and the rate of drift. The resulting data are fit to Equation 24 and Equation 25 using a least squares procedure. The ambient temperature and drift rate are then subtracted from the measurements during processing. A least squares method is used to fit the given data to Equations 24 and 25.

$$\Delta T = \left(\frac{q}{4\pi k}\right) Ei\left(\frac{-r^2}{4Dt}\right) \tag{24}$$

$$\Delta T = \left(\frac{q}{\pi k}\right) Ei\left\{\left(\frac{-r^2}{4D(t-t_h}\right) - Ei\left(\frac{-r^2}{4Dt}\right)\right\} \tag{25}$$

Where, ΔT is the temperature rise at the measuring needle, q is the heat input at the heated needle (W/m), k is the thermal conductivity (W/mK), r is the distance from the heated needle to the measuring needle, D is the thermal diffusivity (m^2/s), t is time (s), t_h is the heating time (s), Ei is the exponential integral and is approximated using polynomials (Abramowitz & Stegun, 1972)

The TEMPOS gathers data to calculate temperature drift at least 30 sec. If the drift is below a certain level, current is delivered to the heater needle for 30 seconds while simultaneously monitoring the temperature of the detecting needle. The current is cut off after 30 s, and another 30 s of temperature monitoring follow. The ΔT values required to solve Equations 24 and 25 are then obtained by subtracting the initial temperature and drift from the temperatures. The tempos can solve for k and D because

the values of q, r, t, and t_h are known. Traditional nonlinear least squares (Marquardt, 1963) may be used for this, but they frequently produce incorrect results because they become stuck in local minima. A linear least squares problem is created when a value for D in Equations 24 and Equation 25 is selected. The tempos then look for the value of D that minimizes the squared deviations between the measured temperature and the temperature predicted by the model. When properly set up, this method yields the global minimum and is just as quick as conventional nonlinear least squares. Equation 1 can be used to calculate the volumetric specific heat capacity once k and D have been established.

For TR-3 sensor, to calculate the temperature drift, the probe temperature is observed for at least 30 s. The measurements are then adjusted for the start temperature and drift. The heater is then powered on for 60 s while the temperature of the probe is being recorded. Equation 24 might be used to predict the temperature of the needle if it were a line-heat source. The exponential integral is expanded in an infinite series using Equation 24 for single-needle analysis, and only the first term of the expansion is kept, as shown in Equation 26. This is the equation used in the ASTM/IEEE mode in TEMPOS.

$$\Delta T = \left(\frac{q}{4\pi k}\right) \ln t + C \tag{26}$$

Early time data are not included in the analysis because it is thought that this expansion only applies after prolonged heating intervals. In fact, it can be showed that Equation 26 produces accurate results after a sufficient long time, but the durations are very long, especially for low-conductivity materials. When temperature is plotted against lnt, Equation 26 demonstrates that conductivity is proportional to the inverse of the slope. Temperature fluctuates very little over long periods of time, therefore measurement noise can have a significant impact. The exponential integral expansion's ignored terms, which are functions of diffusivity, contribute to the problem with shorter measurement times by influencing the conductivity estimates. A bigger issue is that the real probe has a significant heat capacity whereas the line heat source has none. The fact that there is frequently contact resistance between the probe and the material in which it is put is a major issue as well. The Knight et al. (2012) model was

used to replicate sensor data for a variety of conductivities, diffusivities, and contact resistances in order to evaluate these impacts. Equation 25 was fitted to these data, and it was found that the time scale is the main issue. By changing the equation to

$$\Delta T = \left(\frac{q}{4\pi k}\right) \ln(t - t_0) + C \tag{27}$$

The data all matched up well with heating times of 60 seconds where to is a time offset. Diffusivity and contact resistance effects are removed or greatly minimized. Least squares is used to calculate the values of k, to, and C. This is another nonlinear least squares problem, which could be solved using traditional methods (Marquardt, 1963). It is resolved via an alternative iterative process. The value of to that minimizes the standard error of estimation is obtained after different values of are given. This method was applied to dry and wet soil, as well as to samples with known conductivities such glycerin and agar water. The 1-min readings for each of these samples were more precise than 10-min readings using Equation 26. The first 16 s of temperature data were disregarded for all of these estimates.

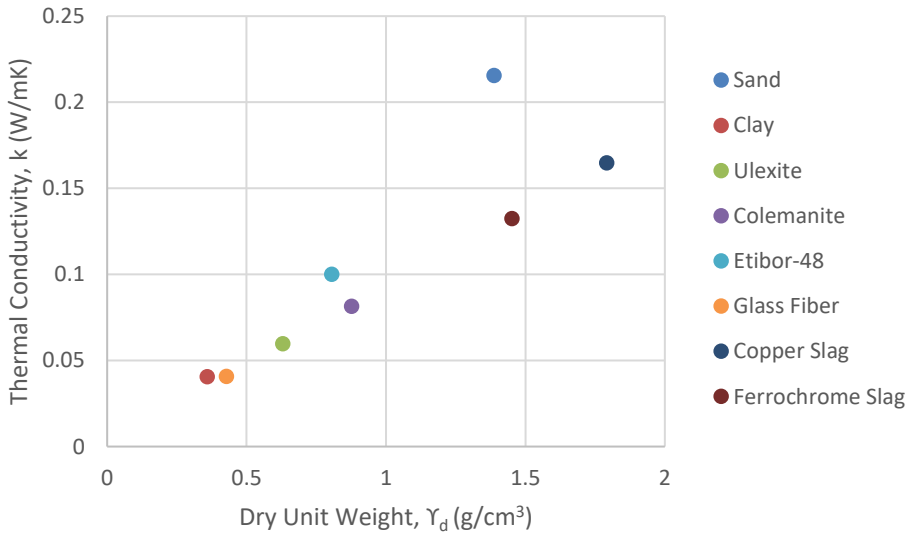


Figure 3.5 Thermal conductivity values of sand, bentonite and additives

The thermal conductivity of the samples was measured by pouring them into the container in Figure 3.7 with maximum void ratio. Thermal conductivity values corresponding to dry unit weight values are given in Figure 3.5. Sand has the highest

thermal conductivity value of 0.2155 W/mK. Copper slag is highest thermal conductivity additive material highest thermal conductivity with a value of 0.1647 W/mK, also it has the highest unit weight value with ϒd = 1.79 g/cm3. Ferrochrome slag, on the other hand, is the second highest thermal conductivity (0.1324 W/mK) additive material with ϒd = 1.45 g/cm3. In borons, the highest thermal conductivity value is in etibor48 (0.10 W/mK), followed by colemanite (0.0815 W/mK) and ulexite (0.0597). Glass fiber is the additive material with the lowest thermal conductivity. Its thermal conductivity value of 0.04075 W/mK is very close to bentonite (0.04056 W/mK).

In this thesis, the variation of the thermal properties of the materials according to the proctor curve, to the degree of saturation and to the temperature were investigated.

The thermal properties of the bentonite mixtures were measured immediately after compaction in standard proctor molds. The TR-3 sensor (single needle) is the main sensor used in thermal conductivity measurements. The measurement is taken from the midpoint of the sample. At least 3 cm diameter area is needed for measurements. Therefore, more than one measurement can be taken on the same sample. The second measurement with the TR-3 sensor is made to confirm the first measurement. After the sensor is immersed in the soil, it is waited for at least 15 minutes for the sensor to reach thermal equilibrium with the soil, then at least 3 measurements are taken with an interval of 15 minutes. The SH-3 sensor (dual needle needle) measures thermal conductivity, volumetric heat capacity and diffusivity values. Bentonite samples are measured from 3 different points with the SH-3 sensor. After the SH-3 sensor is immersed in the soil, it is waited for 15 minutes for the sensor to come to equilibrium with the soil, then at least two measurements are taken with an interval of 15 minutes. An example measurement method is shown in Figure 3.6.

In sand-bentonite mixtures, a metal mold with a diameter of 7 cm and a height of 14 cm in Figure 3.7 was used (the mold was changed to ensure that the amount of sand was sufficient for the experiments). Measurement is taken from the midpoint of the sample with the TR-3 sensor. The TR-3 sensor penetrates the first 10 cm. Then, the sample was turned upside down and measurements were taken from two different

points with the SH-3 sensor from a 4 cm section. The measurement process is the same as for bentonite samples. Also, since the amount of sand was not enough for all experiments, compaction curve-thermal properties experiments were carried out by selecting 3 points on the compaction curve.

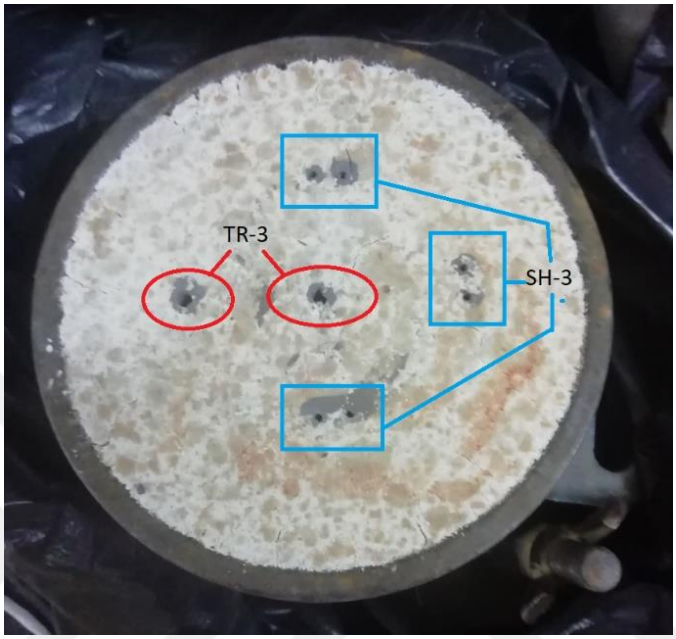


Figure 3.6 Measurement method of bentonite samples in standard proctor mold (Personal archive, 2022)



Figure 3.7 Measurement method of sand-bentonite samples (Personal archive, 2022)

The variation of the thermal conductivity values of the samples depending on the temperature was measured with the TR-3 sensor. The samples were compacted in the mold in Figure 3.7. The thermal conductivity values of the prepared samples were first measured at room temperature. Then, the samples were placed in the oven by wrapping them well with three layers of stretch film and three layers of aluminum foil (Figure

3.8a). For these measurements, lids with holes small enough for the sensor cable to pass through were opened on the sides of the oven (Figure 3.8f). It was waited for at least 16 hours for the samples placed in the oven to reach the desired temperature and equilibrate. After the temperature of soil was stabilized, the aluminum foil on the top layer of the samples was removed, a hole was made in the stretch film enough to pass the needle of the sensor, and the sensor was placed in the sample by applying a small amount of thermal paste (Figures 3.8b and Figure 3.8c). Then, the sample was placed inside the oven by wrapping the upper part with aluminum foil again, the cable was passed through the perforated cover and connected to the TEMPOS device outside (Figure 3.8d and Figure 3.8e). Again, the temperature of the sample and the temperature of the sensor were expected to reach equilibrium. After reaching equilibrium, at least 5 measurements were taken. Since there may be situations such as heating and cooling of the oven and deterioration of the balance, measurements were taken as necessary by looking at the thermal conductivity values of each sample. After the measurements were done, the sensor was removed from the sample, wrapped with aluminum foil again and put back in the oven. The temperatures of the samples were brought to 60°C and 80°C, respectively. The initial weight of the samples and the weight after measurement at 80°C were measured. During the preparation of the samples for thermal conductivity measurements, it was observed that a maximum of 5 grams of water was lost.

The variation of the thermal properties of the samples depending on the degree of saturation was investigated with the SH-3 sensor. The samples were prepared at 0%, 65.8% for bentonite, 60-61% for sand-bentonite and 90% saturation degrees. The samples were prepared in the mold in Figure 3.7. First, samples at the medium saturation degree were prepared. After the measurements were taken with the SH-3 probe, the samples were slowly dried at 60°C. The dried samples were allowed to come to room temperature, then measurements were taken with the SH-3 probe for 0% saturation degree. Since there will be shrinkage due to the presence of bentonite during drying, metal guides with the same dimensions as the sensor were placed in order not to reduce the diameter of the holes.

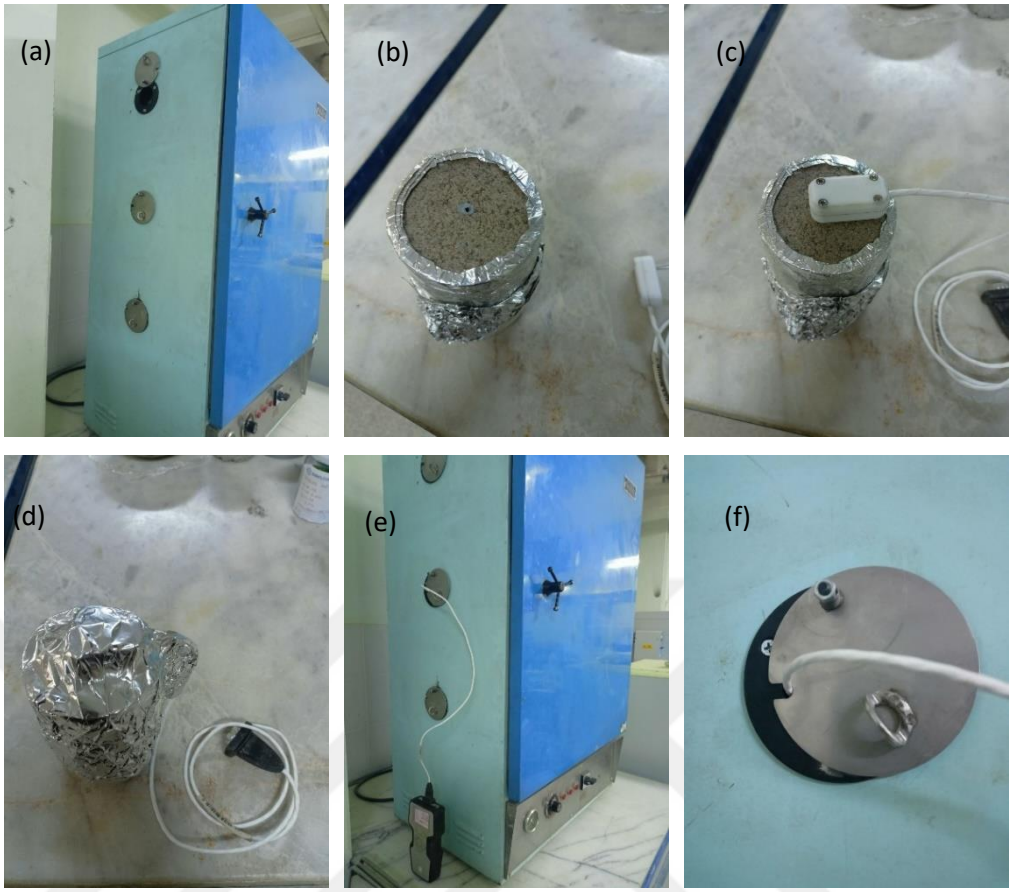


Figure 3.8 a) Modified oven for temperature measurements b) Sample wrapped with stretch film and aluminum foil c) Placement of the TR-3 sensor d) Re-coating the top surface with aluminum foil e) Measurement of the thermal conductivity of the sample f) Closing the lid (Personal archive, 2023)

In bentonite mixtures, additives are used as 10% and 20% by weight of bentonite. For example, 10 grams of additive was added to 100 grams of bentonite for mixtures with 10% colemanite and this mixture is called B10C. However, in sand-bentonite mixtures, the samples were prepared based on the total sample weight, keeping the sand-bentonite ratio constant. For example, a total of 100 grams of sample will be prepared for the mixture with 10% colemanite. 10 grams of 100 grams will be additive and the remaining 90 grams will be sand-bentonite. The sand-bentonite ratio is 90% to 10%, that is, 90% of 90 grams will be sand and 10% of 90 will be bentonite. As a result, 10% additive sand bentonite mixture will be obtained by mixing 10 grams of additive, 9 grams of bentonite and 81 grams of sand. And this mixture will be called SB10C10.

Since the thermal conductivity values depend on many parameters such as saturation degree, void ratio, dry unit volume weight, etc., the void ratios and saturation degrees of the samples were kept constant in order to examine the changes depending on the degree of saturation and temperature. The properties of the prepared samples are given in the Table 3.3, 3.4, 3.5, and 3.6.

Table 3.3 Bentonite Samples

	Specific Gravity	Υ_d (g/cm^3)	S=0.658 e = 1.769		S=0.90 e = 1.769	
			w (%)	Υ (g/cm^3)	w (%)	Υ (g/cm^3)
B	2.600	0.939	44.77	1.359	61.23	1.514
B20C	2.580	0.932	45.12	1.353	61.71	1.507
B20U	2.567	0.927	45.34	1.347	62.02	1.502
B20E48	2.467	0.891	47.18	1.311	64.54	1.466
BGF	2.600	0.939	44.70	1.359	61.23	1.514
B20CS	2.738	0.989	42.51	1.409	58.15	1.564
B20FS	2.703	0.976	43.06	1.396	58.90	1.551

Table 3.4 SB10 Samples

			S=0.606 e = 0.564		S=0.9 e=0.564	
	Specific Gravity	Υ_d (g/cm^3)	w (%)	Υ (g/cm^3)	w (%)	Υ (g/cm^3)
SB10	2.627	1.680	13.00	1.898	19.32	2.005
SB10C20	2.598	1.661	13.10	1.879	19.66	1.988
SB10U20	2.582	1.651	13.24	1.870	19.66	1.976
SB10E4820	2.462	1.574	13.88	1.792	19.32	1.878
SB10GF	2.627	1.680	13.00	1.898	20.62	2.026
SB10CS20	2.788	1.783	12.26	2.002	18.21	2.108
SB10FC20	2.746	1.756	12.45	1.975	18.49	2.081

Table 3.5 SB20 Samples

			S = 0.602 e = 0.632		S = 0.90 e= 0.632	
	Specific Gravity	Υ_d (g/cm^3)	w (%)	Υ (g/cm^3)	w (%)	Υ (g/cm^3)
SB20	2.624	1.608	14.5	1.841	21.68	1.957
SB20C10	2.610	1.599	14.58	1.832	21.79	1.947
SB20C20	2.595	1.59	14.66	1.823	21.92	1.939
SB20U10	2.602	1.594	14.62	1.827	21.86	1.942
SB20U20	2.579	1.58	14.75	1.813	22.06	1.929
SB20E4810	2.542	1.558	14.97	1.791	22.3	1.905
SB20E4820	2.459	1.507	15.47	1.740	23.13	1.856
SB20GF	2.624	1.608	14.5	1.841	21.68	1.957
SB20CS10	2.705	1.657	14.07	1.890	21.03	2.005
SB20CS20	2.785	1.706	13.66	1.939	20.42	2.054
SB20FS10	2.684	1.645	14.18	1.878	21.19	1.994
SB20FS20	2.743	1.681	13.87	1.914	20.74	2.030

Table 3.6 SB30 Samples

			S=0.617 e=0.735		S=090 e=0.735	
	Specific Gravity	Υ_d (g/cm^3)	w (%)	Υ (g/cm^3)	w (%)	Υ (g/cm^3)
SB30	2.621	1.511	17.3	1.772	25.24	1.892
SB30C20	2.593	1.495	17.49	1.756	25.51	1.876
SB30U20	2.577	1.485	17.6	1.746	25.67	1.866
SB30E4820	2.457	1.416	18.46	1.677	26.92	1.797
SB30GF	2.621	1.511	17.3	1.772	25.24	1.892
SB30CS20	2.783	1.604	16.3	1.865	23.77	1.985
SB30FC20	2.741	1.58	16.55	1.841	24.13	1.961

CHAPTER 4
COMPACTION TEST RESULTS

The compaction characteristics of the mixtures were examined by adding 10% and 20% additive to bentonite and SB10 mixtures.

4.1 Compaction Test Results of Bentonite Mixtures

The compaction curve of bentonite is shown in Figure 4.1. The optimum water content is 52.80% and the maximum dry unit weight value is 9.50 kN/m^3.

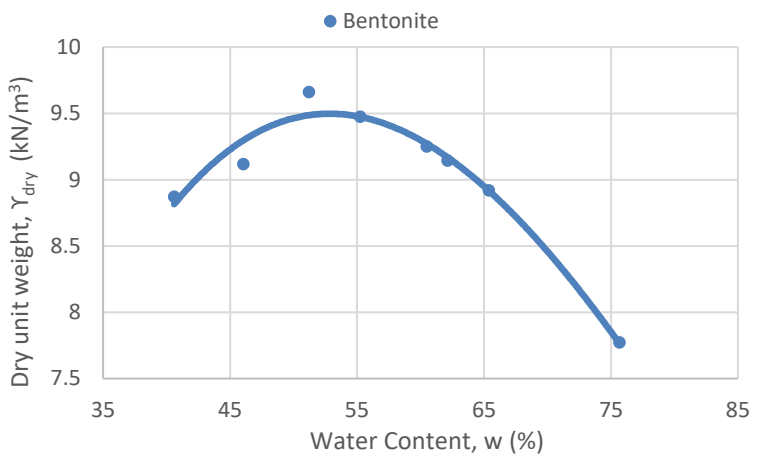


Figure 4.1 Compaction curve of bentonite

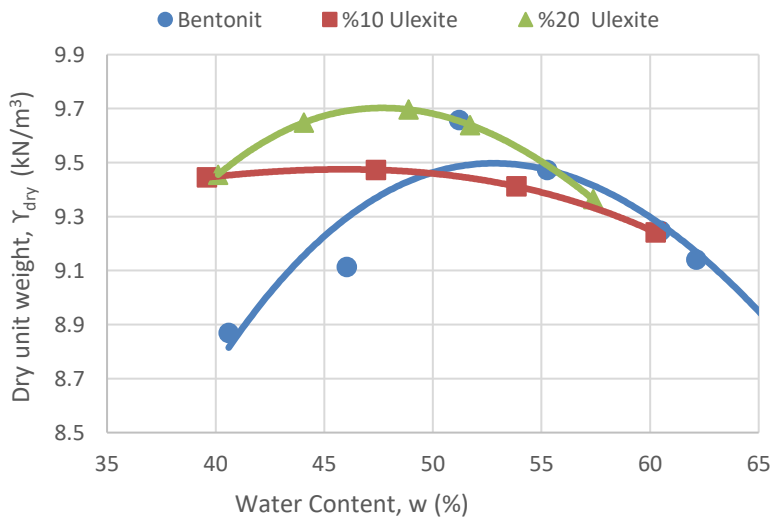


Figure 4.2 Compaction curve of bentonite-ulexite mixtures

Figure 4.2 shows the compaction curve of bentonite and bentonite-ulexite mixtures. When 10% ulexite was added to bentonite, the optimum water content decreased to 45.90% and the maximum dry unit weight decreased to 9.48 kN/m^3. When ulexite was added 20%, the optimum water content decreased to 47.70%, while the maximum dry unit weight increased to 9.70 kN/m^3.

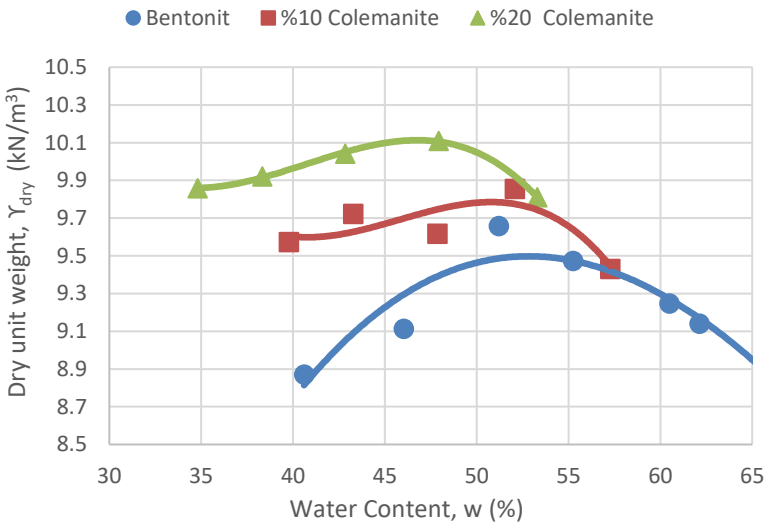


Figure 4.3 Compaction curve of bentonite-colemanite mixtures

In Figure 4.3, compaction curves of bentonite and bentonite-colemanite mixtures are given. When colemanite was added 10%, the optimum water content decreased to 50.80%, while the maximum dry unit weight increased to 9.79 kN/m^3. When 20% colemanite was added to bentonite, the optimum water content decreased to 46.80%, while the maximum dry unit weight reached 10.11 kN/m^3.

Figure 4.4 shows the compaction curves of bentonite and bentonite-etibor48 mixtures. When Etibor48 was added 10% to bentonite, the optimum water content decreased to 51.90% and the maximum dry unit weight was 9.48 kN/m^3. When etibor48 was added at the rate of 20%, the optimum water content increased to 55.10% and the maximum dry unit weight increased to 9.74 kN/m^3.

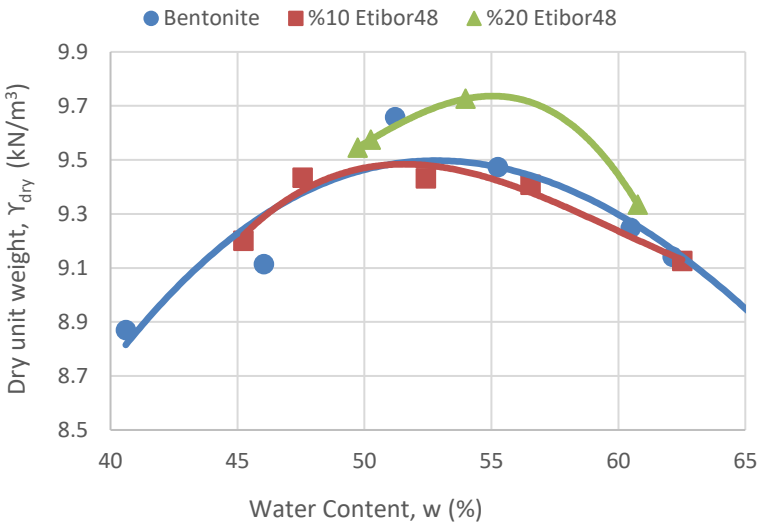


Figure 4.4 Compaction curve of bentonite-etibor48 mixtures

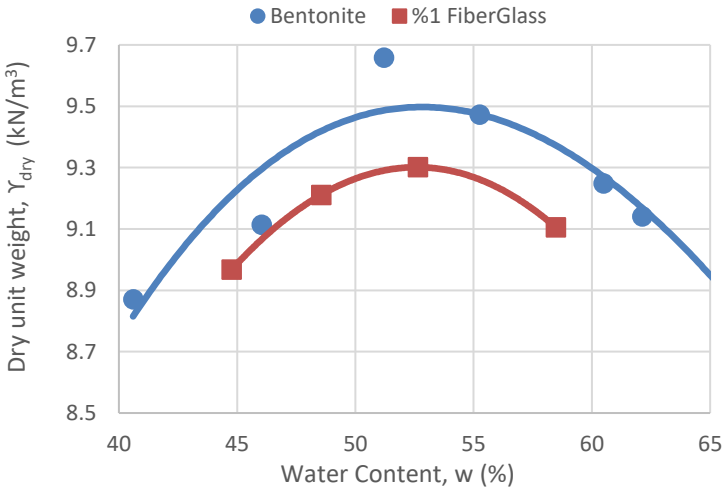


Figure 4.5 Compaction curve of bentonite-fiber glass mixture

As seen in Figure 4.5, when 1% glass fiber was added to bentonite, the optimum water content decreased to 52.2% and the maximum dry unit weight value decreased to 9.29 kN/m^3.

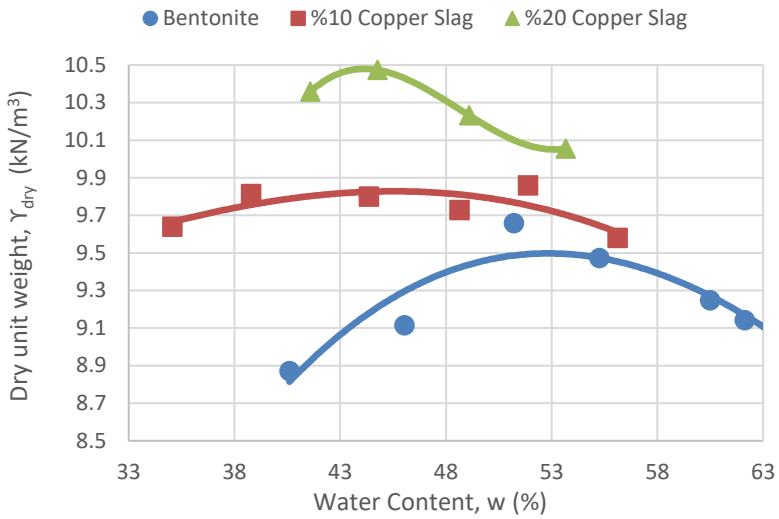


Figure 4.6 Compaction curve of bentonite-copper slag mixtures

As seen in Figure 4.6, while the optimum water content decreased in both ratios, it increased the maximum dry unit volume weight value. When 10% copper slag was used in the mixture, the optimum water content decreases to 45.50%, while the maximum dry unit weight increased to 9.83 kN/m^3. When copper slag was added at the rate of 20%, the optimum water content decreased by 44.10%, while the maximum dry unit weight increased to 10.48 kN/m^3.

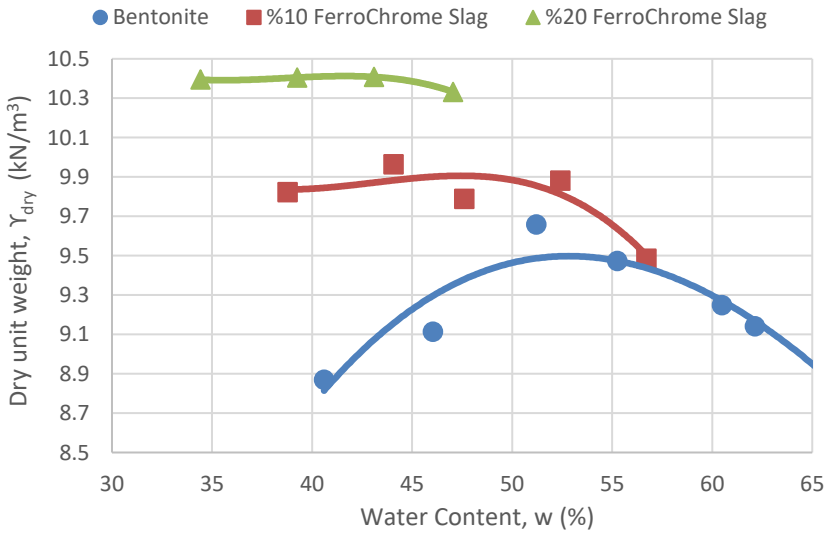


Figure 4.7 Compaction curve of bentonite-ferrochrome slag mixtures

As seen in Figure 4.7, ferrochrome slag also behaved like copper slag. When 10% ferrochrome slag was used in the bentonite mixture, the optimum water content

decreased to 47.50%, and the maximum dry unit weight increased to 9.91 kN/m^3. When ferrochrome slag was added 20% to bentonite, the optimum water content decreased to 41.65% and the maximum dry unit weight increased to 10.41 kN/m^3.

Table 4.1 Compaction results of bentonite mixtures

Sample	Sample Abbreviation	Dry Unit Weight (kN/m^3)	Optimum Water Content (%)
Bentonite	B	9.50	52.8
Bentonite - %10 Etibor48	B10E48	9.48	51.9
Bentonite - %20 Etibor48	B20E48	9.74	55.1
Bentonite - %10 Ulexite	B10U	9.48	45.9
Bentonite - %20 Ulexite	B20U	9.70	44.7
Bentonite - %10 Colemanite	B10C	9.79	50.8
Bentonite - %20 Colemanite	B20C	10.11	46.8
Bentonite - %1 Fiber Glass	BFG	9.39	52.3
Bentonite - %10 Copper Slag	B10CS	9.83	45.5
Bentonite - %20 Copper Slag	B20CS	10.48	44.1
Bentonite - %10 Ferrochrome Slag	B10FS	9.91	47.5
Bentonite - %20 Ferrochrome Slag	B20FS	10.41	41.7

4.2 Compaction Test Results of SB10 Mixtures

When SB10 mixtures mixed (Figure 4.8), the optimum water content is 15.90%, and the maximum dry unit weight increased to 17.76 kN/m^3.

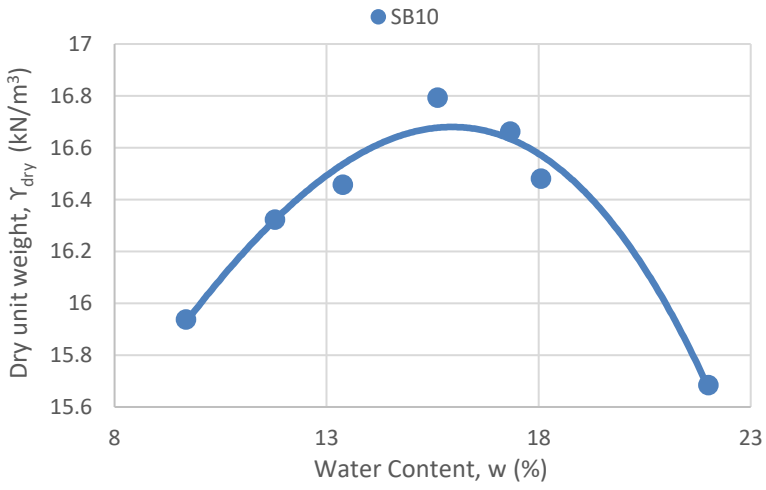


Figure 4.8 Compaction curve of SB10

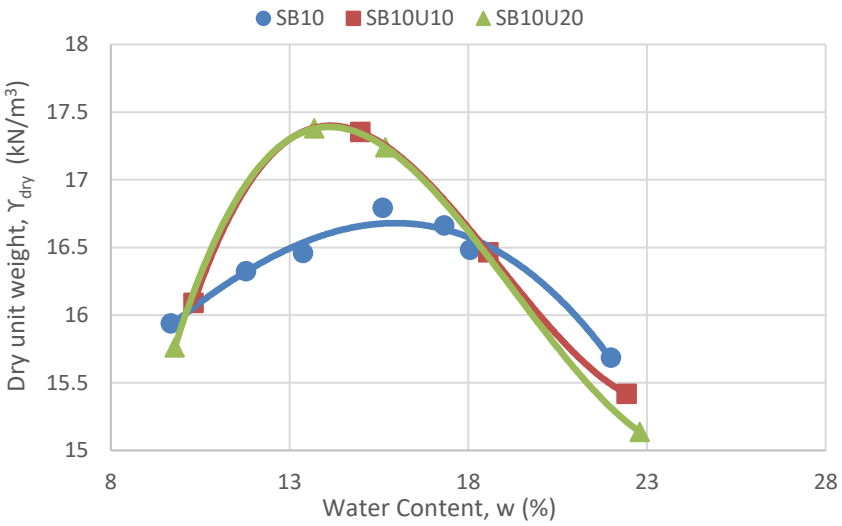


Figure 4.9 Compaction curves of SB10-ulexite mixtures

Figure 4.9 shows the compaction curve of SB10 and SB10-ulexite mixtures. When 10% ulexite was added to SB10, the optimum water content decreased to 14.10%, and the maximum dry unit weight increased to 17.40 kN/m^3. When 20% ulexite was used in the SB10 mixture, the optimum water content decreased to 14.10% while the maximum dry unit weight increased to 17.39 kN/m^3.

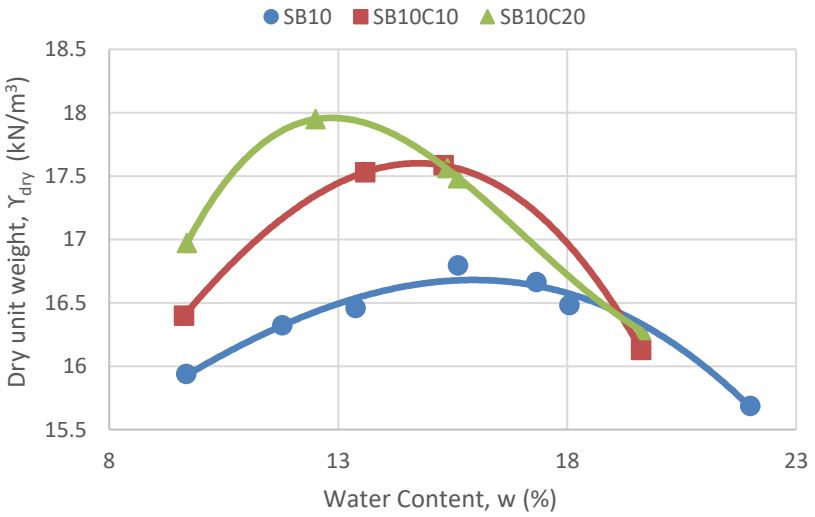


Figure 4.10 Compaction curves of SB10-colemanite mixtures

In Figure 4.10, compaction curves of SB10 and SB10-colemanite mixtures are given. When colemanite was added 10% to SB10, the optimum water content decreased to 14.70%, and the maximum dry unit weight increased to 17.60 kN/m^3.

Also, when 20% ulexite was added to SB10, the optimum water content decreased to 13.00% while the maximum dry unit weight increased to 17.96 kN/m^3.

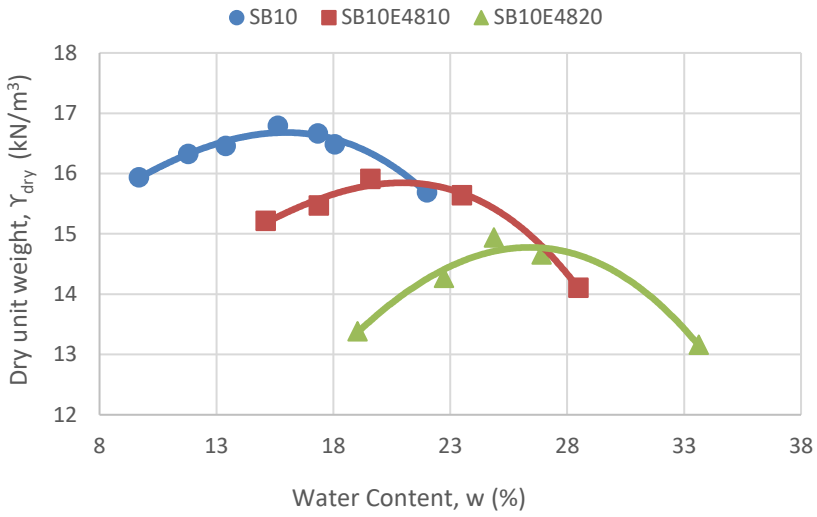


Figure 4.11 Compaction curves of SB10-etibor48 mixtures

Figure 4.11 shows the compaction curves of SB10 and SB10-etibor48 mixtures. When etibor48 was added %10, the optimum water content increased to 20.90%, and the maximum dry unit weight decreased to 15.85 kN/m^3. Also, when 20% ulexite was added to SB10, the optimum water content increased to 26.40% while the maximum dry unit weight decreased to 14.78 kN/m^3.

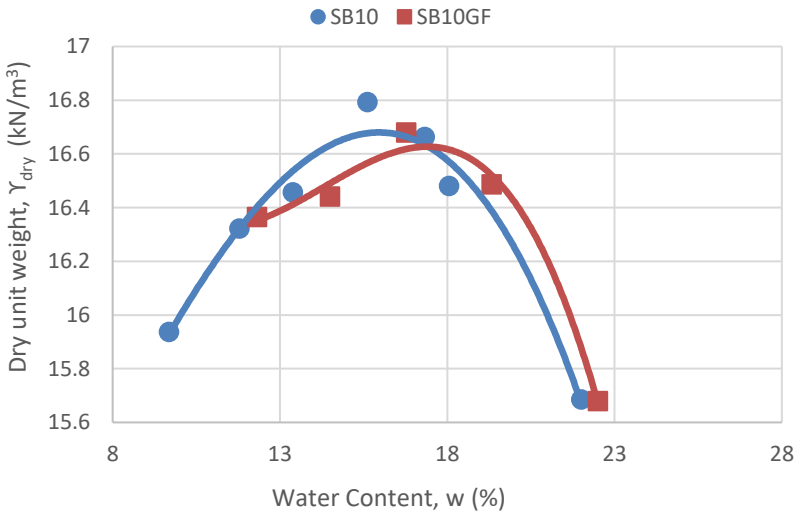


Figure 4.12 Compaction curves of SB10-glass fiber mixture

When 1% glass fiber was added to SB10 (Figure 4.12), the optimum water content increased to 17.4%, and the maximum dry unit weight decreased to 1.70 kN/m^3.

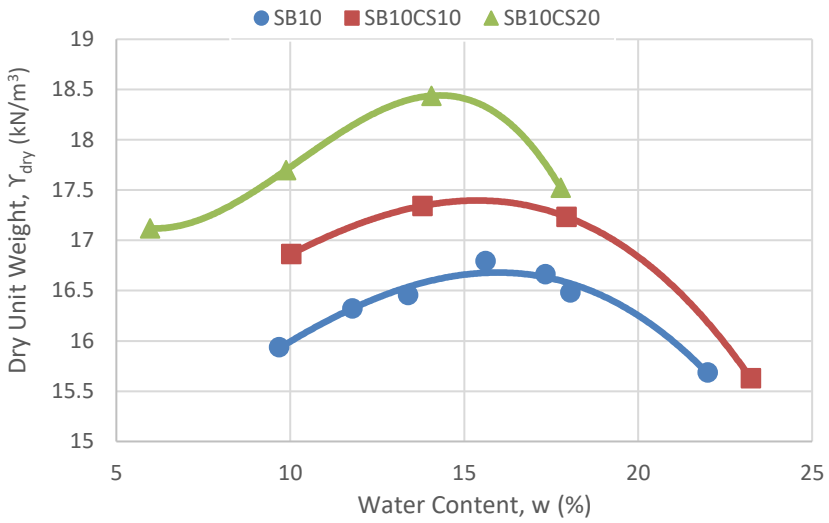


Figure 4.13 Compaction curves of SB10-copper slag mixtures

Figure 4.13 shows the compaction curve of SB10 and SB10-copper slag mixtures. When copper slag was used as 10% additive, the optimum water content decreased to 15.40%, while the maximum dry unit weight increased to 17.40 kN/m^3. In the SB10CS20 mixture, while the optimum water content decreased to 14.30%, the maximum dry unit weight reached 18.44 kN/m^3.

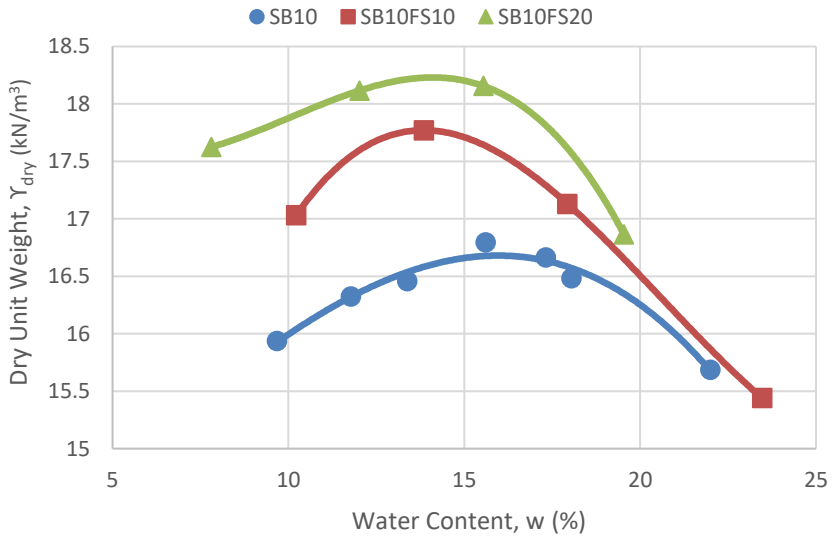


Figure 4.14 Compaction curves of SB10-ferrochrome slag mixtures

In Figure 4.14, compaction curves of SB10 and SB10-ferrochrome slag mixtures are given. While the optimum water content decreased to 13.80% in the SB10FS10 mixture, the maximum dry unit volume weight value reached 17.70 kN/m^3. In the 20% Ferrochrome additive, while the maximum dry unit volume weight value increased to 18.23 kN/m^3, the optimum water content decreased to 14.10%.

Table 4. 2 Compaction results of sand-bentonite mixtures

Sample	Sample Abbreviation	Dry Unit Weight (kN/m3)	Optimum Water Content (%)
Sand-Bentonite	SB10	16,68	16,00
Sand-Bentonite - %10 Etibor48	SB10E4810	15.85	20.90
Sand-Bentonite - %20 Etibor48	SB10E4820	14.78	26.40
Sand-Bentonite - %10 Ulexite	SB10U10	17.40	14.10
Sand-Bentonite - %20 Ulexite	SB10U20	17.36	14.10
Sand-Bentonite - %10 Colemanite	SB10C10	17.60	14.70
Sand-Bentonite - %20 Colemanite	SB10C20	17.96	13.00
Sand-Bentonite - %1 Glass Fiber	SB10GF	16.70	17.40
Sand-Bentonite - %10 Copper Slag	SB10CS10	17.40	15.40
Sand-Bentonite - %20 Copper Slag	SB10CS20	18.44	14.30
Sand-Bentonite - %10 Ferrochrome Slag	SB10FS10	17.70	13.80
Sand-Bentonite - %20 Ferrochrome Slag	SB10FS20	18.23	14.10

CHAPTER 5
THERMAL PROPERTIES DEPENDING ON PROCTOR CURVE

5.1 Thermal Properties of Bentonite Depending on Proctor Curve

In Figure 5.1, the thermal properties of bentonite were investigated within ∓10 from optimum water content. Bentonite is expected to reach approximately the maximum thermal conductivity value when the water content is 62% because the plastic limit of bentonite is 62.7%. Yan et al. (2021) stated in their research that the thermal conductivity values decrease after the plastic limit. The highest thermal conductivity value of the bentonite is 0.971 W/mK (Figure 5.1a) when w = 62% and ϒdry is 9.18 kN/m^3, its volumetric specific heat capacity is 2.961 MJ/m^3K (Figure 5.1b) and its diffusivity is 0.326 mm^2/s (Figure 5.1c). Thermal conductivity, volumetric heat capacity and diffusivity values started to decrease on the wet side of the optimum (Figure 5.1c). In the dry part of the compaction curve, the degree of saturation continued to increase while the porosity decreased. On the wet side, while the soil tried to become saturated, and the void ratios started to increase.

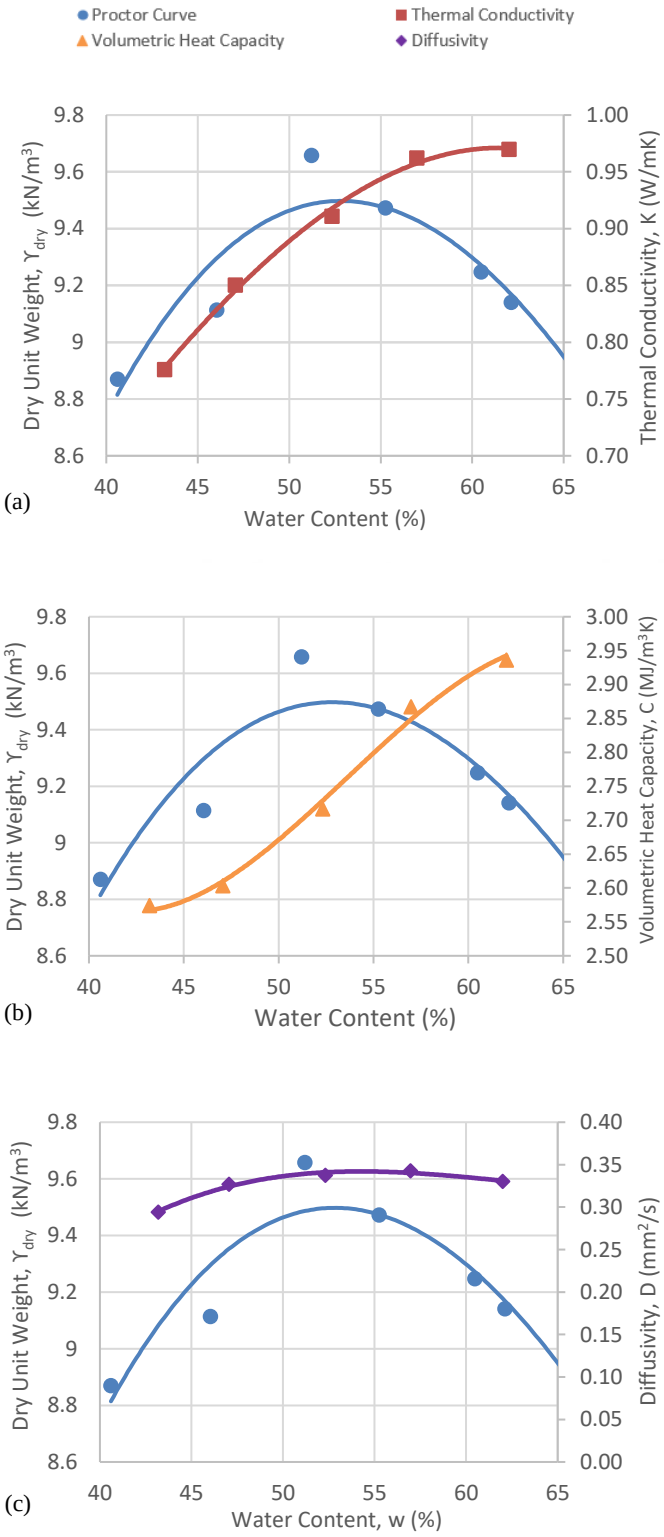


Figure 5.1 Variation of thermal properties of bentonite according to the compaction curve a) Thermal conductivity b) Volumetric heat capacity c) Diffusivity

5.1.1 Thermal Properties of Bentonite Depending on Proctor Curve in their Presence of Boron Minerals

When 10% ulexite was used in the mixture, the highest thermal conductivity value (0.966 W/mK) was obtained when the water content was 58% and Υ_{dry} was 9.32 kN/m^3. At this value, the volumetric specific heat capacity was 3.03 MJ/m^{3}K and the diffusivity value was 0.318 mm^2/s. The highest thermal conductivity value was obtained when there was a 12.1% increase from the optimum water content (45.9%) (Figure 5.2a). However, due to the differences in the increase in thermal conductivity and the increase in volumetric heat capacity (Figure 5.2b), the highest diffusivity value was obtained at 56.70% water content (Figure 5.2c). The values in these two water contents were quite close to each other.

In Figure 5.2, the highest thermal conductivity value (0.965 W/mK) was obtained when Υ_{dry} was 9.36 kN/m^3 and w = 57.4%. At this value, the volumetric specific heat capacity is 2.935 MJ/m^{3}K and its diffusivity is 0.328 mm^2/s. The thermal conductivity value continued to increase after the optimum water content (44.7%) and although there was an increase of 12.7%, no peak value was observed (Figure 5.3a). However, there was a decrease in the volumetric heat capacity (Figure 5.3b). So, this caused the diffusivity value to continue to increase after the optimum water content (Figure 5.3c).

When colemanite was used at the rate of 10%, it obtained the highest thermal conductivity value with 0.963 W/mK when Υ_{dry} was 9.56 kN/m^3 and w = 56.1%. Its volumetric specific heat capacity was 2.954 MJ/m^{3}K and its diffusivity value is 0.327 mm^2/s. Thermal conductivity values between 52.1% and 57.3% water content of the colemanite additive started to converge (Figure 5.4a), and there were decreasing trend in the volumetric heat capacity (Figure 5.4b). Thus, the increase in diffusivity values continued (Figure 5.4c).

When 20% colemanite was used in the mixture, the highest thermal conductivity value (0.989 W/mK) was obtained when the water content was 50.2% and Υ_{dry} was 10.04 kN/m^3. At this value, the volumetric specific heat capacity was 3.086 MJ/m^{3}K and the diffusivity value is 0.321 mm^2/s. It showed the best thermal properties between 47.7% and 50.2% water content (Figure 5.5a). There were decrease in thermal

conductivity, volumetric heat capacity (Figure 5.5b) and diffusivity (Figure 5.5c) values were parallel to each other on the optimum wet sides.

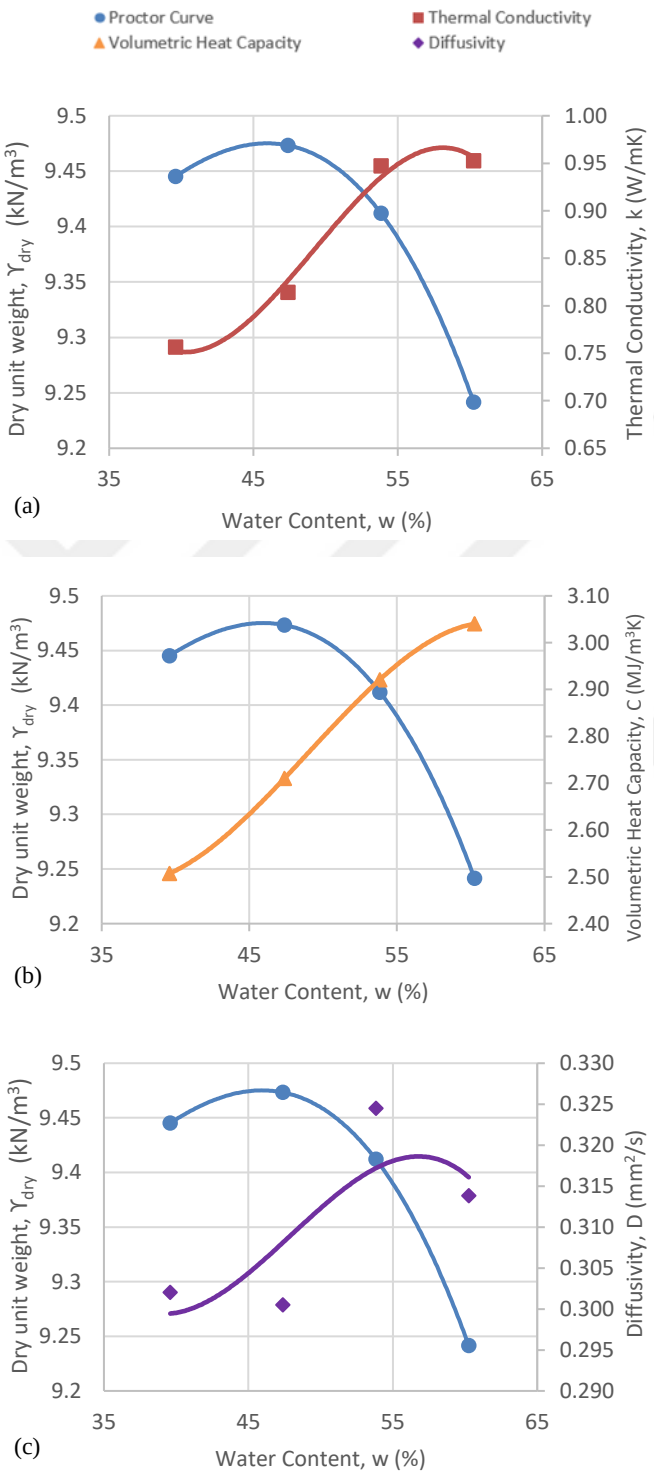


Figure 5.2 Variation of thermal properties of B10U according to the compaction curve a) Thermal conductivity b) Volumetric heat capacity c) Diffusivity

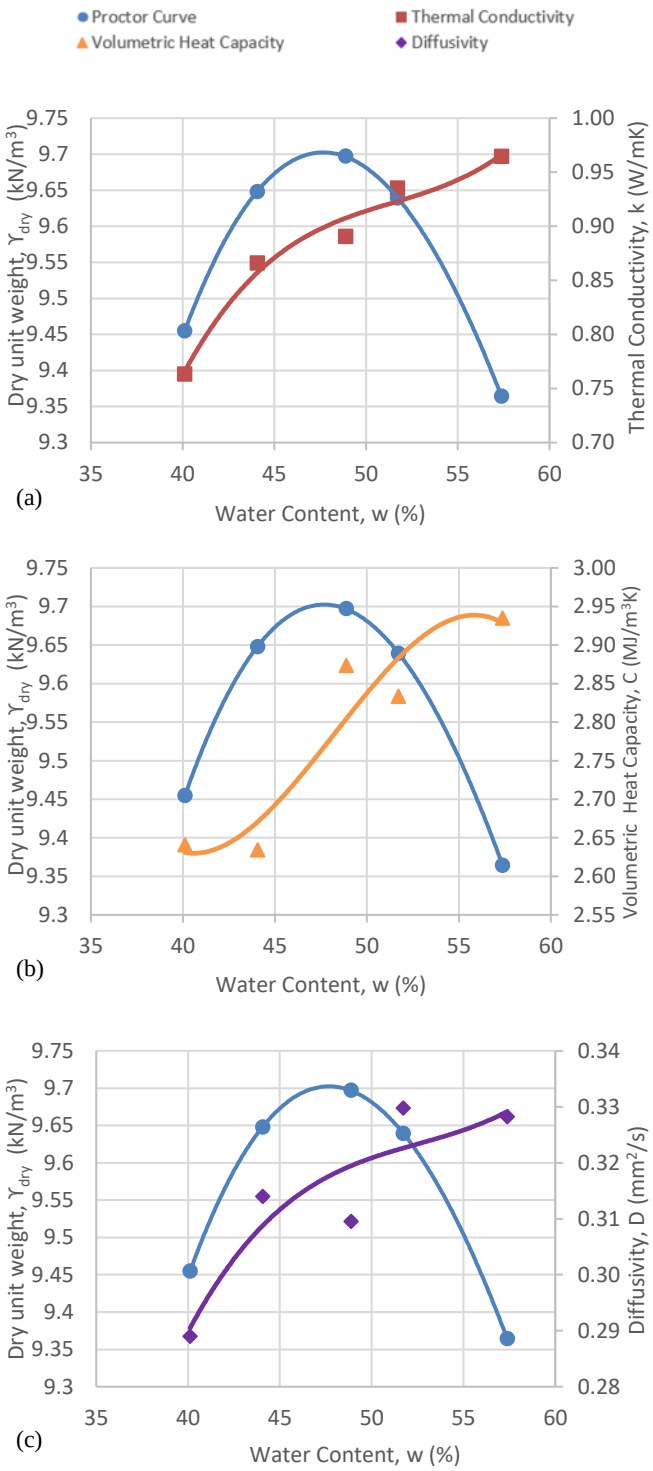
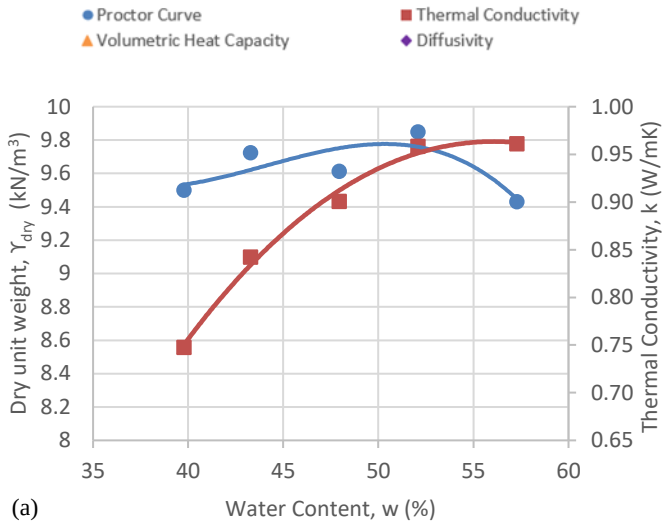
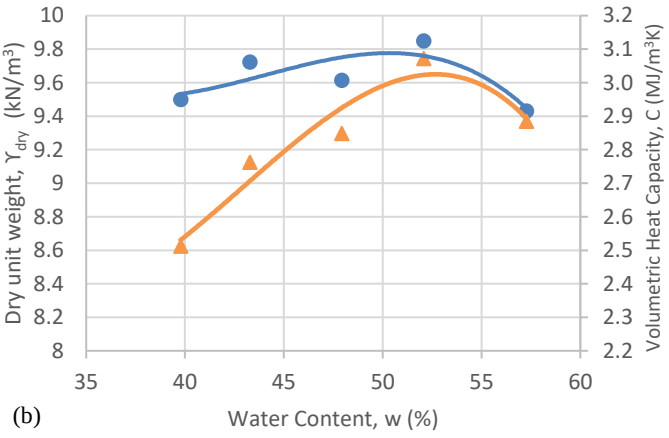


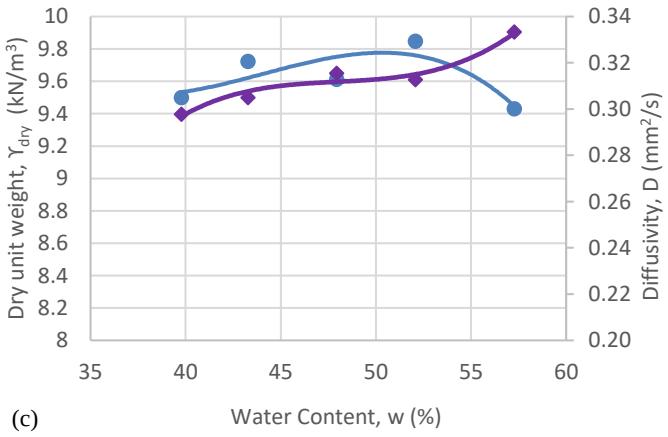
Figure 5.3 Variation of thermal properties of B20U according to the compaction curve a) Thermal conductivity b) Volumetric heat capacity c) Diffusivity



(a)

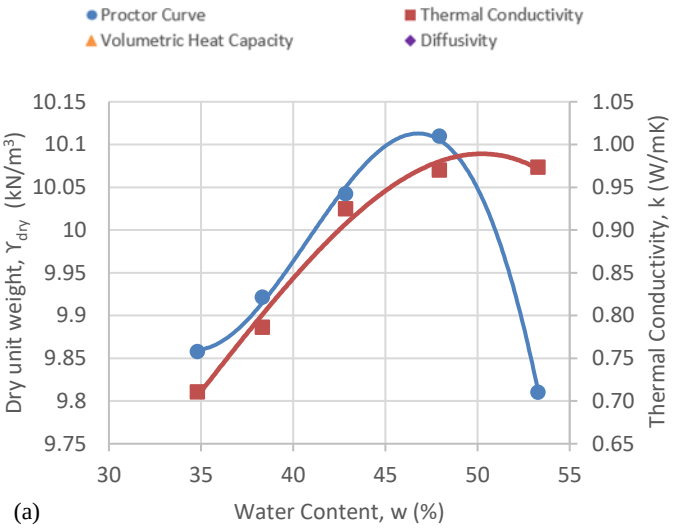


(b)

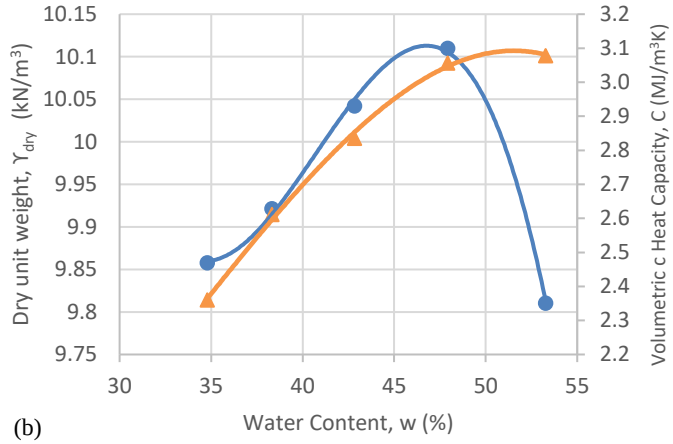


(c)

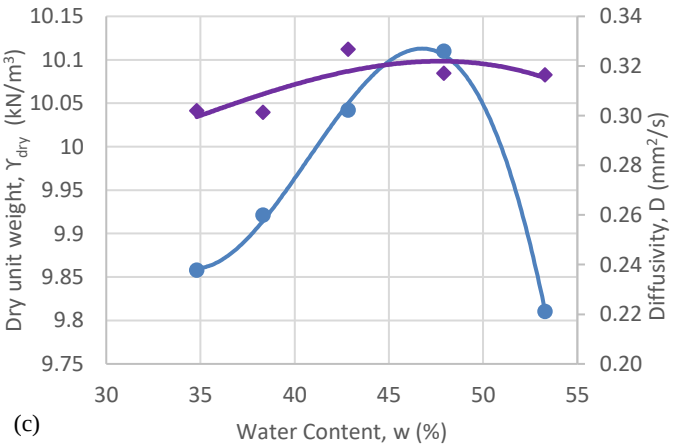
Figure 5.4 Variation of thermal properties of B10C according to the compaction curve a) Thermal conductivity b) Volumetric heat capacity c) Diffusivity



(a)



(b)



(c)

Figure 5.5 Variation of thermal properties of B20C according to the compaction curve a) Thermal conductivity b) Volumetric heat capacity c) Diffusivity

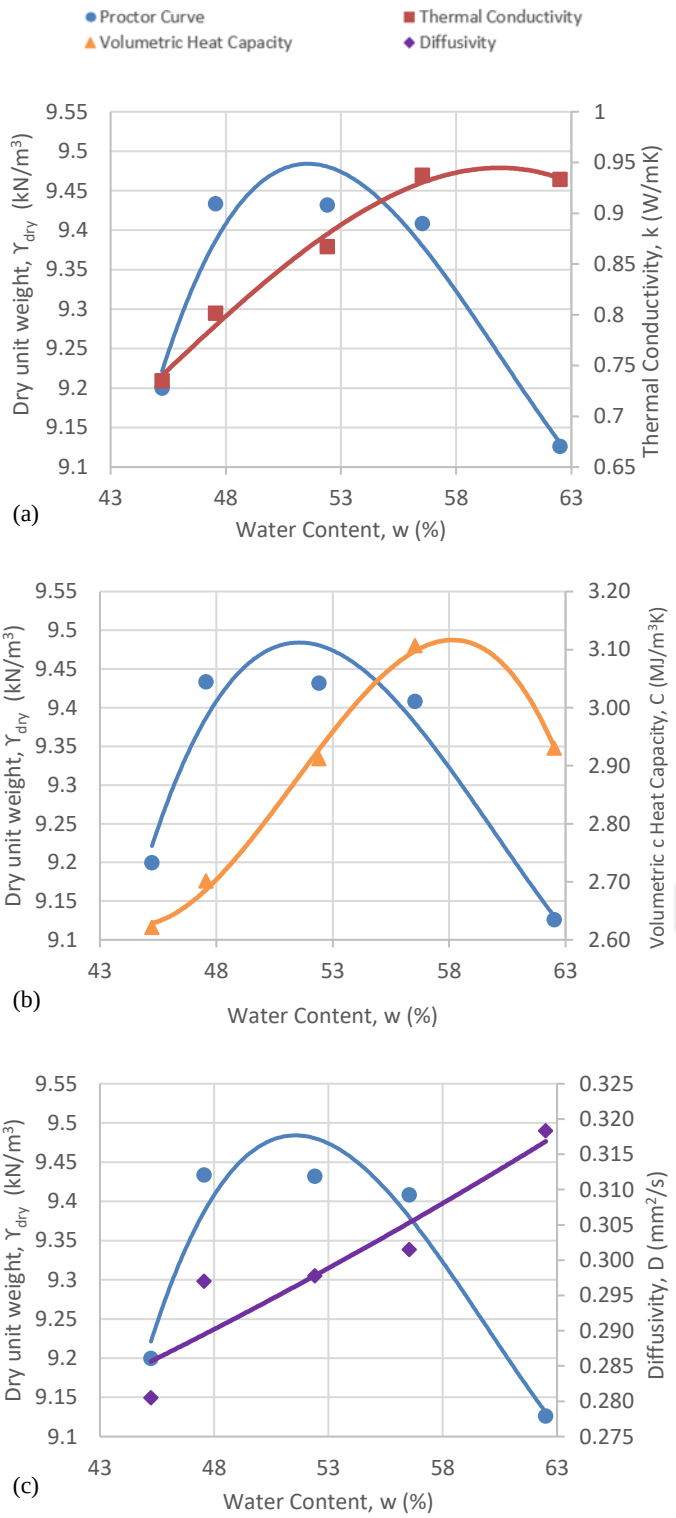


Figure 5.6 Variation of thermal properties of B10E48 according to the compaction curve a) Thermal conductivity b) Volumetric heat capacity c) Diffusivity

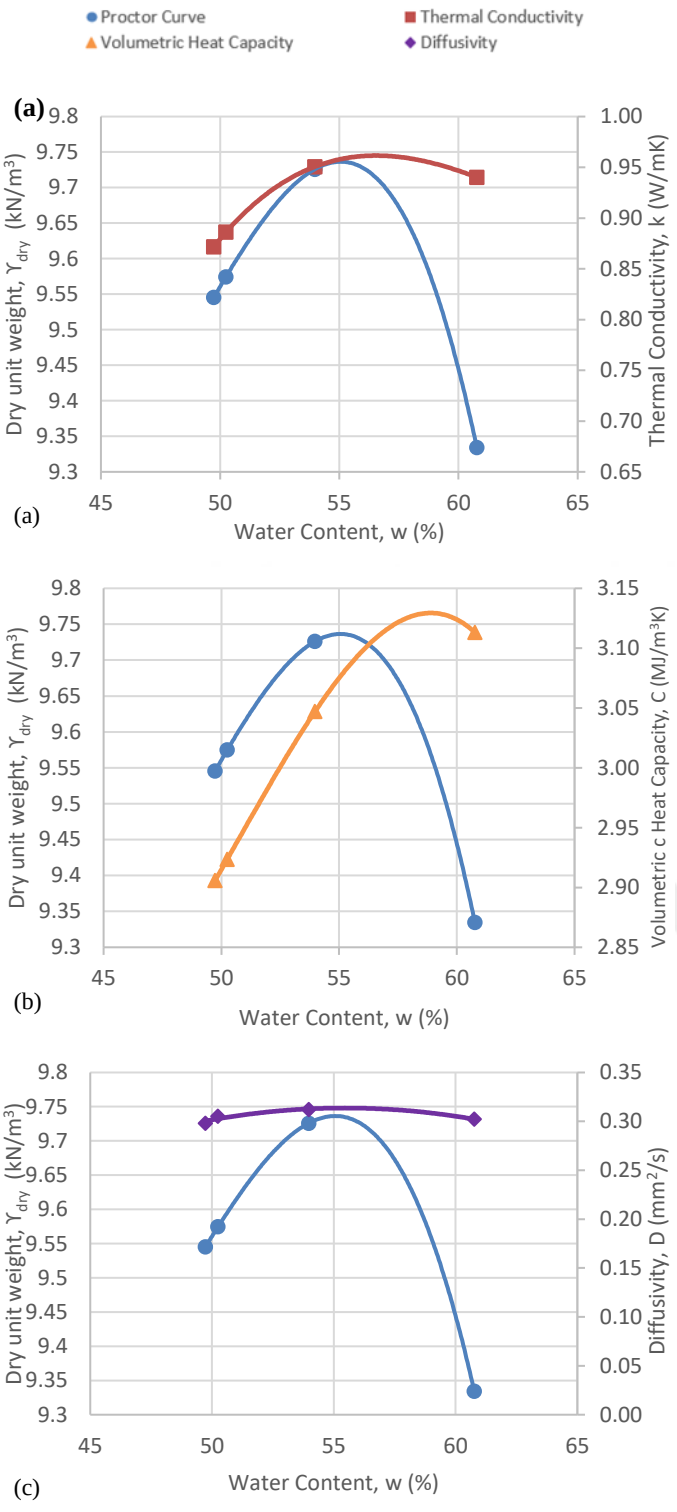


Figure 5.7 Variation of thermal properties of B20E48 according to the compaction curve a) Thermal conductivity b) Volumetric heat capacity c) Diffusivity

In Figure 5.6, the highest thermal conductivity value (0.951 W/mK) was obtained when Υ_{dry} was 9.25 kN/m^3 and w = 59.7%. At this value, the volumetric specific heat

capacity is 3.097 MJ/m^{3}K and its diffusivity is 0.312 mm^2/s. When the optimum water content increased by 7.9%, the decrease in thermal conductivity started (Figure 5.6a). The volumetric heat capacity decreased after 58.1% water content (Figure 5.6b). On the other hand, the diffusivity values continued to increase continuously (Figure 5.6c).

When 20% etibor48 was used in the mixture, the highest thermal conductivity value was obtained as 0.962 W/mK. At this value, the water content was 56.7% and the Υ_{dry} was 9.71 kN/m^3, the volumetric specific heat capacity was 3.109 MJ/m^{3}K and the diffusivity value was 0.313 mm^2/s. The thermal conductivity value started to decrease after 1.6% increase in the optimum water content (Figure5.7a). The volumetric heat capacity, on the other hand, started to decrease after 58.9% (Figure 5.7b). The diffusivity values were very close to each other at water contents between 49.7% and 60.8% (Figure 5.7c).

5.1.2 Thermal Properties of Bentonite Depending on Proctor Curve in their Presence of Slags

When 10% copper slag was used in the mixture, the highest thermal conductivity value (0.972 W/mK) was obtained when the water content was 56.1% and Υ_{dry} was 9.58 kN/m^3. At this value, the volumetric specific heat capacity was 2.904 MJ/m^{3}K and the diffusivity value was 0.335 mm^2/s. Thermal conductivity (Figure 5.8a), volumetric heat capacity (Figure 5.8b) and diffusivity (Figure 5.8c) values continued to increase along the compaction curve.

When copper slag was added to the mixture at the rate of 20%, the thermal conductivity value was 0.996 W/mK and w=53.7%, Υ_{dry} = 10.06 kN/m^3. Its volumetric specific heat capacity was 3.184 MJ/m^{3}K and its diffusivity value was 0.313 mm^2/s. While the thermal conductivity (Figure 5.9a) and volumetric heat capacities (Figure 5.9b) continued to increase along the compaction curve, the diffusivity (Figure 5.9c) values decreased after the optimum water content.

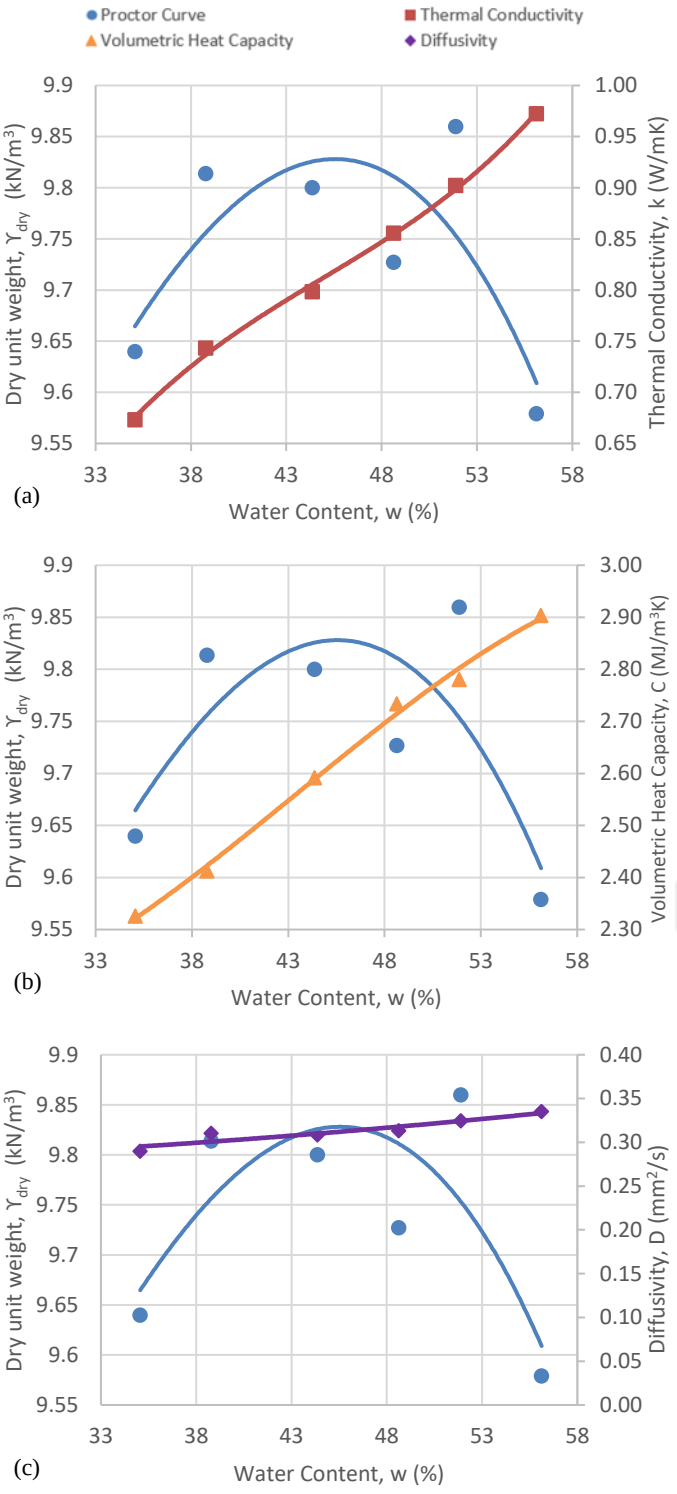


Figure 5.8 Variation of thermal properties of B10CS according to the compaction curve a) Thermal conductivity b) Volumetric heat capacity c) Diffusivity

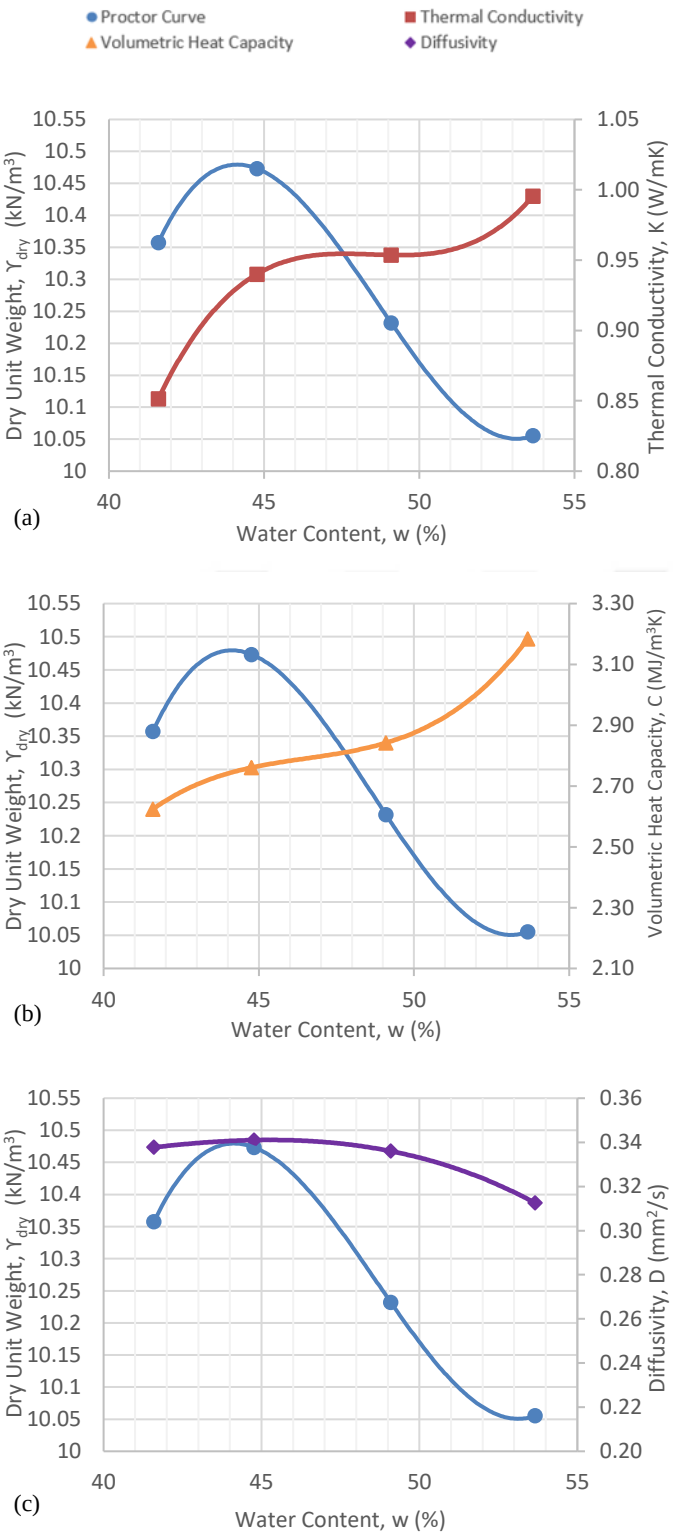


Figure 5.9 Variation of thermal properties of B20CS according to the compaction curve a) Thermal conductivity b) Volumetric heat capacity c) Diffusivity

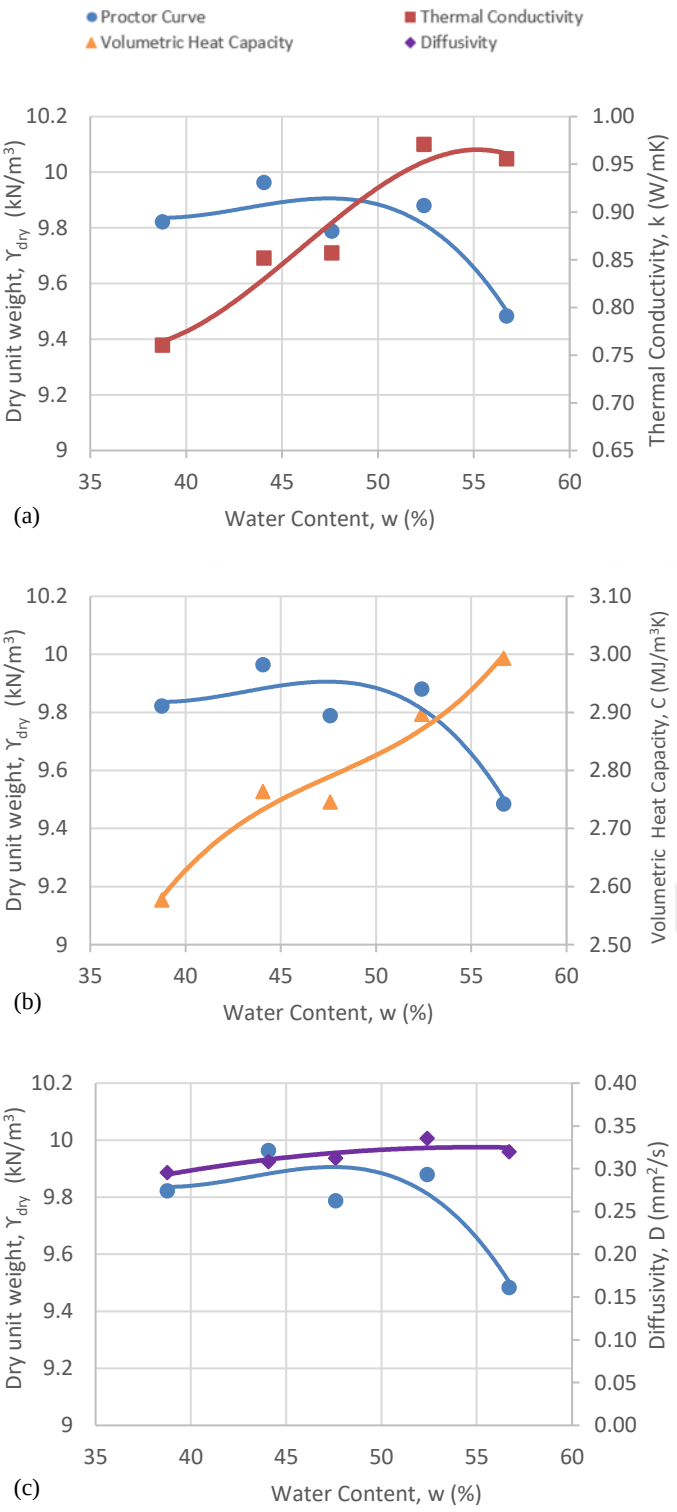


Figure 5.10 Variation of thermal properties of B10FS according to the compaction curve a) Thermal conductivity b) Volumetric heat capacity c) Diffusivity

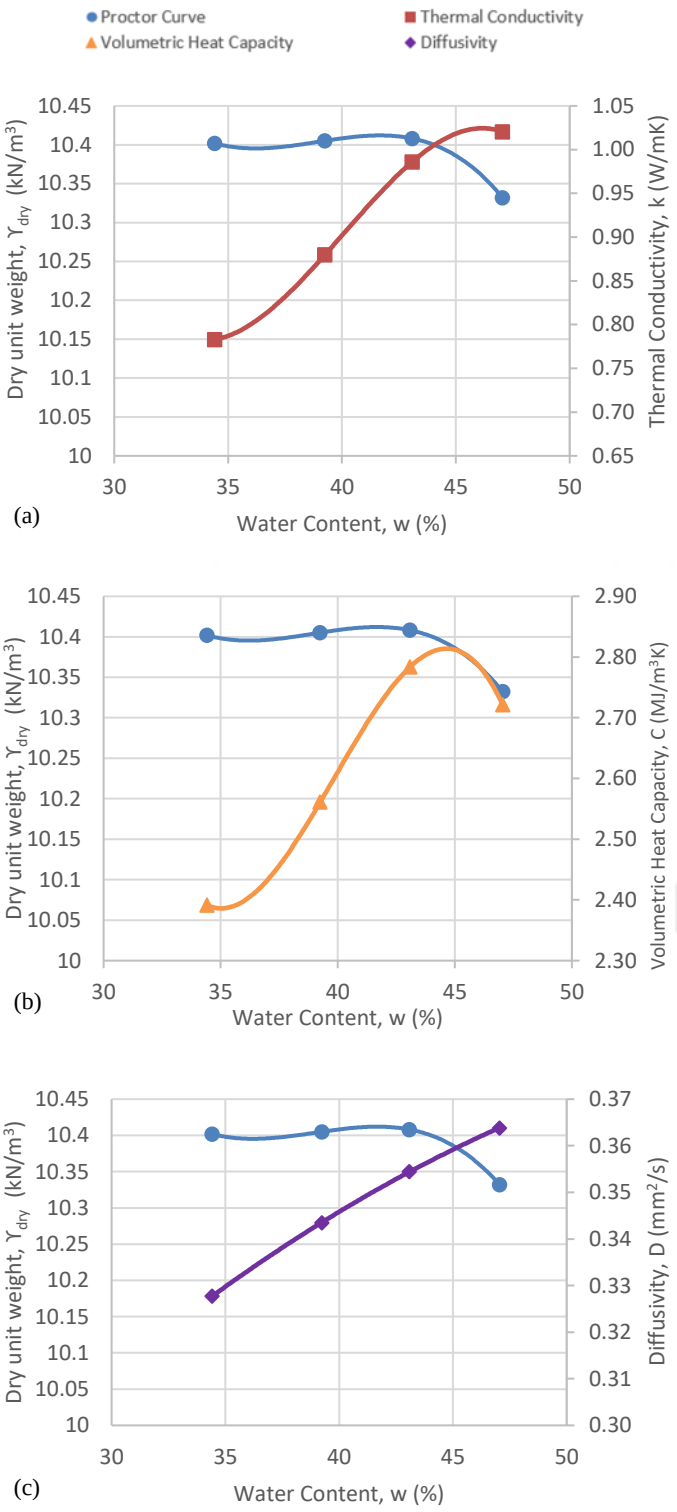


Figure 5.11 Variation of thermal properties of B20FS according to the compaction curve a) Thermal conductivity b) Volumetric heat capacity c) Diffusivity

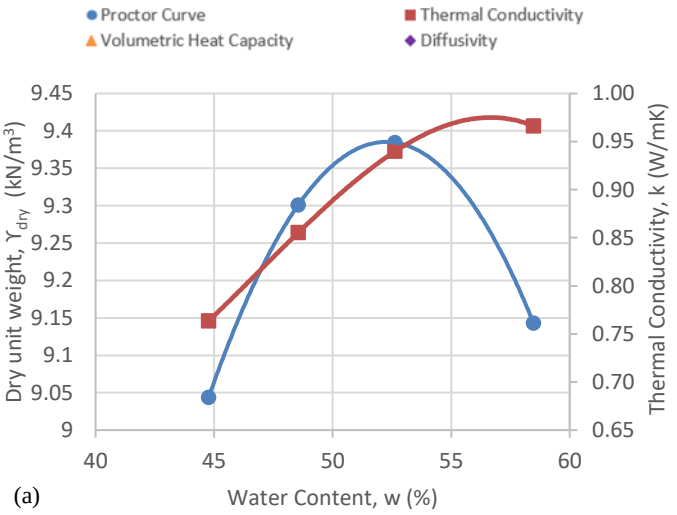
When 10% of ferrochrome slag was used, it was obtained the highest thermal conductivity value as 0.965 W/mK. At this value, Υ_{dry}=9.64 kN/m^3 and w = 55.2%,

volumetric specific heat capacity was 2.943 MJ/m^{3}K and diffusivity value was 0.328 mm^2/s. Although the thermal conductivity value reached its highest value and started to decrease (Figure 5.10a), the volumetric heat capacity (Figure 5.10b) and diffusivity (Figure 5.10c) values continued to increase.

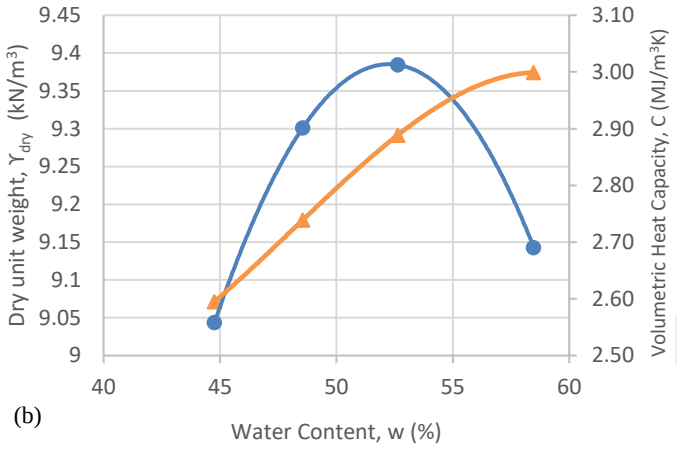
When 20% ferrochrome slag was used in the mixture, the highest thermal conductivity value (1.025 W/mK) was obtained when water content was 46.2% and Υ_{dry} was 10.36 kN/m^3. At this value, the volumetric specific heat capacity was 2.774 MJ/m^{3}K and the diffusivity value was 0.362 mm^2/s. While the thermal conductivity value started to decrease at 46.2% water content (Figure 5.11a), the volumetric heat capacity started to decrease after 44.6% water content (Figure 5.11b), and the diffusivity values continued to increase continuously (Figure 5.11c).

5.1.3 Thermal Properties of Bentonite Depending on Proctor Curve in their Presence of Fiber Glass

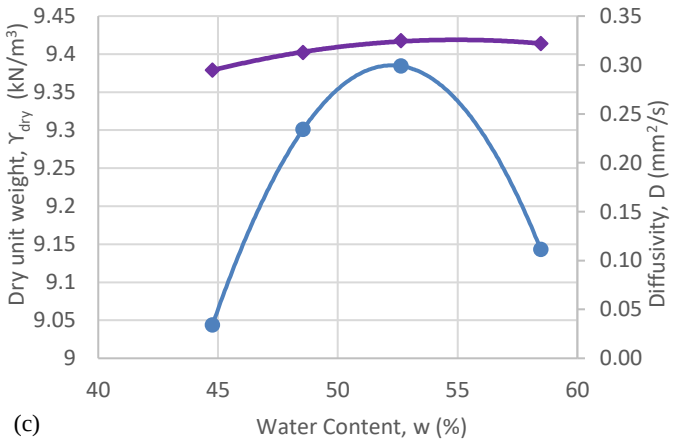
When glass fiber was used at the rate of 1%, it was obtained the highest thermal conductivity value with a value of 0.976 W/mK when Υ_{dry} was 9.26 kN/m^3 and w = 56.7%. Its volumetric specific heat capacity was 3.081 MJ/m^{3}K and its diffusivity value was 0.326 mm^2/s. While the thermal conductivity value reached its highest value at 56.7% water content (Figure 5.12a), the volumetric heat capacity continued to increase continuously (Figure 5.12b). In the diffusivity value (Figure 5.12c), it reached its highest value at 55% water content, but the diffusivity values were quite close to each other.



(a)



(b)



(c)

Figure 5.12 Variation of thermal properties of BGF according to the compaction curve a) Thermal conductivity b) Volumetric heat capacity c) Diffusivity

5.2 Thermal Properties of Sand-Bentonite Mixtures Depending on Proctor Curve

In sandy soils, thermal conductivity and volumetric heat capacity are expected to behave similarly to bentonite mixtures. It is expected that the values increase as the water content and dry unit weight increase and then decreases at wet side of optimum. It is expected that the diffusivity values will reach peak and then decrease and the diffusivity value will continue close to decreased value.

For SB10 mixture while at the highest thermal conductivity value (2.134 W/mK), the water content was 17.9%, Υ_{dry} was 16.52 kN/m^3, volumetric specific heat capacity was 2.550 MJ/m^{3}K and diffusivity was 0.828 mm^2/s. For the highest diffusivity value (0.835 mm^2/s), the water content was 15.5%, Υ_{dry} was 16.83 kN/m^3, thermal conductivity was 2.082 W/mK and volumetric specific heat capacity was 2.518 MJ/m^{3}K. The reason why the diffusivity (Figure 5.13c) value was higher at low water content is due to the difference in the amount of increase in thermal conductivity (Figure 5.13a) and volumetric heat capacity (Figure 5.13b).

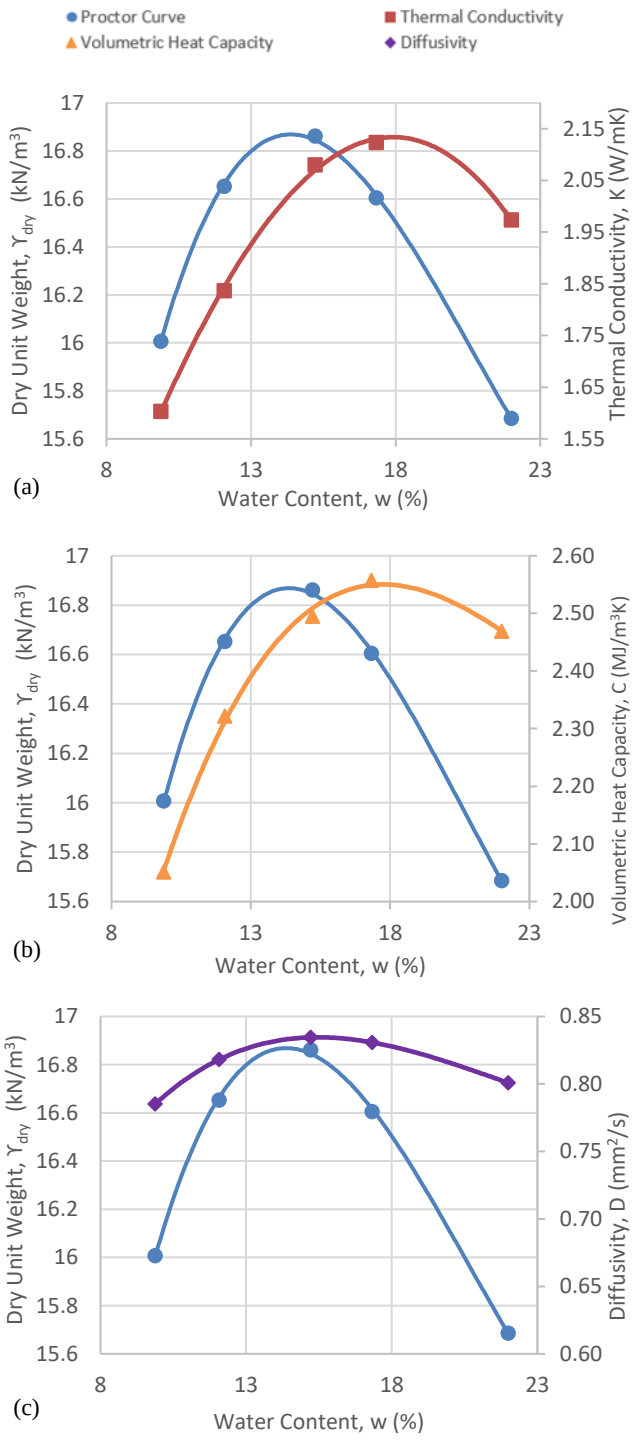


Figure 5.13 Variation of thermal properties of SB10 according to the compaction curve a) Thermal conductivity b) Volumetric heat capacity c) Diffusivity

5.2.1 Thermal Properties of SB10 Depending on Proctor Curve in their Presence of Boron Minerals

The optimum thermal properties of SB10U10 were obtained while Υ_{dry}=17.05 kN/m^3 and w=16.6%. Thermal conductivity value was 2.198 W/mK, volumetric specific heat capacity was 2.645 MJ/m^{3}K and diffusivity was 0.841 mm^2/s. While the highest thermal conductivity (Figure 5.14a) and diffusivity (Figure 5.14c) values were obtained at the same water content, the volumetric heat capacity (Figure 5.14b) continued to increase up to 17.5% water content and then decreased somewhat.

For SB10U20 mixture while at the highest thermal conductivity value (2.019 W/mK), the water content was 17.5%, Υ_{dry} was 16.78 kN/m^3, volumetric specific heat capacity was 2.585 MJ/m^{3}K and diffusivity was 0.788 mm^2/s. For the highest diffusivity value (0.789 mm^2/s), the water content was 16.9%, Υ_{dry} was 16.97 kN/m^3, thermal conductivity was 2.013 W/mK and volumetric specific heat capacity was 2.570 MJ/m^{3}K. The highest diffusivity (Figure 5.15c) and thermal conductivity (Figure 5.15a) values occurred at different water content levels. But these values were quite close to each other. Thermal property values between 16.9% and 17.5% water content are the most ideal values for this mixture (Figure 5.15a, Figure 5.15b, Figure 5.15c).

The optimum thermal properties of SB10C10 were obtained while Υ_{dry}=17.57 kN/m^3 and w=15.5%. Thermal conductivity value was 2.026 W/mK, volumetric specific heat capacity was 2.590 MJ/m^{3}K and diffusivity was 0.789 mm^2/s. When colemanite was added to the 10% mixture, the highest thermal conductivity (Figure 5.16a) and diffusivity (Figure 5.16c) values were obtained at the same point. The volumetric heat capacity (Figure 5.16b), on the other hand, started to decrease after a while.

For SB10C20 mixture while at the highest thermal conductivity value (2.179 W/mK), the water content was 15.8%, Υ_{dry} was 17.43 kN/m^3, volumetric specific heat capacity was 2.397 MJ/m^{3}K and diffusivity was 0.926 mm^2/s. For the highest diffusivity value (0.949 mm^2/s), the water content was 13.9%, Υ_{dry} was 17.88 kN/m^3, thermal conductivity was 2.128 W/mK and volumetric specific heat capacity was

2.254 MJ/m^{3}K. While the thermal conductivity (Figure 5.17a) and diffusivity (Figure 5.17c) values reached their peak values in the SB10C20 mixture, the volumetric heat capacity (Figure 5.17b) continued to increase continuously.

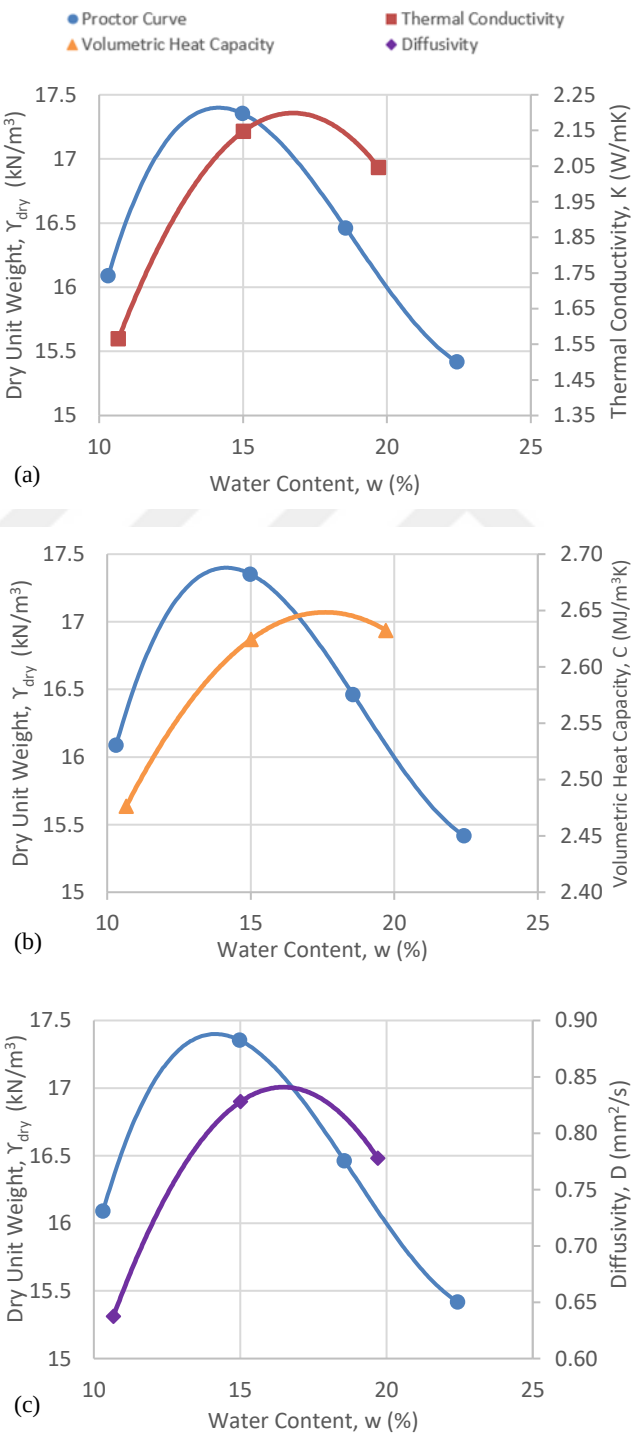


Figure 5.14 Variation of thermal properties of SB10U10 according to the compaction curve a) Thermal conductivity b) Volumetric heat capacity c) Diffusivity

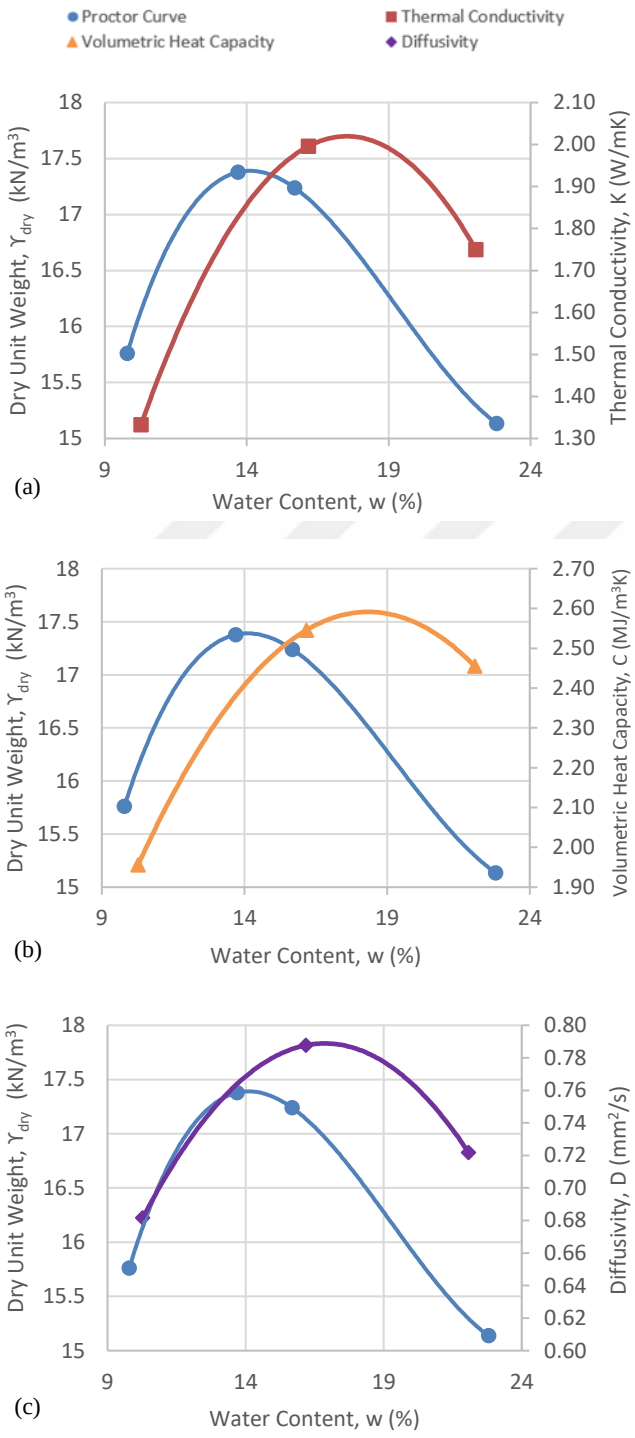


Figure 5.15 Variation of thermal properties of SB10U20 according to the compaction curve a) Thermal conductivity b) Volumetric heat capacity c) Diffusivity

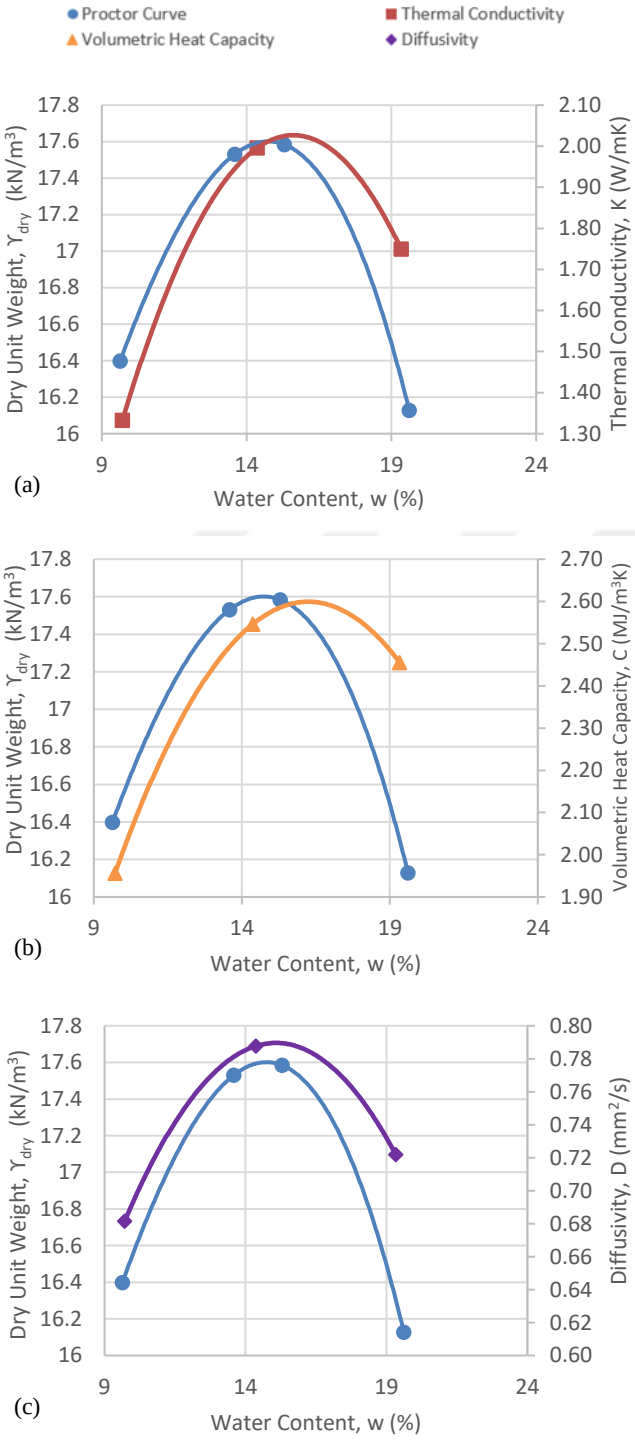


Figure 5.16 Variation of thermal properties of SB10C10 according to the compaction curve a) Thermal conductivity b) Volumetric heat capacity c) Diffusivity

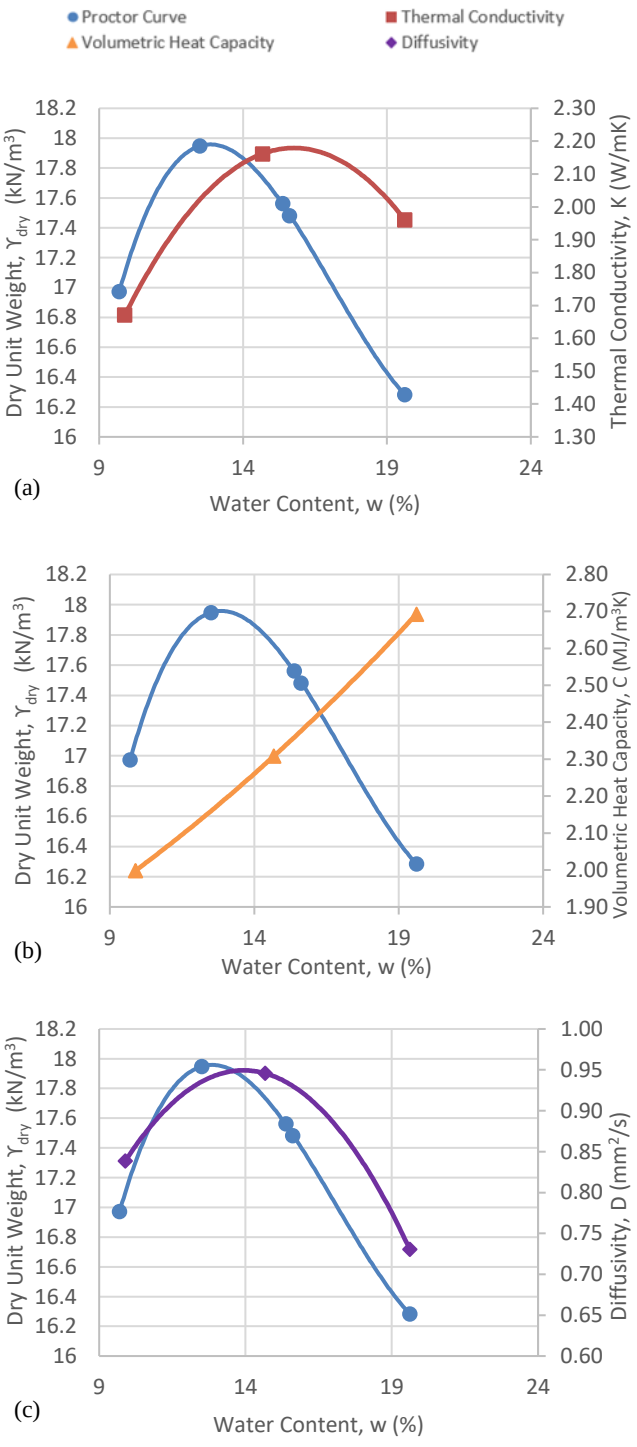


Figure 5.17 Variation of thermal properties of SB10C20 according to the compaction curve a) Thermal conductivity b) Volumetric heat capacity c) Diffusivity

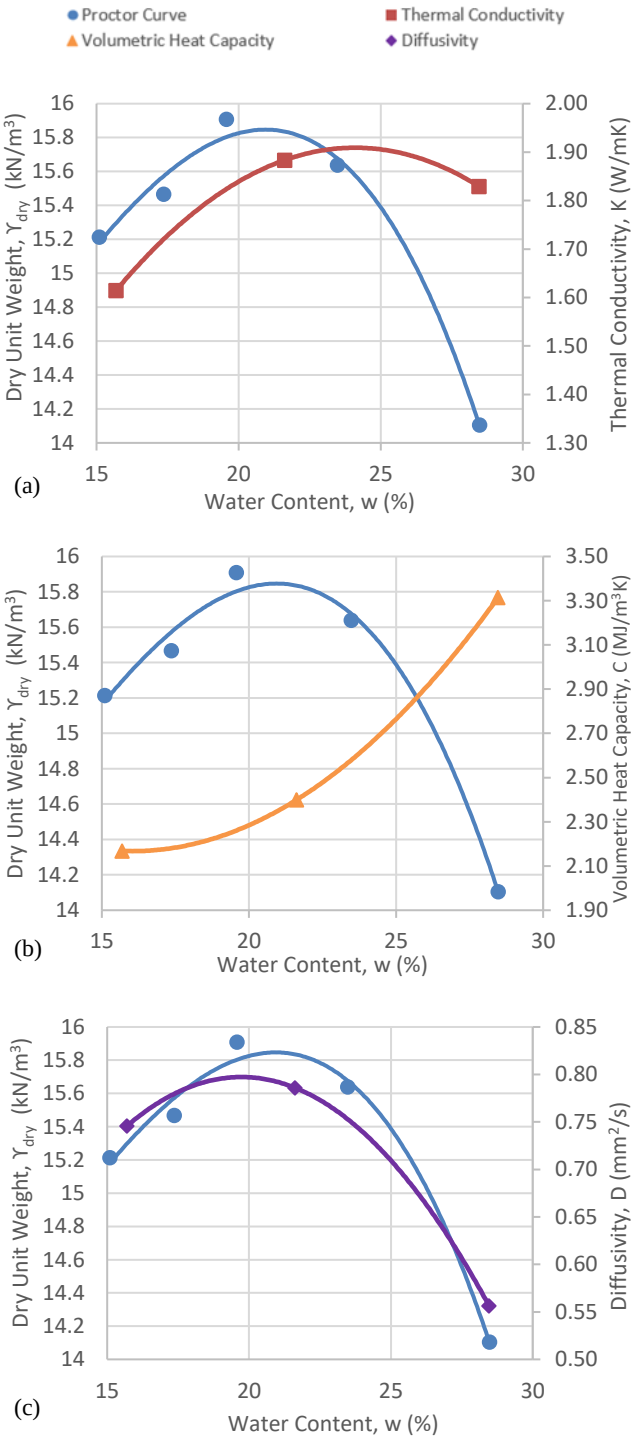


Figure 5.18 Variation of thermal properties of SB10E4810 according to the compaction curve a) Thermal conductivity b) Volumetric heat capacity c) Diffusivity

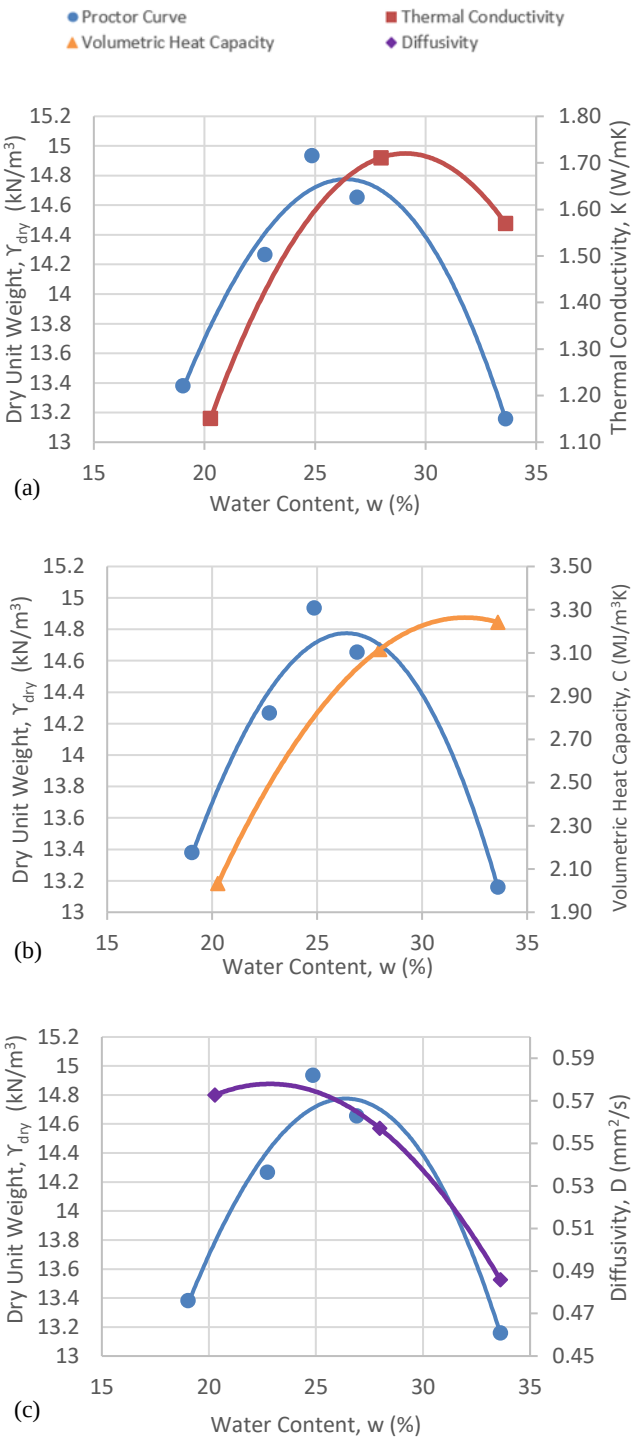


Figure 5.19 Variation of thermal properties of SB10E4820 according to the compaction curve a) Thermal conductivity b) Volumetric heat capacity c) Diffusivity

For SB10E4810 mixture while at the highest thermal conductivity value (1.909 W/mK), the water content was 24.1%, Υ_{dry} was 15.58 kN/m^3, volumetric specific heat capacity was 2.651 MJ/m^{3}K and diffusivity was 0.737 mm^2/s. For the highest

diffusivity value (0.797 mm^2/s), the water content was 19.1%, Υ_{dry} was 15.81 kN/m^3, thermal conductivity was 1.828 W/mK and volumetric specific heat capacity was 2.267 MJ/m^3K. In the SB10E4810 mixture, the water contents, where the highest diffusivity and thermal conductivity (Figure 5.18b) were obtained, they were quite far from each other. While the diffusivity value was obtained on the dry side of the optimum (Figure 5.18c), the highest thermal conductivity value occurred on the wet side of the optimum (Figure 5.18a). The volumetric heat capacity (Figure 5.18b), on the other hand, continued to increase continuously.

For SB10E4820 mixture while at the highest thermal conductivity value (1.720 W/mK), the water content was 29.1%, Υ_{dry} was 14.56 kN/m^3, volumetric specific heat capacity was 3.186 MJ/m^3K and diffusivity was 0.588 mm^2/s.

The SB10E4820 mixture showed similar behavior with the SB10E4810 mixture. The highest thermal conductivity value was obtained on the wet side of the optimum (Figure 5.19a), while the highest diffusivity value was obtained on the dry side of the optimum (Figure 5.19c). It was seen that the volumetric heat capacity started to decrease towards the end (Figure 5.19b).

In boron mixtures, the highest thermal conductivity and diffusivity values of the mixtures with a higher fine ratio (or lower mean particle size) occurred on the wet side of the optimum, while the highest diffusivity value occurred on the dry side of the optimum with a decrease in the fine grain ratio.

5.2.2 Thermal Properties of SB10 Depending on Proctor Curve in their Presence of Slags

For SB10CS10 mixture while at the highest thermal conductivity value (2.196 W/mK), the water content was 19.3%, Υ_{dry} was 17.00 kN/m^3, volumetric specific heat capacity was 2.897 MJ/m^3K and diffusivity was 0.714 mm^2/s. For the highest diffusivity value (0.826 mm^2/s), the water content was 12.00%, Υ_{dry} was 17.16 kN/m^3, thermal conductivity was 1.833 W/mK and volumetric specific heat capacity was 2.415 MJ/m^3K.

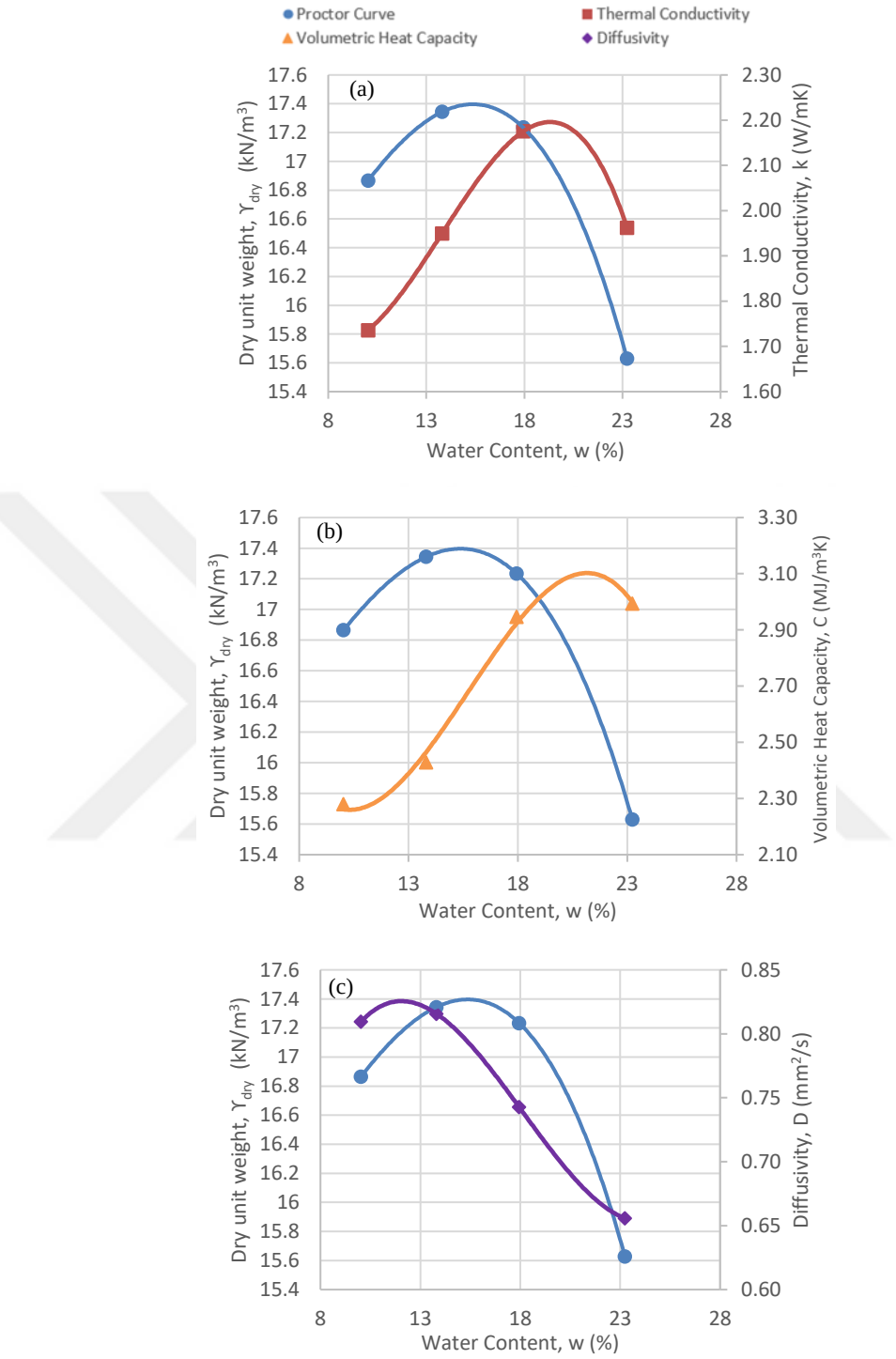


Figure 5.20 Variation of thermal properties of SB10CS10 according to the compaction curve a) Thermal conductivity b) Volumetric heat capacity c) Diffusivity

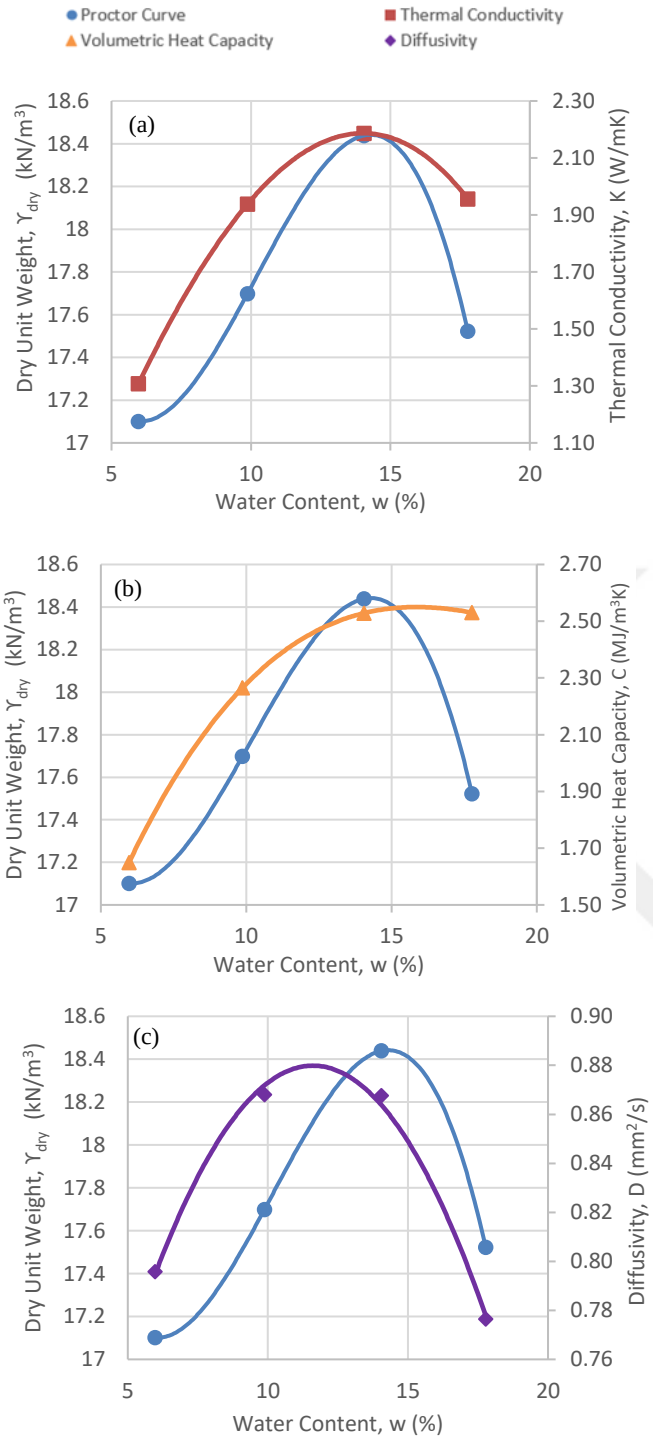


Figure 5.21 Variation of thermal properties of SB10CS20 according to the compaction curve a) Thermal conductivity b) Volumetric heat capacity c) Diffusivity

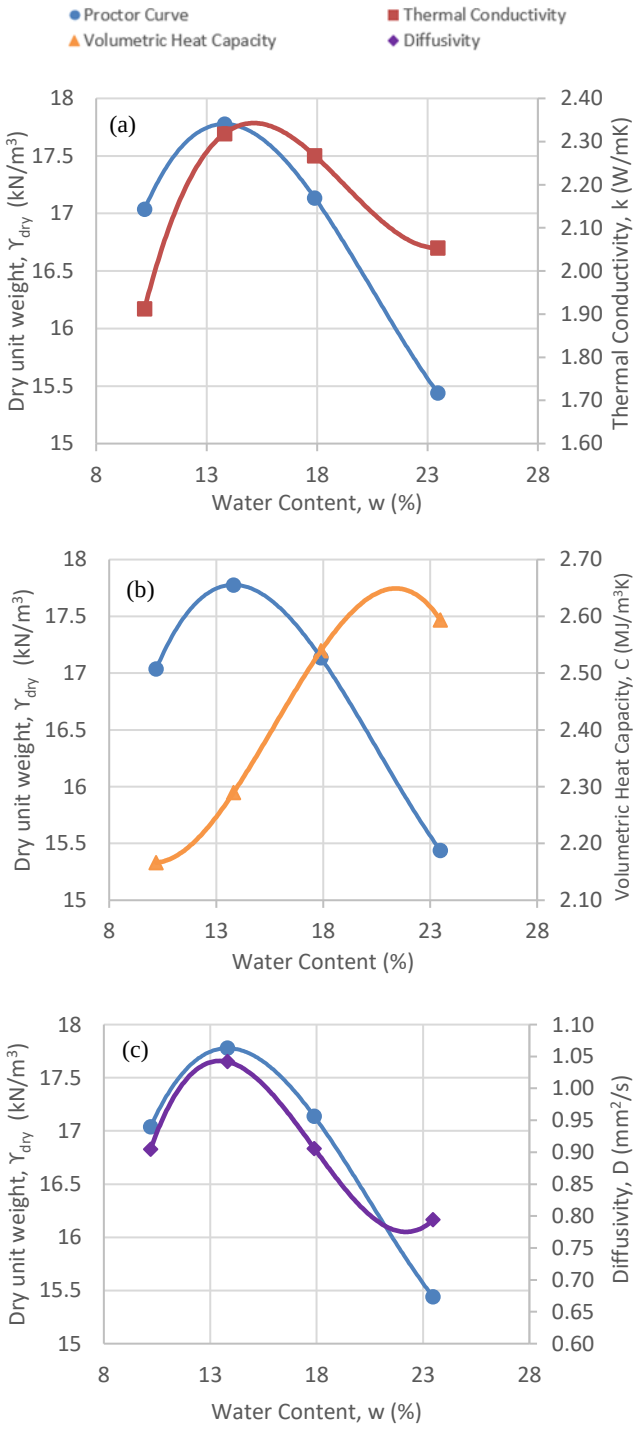


Figure 5.22 Variation of thermal properties of SB10FS10 according to the compaction curve a) Thermal conductivity b) Volumetric heat capacity c) Diffusivity

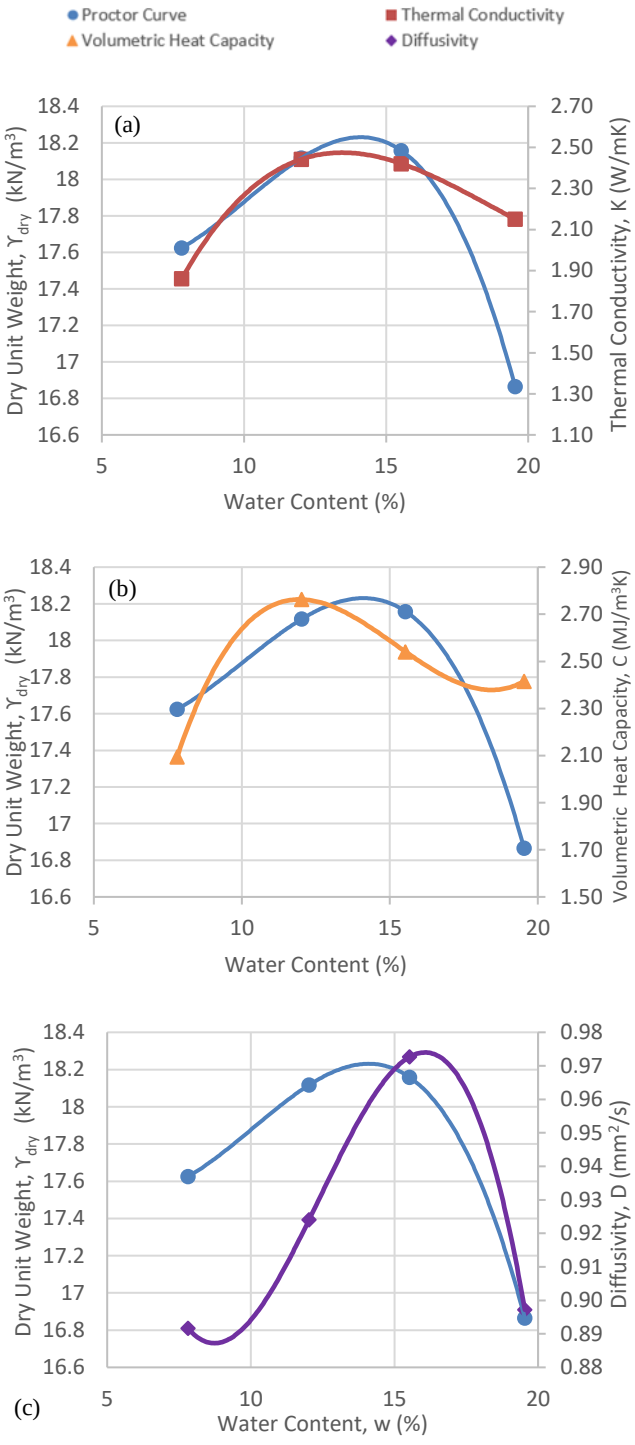


Figure 5.23 Variation of thermal properties of SB10FS20 according to the compaction curve a) Thermal conductivity b) Volumetric heat capacity c) Diffusivity

For SB10CS20 mixture while at the highest thermal conductivity value (2.187 W/mK), the water content was 14.0%, Υ_{dry} was 18.44 kN/m^3, volumetric specific heat capacity was 2.527 MJ/m^{3}K and diffusivity was 0.868 mm^2/s. For the highest

diffusivity value (0.880 mm^2/s), the water content was 12.0%, Υ_{dry} was 18.19 kN/m^3, thermal conductivity was 2.126 W/mK and volumetric specific heat capacity was 2.442 MJ/m^3K. While the highest thermal conductivity (Figure 5.20a) and diffusivity (Figure 5.20c) values were found on the opposite sides of the optimum in the mixtures where 10% copper slag was used, both values (Figure 5.21a and Figure 5.21c) were on the dry side of the optimum in the mixtures with 20% additives. On the other hand, the volumetric heat capacities continued to increase and started to decrease on the wet side of the optimum water content (Figure 5.20b and Figure 5.21b).

For SB10FS10 mixture while at the highest thermal conductivity value (2.453 W/mK), the water content was 15.4%, Υ_{dry} was 17.66 kN/m^3, volumetric specific heat capacity was 2.387 MJ/m^3K and diffusivity was 1.009 mm^2/s. For the highest diffusivity value (1.043 mm^2/s), the water content was 13.40%, Υ_{dry} was 17.77 kN/m^3, thermal conductivity was 2.397 W/mK and volumetric specific heat capacity was 2.267 MJ/m^3K.

For SB10FS20 mixture while at the highest thermal conductivity value (2.474 W/mK), the water content was 13.5%, Υ_{dry} was 18.22 kN/m^3, volumetric specific heat capacity was 2.698 MJ/m^3K and diffusivity was 0.953 mm^2/s. For the highest diffusivity value (0.973 mm^2/s), the water content was 15.80%, Υ_{dry} was 18.13 kN/m^3, thermal conductivity was 2.408 W/mK and volumetric specific heat capacity was 2.520 MJ/m^3K. 10% and 20% of ferrochrome additives behave opposite to each other. While the highest thermal conductivity value from the 10% added mixture was on the wet side of the optimum (Figure 5.22a), the highest diffusivity value was obtained on the dry side of the optimum (Figure 5.22c). This situation was the opposite for the mixture with 20% additive (Figure 5.23a and Figure 5.23c). SB10FS10 mixture's volumetric heat capacity decreased after optimum water content (Figure 5.22b). However, the volumetric heat capacity of the SB10FS20 mixture started to decrease on the dry side of the optimum (Figure 5.23b).

It was seen that the highest thermal conductivity value shifts to the dry side of the optimum as the fine grain ratio increases in the slag mixtures, while the highest thermal conductivity value shifts to the wet side of the optimum.

5.2.3 Thermal Properties of SB10 Depending on Proctor Curve in their Presence of Fiber Glass

For SB10GF mixture while at the highest thermal conductivity value (1.912 W/mK), the water content was 20.0%, Υ_{dry} was 16.42 kN/m^3, volumetric specific heat capacity was 2.339 MJ/m^{3}K and diffusivity was 0.814 mm^2/s.

When glass fiber additive was used, it was seen that the thermal conductivity (Figure 5.24a) and volumetric heat capacity (Figure 5.24b) reach a peak value on the wet side of the optimum and then decrease, while it was seen that the diffusivity (Figure 5.24c) value decreases continuously from the highest value on the dry side of the optimum.

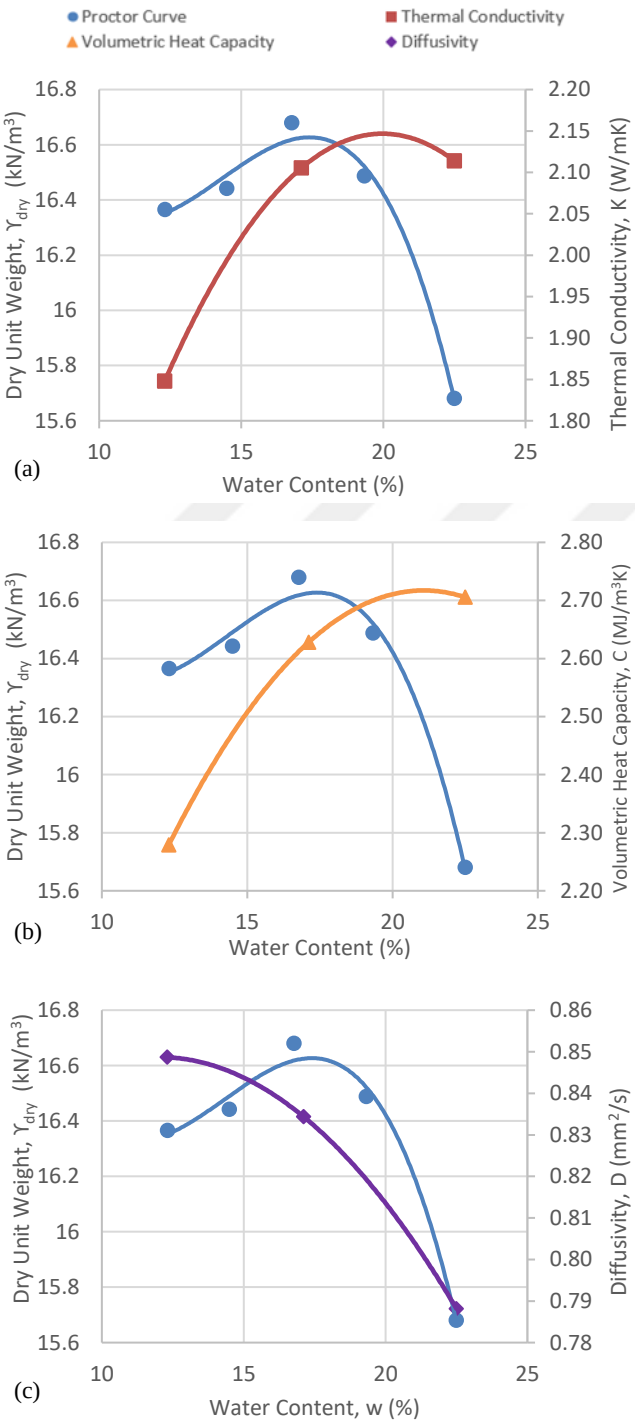


Figure 5.24 Variation of thermal properties of SB10GF according to the compaction curve a) Thermal conductivity b) Volumetric heat capacity c) Diffusivity

CHAPTER 6
THERMAL CONDUCTIVITY DEPENDING ON TEMPERATURE

6.1 Thermal Conductivity of Bentonite Depending on Temperature

Bentonite has a thermal conductivity value of 0.658 W/mK at 25 °C, 0.808 W/mK at 60 °C and 1.077 W/mK at 80 °C (Figure 6.1). The effects of the additives were examined by comparing them with these values. In the literature, it is reported that the changes in thermal conductivity up to 60 °C are negligible and low. For this reason, measurements were performed at 25 °C, 60 °C and 80 °C.

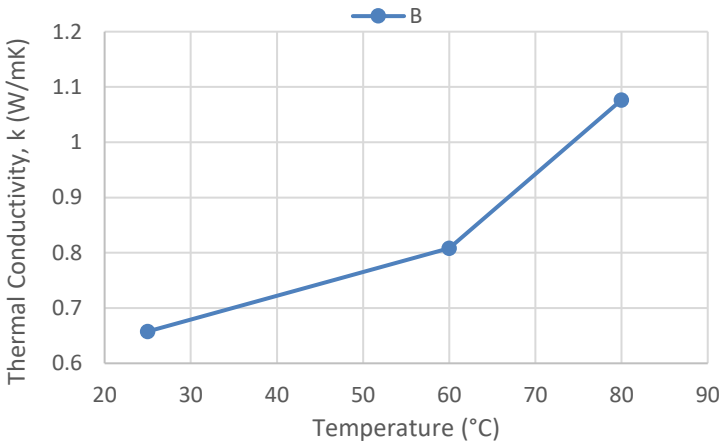


Figure 6.1 Variation of thermal conductivity of bentonite at different temperatures (S = 0.658 and e =1.769)

6.1.1 Thermal Conductivity of Bentonite-Boron Mixtures Depending on Temperature

Figure 6.2 shows the thermal conductivity values of boron added bentonite mixtures at different temperatures. Thermal conductivity values of ulexite and colemanite additives are very close to bentonite. Although the thermal conductivity value of

etibor48 at room temperature was close to bentonite, etibor48 caused a decrease in the thermal conductivity value as the temperature increased.

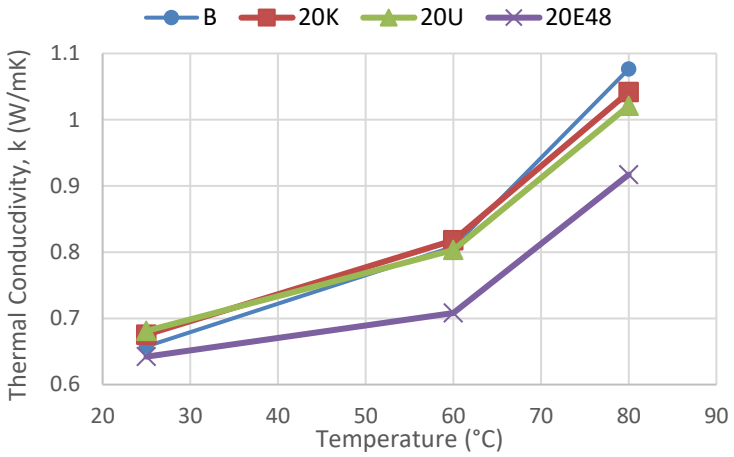


Figure 6.2 Variation of thermal conductivity of bentonite-boron mixtures at different temperatures (S = 0.658 and e =1.769)

6.1.2 Thermal Conductivity of Bentonite-Slag Mixtures Depending on Temperature

It was observed that when ferrochrome slag was used as an additive, it increased the thermal conductivity value at all temperatures as seen in Figure 6.3. However, the effect of copper slag was negligible (Figure 6.3).

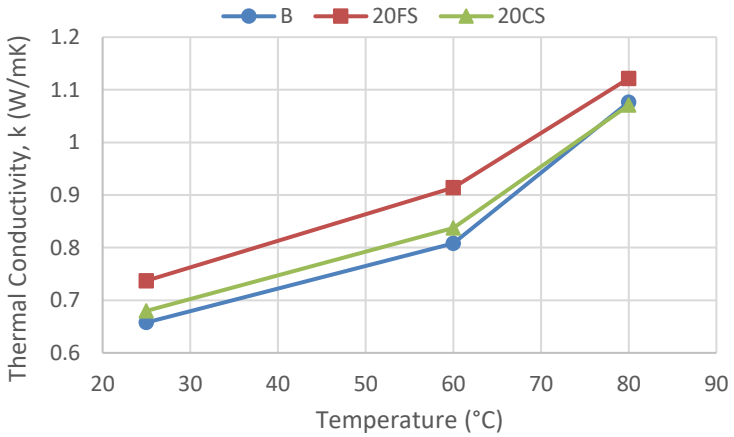


Figure 6.3 Variation of thermal conductivity of bentonite-slag mixtures at different temperatures (S = 0.658 and e =1.769)

6.1.3 Thermal Conductivity of Bentonite-Fiber Glass Mixture Depending on Temperature

It was observed that when the glass fiber added bentonite mixture (Figure 6.4), there was a slight decrease in the thermal conductivity value at 80 °C, while the effect of glass fiber was negligible at other temperatures.

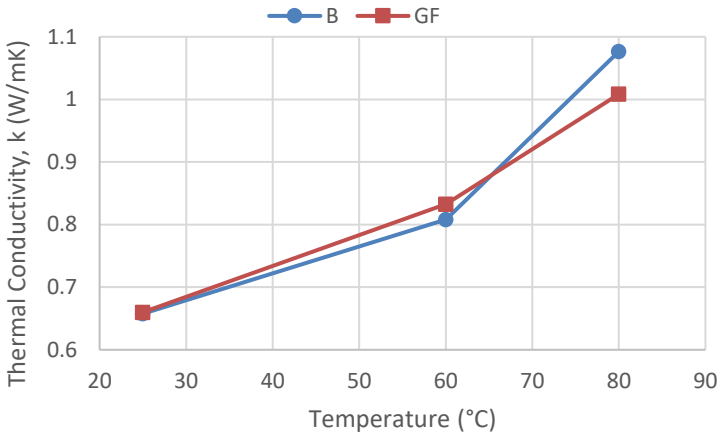


Figure 6.4 Variation of thermal conductivity of bentonite-glass fiber mixture at different temperatures (S = 0.658 and e =1.769)

6.2 Thermal Conductivity of Sand-Bentonite Mixtures Depending on Temperature

Figure 6.5 shows thermal conductivities of SB10, SB20 and SB30 mixtures. The thermal conductivity value of the SB10 mixture was 1.886 W/mK at 25 °C, 2.041 W/mK at 60 °C and 2.357 W/mK at 80 °C. SB20 has a thermal conductivity value of 1.589 W/mK at 25 °C, 1.704 W/mK at 60 °C and 1.900 W/mK at 80 °C. The SB30 has a thermal conductivity value of 1.386 W/mK at 25 °C, 1.510 W/mK at 60 °C and 1.817 W/mK at 80 °C.

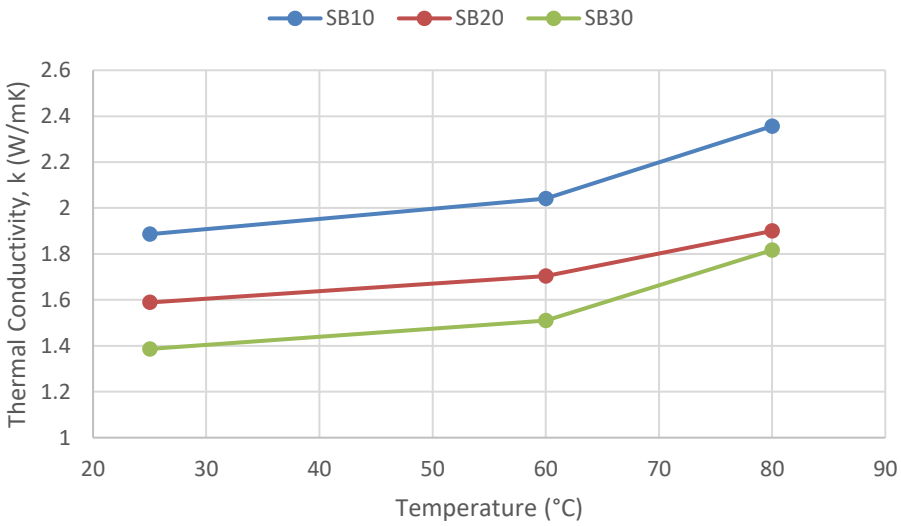


Figure 6.5 Variation of thermal conductivity of SB10 (S = 0.606 and e =0.564), SB20 (S = 0.602 and e =0.632) and SB30 (S = 0.617 and e =0.735) mixtures at different temperatures

6.2.1 Thermal Conductivity of Sand-Bentonite-Boron Mixtures Depending on Temperature

With etibor48 additive, the sample at constant void ratio and degree of saturation could not be prepared because it remained on the dry side of the compaction curve and did not comply with these values (Figure 4.4). It was observed that the thermal conductivity values decreased significantly in the compaction curve-thermal conductivity graphs (Figure 5.18 and Figure 5.19). For this reason, it was considered that there was no need to examine the effect of etibor48 additive here. It was seen that the thermal conductivity value of colemanite and ulexite additive was lower than that of the SB10 mixture at all temperatures (Figure 6.6). The structure of the soil changes with the addition of additives. Low thermal conductive boron minerals fill the voids of the soil together with bentonite. At the same time, the proportion of high thermal conductive sand decreases due to the method of mixture preparation. Mixtures with additives have a higher fine ratio than sand-bentonite mixtures without additives. For these reasons, it was thought that there was a decrease in thermal conductivity values. Colemanite additive showed higher thermal conductivity values than ulexite additive at all temperature values.

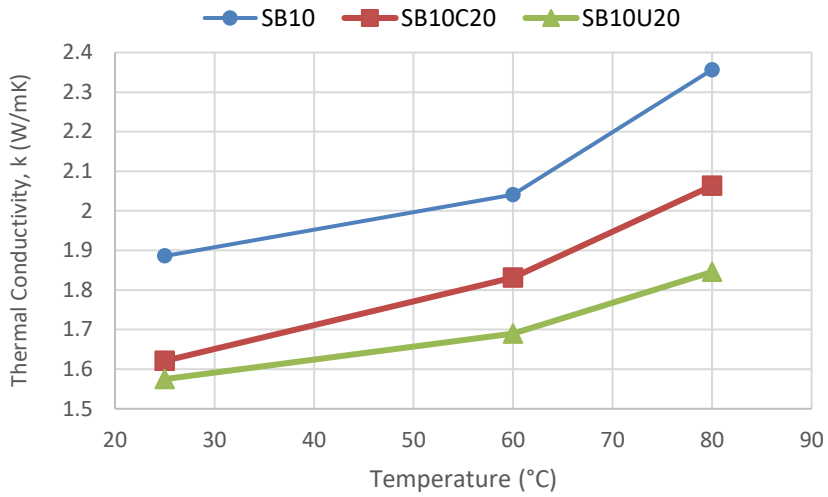


Figure 6.6 Variation of thermal conductivity of SB10-boron mixtures at different temperatures (S = 0.606 and e =0.564)

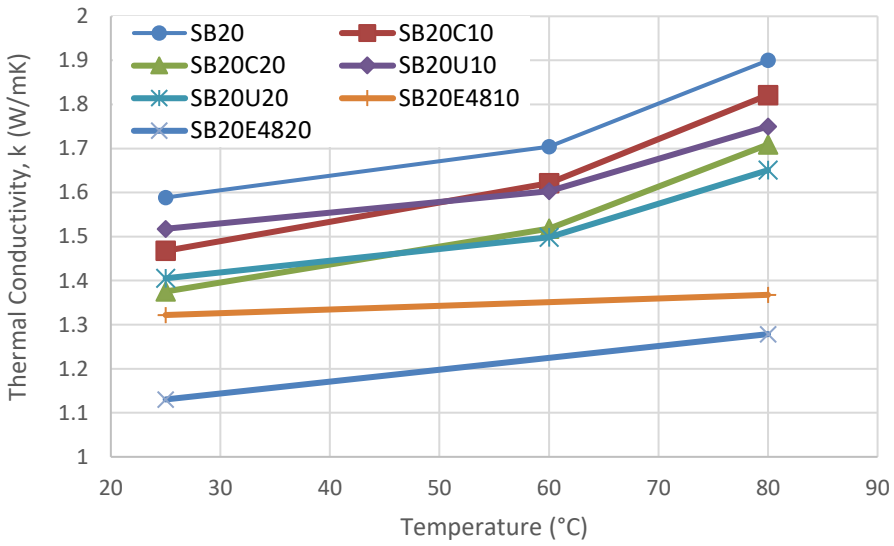


Figure 6.7 Variation of thermal conductivity of SB20-Boron mixtures at different temperatures (S = 0.602 and e =0.632)

Boron additives used in the SB20 mixture decreased the thermal conductivity values (Figure 6.7). When ulexite and colemanite were used as 10% additives at room temperature, the thermal conductivity values decreased by 4.5% and 7.6%, respectively. Thermal conductivity decreased 11.5% and 13.4% in mixtures with 20% additives. Etibor48, on the other hand, decreased the thermal conductivity value by 16.8% and 28.9% when 10% and 20% were added. Etibor48 significantly reduced the

thermal conductivity value at room temperature, and the negative effect of colemanite on thermal conductivity was more than ulexite.

When the temperature was increased to 60 °C, 10% of ulexite and 20% of ulexite decreased the thermal conductivity values by 5.9% and 12.1%, respectively. Colemanite decreased the thermal conductivity value by 4.9% and 10.9% in the mixtures with 10% and 20% additives. Contrary to room temperature, ulexite has a greater negative effect on thermal conductivity than colemanite at 60 °C. In addition, it was seen that the thermal conductivity values of 10% and 20% added ulexite and colemanite are very close to each other.

When the temperature was 80 °C, the behavior of boron minerals was similar to 60 °C. Colemanite exhibits better thermal conductivity behavior at high temperatures than ulexite. The difference between the SB20E4810's thermal conductivity at room temperature and 80 °C was 0.0458 W/mK. At 80 °C, Etibor48 shows very low thermal conductivity values. Despite SB20E4820 refining the thermal conductivity value of 0.148 W/mK at 80 °C, it has a very low thermal conductivity value compared to SB20 mixture. At 80 °C, the thermal conductivity values were reduced by 28% and 32.7% at 10% and 20% additive rates.

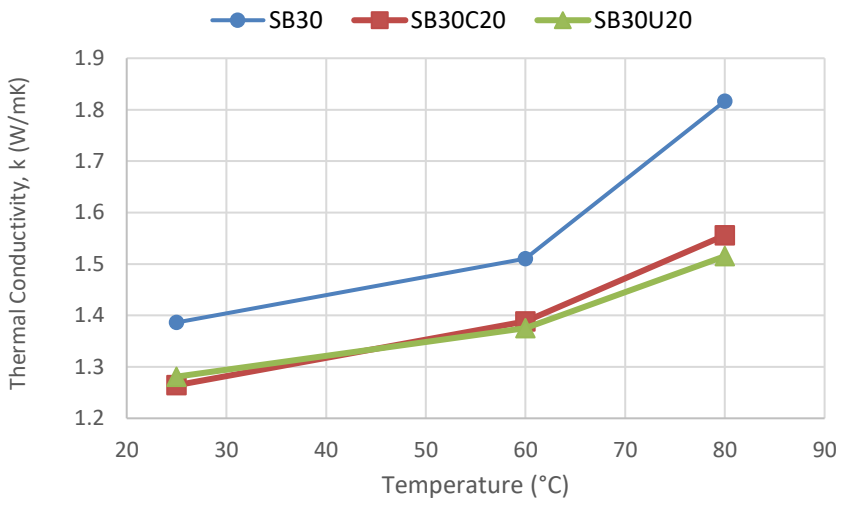


Figure 6.8 Variation of thermal conductivity of SB30-Boron mixtures at different temperatures (S = 0.617 and e =0.735)

The effects of ulexite and colemanite additives on thermal conductivity in SB30 mixtures were quite close to each other (Figure 6.8). While ulexite performed better at room temperature, colemanite performed better at higher temperatures. The same trend was seen in SB20 mixtures. An average of 8.2%, 8.5% and 15.5% decreases occurred on thermal conductivity values at room temperature, 60 °C and 80 °C, respectively.

6.2.2 Thermal Conductivity of Sand-Bentonite-Slag Mixtures Depending on Temperature

Ferrochrome slag increased the thermal conductivity in SB10 mixtures and copper slag decreased the thermal conductivity (Figure 6.9). Copper slag has a lower fine ratio and a narrower grain size range that can fill the voids compared to other mixtures except etibor48. In addition, the thermal conductivity value of the granular form of copper slag was lower than that of sand. On the other hand, ferrochrome slag the grain size range was wider and had a higher fine ratio than copper slag. While copper slag showed better results in the compaction curve, there was a slight decrease at constant volume and void ratio. Ferrochrome slag generally had a positive effect on thermal conductivity. It was thought that ferrochrome slag both fills the intergranular spaces better and has a higher thermal conductivity value as an additive, thus increasing the thermal conductivity.

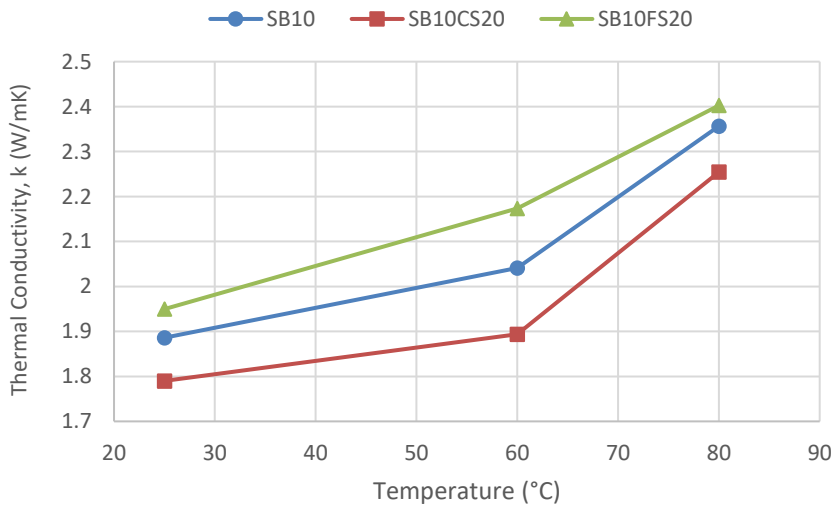


Figure 6.9 Variation of thermal conductivity of SB10-Slag mixtures at different temperatures (S = 0.606 and e =0.564)

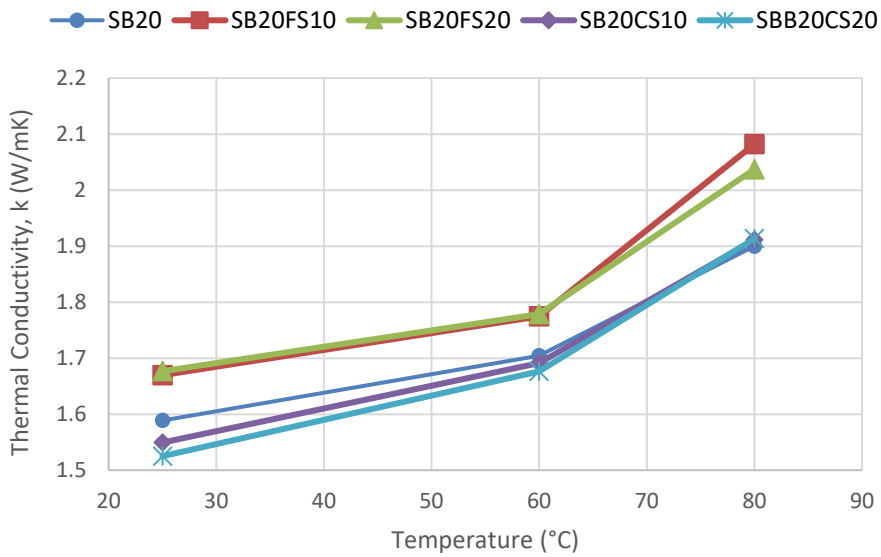


Figure 6.10 Variation of thermal conductivity of SB20-Slag mixtures at different temperatures (S = 0.602 and e =0.632)

In SB20 mixtures, while ferrochrome slag increases, it was seen that copper slag slightly affected the thermal conductivity values (Figure 6.10). 10% Ferrochrome slag increased the thermal conductivity value by 5.1%, 4.1% and 9.6% at room temperature at 60 °C and 80 °C, respectively. When ferrochrome was used as 20% additive, it increased the thermal conductivity values of 5.5%, 4.3% and 7.2% at room temperature, 60 °C and 80 °C, respectively. Copper slag slightly reduced the thermal conductivity value when used as 10% and 20% additives at room temperature and 60 °C, while it showed approximately the same values at 80 °C.

Figure 6.11 shows thermal conductivitiy values of slag added SB30 mixtures at different temperatures. While the effect of slags in SB30 mixtures showed similar behavior at room temperature and 60 °C, the thermal conductivity of the SB30FS20 at 80 °C fell below the SB30. Ferrochrome slag increased the thermal conductivities by 5.9% at room temperature and 60 °C and decreased by 1.8% at 80 °C. Copper slag decreased the thermal conductivity values by 3.7%, 1.9% and 6.9% at room temperature, 60 °C and 80 °C, respectively.

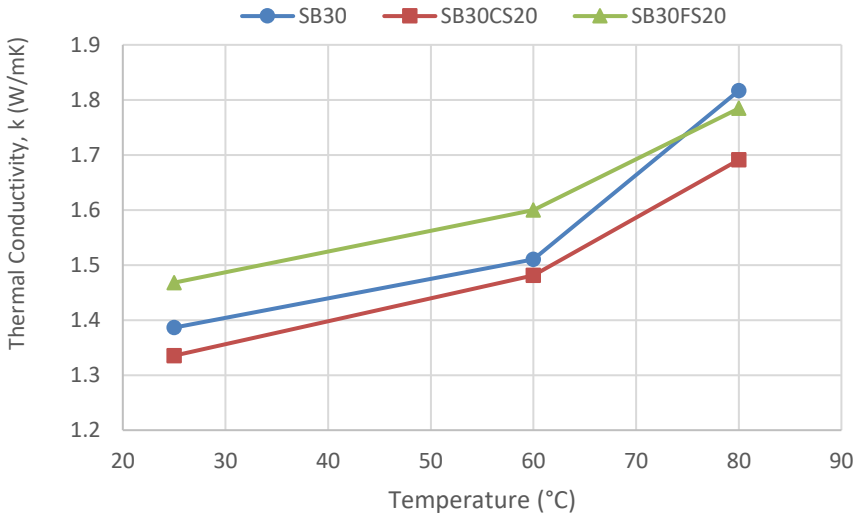


Figure 6.11 Variation of thermal conductivity of SB30-Slag mixtures at different temperatures (S = 0.617 and e =0.735)

6.2.3 Thermal Conductivity of Sand-Bentonite-Fiber Glass Mixtures Depending on Temperature

The thermal conductivity values of the SB10GF mixture were very close to the SB10 mixture at all temperatures (Figure 6.12). The effect was thought to be low due to the very low additive percent. In SB20 mixtures, unlike the glass fiber SB10GF mixture, the thermal conductivity value decreased by 4.3% and 3% at room temperature and 60 °C as seen in Figure 6.13. The thermal conductivity values were very close to each other at 80 °C. In glass fiber added SB30 mixtures, an average of 3.4% decrease occurred in all temperature values (Figure 6.14).

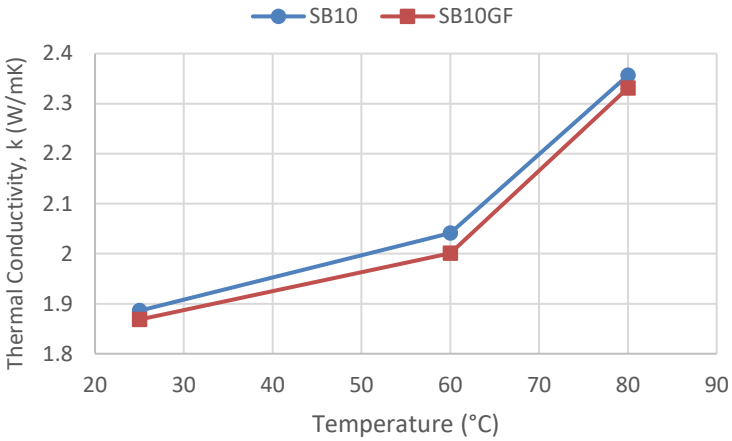


Figure 6.12 Variation of thermal conductivity of SB10-Glass Fiber mixture at different temperatures (S = 0.606 and e =0.564)

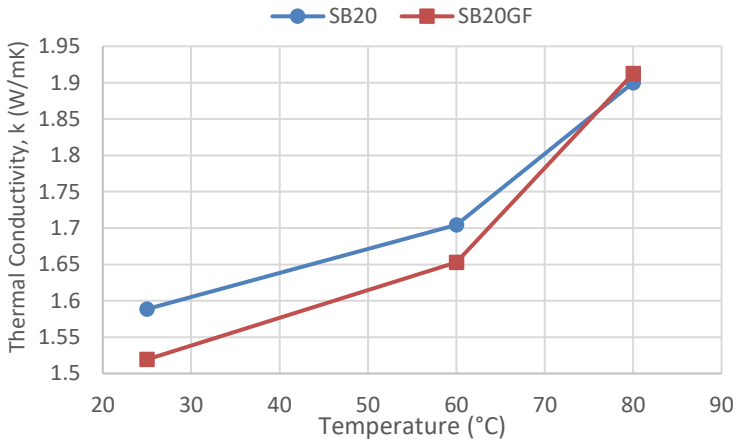


Figure 6.13 Variation of thermal conductivity of SB20-Glass Fiber mixture at different temperatures (S = 0.602 and e =0.632)

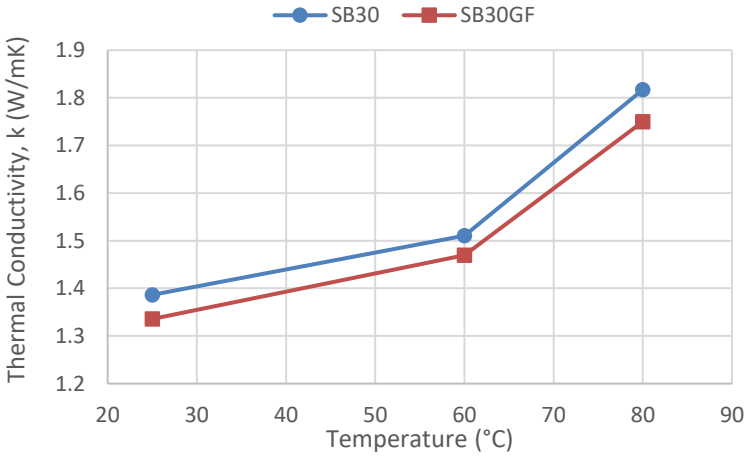


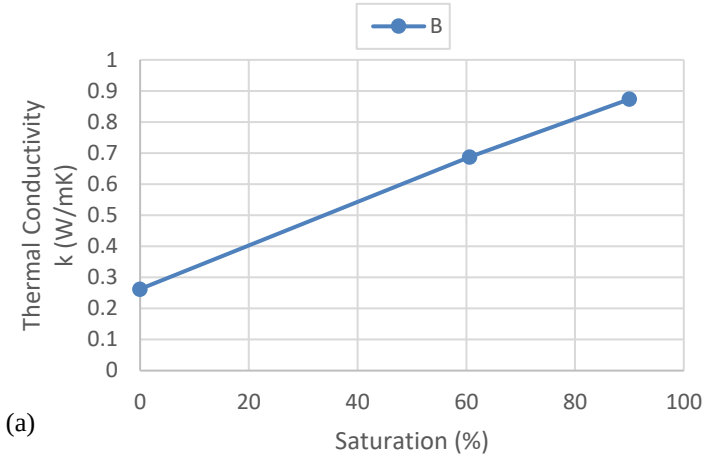
Figure 6.14 Variation of thermal conductivity of SB30-Glass Fiber mixture at different temperatures (S = 0.617 and e =0.735)

CHAPTER 7
THERMAL PROPERTIES DEPENDING ON SATURATION

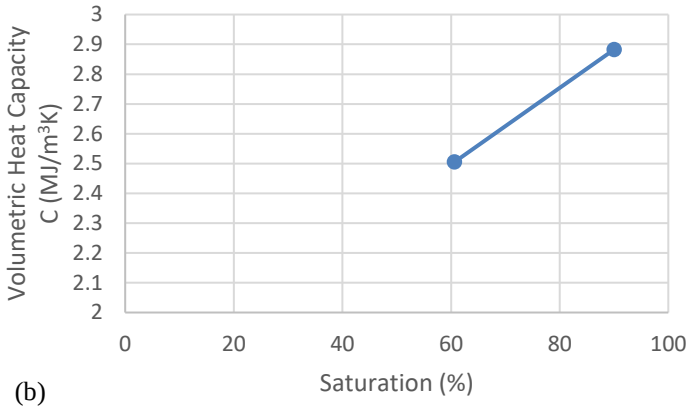
Measurements depending on the degree of saturation are based on the values of the SH-3 sensor. However, the TR-3 sensor was also used in the measurements. The differences between the two sensors were in acceptable range. Measurements could not be taken from the SH-3 sensor due to the shrinkage of the bentonite samples when they dried. When bentonite shrinks, the distance between the two holes gets shorter. These results in the probes being unable to penetrate the holes of the sample. When the guides were inserted into the holes, the bentonite samples compressed the guide after drying. When the guides are removed, the sample disintegrated. For this reason, only thermal conductivity values of dry bentonite samples will be given. At other saturation levels, also the volumetric heat capacity and diffusivity values will be given.

7.1 Thermal Properties of Bentonite Depending on Saturation

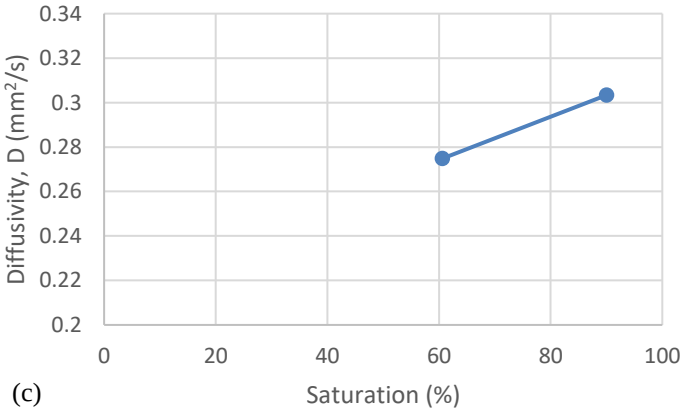
Thermal properties of bentonite are given in Figure 7.1. Bentonite has a value of 0.2646 W/mK in dry form. When the degree of saturation was 65.8%, the thermal conductivity value of bentonite was 0.658 W/mK, the volumetric heat capacity was 2.505 MJ/m^{3}K, and the diffusivity value was 0.275 mm^2/s. At 90% saturation, the thermal conductivity, volumetric heat capacity and dwassipation values are 0.874 W/mK, 2.882 MJ/m^{3}K and 0.303 mm^2/s, respectively.



(a)



(b)



(c)

Figure 7.1 Variation of thermal properties of bentonite at different degrees of saturation (e = 1.769) a) Thermal conductivity b) Volumetric heat capacity c) Diffusivity

7.1.1 Thermal Properties of Bentonite-Boron Mixtures Depending on Saturation

The thermal conductivity values of boron added bentonite mixtures were very close to each other at the measured saturation degrees (Figure 7.2a). At 65.8% saturation,

ulexite had the lowest volumetric heat capacity, while the volumetric heat capacities of colemanite and etibor48 were quite close to the volumetric heat capacity of bentonite as seen in Figure 7.2b. When the diffusivity values (Figure 7.2c) were considered, it was seen that the lowest diffusivity value was in etibor48, the highest diffusivity value was in ulexite, followed by colemanite. At 90% saturation (Figure 7.2b), the lowest volumetric heat capacity belonged to colemanite, the volumetric heat capacities of bentonite and ulexite were very close to each other, and the mixture of etibor48 had the highest volumetric heat capacity. Considering the diffusivity values (Figure 7.2c), etibor48 had the lowest diffusivity, while colemanite and ulexite had the highest diffusivity values, which were quite close to each other. Although the effect of boron additives on thermal conductivity was negligible (Figure 7.2a), differences occurred in diffusivity due to changing the volumetric heat capacities (Figure 7.2b). It was seen that while etibor48 reduced the diffusivity, ulexite and colemanite increased the diffusivity (Figure 7.2c).

7.1.2 Thermal Properties of Bentonite-Slag Mixtures Depending on Saturation

The thermal conductivity values of the slag mixtures in the dry state were quite close to the thermal conductivity value of bentonite (Figure 7.3a). At medium saturation, the thermal conductivity values of slag mixtures were very close to bentonite, also the thermal conductivity values of the slags were higher than bentonite (Figure 7.3a). Volumetric heat capacities were also very close to each other (Figure 7.3b). When the diffusivity values are compared (Figure 7.3c), bentonite had the lowest diffusivity value, while ferrochrome slag had the highest diffusivity value. In the high saturation degree (Figure 7.3a), the thermal conductivity values were close to each other as in the other saturation degrees, the thermal conductivity of the slags was slightly higher than the bentonite, as in medium saturation. Also, volumetric heat capacities were very close to each other, as at medium saturation levels (Figure 7.3b). In the diffusivity values (Figure 7.3c), the highest diffusivity value was the ferrochrome slag additive with 0.338 mm^2/s, and copper slag was followed by 0.320 mm^2/s diffusivity (Figure 7.3c).

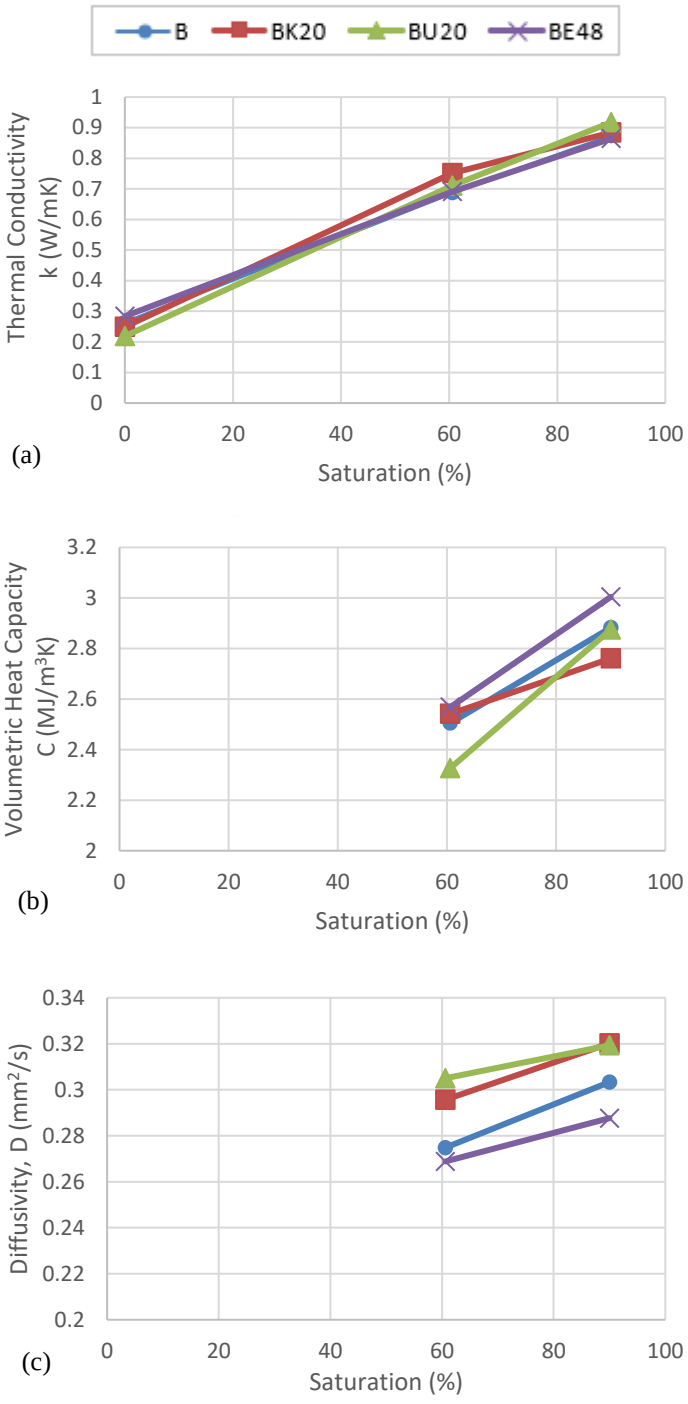
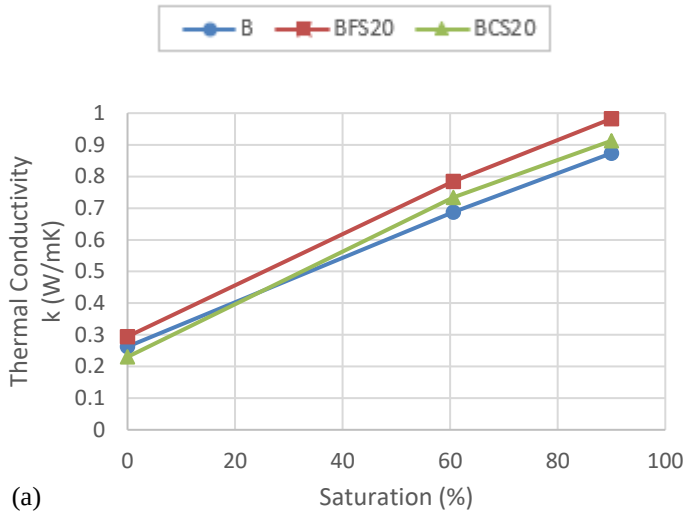
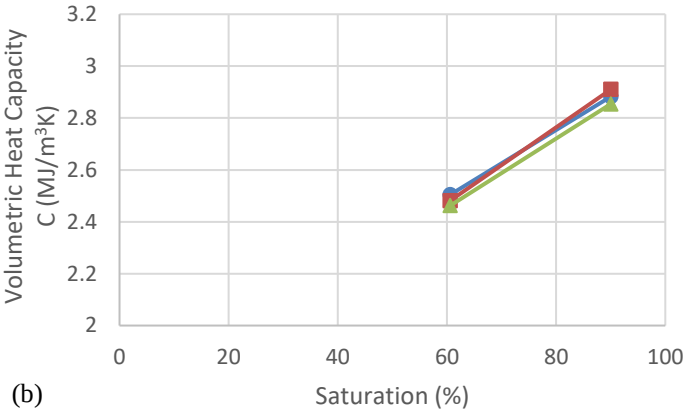


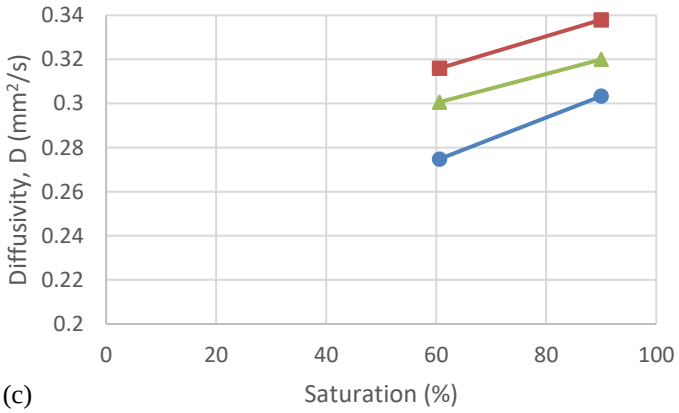
Figure 7.2 Variation of thermal properties of bentonite-boron mixtures at different degrees of saturation (e = 1.769) a) Thermal conductivity b) Volumetric heat capacity c) Diffusivity



(a)



(b)



(c)

Figure 7.3 Variation of thermal properties of bentonite-slag mixtures at different degrees of saturation (e = 1.769) a) Thermal conductivity b) Volumetric heat capacity c) Diffusivity

7.1.3 Thermal Properties of Bentonite-Fiber Glass Mixture Depending on Saturation

The thermal conductivity values of the glass fiber additive at all saturation degrees were remarkably close to each other (Figure 7.4a). At medium saturation (Figure 7.4b), the volumetric heat capacity of glass fiber was lower than that of bentonite, but the opposite was true for high saturation degrees. This situation in the volumetric heat capacity resulted in higher diffusivity of BGF at medium saturation degree and higher diffusivity of bentonite at high saturation degree (Figure 7.4c).

7.2 Thermal Properties of Sand-Bentonite Mixtures Depending on Saturation

Figure 7.5 shows thermal properties of SB10 mixture. The SB10 mixture had a thermal conductivity value of 0.703 W/mK, a volumetric heat capacity of 1.247 MJ/m^{3}K and a diffusivity value of 0.566 mm^2/s in dry condition. When the saturation degree increased to 60.6%, the thermal conductivity value reached 1.895 W/mK, the volumetric heat capacity reached 2.105 MJ/m^{3}K, and the diffusivity value reached 0.902 mm^2/s. The highest diffusivity value was obtained at medium saturation. At 90% saturation, the thermal conductivity showed the highest value of 2.175 W/mK, the volumetric heat capacity continued to increase and reached the value of 2.534 MJ/m^{3}K, and the diffusivity value decreased to 0.882 mm^2/s.

Thermal properties of SB20 mixture are given in Figure 7.5. The SB20 mixture had a thermal conductivity value of 0.586 W/mK, a volumetric heat capacity of 1.319 MJ/m^{3}K and a diffusivity value of 0.447 mm^2/s in dry condition. When the saturation degree increased to 60.2%, the thermal conductivity value reached 1.569 W/mK, the volumetric heat capacity reached 1.963 MJ/m3K, and the diffusivity value reached 0.820 mm^2/s. The highest diffusivity value was obtained at medium saturation. At 90% saturation, the thermal conductivity showed the highest value of 1.858 W/mK, the volumetric heat capacity continued to increase and reached the value of 2.271 MJ/m^{3}K, and the diffusivity value decreased to 0.832 mm^2/s. It was seen that the thermal conductivity values decreased at all saturation degrees with the increase in the bentonite ratio. Likewise, the volumetric heat capacity was lower than the SB10 mixtures. When the diffusivity values were compared, it was seen that SB20 mixture

had lower diffusivity than the SB10 mixtures, but in the SB20 mixtures, the highest diffusivity value was obtained at 90% saturation.

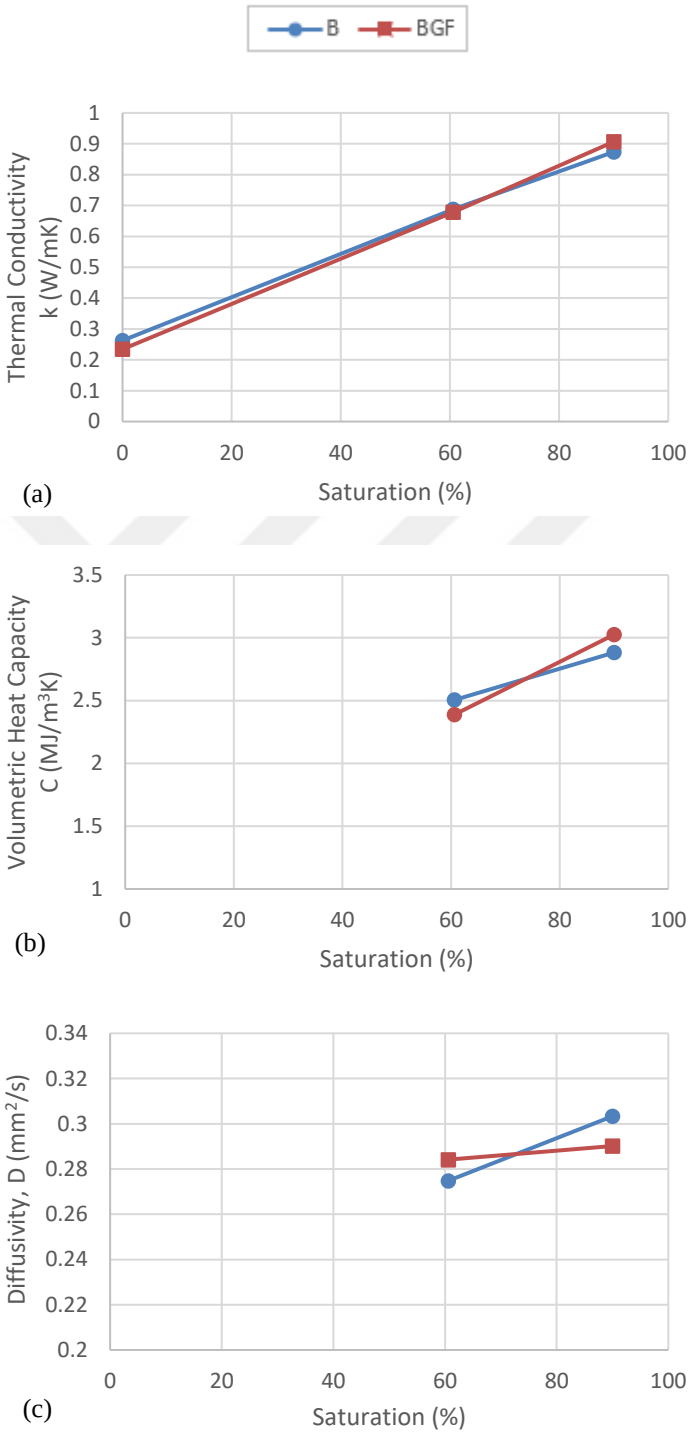


Figure 7.4 Variation of thermal properties of bentonite-glass fiber mixture at different degrees of saturation (e = 1.769) a) Thermal conductivity b) Volumetric heat capacity c) Diffusivity

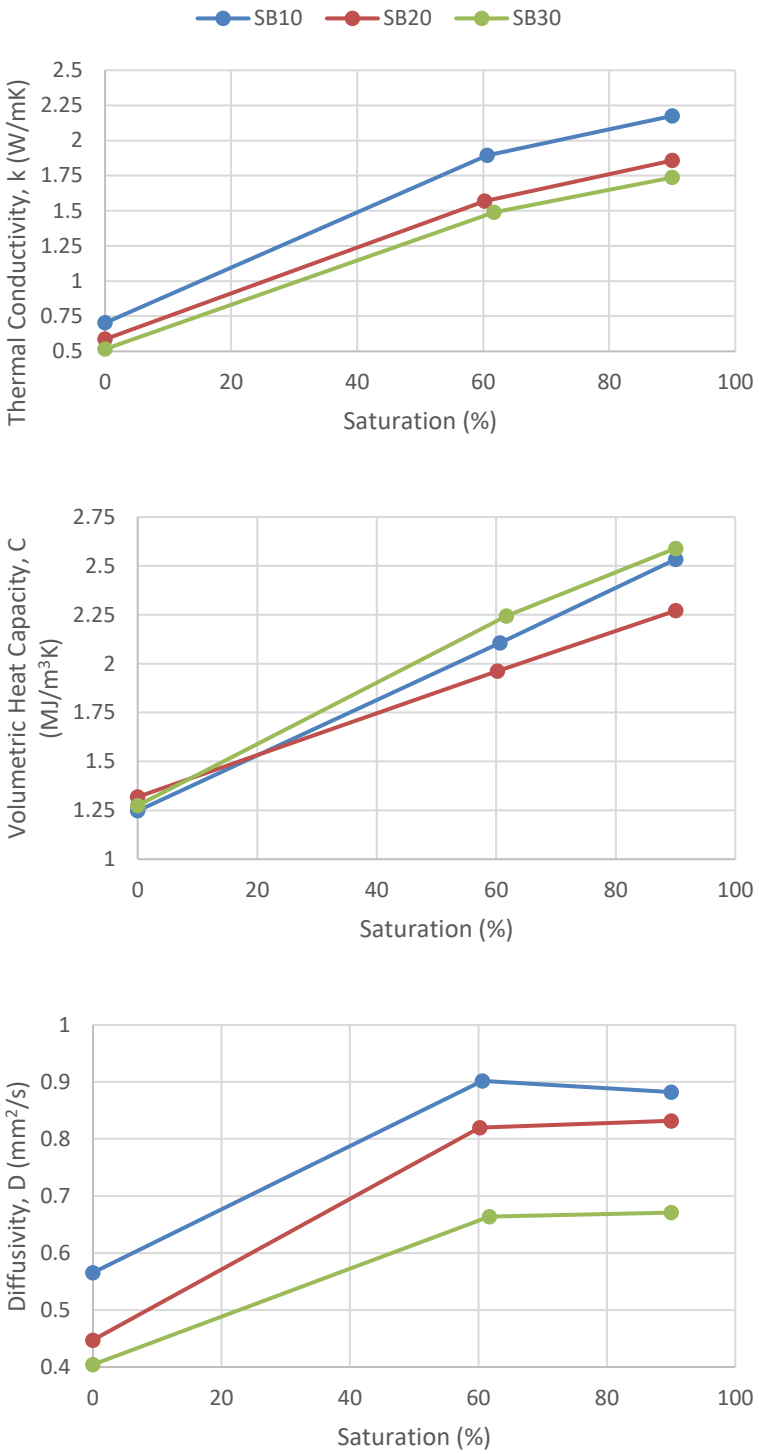


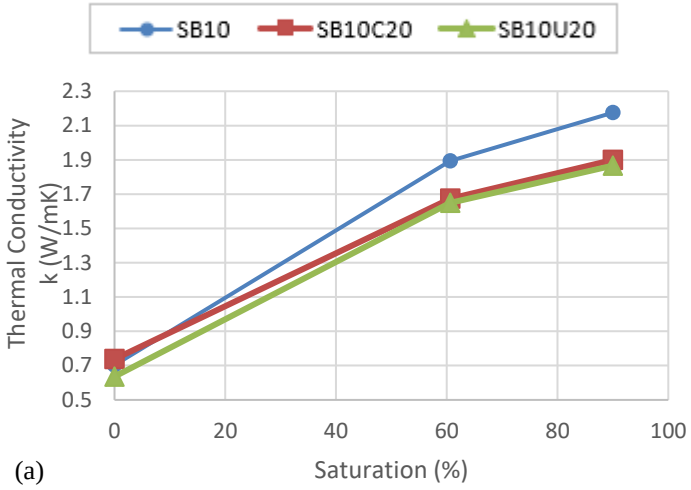
Figure 7.5 Variation of thermal properties of SB10 (e = 0.564), SB20 (e = 0.632) and SB30 (e = 0735) at different degrees of saturation (e = 0.564) a) Thermal conductivity b) Volumetric heat capacity c) Diffusivity

In Figure 7.5, thermal properties of SB30 mixture are given. The SB30 mixture had a thermal conductivity value of 0.516 W/mK, a volumetric heat capacity of 1.275

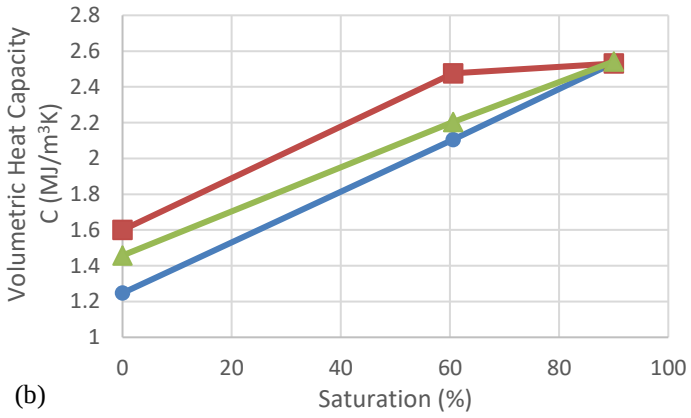
MJ/m^{3}K and a diffusivity value of 0.404 mm^2/s in dry condition. When the saturation degree increased to 61.7%, the thermal conductivity value reached 1.488 W/mK, the volumetric heat capacity reached 2.244 MJ/m^{3}K, and the diffusivity value reached 0.664 mm^2/s. The highest diffusivity value was obtained at medium saturation. At 90% saturation, the thermal conductivity showed the highest value of 1.737 W/mK, the volumetric heat capacity continued to increase and reached the value of 2.590 MJ/m^{3}K, and the diffusivity value decreased to 0.671 mm^2/s. It was seen that the thermal conductivity values decrease at all saturation degrees with the increase of the bentonite content. The volumetric heat capacity was also higher than the SB20 mixtures and closer to the values of the SB10 mixtures. The diffusivity values were lower than the SB10 and SB20 mixtures, the highest diffusivity value was obtained at 90% saturation for SB30 mixture, as in the SB20 mixture.

7.2.1 Thermal Properties of Sand-Bentonite-Boron Mixtures Depending on Saturation

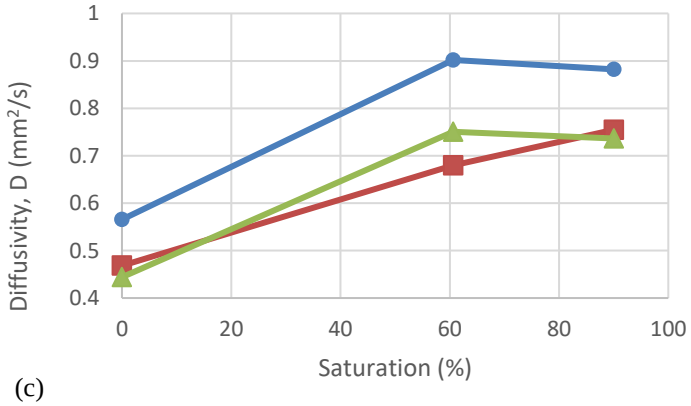
It was seen that the thermal conductivity values of boron added SB10 mixture in the dry condition were close to each other (Figure 7.6a). The volumetric heat capacity was seen to be the highest in colemanite (Figure 7.6b). Compared to the SB10 mixture, colemanite and ulexite were higher values as 28.3% and 16.8%, respectively (Figure 7.8b). In parallel, the diffusivity values were lower than the SB10 mixture (Figure 7.6c). The thermal conductivity values of colemanite and ulexite at medium saturation degrees were very close to each other and lower than the SB10 mixture (Figure 7.6a). The volumetric heat capacities were higher than the SB10 mixture (Figure 7.6b), with colemanite and ulexite were higher as 17.6% and 4.7%, respcetively. The lowest diffusivity values were 0.680 mm^2/s for colemanite and 0.751 mm^2/s for ulexite (Figure 7.6c). When the saturation degree was 90%, the behavior in the thermal conductivity values was similar to the medium saturation degree (Figure 7.6a). The volumetric heat capacities were remarkable close to the value of the SB10 mixture (Figure 7.6b). The diffusivity values were lower than the SB10 mixture and the colemanite and ulexite values were close to each other (Figure 7.6c).



(a)



(b)



(c)

Figure 7.6 Variation of thermal properties of SB10-Boron mixtures at different degrees of saturation (e = 0.564) a) Thermal conductivity b) Volumetric heat capacity c) Diffusivity

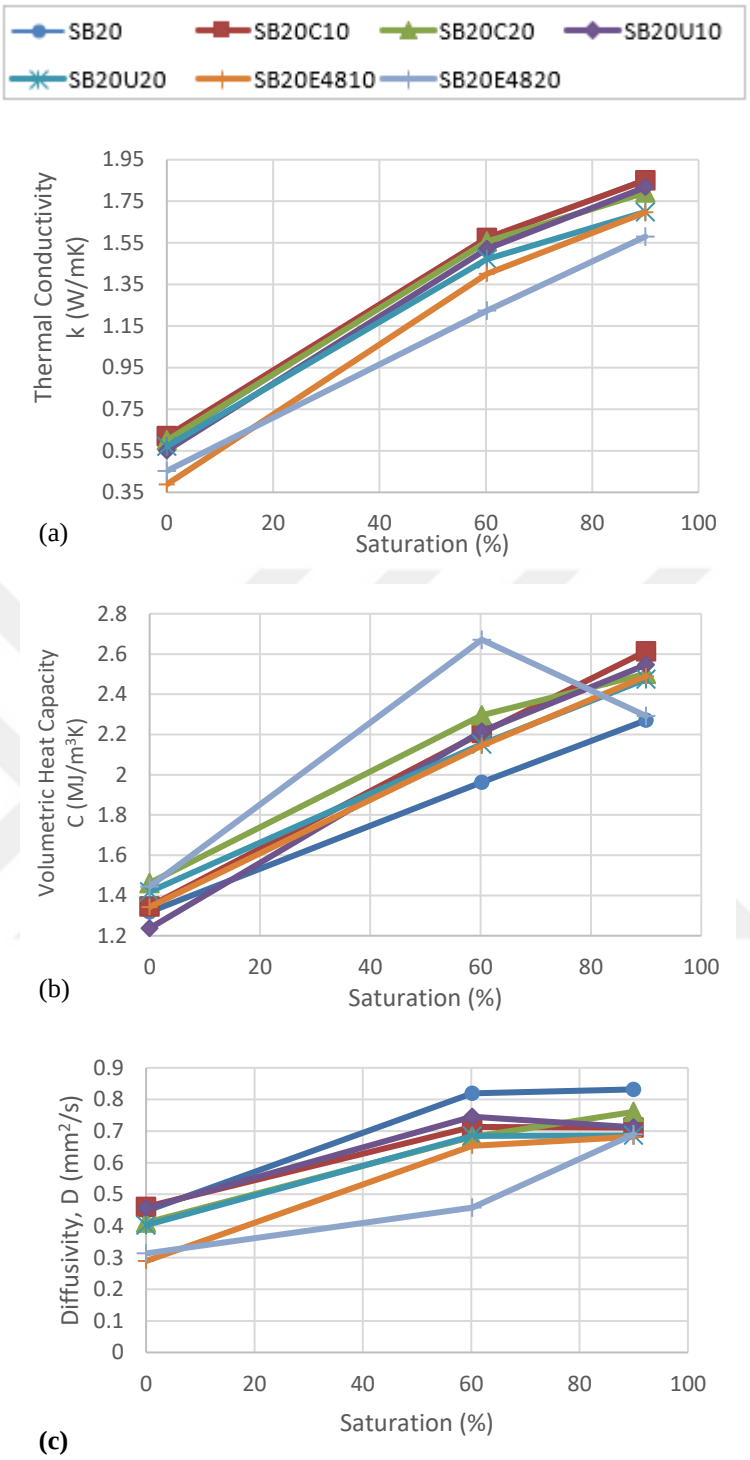
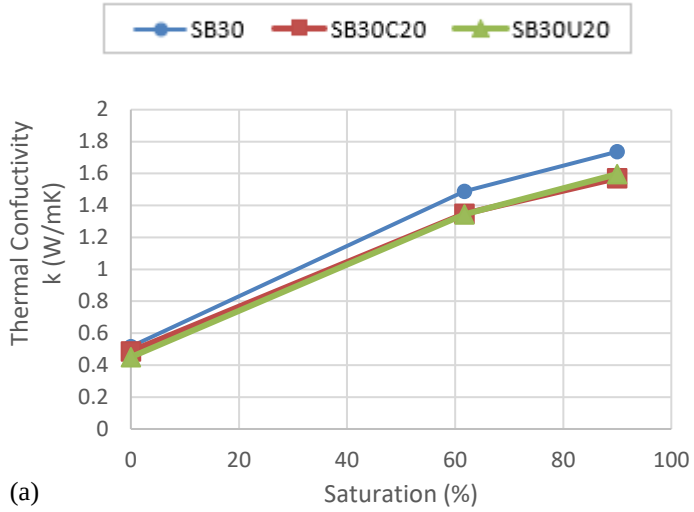


Figure 7.7 Variation of thermal properties of SB20-Boron mixtures at different degrees of saturation (e = 0.632) a) Thermal conductivity b) Volumetric heat capacity c) Diffusivity

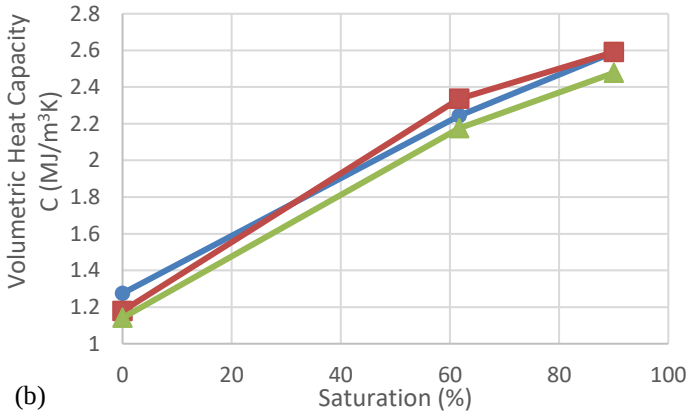
Figure 7.7 shows thermal properties of boron added SB20 mixtures. Etibor48 mixtures had the lowest thermal conductivity value when the mixtures were dry, colemanite added SB20 slightly increased the thermal conductivity value, while

ulexite added SB20 slightly decreased it (Figure 7.7a). As the degree of saturation increased, thermal conductivity values of colemanite and ulexite mixtures decreased compared to SB20 mixtures (Figure 7.7a). At the same time, with the increase in saturation degree, the volumetric heat capacities increased (Figure 7.7b) and SB20 mixtures had lower volumetric heat capacities compared to SB10 mixtures (Figure 7.6b). In the SB10E4820 mixture, the highest volumetric heat capacity reached 2.671 MJ/m^3K at 60.2% saturation, and then decreased to 2.292 MJ/m^3K at %90 saturation (Figure 7.7b). While etibor48 mixtures had the lowest diffusivity value (Figure 7.7c), 10% ulexite and 10% colemanite mixtures were quite close to the value of SB10 mixture. When the content of ulexite and colemanite were increased to 20%, the diffusivity values decreased slightly (Figure 7.7c). In Figure 7.7c, it was seen that with the increase in saturation degree, it was seen that while the SB20 mixture had the highest diffusivity value at medium saturation, the diffusivity value of boron decreased and diffusivity values were close to each other except for the SB20E4820 mixture. At the high saturation degree, the diffusivity values of boron mixtures were lower than the diffusivity value of the SB20 mixture (Figure 7.7c). It was seen that SB20K10, SB20U10, SB20U20 diffusivity values start to decrease after medium saturation degree (Figure 7.7c). The diffusivity values of SB20K20, SB20E4810 and SB20E4820 mixtures continued to increase (Figure 7.7c).

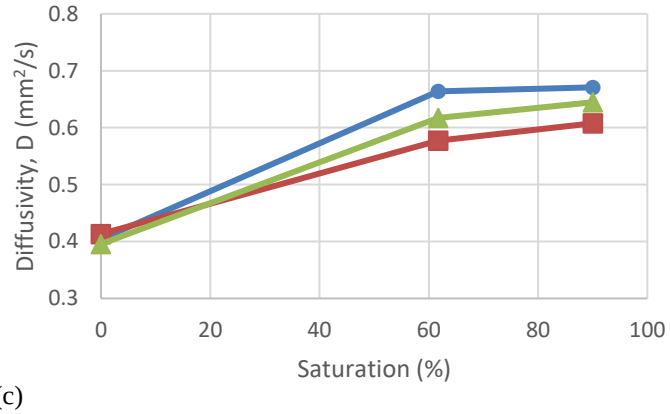
Figure 7.8 shows that the thermal properties of the slag additives were close to the values of the SB30 mixture in dry condition. As the degree of saturation increased, the thermal conductivity values of the slags added SB30 increased but the thermal conductivity values of SB30-slags were lower than that of the SB30 mixture (Figure 7.8 a). Ulexite had the lowest volumetric heat capacity as seen in Figure 7.8 b. While colemanite had a higher volumetric heat capacity than SB30 mixture at 61.7% saturation degree, it reached the same value with SB30 mixture at 90% saturation degree (Figure 7.8 b). When the diffusivity values were examined (Figure 7.8 c), it was seen that the diffusivity values increase continuously with the increase in the degree of saturation. Colemanite has generally the lowest diffusivity values, ulexite diffusivity values are between diffusivity values of colemanite additive and SB30 mixtures at middle and high degree of saturations (Figure 7.8c). The diffusivity value of the ulexite admixture has the lowest diffusivity value at dry state (Figure 7.8c).



(a)



(b)



(c)

Figure 7.8 Variation of thermal properties of SB30-Boron mixtures at different degrees of saturation (e = 0.735) a) Thermal conductivity b) Volumetric heat capacity c) Diffusivity

7.2.2 Thermal Properties of Sand-Bentonite-Slag Mixtures Depending on Saturation

In Figure 7.9a, while the thermal conductivity of the ferrochrome additive at all saturation levels was quite close to the SB10 mixture, %20 copper slag additive mixture had 0.155 W/mK lower thermal conductivity SB10 mixture. Figure 7.9b shows volumetric heat capacities of slag added SB10 mixture. The volumetric heat capacity of the slag was 28.8% higher than the SB10 mixture on average at dry state. At medium saturation, the volumetric heat capacity of the copper slag was lower than SB10 mixture. Ferrochrome slag still had a higher value, although its volumetric heat capacity approaches that of the SB10 mixture. When it reached 90% saturation, the ferrochrome additive decreased the volumetric heat capacity, while the copper slag increased the volumetric heat capacity, approaching the value of the SB10 mixture. At the dry state, since the volumetric heat capacity of the slag added samples were higher than the SB10 mixture, the diffusivity value of the SB10 mixture was higher than the slag added mixtures (Figure 7.9c). At medium saturation, the diffusivity values were quite close to each other (Figure 7.9c). At high saturation, ferrochrome slag reached the highest diffusivity value of 0.972 mm^2/s (Figure 7.9c). Copper slag had a lower diffusivity value (0.825 mm^2/s) than the SB10 mixture (Figure 7.9c).

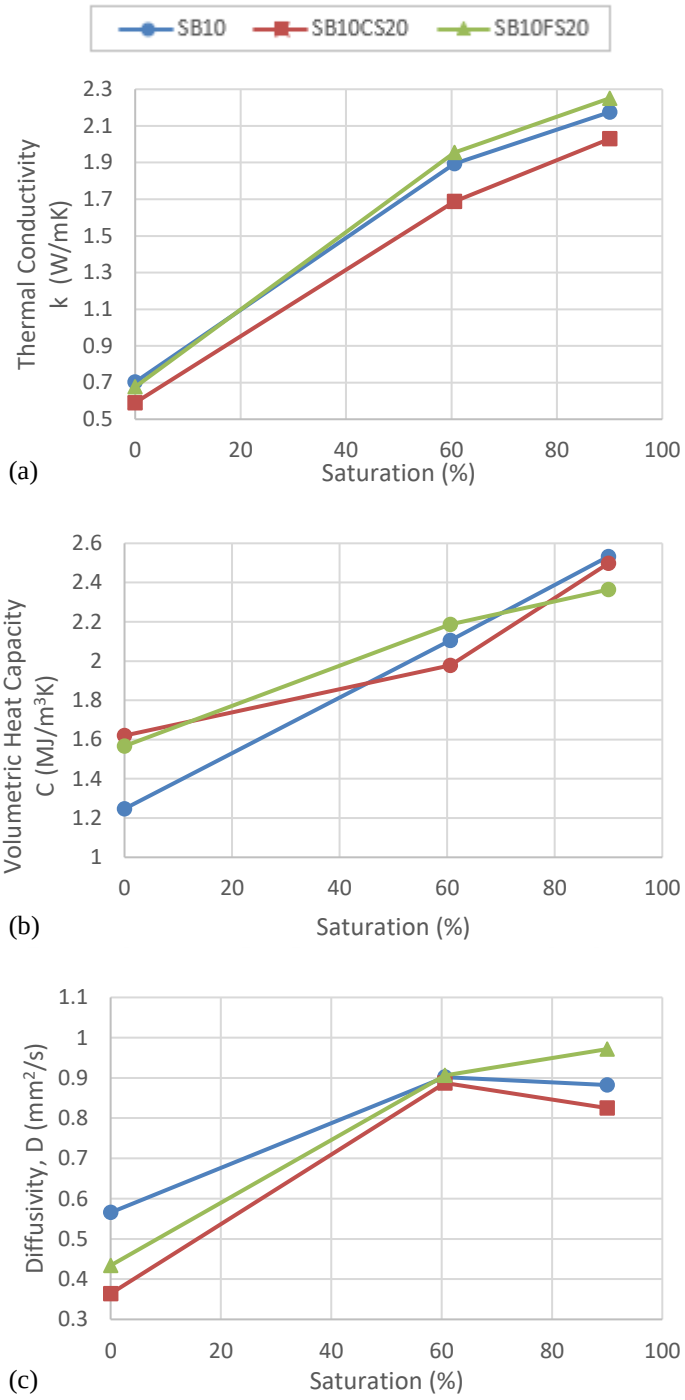


Figure 7.9 Variation of thermal properties of SB10-Slag mixtures at different degrees of saturation (e = 0.564) a) Thermal conductivity b) Volumetric heat capacity c) Diffusivity

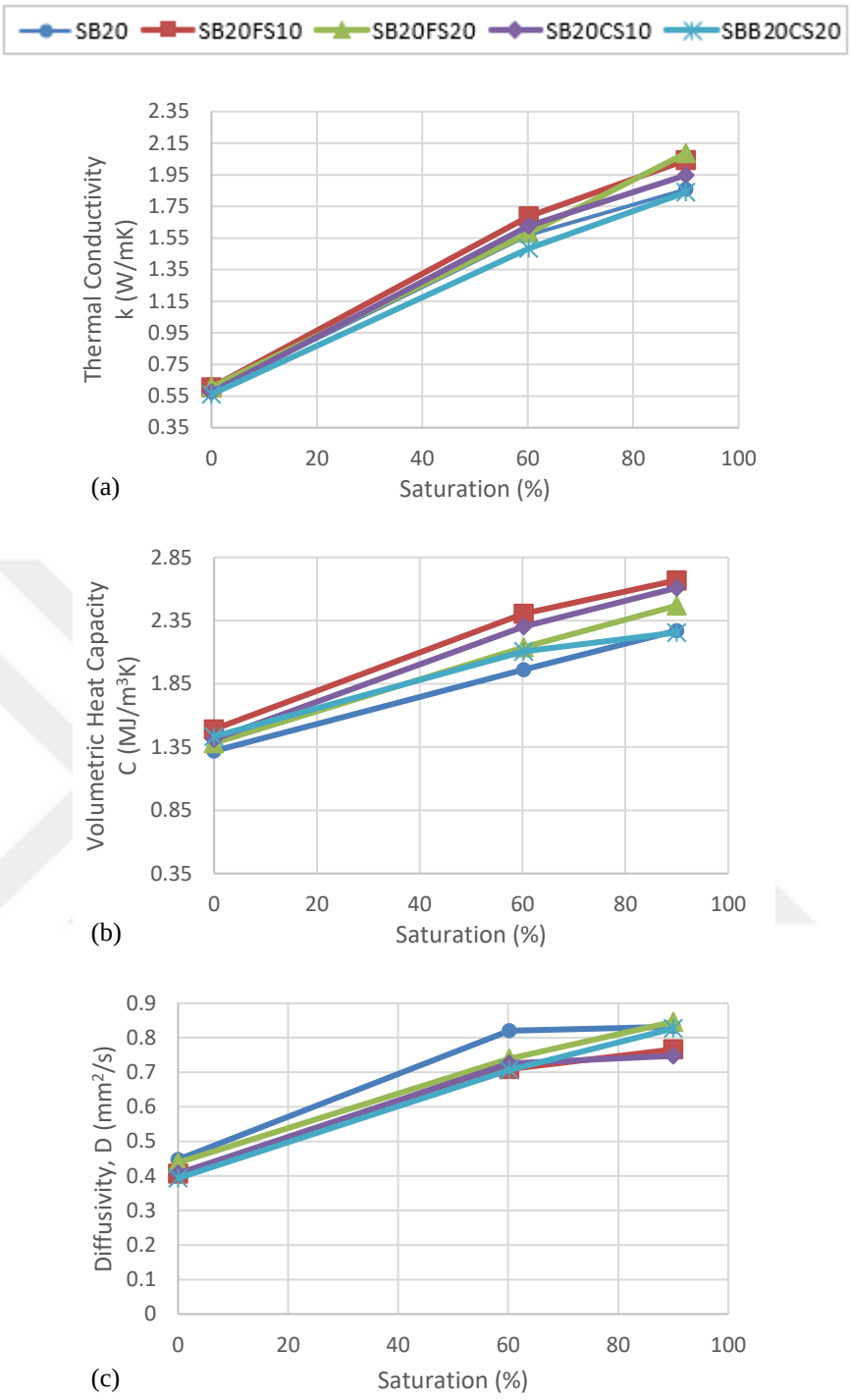


Figure 7.10 Variation of thermal properties of SB20-Slag mixtures at different degrees of saturation (e = 0.632) a) Thermal conductivity b) Volumetric heat capacity c) Diffusivity

It was observed that the thermal properties of the slag additives in the dry state were quite close to the SB20 mixture (Figure 7.10). Figure 7.10a shows thermal conductivity of slag added SB20 mixtures at different degree of saturation. The thermal conductivity value of 10% added slags increased with the increase in

saturation degree to 60.2%. It was seen that the thermal conductivity adversely affected with the increase of the additive ratio to 20% slag added mixtures approached the thermal conductivity value of SB20 mixture. In fact, the thermal conductivity value of the mixture with 20% copper slag was below the SB20 mixture. With the saturation degree reaching 90%, it was seen that the thermal conductivity value of ferrochrome slag increased by 11.2% on average in both ratios. For copper slag, 10% additive increased the thermal conductivity, while 20% additive decreased the thermal conductivity slightly. In Figure 7.10b, volumetric heat capacities of slag added SB20 mixtures were given. When the volumetric heat capacities at medium saturation were examined, it was seen that 10% ferrochrome and copper slag were increased the volumetric heat capacities most. Although the volumetric heat capacity decreases with the 20% additive ratio, it was still higher than the value of the SB20 mixture. At high saturation, the same trend of ferrochrome slag and 10% copper slag continued. It was seen that the volumetric heat capacity of the SB20CS20 mixture approached the SB20 mixture. Due to these changes in volumetric heat capacity and thermal conductivity, the SB20 mixture showed the best diffusivity at medium saturation (Figure 7.10c). Because slag additives increased the volumetric heat capacity considerably at medium saturation degree (Figure 7.10b). At the same time, the diffusivity values of all slag mixtures were very close to each other (Figure 7.10c). With the saturation degree reaching 90%, SB20, SB20FC20 and SB20CS20 showed close diffusivity values (Figure 7.10c). On the other hand, 10% added slag mixtures decreased the diffusivity values (Figure 7.10c).

While copper slag showed a thermal conductivity value very close to the SB30 mixture at dry state, there was a slight decrease in the thermal conductivity value with the increase in saturation degree (Figure 7.11a). The volumetric heat capacities of copper slag added SB30 were higher than the SB30 mixture at all saturation degree values (Figure 7.11b). The use of copper slag as an additive adversely affected the diffusivity value (Figure 7.11c). The contribution of the ferrochrome slag to the thermal properties was revealed at a high degree of saturation. While ferrochrome slag increased the thermal conductivity (Figure 7.11a) and diffusivity values (Figure 7.11c) and decreased the volumetric heat capacity (Figure 7.11b).

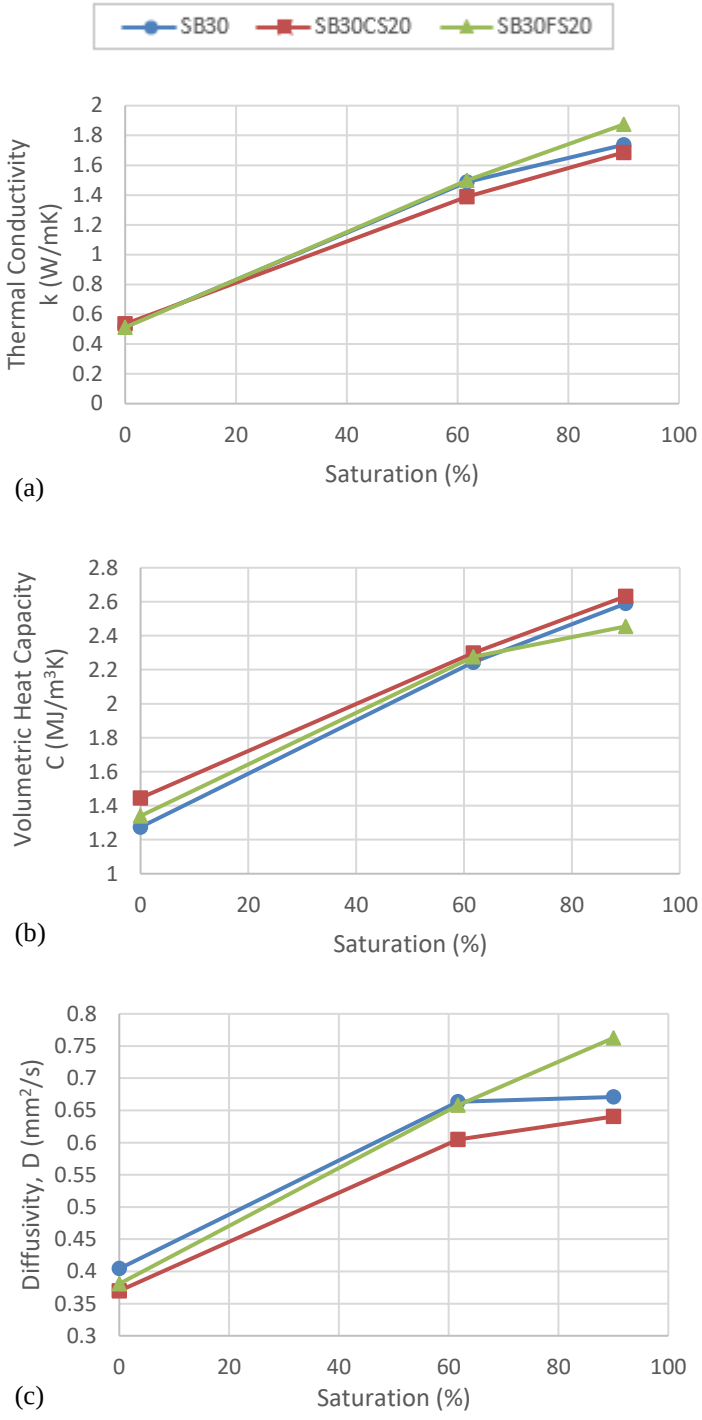
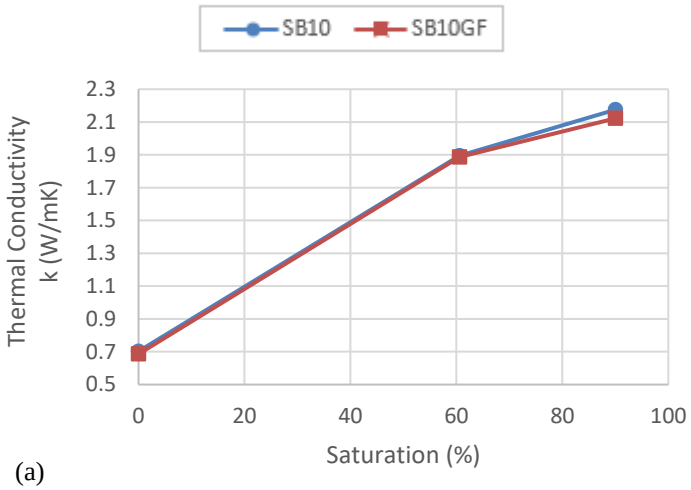


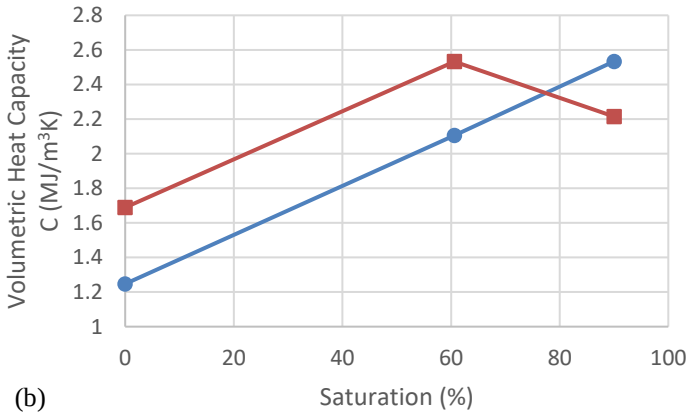
Figure 7.11 Variation of thermal properties of SB30-Slag mixtures at different degrees of saturation (e = 0.735) a) Thermal conductivity b) Volumetric heat capacity c) Diffusivity

7.2.3 Thermal Properties of Sand-Bentonite-Fiber Glass Mixtures Depending on Saturation

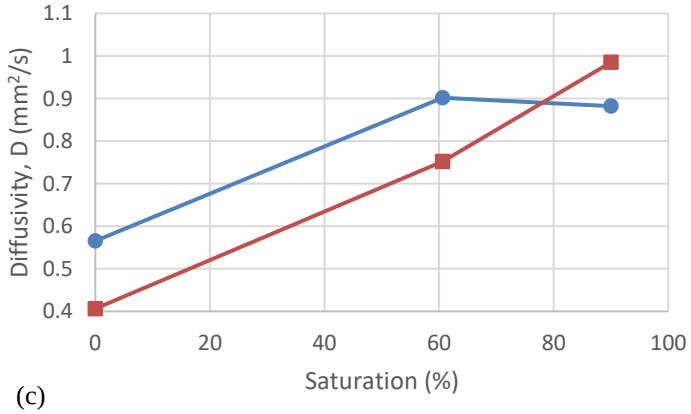
It was observed that glass fiber additive had a great effect on thermal conductivity in SB10 (Figure 7.12a), SB20 (Figure 7.13a) and SB30 (Figure 7.14a) mixtures. While the volumetric heat capacities of sand-bentonite mixtures increased continuously till medium saturation, it was seen that glass fiber-added sand-bentonite mixtures reached their highest value at medium saturation level and then decreased (Figure 7.12b, Figure 7.13b and Figure 7.14b). At medium saturation levels, the fiber glass may had bridged the water, increasing the specific heat capacity. With the increase in saturation degree, the low specific heat capacity of the glass fiber compared to water may had its effect. In the SB20 mixture, the glass fiber decreased diffusivity values at all degrees of saturation (Figure 7.13c), while glass fiber increased the diffusivity values in the SB10 (Figure 7.12c) and SB30 (Figure 7.14c) mixtures at high saturation.



(a)

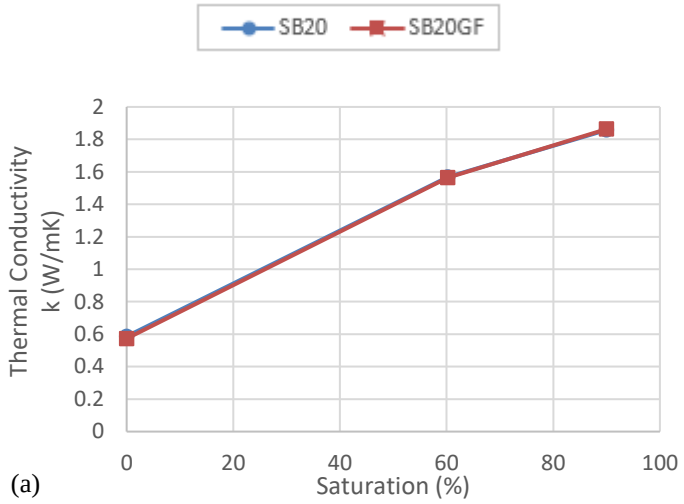


(b)

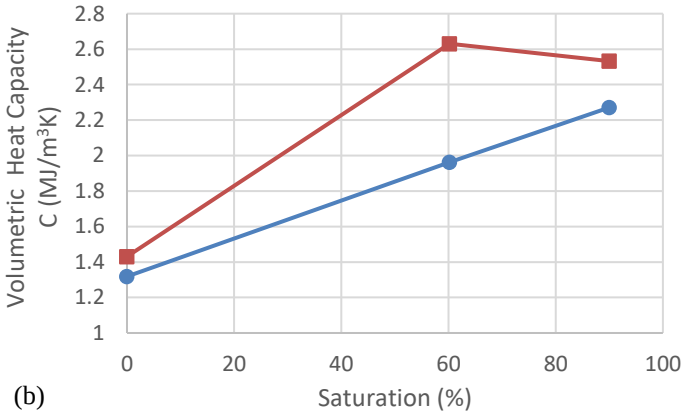


(c)

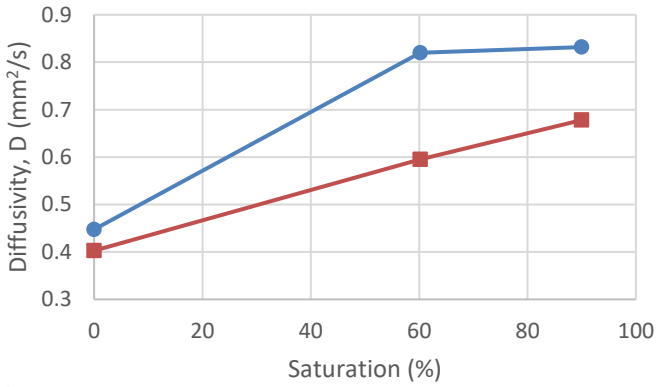
Figure 7.12 Variation of thermal properties of SB10-Glass Fiber mixture at different degrees of saturation (e = 0.564) a) Thermal conductivity b) Volumetric heat capacity c) Diffusivity



(a)

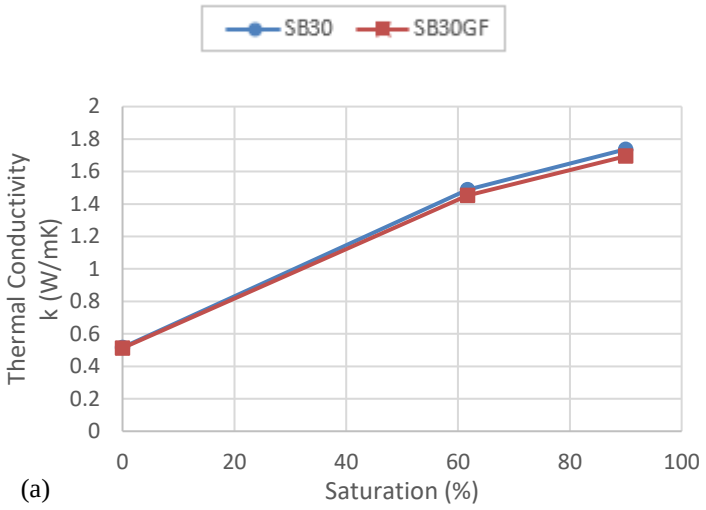


(b)

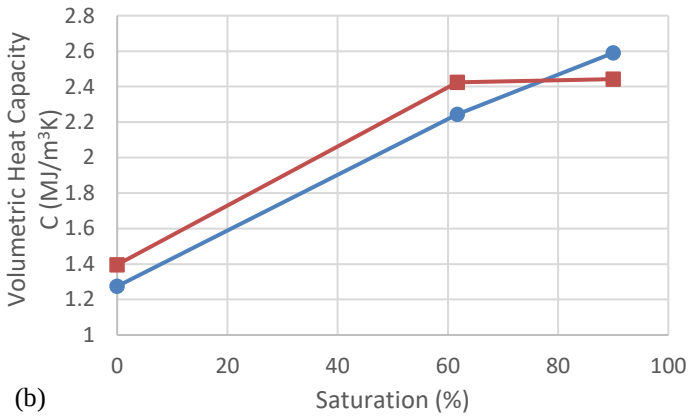


(c)

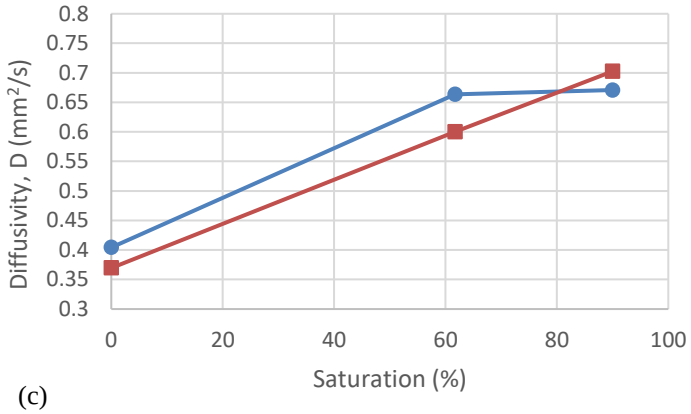
Figure 7.13 Variation of thermal properties of SB20-Slag mixture at different degrees of saturation (e = 0.632) a) Thermal conductivity b) Volumetric heat capacity c) Diffusivity



(a)



(b)



(c)

Figure 7.14 Variation of thermal properties of SB30-Glass Fiber mixture at different degrees of saturation (e = 0.735) a) Thermal conductivity b) Volumetric heat capacity c) Diffusivity

CHAPTER 8
CONCLUSIONS AND FUTURE RECOMMENDATIONS

8.1 Results of Thermal Properties-Compaction Curve of Bentonite

The highest thermal conductivity values of the samples and the point on the compaction curve where this value corresponds are given in Table 8.1. In table 8.2, the water content and dry unit weight values corresponding to the highest thermal conductivity and diffusivity values of the samples are given. The diffusivity value shows how fast the heat dissipates. The diffusivity value was obtained by dividing the thermal conductivity by the volumetric heat capacity. Since the change of thermal conductivity and volumetric heat capacities are different, although the thermal conductivity value was high, the diffusivity value may be low. For this reason, diffusivity and thermal conductivity values were taken into account in the examinations. The measurement differences between TR-3 sensor and SH-3 sensors do not exceed 10%. It was known in the literature that thermal conductivity measurements have a margin of error of approximately 10%. For this reason, these values are accepted as confirming each other and being correct.

Table 8.1 Highest thermal conductivity values of bentonite and additive mixtures measured by TR-3 sensor

Numune	Υ_d (kN/m^3)	w (%)	k (W/mK)	R (°Ccm/W)
Bentonit	9.18	62.00	0.913	109.6
B10U	9.24	60.00	0.893	112
B20U	9.36	57.40	0.911	110
B10C	9.62	55.35	0.900	110
B20C	9.96	51.60	0.942	106
B10E48	9.12	62.50	0.890	112
B20E48	9.32	56.65	0.969	105.5
BFG	9.31	56.75	0.915	109
B10CS	9.58	56.10	0.954	105
B20CS	10.06	53.70	0.946	106
B10FS	9.80	52.70	0.900	110
B20FS	10.33	47.00	0.914	109.5

The results of the TR-3 sensor are given in Table 8.1, it was seen that the increase in thermal conductivity values are negligible. Table 8.2 was prepared according to the

highest thermal conductivity and diffusivity values from compaction curve-thermal properties graphs.

Table 8.2 Best thermal properties of bentonite and additive mixtures measured by SH-3 sensor

Numune	Υ_d (kN/m^3)	w (%)	k (W/mK)	C (MJ/m^{3}K)	D (mm^2/s)
Bentonit	9.18	62.00	0.971	2.961	0.326
Bentonit	9.49	54.25	0.951	2.786	0.342
B10U	9.32	58.00	0.966	3.030	0.318
B10U*	9.35	56.70	0.962	3.009	0.319
B20U	9.36	57.80	0.965	2.935	0328
B10C	9.56	56.10	0.963	2.954	0.327
B10C*	9.45	57.30	0.962	2.892	0.333
B20C	10.04	50.20	0.989	3.086	0.321
B20C*	10.11	47.70	0.978	3.041	0.322
B10E48	9.25	59.70	0.951	3.097	0.312
B10E48*	9.13	62.50	0.934	2.934	0.317
B20E48	9.71	56.70	0.962	3.109	0.313
B20E48*	9.74	55.45	0.960	3.084	0.314
BFG	9.26	56.70	0.976	3.081	0.326
BFG*	9.34	55.00	0.969	3.109	0.327
B10CS	9.58	56.10	0.972	2.904	0.335
B20CS	10.06	53.70	0.996	3.184	0.313
B20CS*	10.46	45.30	0.945	2.763	0.341
B10FS	9.64	55.20	0.965	2.943	0.328
B10FS*	9.79	52.90	0.956	2.880	0.332
B20FS	10.33	47.00	1.021	2.721	0.364

* The highest diffusivity value.

Considering the thermal conductivity values in Table 8.2, the increments are negligible. However, when the diffusivity values are examined, it was seen that 20% ferrochrome additive provides 6.7% faster heat conduction.

Since the fine grain content of bentonite and bentonite mixtures were high, resistance occurs in the transfer between grains in heat conduction. Although materials with high thermal conductivity were added as additives, the high void ratio of the samples, the absence of particles that can fill these voids even though the void ratios were high, the fact that water has a more dominant effect on thermal conductivity than the particles, the amount of bentonite grains in the soil is higher than other materials. It is thought that bentonite governs the behavior in thermal conductivity because it suppresses the effects of other grains. In this project, all additives were sifted through

a no.40 sieve and used. And all additives except etibor48 have high fine grain ratio. If it is desired to change the thermal conductivity value of bentonite, the use of coarser materials is recommended.

8.2 Results of Thermal Properties – Compaction Curve of SB10

Table 8.3 shows the highest thermal conductivity values obtained in the measurements made with the TR-3 sensor. In the measurements made with the TR-3 sensor, the effects of ulexite, colemanite and glass fiber were found to be negligible. It was observed that etibor48 reduces thermal conductivity. When etibor48 was used as a 10% additive, the thermal conductivity decreased by 5%, and when it was added as a 20% additive, by 22.4%. Copper slag, on the other hand, provided an increase of 6.4% when 10% was added, while this increase decreased to 4.1% when 20% was added. When ferrochrome slag was used as an additive of 10%, an increase of 15.5% was obtained in thermal conductivity, and an increase of 17.6% was obtained when used as an additive of 20%. In general, the additives that affect the thermal conductivity the most were ferrochrome slag and etibor48.

Table 8.3 Highest thermal conductivity values of SB10 and additive mixtures measured by TR-3 sensor

Sample	Υ_{dry} (kN/m^3)	w (%)	k (W/mK)	R (°Ccm/W)
SB10	16.67	16.40	2.088	47.83
SB10U10	17.10	16.40	2.042	48.60
SB10U20	16.67	17.85	2.011	49.03
SB10C10	17.45	16.35	2.139	46.41
SB10C20	17.29	16.25	2.042	48.62
SB10E4810	15.75	22.85	1.984	50.13
SB10E4820	14.52	29.35	1.621	61.39
SB10GF	16.62	17.75	2.156	46.44
SB10CS10	17.15	18.50	2.222	45.08
SB10CS20	18.42	14.85	2.173	46.22
SB10FS10	17.26	15.65	2.413	40.38
SB10FS20	17.67	14.60	2.456	40.64

Table 8.4 Best thermal properties of SB10 and additive mixtures measured by SH-3 sensor

Sample	Υ_{dry} (kN/m^3)	w (%)	k (W/mK)	C (MJ/m^{3}K)	D (mm^2/s)
SB10	16.52	17.90	2.134	2.550	0.828
SB10*	16.83	15.50	2.082	2.518	0.835
SB10U10	17.05	16.60	2.198	2.645	0.841
SB10U20	16.78	17.50	2.019	2.585	0.788
SB10U20*	16.97	16.85	2.013	2.570	0.789
SB10C10	17.57	15.45	2.026	2.590	0.789
SB10C20	17.43	15.80	2.179	2.397	0.926
SB10C20*	17.88	13.90	2.128	2.254	0.949
SB10E4810	15.58	24.10	1.909	2.651	0.737
SB10E4810*	15.81	19.10	1.828	2.267	0.797
SB10E4820	14.56	29.10	1.720	3.186	0.547
SB10E4820*	14.44	22.90	1.440	2.520	0.578
SB10GF	16.42	20.00	2.147	2.711	0.814
SB10GF*	16.39	12.30	1.848	2.279	0.849
SB10CS10	17.00	19.30	2.196	3.036	0.714
SB10CS10*	17.16	12.00	1.833	2.314	0.826
SB10CS20	18.44	14.00	2.187	2.527	0.868
SB10CS20*	18.19	12.00	2.126	2.442	0.880
SB10FS10	17.66	15.40	2.453	2.387	1.009
SB10FS10*	17.77	13.40	2.397	2.267	1.043
SB10FS20	17.79	13.50	2.475	2.708	0.950
SB10FS20*	17.35	16.10	2.392	2.492	0.974

* The highest diffusivity value.

The thermal conductivity is expected to increase as the degree of saturation increases and to remain constant or decrease after a certain degree. The volumetric heat capacity is expected to increase as the amount of water in the soil increases. However, a decrease in the volumetric heat capacity may occur due to the changes in the void ratio of the points on the compaction curve, the dry unit weight and the degree of saturation.

For these reasons, there were also changes in the diffusivity value. Although the highest thermal conductivity values of sand-bentonite mixtures were observed on the wet side of the compaction curve, the highest diffusivity value can occur at lower water contents due to the variability of volumetric heat capacities. It is expected that the diffusivity values reach a peak and then decrease in the mixtures where sand is present.

Considering the thermal conductivity values according to Table 8.4, the effects of ulexite, colemanite, glass fiber and copper slag were negligible. While etibor48

significantly decreased the thermal conductivity, ferrochrome slag increased. Etibor48 decreased the thermal conductivity values 10.5% when it was 10% as an additive, and 19.4% when it was 20%. On the other hand ferrochrome slag increased the thermal conductivity value by 15% when 10% was added to SB10 and 16% when 20% was added.

When the diffusivity values are examined according to Table 8.4, it was seen that the effects of 10% ulexite, 10% etibor48, 1% glass fiber and 10% copper slag were at a negligible level. While 20% ulexite and 10% colemanite decreased the diffusivity by 5.5%, 20% colemanite increased the diffusivity by 13.7%. SB10E4820, on the other hand, caused a decrease of 30.8% on the diffusivity. The diffusivity increased by 5.4% when 20% copper slag was added, 24.9% increased when 10% ferrochrome slag was added, and 16.6% increased when 20% ferrochrome slag was added. It was observed that when etibor48 was used at 20%, it significantly reduced the diffusivity of the soil, while it was significantly increased when the ferrochrome slag was used at 10%.

8.3 Results of Bentonite and Additive Mixtures Depending on Temperature and Saturation

The values of thermal conductivities of bentonite mixtures at different temperatures are shown in detail in Table 8.5. In order to better understand the effect of additives on the thermal conductivity behavior of bentonite, the samples were prepared with constant void ratio and saturation degree.

Except for the ferrochrome slag, the effects of the additives at room temperature were negligible. Ferrochrome slag, on the other hand, increased thermal conductivity value by 12%.

When the temperature was 60 °C, it was seen that there was an average increase of 20.8% in the thermal conductivity values. While ferrochrome slag increased the thermal conductivity value by 13.1%, etibor48 decreased it by 12.4%. The effects of other additives were negligible.

Table 8.5 Variation of thermal conductivity of bentonite and additive mixtures at different temperatures (at constant S=0.658 and e=1.769)

Sample	ϒdry (kN/m^3)	w (%)	25 °C		60 °C		80 °C	
			k (W/mK)	R (°Ccm/W)	k (W/mK)	R (°Ccm/W)	k (W/mK)	R (°Ccm/W)
B	9.21	44.77	0.658	152	0.808	124	1.077	93
B20K	9.09	45.34	0.681	147	0.803	125	1.021	98
B20U	9.14	45.12	0.675	148	0.818	122	1.042	96
B20E48	8.74	47.18	0.642	156	0.708	141	0.917	109
BGF	9.21	44.70	0.660	152	0.832	120	1.008	99
B20FS	9.70	42.51	0.737	136	0.914	109	1.122	89
B20CS	9.57	43.06	0.680	147	0.837	120	1.071	96

When the sample temperatures reached 80°C, there was an average increase of 53.3% in the thermal conductivity values compared to the room temperature, while there was an increase of 27% compared to 60 °C. The effect of ferrochrome on increasing thermal conductivity was 4.2%. Ulexite decreased the thermal conductivity by 5.2%, etibor48 decreased by 14.9% and glass fiber decreased by 6.4%. In general, it was seen that copper slag had no effect on thermal conductivity in bentonite mixtures. While etibor48 lowered the thermal conductivity, the ferrochrome slag elevated. It was determined that the effects of ulexite, colemanite and glass fiber on the thermal conductivity of bentonite were generally negligible.

Thermal properties of bentonite mixtures at different saturation degrees shown in details in Table 8.6. It is expected that thermal conductivity (Xu et al., 2019), volumetric heat capacity (Abu-Hamdeh, 2003) and diffusivity (Abu-Hamdeh, 2003) increase with the increase in saturation degree. The evaluations were made according to diffusivity. Even if the thermal conductivity value increases, there may be differences in the diffusivity values as the volumetric heat capacity will change. Also, it is expected that the diffusivity value at constant dry unit weight in clay samples will increase slowly with increasing saturation degree. While the degree of saturation was 65.8%, the effects of etibor48 and glass fiber were negligible. Colemanite increased diffusivities by 7.5%, ulexite by 10.9%, ferrochrome slag by 14.9% and copper slag by 9.3%. When the degree of saturation was 90%, etibor48 decreased the diffusivity by 4.2%, while glass fiber decreased it by 5.1%. Colemanite, ulexite, ferrochrome slag

and copper slag increased its diffusivities by 5.7%, 5.4%, 11.6% and 5.6%, respectively.

Table 8.6 Variation of thermal properties of bentonite and additive mixtures according to saturation degree (at constant e =1.769)

	Saturation (%)						
	0	65.8	90	65.8	90	65.8	90
	Thermal Conductivity (W/mK)			Volumetric Heat Capacity (MJ/m^{3}K)		Diffusivity (mm^2/s)	
B	0.263	0.688	0.874	2.505	2.882	0.275	0.303
B20K	0.249	0.751	0.884	2.541	2.761	0.296	0.320
B20U	0.219	0.711	0.918	2.327	2.875	0.305	0.319
B20E48	0.284	0.690	0.864	2.568	3.004	0.269	0.288
BGF	0.234	0.678	0.907	2.388	3.025	0.284	0.290
B20FS	0.295	0.785	0.983	2.482	2.910	0.316	0.338
B20CS	0.230	0.734	0.913	2.463	2.854	0.301	0.320

8.4 Results of Sand-Bentonite and Additive Mixtures Depending on Temperature

Thermal conductivities of SB10 mixtures at different temperatures are shown in details in Table 8.7. In the samples prepared at room temperature, it was seen that colemanite, ulexite and copper slag decreased the thermal conductivity, glass fiber had no effect and ferrochrome slag increased the thermal conductivity. It was thought that the negligible effect of glass fiber on thermal conductivity was due to the use of 1% additive ratio. Colemanite decreased the thermal conductivity by 14.1%, ulexite by 16.5% and copper slag by 5.1%. Ferrochrome slag increased the thermal conductivity by 3.4%, but this increase was negligible.

When the samples were brought to 60 °C, there was an average 8.8% increase in thermal conductivity values. Colemanite reduced thermal conductivity by 10.2%, ulexite by 1.2% and copper slag by 7.2%. The effect of glass fiber on thermal conductivity was negligible at 60 °C. Ferrochrome slag, on the other hand, increased the thermal conductivity value by 6.5%.

Table 8.7 Variation of thermal conductivity of SB10 and additive mixtures at different temperatures (at constant S = 0.606 and e =0.564)

Sample	Υ_{dry} (kN/m^3)	w (%)	25 °C		60 °C		80 °C	
			k (W/mK)	R (°Ccm/W)	k (W/mK)	R (°Ccm/W)	k (W/mK)	R (°Ccm/W)
SB10	18.62	13.00	1.886	53.0	2.041	49.1	2.357	42.5
SB10C20	18.43	13.10	1.621	61.7	1.832	54.7	2.063	48.5
SB10U20	18.34	13.24	1.575	63.5	1.690	59.2	1.846	54.2
SB10GF	18.62	13.00	1.868	53.5	2.001	50.0	2.331	43.5
SB10CS20	19.64	12.26	1.790	55.9	1.894	52.9	2.254	44.5
SB10FS20	19.37	12.45	1.950	51.3	2.174	46.1	2.402	41.7

When the samples reach 80 °C, the highest thermal conductivity values of sand-bentonite and additive mixtures were observed. There was an average increase of 23.9% on thermal conductivity values according to room temperature, and an average increase of 13.9% compared to 60 °C. Colemanite decreased its thermal conductivity by 12.5%, ulexite by 21.7% and copper slag by 4.4%. The effects of glass fiber and ferrochrome slag were negligible.

Table 8.8 shows thermal conductivities of SB20 mixtures at different temperatures. It was seen that boron minerals decreased the thermal conductivity value at all temperatures. While 10% colemanite decreased the thermal conductivity value by 7.6% at room temperature, it decreased by 4.5% at other temperatures. On the other hand, 20% colemanite decreased the thermal conductivity by 13.4% at room temperature, while it decreased by about 10.5% at other temperatures. When ulexite additive was added 10%, the thermal conductivity value decreased on average 5.2% at room temperature and 60 °C, while it decreased by 7.9% at 80 °C. When the additive ratio was increased to 20%, an average of 12.2% decrease occurred in all temperatures. Mixtures with etibor48 additives were with the lowest thermal conductivity values at all temperatures. While 10% etibor48 decreased by 16.8% at room temperature, thermal conductivity decreased by 28% at 80 °C. When the additive was used 20%, there was a 28% decrease in room temperature, while a 32.7% decrease occurred at 80 °C. Glass fiber and copper slag additives had a negligible effect on thermal conductivity at all temperatures. When ferrochrome slag was used at a ratio of 10%,

an average decrease of 4.62% was observed at room temperature and 60 °C, while the thermal conductivity value increased by 9.6% at 80 °C. In 20% ferrochrome slag, an increase of 7.22% occurred in thermal conductivity at 80 °C, while an average increase of 5% occurred at other temperatures.

Table 8.8 Variation of thermal conductivity of SB20 and additive mixtures at different temperatures (at constant S = 0.602 and e =0.632)

Sample	Υ_{dry} (kN/m^3)	w (%)	25 °C		60 °C		80 °C	
			k (W/mK)	R (°Ccm/W)	k (W/mK)	R (°Ccm/W)	k (W/mK)	R (°Ccm/W)
SB20	1.841	14.5	1.589	62.97	1.704	58.80	1.900	53.27
SB20C10	1.832	14.58	1.468	68.10	1.622	61.70	1.821	55.02
SB20C20	1.823	14.66	1.375	72.70	1.518	66.43	1.709	59.53
SB20U10	1.827	14.62	1.518	65.90	1.603	62.38	1.750	57.44
SB20U20	1.813	14.75	1.405	71.70	1.499	66.72	1.651	61.03
SB20E4810	1.791	14.97	1.322	75.63	-	-	1.368	73.32
SB20E4820	1.740	15.47	1.130	88.47	-	-	1.279	78.24
SB20GF	1.841	14.5	1.519	66.10	1.653	60.75	1.913	52.41
SB20CS10	1.890	14.07	1.549	64.53	1.691	59.16	1.911	52.56
SB20CS20	1.939	13.66	1.525	65.58	1.677	59.63	1.913	52.39
SB20FS10	1.878	14.18	1.670	59.90	1.775	56.46	2.082	48.15
SB20FS20	1.914	13.87	1.677	59.67	1.779	56.28	2.037	49.13

Thermal conductivities of SB30 mixtures at different temperatures are shown in Table 8.9. At room temperature, boron minerals decreased the thermal conductivity value by an average of 8.2%. Copper slag and glass fiber decreased by about 3.6%, while ferrochrome slag increased the thermal conductivity value by 5.9%. When the temperature was 60 °C, the effects of glass fiber and copper slag on thermal conductivity were negligible. While boron minerals decreased the thermal conductivity value by 8.5% on average, ferrochrome slag increased by 6%. When the temperature of the samples was 80 °C, boron minerals reduced the thermal conductivity by about 16%. While the effects of glass fiber and ferrochrome slag were negligible, copper slag was reduced by 6.9%.

Table 8.9 Variation of thermal conductivity of SB30 and additive mixtures at different temperatures (at constant S = 0.617 and e =0.735)

Sample	Υ_{dry} (kN/m^3)	w (%)	25 °C		60 °C		80 °C	
			k (W/mK)	R (°Ccm/W)	k (W/mK)	R (°Ccm/W)	k (W/mK)	R (°Ccm/W)
SB30	1.772	17.3	1.386	72.23	1.510	66.26	1.817	55.20
SB30C20	1.756	17.49	1.264	79.10	1.389	72.04	1.556	64.36
SB30U20	1.746	17.6	1.281	78.07	1.376	72.74	1.515	66.05
SB30GF	1.772	17.3	1.336	74.87	1.469	67.10	1.750	57.16
SB30CS20	1.865	16.3	1.335	74.87	1.481	67.58	1.691	59.47
SB30FS20	1.841	16.55	1.468	68.13	1.600	62.54	1.785	56.18

8.5 Results of Sand-Bentonite and Additive Mixtures Depending on Saturation

In Table 8.10, thermal properties of SB10 mixtures at different saturation degrees are shown. The values of thermal conductivity and volumetric heat capacity of sandy samples are expected to increase as the water content increases. However, it is expected that the diffusivity values reach their highest value and decrease in certain water contents, and then may be slowly increase or give diffusivity values close to the value they decrease (a graph that oscillates by increasing and decreasing) (Abu-Hamdeh, 2003). It is not known at which saturation the diffusivity values of the samples will reach the peak value. The selected saturation degrees were selected as low, medium and high. It is expected that the highest diffusivity values will be reached at the medium saturation level. The highest values of thermal conductivity and volumetric heat capacity are expected to be reached at high saturation degrees. On soils where heat transfer is important, soils with high thermal conductivity and low volumetric heat capacity should be used. Since the diffusivity will be higher on such soils, more efficient results will be obtained.

Table 8.10 Variation of thermal properties of SB10 and additive mixtures according to saturation degree (at constant e =0.564)

Sample	Saturation (%)								
	0	60.6	90	0	60.6	90	0	60.6	90
	Thermal Conductivity (W/mK)			Volumetric Heat Capacity (MJ/m^3K)			Diffusivity (mm^2/s)		
SB10	0.703	1.895	2.175	1.247	2.105	2.534	0.566	0.902	0.882
SB10C20	0.738	1.674	1.900	1.600	2.475	2.531	0.468	0.680	0.755
SB10U20	0.636	1.649	1.866	1.458	2.204	2.542	0.444	0.751	0.737
SB10GF	0.686	1.887	2.122	1.689	2.532	2.215	0.406	0.752	0.985
SB10FS20	0.676	1.954	2.251	1.567	2.186	2.365	0.434	0.906	0.972
SB10CS20	0.590	1.688	2.029	1.620	1.978	2.498	0.364	0.887	0.825

The best diffusivity value at low saturation was in SB10 mixture. Although the thermal conductivity values were close, it was seen that the diffusivity values were significantly reduced as a result of the increase in the volumetric heat capacity of the additives. In general, it was seen that there was an average of 5% change in thermal conductivity values, while an average of 25.2% change in volumetric heat capacity had occurred.

As expected for samples with medium saturation, thermal conductivity values increased with increasing saturation degree. Likewise, the volumetric heat capacities also increased. It was observed that the diffusivity values of copper slag and ferrochrome slag change negligibly, while colemanite, ulexite and glass fiber decreased significantly. Although the contribution to the thermal conductivity value of copper slag was lower than SB10 mixture, it was seen that the diffusivity was high due to its low volumetric heat capacity. While colemanite and ulexite decreased the thermal conductivity value, they increased the volumetric heat capacity, which caused the diffusivity to be low. For glass fiber, although its effect on thermal conductivity was negligible, it increased the volumetric heat capacity and thus the diffusivity value decreased. While colemanite, ulexite and copper slag decreased the thermal conductivity value, they did not cause a significant change in the volumetric heat capacity.

In the samples with high saturation degree, the best diffusivity value was seen in ferrochrome slag and glass fiber additives. While ferrochrome slag and glass fiber additives did not cause a significant change in the thermal conductivity value, it was seen that the diffusivity values were high due to the fact that their volumetric heat capacity was less than the SB10 mixture. Therefore, the diffusivity values decreased. Ferrochrome slag increased the diffusivity value by 10.2%, while glass fiber increased 11.7%.

Table 8.11 Variation of thermal properties of SB20 and additive mixtures according to saturation degree (at constant e =0.632)

Sample	Saturation (%)								
	0	60.2	90	0	60.2	90	0	60.2	90
	Thermal Conductivity (W/mK)			Volumetric Heat Capacity (MJ/m^3K)			Diffusivity (mm^2/s)		
SB20	0.586	1.569	1.858	1.319	1.963	2.271	0.447	0.820	0.832
SB20C10	0.620	1.346	1.851	1.346	2.208	2.613	0.460	0.713	0.711
SB20C20	0.600	1.556	1.792	1.462	2.295	2.502	0.410	0.682	0.761
SB20U10	0.551	1.522	1.818	1.237	2.216	2.546	0.456	0.745	0.712
SB20U20	0.571	1.472	1.699	1.419	2.152	2.475	0.403	0.685	0.686
SB20E4810	0.388	1.402	1.697	1.343	2.145	2.490	0.289	0.654	0.682
SB20E4820	0.453	1.224	1.580	1.445	2.631	2.292	0.313	0.458	0.690
SB20GF	0.573	1.564	1.863	1.431	2.671	2.532	0.403	0.595	0.678
SB20CS10	0.574	1.628	1.948	1.412	2.304	2.610	0.407	0.726	0.748
SB20CS20	0.561	1.483	1.839	1.434	2.106	2.256	0.393	0.707	0.827
SB20FS10	0.606	1.686	2.043	1.491	2.405	2.669	0.406	0.709	0.766
SB20FS20	0.606	1.581	2.087	1.382	2.138	2.468	0.439	0.739	0.846

Table 8.11 shows thermal properties of SB20 mixtures at different saturation degrees. The effect of additives (except etibor48) on thermal conductivity in dry condition was in the range of ∓ 6. While 10% etibor48 decreased the thermal conductivity value by 34%, 20% etibor48 decreased by 23%. With the degree of saturation being 60.2%, the thermal conductivity values increased by approximately 268% (except SB20E4810, it increased 361%). The effects of colemanite, 10% ulexite, glass fiber, 20% ferrochrome and 10% copper slag on thermal conductivity were negligible. Thermal conductivity values decreased by 6.2%, 10.7%, 22%, and 5.5%

respectively, with the addition of 20% ulexite, 10% etibor48, 20% etibor48 and 20% copper slag. 10% ferrochrome slag increased the thermal conductivity value by 7.5%. At high saturation, the effects of colemanite, 10% ulexite, glass fiber and copper slag on thermal conductivity were below 5%. 20% ulexite, 10% etibor48, 20% etibor48 decreased the thermal conductivities by 8.6%, 8.7% and 15%, respectively. Thermal conductivity values increased by 10% and 12.3%, respectively, due to the effect of 10% and 20% ferrochrome slag.

The effects of 10% colemanite, 10% etibor48, 20% ferrochrome slag in dry form on the volumetric heat capacity were below 5%. The volumetric heat capacity of 20% colemanite, 20% ulexite, 20% etibor48, glass fiber and copper slag increased between 7% and 10%. While 10% ferrochrome slag increased by 12.3%, 10% ulexite decreased 6.3%. While the degree of saturation was 60.2%, the volumetric heat capacity of all additive mixtures was higher than the SB20 mixture. Etibor48, glass fiber and 10% ferrochrome slag increased the volumetric heat capacity the most by 20%, 36.1%, 34% and 22.5%, respectively. 10% colemanite, ulexite, 10% etibor48, 20% ferrochrome slag and 20% copper slag increased the volumetric heat capacity by 10% on average, while 20% colemanite and 10% copper slag increased it by 17% on average. At high saturation, the lowest volumetric heat capacity was in the SB20 mixture. In all mixtures with additives, it was seen that the volumetric heat capacity decreased with the increase of the additive ratio to 20%. While the volumetric heat capacity of the mixtures with 10% additives (except etibor48) increased by 15% on average, the increase was 10% on average when the additive ratio was 20% (excluding etibor48 and copper slag). While 10% etibor48 increases the volumetric heat capacity by 10%, it was seen that the effects of 20% etibor48 and 20% copper slag on the volumetric heat capacity were negligible. It was seen that glass fiber increased the volumetric heat capacity at all degrees of saturation. While the effect was 10% on average at low and high saturation, it was the highest with 34% at medium saturation.

Considering the diffusivity values, the best diffusivity values in dry state are 10% ulexite, 10% colemanite, 20% ferrochrome slag and SB20 mixtures. While etibor48 significantly decreased the diffusivity values (average 33%), other mixtures decreased the diffusivity values by 10% on average. At medium saturation, the best diffusivity

value was in SB20. It was seen that all additives reduce the diffusivity. 10% ulexite and 10% colemanite decreased the diffusivity value by 11.5% on average, while 20% added mixtures decreased about 17%. Ferrochrome slag reduced the diffusivity by 12% on average, while copper slag reduced it by 13% on average. While 10% etibor48 decreased the diffusivity value by 20.3%, 20% etibor48 was the additive that reduced the diffusivity value the most with a decrease of 44.1%. Glass fiber, on the other hand, reduced the diffusivity of 13.5%. When the saturation degree was 90%, it was seen that the best diffusivity values were in SB20, 20% ferrochrome slag and 20% copper slag. 10% colemanite and 10% ulexite reduced the diffusivity by 14.5%, while 20% ulexite, 10% etibor48, 20% etibor48 and glass fiber decreased about 17.8%. 20% colemanite and 10% copper slag caused an average of 9.4% reduction.

Table 8.12 Variation of thermal properties of SB30 and additive mixtures according to saturation degree (at constant e =0.735)

Sample	Saturation (%)								
	0	61.7	90	0	61.7	90	0	61.7	90
	Thermal Conductivity (W/mK)			Volumetric Heat Capacity (MJ/m^3K)			Diffusivity (mm^2/s)		
SB30	0.516	1.488	1.737	1.275	2.244	2.590	0.404	0.664	0.671
SB30C20	0.487	1.349	1.571	1.179	2.337	2.591	0.413	0.577	0.608
SB30U20	0.450	1.344	1.597	1.141	2.176	2.477	0.396	0.617	0.645
SB30GF	0.510	1.452	1.694	1.396	2.424	2.442	0.370	0.600	0.703
SB30CS20	0.534	1.388	1.686	1.446	2.276	2.455	0.370	0.605	0.641
SB30FS20	0.512	1.498	1.874	1.340	2.298	2.632	0.381	0.658	0.763

Thermal properties of SB30 mixtures at different saturations are shown in Table 8.12. In the dry state, the effect of glass fiber, ferrochrome slag and copper slag on thermal conductivity was negligible, while colemanite and ulexite decreased by 5.7% and 12.5%, respectively. Glass fiber, ferrochrome slag and copper slag increased the volumetric heat capacity by 9.5%, 5.1% and 13.4%, respectively. Boron minerals, on the other hand, decreased by about 9.4%. However, when the diffusivity values were examined, it was seen that the changes were generally at a negligible level. Glass fiber and copper slag, on the other hand, had the biggest impact with a 8.5% decrease in the diffusivity.

It was seen that glass fiber and ferrochrome additives had no effect on thermal conductivity when the saturation degree was 61.7%. Boron minerals reduced thermal conductivity approximately 9.5% and copper slag by 6.7%. The volumetric heat capacities were quite close to each other. Except for glass fiber, the effect of all additives on the volumetric heat capacity was below 5%, while glass fiber increased it by 8%. In the diffusivity value, SB30 and SB30FC20 show the highest values, while other additives caused a decrease of about 10%.

While the thermal conductivity values decreased by 8.8% on average with the effect of boron minerals at 90% saturation degree, thermal conductivity increased by 7.9% with the effect of ferrochrome slag. The effects of glass fiber and copper slag were negligible. Volumetric heat capacity values were very close to each other and the changes were negligible. Glass fiber and ferrochrome slags showed higher diffusivity than the SB30 mixture. The effects of copper slag, ulexite and glass fiber on the diffusivity were below 5%. While colemanite decreased by 9.4%, ferrochrome slag increased diffusivity by 13.6%.

8.6 General Conclusions and Future Recommendations

Thermal conductive soils are a general requirement for energy structures. Better efficiency can be obtained in heat exchangers with the quick heat transfer, while the life of the cables can be extended by preventing temperature-related damage to buried power cables. Various models are available for the disposal of nuclear waste, and both thermal conductive and thermal resistive engineering barriers need to be investigated. When the compaction curve-thermal conductivity graphs of bentonite mixtures are examined;

- Bentonite appears to suppress the effects of additives. Increase or decrease in the thermal properties of mixtures with additives remained at a negligible level.

When the compaction curve-thermal conductivity graphs of SB10 mixtures are examined;

- It was seen that ulexite had little effect on thermal conductivity. Likewise, the volumetric heat capacities were quite close to the SB10 mixture. However, there was a slight decrease in the diffusivity value at the 20% ulexite additive.
- Although the colemanite additive had insignificant effect on thermal conductivity, it was seen that the volumetric heat capacity decreased as the additive ratio increased. Colemanite, which was expected to provide thermal insulation to the soil, increased the heat dissipation rate of the soil by increasing the diffusivity value here.
- Etibor48 significantly decreased the thermal conductivity as its content increased. However, it also increased the volumetric heat capacity significantly, which caused the diffusivity values to be quite low compared to SB10.
- Since the proportion of glass fiber additive was very low, its effect on thermal properties was generally negligible.
- Although copper slag had little effect on thermal conductivity, it reduced the volumetric heat capacity and increased the diffusivity, albeit slightly.
- Ferrochrome slag was the additive material that increased the thermal properties the most.

Since temperature is a very important parameter in nuclear disposal area, it is necessary to examine the thermal conductivity values of bentonite mixtures at different temperatures. When the results of the change of bentonite mixtures according to temperature are examined;

- It was observed that the effect of the additives was negligible at room temperature, except for the ferrochrome slag.
- With the temperature of 60 ℃, etibor48 decreased the thermal conductivity, while ferrochrome slag continued to increase the thermal conductivity.
- When the temperature was 80 ℃, while etibor48 reduced the thermal conductivity, the effect of other additives were negligible.

The effect of additives on sand-bentonite mixtures investigated, since temperature is an important parameter in buried power cables, and it is a necessary parameter in strength.

- First of all, it was seen that the thermal conductivity values decreased with the increase of the bentonite content.
- Boron minerals reduced thermal conductivity at all temperatures. At high temperatures, colemanite showed higher thermal conductivity values than other boron minerals.
- The effect of glass fiber on the thermal conductivity was negligible.
- Contrary to the compaction curve, copper slag could not show its effect on thermal conductivity at constant saturation degree and void ratio. In some cases, it even reduced the thermal conductivity value.
- Ferrochrome slag was an additive that increases thermal conductivity at all temperatures. However, as the temperature was increased, the contribution of ferrochrome to the thermal conductivity decreased.

It is very important that bentonite seals the canister in nuclear waste landfills. Bentonite is expected to become saturated by feeding from ground water. For this reason, it is necessary to examine the thermal conductivity values of the mixtures at different saturation degrees. When the graphs of the change of bentonite mixtures according to the degree of saturation are examined;

- As in the results of the compaction curve-thermal conductivity of bentonite mixtures, the effects of the additives were very small. While ferrochrome slag affected the thermal properties positively, etibor48 had a negative effect. The effects of other additives were negligible.

Other energy structures are expected to be affected by changes in water level due to seasonal changes. For this reason, the thermal conductivity values of sand-bentonite mixtures at different saturation degrees should be investigated. When the results of the change of bentonite mixtures according to the degree of saturation are examined;

- Boron minerals affected the thermal properties of sand-bentonite mixtures negatively.
- Contrary to other additives, glass fiber showed the highest volumetric heat capacity at medium saturation degrees. Contrary to expectations, it showed the highest diffusivity value in SB10 mixtures.
- Copper slag showed lower and close thermal conductivity and volumetric heat capacity values compared to sand-bentonite mixtures. Therefore, the diffusivity values were very close to the sand-bentonite mixture.
- In ferrochrome slag mixtures, although the thermal conductivity and volumetric heat capacity increased, the diffusivity values were always higher than the other mixtures, since the increase in thermal conductivity was higher. It also affected the thermal conductivity values positively in all mixtures.
- It was found that as the bentonite ratio increased and the percentage of additives increased, the thermal conductivity behavior affected by the fine particles and the change in rate decreased.

Based on the thesis, the following recommendations for future research are suggested;

- Although the thermal behavior of bentonite and sand-bentonite mixtures with additives investigated, their hydro-mechanical properties should also be examined.
- It is recommended to continue research on ferrochrome slags, especially since it was shown that ferrochrome slag has a positive effect on thermal properties.
- Fine grain content of bentonite mixtures are quite high, it is recommended to examine the thermal conductivity behavior by using additives with larger grain sizes.
- It is known that the mechanical properties of slags are high, hydro-mechanical-thermal properties can be examined by using slag instead of sand.

REFERENCES

Abdelaziz, S. L., Olgun, C. G., & Martin, II, J. R. (2011). Design and operational considerations of geothermal energy piles. In *Geo-frontiers 2011: Advances in geotechnical engineering* (pp. 450-459). https://doi.org/10.1061/41165(397)47

Abramowitz, M., & Stegun, I. A. (1972). Handbook of Mathematical Functions with Formulas, Graphs, and Mathematical Tables. National Bureau of Standards Applied Mathematics Series 55. Tenth Printing. https://doi.org/10.1119/1.15378

Abu-Hamdeh, N. H., & Reeder, R. C. (2000). Soil thermal conductivity effects of density, moisture, salt concentration, and organic matter. *Soil science society of America Journ*al, *64*(4), 1285-1290. https://doi.org/10.2136/sssaj2000.6441285x

Abu-Hamdeh, N. H. (2003). Thermal properties of soils as affected by density and water content. *Biosystems engineering*, *86*(1), 97-102. https://doi.org/10.1016/S1537-5110(03)00112-0

Abuel-Naga, H., Raouf, M. I. N., Raouf, A. M., & Nasser, A. G. (2015). Energy piles: current state of knowledge and design challenges. *Environmental Geotechnics*, 2(4), 195-210. https://doi.org/10.1680/envgeo.13.00019

Ahn, J., & Jung, J. (2017). Effects of fine particles on thermal conductivity of mixed silica sands. *Applied Sciences*, 7(7), 650. https://doi.org/10.3390/app7070650.

Al Nakshabandi, G., & Kohnke, H. (1965). Thermal conductivity and diffusivity of soils as related to moisture tension and other physical properties. *Agricultural Meteorology*, 2(4), 271-279. https://doi.org/10.1016/0002-1571(65)90013-0

Al-Jabri, K. S. (2018). Research on the use of Ferro-Chrome slag in civil engineering applications. In *MATEC Web of Conferences* (Vol. 149, p. 01017). EDP Sciences. https://doi.org/10.1051/matecconf/201814901017

Alnefaie, K. A., & Abu-Hamdeh, N. H. (2013, September). Specific heat and volumetric heat capacity of some saudian soils as affected by moisture and density. In *International conference on mechanics, fluids, heat, elasticity and electromagnetic fields* (pp. 139-143). https://doi.org/10.46300/91018.2020.7.8

Alpaydın, Ş. G. (2019). *An investigation of effects of boron additives on the permeability and shear strength behavior of sand bentonite mixtures under high temperatures* [Master dissertation, Dokuz Eylül University]. YOK Ulusal Tez Merkezi

Army, U. S., & Force, A. (1988). *Arctic and subarctic construction calculation methods for determination of depths of freeze and thaw in soils*. Technical Manual: TM5-852-6/AFM, 88-19, 6.

Arslan, D. S., & Drelich, J. W. (2022). Diffuse-layer surface potentials of colemanites mined in Turkey. *Physicochemical Problems of Mineral Processing, 58*. https://doi.org/ 10.37190/ppmp/151933

ASTM:D422-63. (2007). Standard test method for particle-size analysis of soils (Withdrawn 2016), ASTM International, West Conshohocken, PA, USA, 1-8.

ASTM:D4318-17e1. (2017). Standard test methods for liquid limit, plastic limit, and plasticity index of soils. ASTM International, West Conshohocken, PA, USA, 1-20.

ASTM:D4972-19. (2019). Standard test methods for ph of soils. *ASTM International, West Conshohocken, PA, USA*, 1-6

ASTM:D698-12. (2012). Standard test methods for laboratory compaction characteristics of soil using standard effort (12 400 ft-lbf/ft3 (600 kN-m/m3)). *ASTM International, West Conshohocken, PA, USA*, 1–13.

ASTM:D854-14. (2014). Standard test methods for specific gravity of soil solids by water pycnometer. *ASTM International, West Conshohocken, PA, USA*, 1-8.

Ateş, A. (2016). Mechanical properties of sandy soils reinforced with cement and randomly distributed glass fibers (GRC). *Composites Part B: Engineering, 96*, 295-304. https://doi.org/10.1016/j.compositesb.2016.04.049

Barry-Macaulay, D., Bouazza, A., Singh, R. M., Wang, B., & Ranjith, P. G. (2013). Thermal conductivity of soils and rocks from the Melbourne (Australia) region. *Engineering Geology, 164*, 131-138. https://doi.org/10.1016/j.enggeo.2013.06.014

Baruah, H. (2015). Effect of glass fibers on red soil. *International Journal of Advanced Technology in Engineering and Science, 3*(1), 217-223. ISBN: 978-81-931039-7-5

Bejan, A., & Kraus, A. D. (Eds.). (2003). *Heat transfer handbook* (Vol. 1). John Wiley & Sons.

Bi, J., Zhang, M., Chen, W., Lu, J., & Lai, Y. (2018). A new model to determine the thermal conductivity of fine-grained soils. *International Journal of Heat and Mass Transfer, 123*, 407-417. https://doi.org/10.1016/j.ijheatmasstransfer.2018.02.035

Boukelia, A., Eslami, H., Rosin-Paumier, S., & Masrouri, F. (2019). Effect of temperature and initial state on variation of thermal parameters of fine compacted soils. *European Journal of Environmental and Civil Engineering, 23*(9), 1125-1138. https://doi.org/10.1080/19648189.2017.1344144

Campbell, G. S., Jungbauer Jr, J. D., Bidlake, W. R., & Hungerford, R. D. (1994). Predicting the effect of temperature on soil thermal conductivity. *Soil science, 158*(5), 307-313. https://doi.org/10.1097/00010694-199411000-00001

Chandrshekhar, J., Chokshi, T. A., & Chauhan, D. V. (2015). A review on utilization of waste material "Copper Slag" in geotechnical applications. *Int J Innov Res Sci Technol, 1*, 2349. ISSN (online): 2349-6010

Chen, S. X. (2008). Thermal conductivity of sands. *Heat and mass transfer, 44*(10), 1241-1246. https://doi.org/10.1007/s00231-007-0357-1

Chen, W., Zhao, J., Fan, L., Li, J., Yuan, B., Li, H., ... & Chen, T. (2022). The Effect of Length and Content of Fiber on Glass Fiber and Basalt Fiber-Reinforced Granite Residual Soil. *Advances in Civil Engineering, 2022.* https://doi.org/10.1155/2022/7803002

Chen, Y. G., Liu, X. M., Mu, X., Ye, W. M., Cui, Y. J., Chen, B., & Wu, D. B. (2018). Thermal conductivity of compacted GO-GMZ bentonite used as buffer material for a high-level radioactive waste repository. *Advances in Civil Engineering, 2018.* https://doi.org/10.1155/2018/9530813

Cho, G. C., & Santamarina, J. C. (2001). Unsaturated particulate materials—particle-level studies. *Journal of geotechnical and geoenvironmental engineering, 127*(1), 84-96. https://doi.org/10.1061/(ASCE)1090-0241(2001)127:1(84)

Cho, W. J., Lee, J. O., & Kwon, S. (2010). Analysis of thermo–hydro–mechanical process in the engineered barrier system of a high-level waste repository. *Nuclear Engineering and Design, 240*(6), 1688-1698. https://doi.org/10.1016/j.nucengdes.2010.02.027

Côté, J., & Konrad, J. M. (2005). A generalized thermal conductivity model for soils and construction materials. *Canadian Geotechnical Journal, 42*(2), 443-458. https://doi.org/10.1139/t04-106

De Vries, D. A. (1963). Thermal properties of soils. Physics of plant environment., 210-235.

Desenerji. (2019). *Yer ısısı – en sıcak şekilde önerilir yer ısısı enerji kullanımı için rehau system tekniği* [Brochure]. https://desenerji.com/wp-content/uploads/2019/06/yer-isisi-brosur.pdf

Dhanesh, P., Amit, R., & Pitroda, J. R. (2019). Sustainable construction material-copper slag: A review. *International Journal of Engineering Research, 8*, 10-18. ISSN:2319-6890 (online),2347-5013

Etimaden. (2023, Jan 10). *Bor*. https://www.etimaden.gov.tr/

Fares, A. I., Sohel, K. M. A., Al-Jabri, K., & Al-Mamun, A. (2021). Characteristics of ferrochrome slag aggregate and its uses as a green material in concrete–A review. *Construction and Building Materials, 294*, 123552. https://doi.org/10.1016/j.conbuildmat.2021.123552

Fricke, B. A., Misra, A., Becker, B. R., & Stewart, W. E. (1992, December). Soil thermal conductivity: effects of saturation and dry density. In *Thermal Performance of the Exterior Envelopes of Whole Buildings V International Conference, Clearwater Beach, Florida, USA.*

Georgiev, D., Georgiev, G., Rangelov, Y., & Kamenov, Y. (2020, June). Analysis of the Effect of Soil Thermal Resistivity on High-Voltage Cables Sizing. In *2020 21st*

International Symposium on Electrical Apparatus & Technologies (SIELA) (pp. 1-4). IEEE. https://doi.org/10.1109/SIELA49118.2020.9167058.

Ghuman, B. S., & Lal, R. (1985). Thermal conductivity, thermal diffusivity, and thermal capacity of some Nigerian soils. *Soil Science*, *139*(1), 74-80. https://doi.org/10.1097/00010694-198501000-00011

Go, G. H., Lee, S. R., Kim, Y. S., Park, H. K., & Yoon, S. (2014). A new thermal conductivity estimation model for weathered granite soils in Korea. *Geomech. Eng*, *6*(4), 359-376. https://doi.org/10.12989/gae.2014.6.4.359

Gul, N., & Mir, B. A. (2022). Influence of glass fiber and cement kiln dust on physicochemical and geomechanical properties of fine-grained soil. *Innovative Infrastructure Solutions, 7*(6), 344. https://doi.org/10.1007/s41062-022-00943-4

Haigh, S. K. (2012). Thermal conductivity of sands. *Geotechnique, 62*(7), 617-625. https://doi.org/10.1680/geot.11.P.043

Hakhamaneshi, M., & Black, J. A. (2016, June). Centrifuge modeling of energy foundations–effect of seasonal temperature fluctuation and soil state. In *Proceedings of the 3rd European Conference on Physical Modelling in Geotechnics (Eurofuge 2016)* (pp. 141-147). Eurofuge 2016. ISBN 9782857827177

Havanagi, V. G., Mathur, S., Prasad, P. S., & Kamaraj, C. (2007). Feasibility of copper slag–fly ash–soil mix as a road construction material. *Transportation research record, 1989*(1), 13-20. https://doi.org/10.3141/1989-43

Hiraiwa, Y., & Kasubuchi, T. (2000). Temperature dependence of thermal conductivity of soil over a wide range of temperature (5–75 C). *European Journal of Soil Science, 51*(2), 211-218. https://doi.org/10.1046/j.1365-2389.2000.00301.x

Islam, M. Z., Sohel, K. M., Al-Jabri, K., & Al Harthy, A. (2021). Properties of concrete with ferrochrome slag as a fine aggregate at elevated temperatures. *Case Studies in Construction Materials, 15*, e00599. https://doi.org/10.1016/j.cscm.2021.e00599

Jackson, R. D., & Taylor, S. A. (1986). Thermal conductivity and diffusivity. *Methods of Soil Analysis: Part 1 Physical and Mineralogical Methods, 5*, 945-956 https://doi.org/10.2136/sssabookser5.1.2ed.c39

Johansen, O. (1977). *Thermal conductivity of soils*. Cold Regions Research and Engineering Lab Hanover NH. https://doi.org/10.21236/ada044002

Johnston, I. W., Narsilio, G. A., & Colls, S. (2011). Emerging geothermal energy technologies. *KSCE Journal of Civil Engineering, 15*, 643-653. https://doi.org/10.1007/s12205-011-0005-7

Kavak, O., & Kaya, S. (2022). Dünya Bor Mineralleri ve Bileşikleri Üretiminde Türkiye'nin Yeri. In B. TURAL, S. TURAL, Y. K. HASPOLAT (Eds.), Farklı yaklaşımlarla endüstriyel ve sağlık alanında bor (pp. 1-25). Retrieved https://www.researchgate.net/publication/366177556_Dunya_Bor_Mineralleri_ve_Bilesikleri_Uretiminde_Turkiye'nin_Yeri

Kersten, M. S. (1949). Laboratory research for the determination of thermal properties of soils. https://doi.org/11681/6576

Knight, J. H., Kluitenberg, G. J., Kamai, T., & Hopmans, J. W. (2012). Semianalytical solution for dual-probe heat-pulse applications that accounts for probe radius and heat capacity. *Vadose Zone Journal, 11*(2). https://doi.org/10.2136/vzj2011.0112

Krishnaiah, S., & Singh, D. N. (2003). Determination of influence of various parameters on thermal properties of soils. http://doi.org/10.1016/S0735-1933(03)00134-9

Kubičár, L. U., Vretenár, V., Štofanik, V., & Boháč, V. (2010). Hot-ball method for measuring thermal conductivity. *International Journal of Thermophysics, 31*, 1904-1918. https://doi.org/10.1007/s10765-008-0544-4

Lavanya, C., Rao, A. S., & Kumar, N. D. (2011, December). A review on utilization of copper slag in geotechnical applications. *In Indian Geotechnical Conference, Kochi* (pp. 445-448).

Lee, G. J., Yoon, S., & Cho, W. J. (2021). Effect of bentonite type on thermal conductivity in a HLW repository. *방사성폐기물학회지, 19*(3), 331-338. https://doi.org/10.7733/jnfcwt.2021.19.3.331

Lee, S. J., Kim, K. Y., Choi, J. C., & Kwon, T. H. (2016). Experimental investigation on the variation of thermal conductivity of soils with effective stress, porosity, and water saturation. *Geomech. Eng, 11*(6), 771-785. http://doi.org/10.12989/gae.2016.11.6.771

Li, R., Zhao, L., Wu, T., Wang, Q., Ding, Y., Yao, J., ... & Shi, J. (2019). Soil thermal conductivity and its influencing factors at the Tanggula permafrost region on the Qinghai–Tibet Plateau. *Agricultural and Forest Meteorology, 264*, 235-246. https://doi.org/10.1016/j.agrformet.2018.10.011

Lind, B. B., Fällman, A. M., & Larsson, L. B. (2001). Environmental impact of ferrochrome slag in road construction. *Waste Management, 21*(3), 255-264. https://doi.org/10.1016/S0956-053X(00)00098-2

López-Acosta, N. P., Zaragoza-Cardiel, A. I., & Barba-Galdámez, D. F. (2021). Determination of Thermal Conductivity Properties of Coastal Soils for GSHPs and Energy Geostructure Applications in Mexico. *Energies, 14*(17), 5479. https://doi.org/10.3390/en14175479

Lu, S., Ren, T., Gong, Y., & Horton, R. (2007). An improved model for predicting soil thermal conductivity from water content at room temperature. *Soil Science Society of America Journal, 71*(1), 8-14. https://doi.org/10.2136/sssaj2006.0041

Lu, S., Ren, T., & Horton, R. (2020). Estimating the components of apparent thermal conductivity of soils at various water contents and temperatures. *Geoderma, 376*, 114530. https://doi.org/10.1016/j.geoderma.2020.114530

Lu, Y., Yu, W., Hu, D., & Liu, W. (2018). Experimental study on the thermal conductivity of aeolian sand from the Tibetan Plateau. *Cold Regions Science and Technology, 146*, 1-8. https://doi.org/10.1016/j.coldregions.2017.11.006

Lyu, C., Sun, Q., & Zhang, W. (2020). Effects of NaCl concentration on thermal conductivity of clay with cooling. *Bulletin of Engineering Geology and the Environment, 79*, 1449-1459. https://doi.org/10.1007/s10064-019-01624-w

Łydżba, D., Rajczakowska, M., Różański, A., & Stefaniuk, D. (2014). Influence of the moisture content and temperature on the thermal properties of soils: laboratory investigation and theoretical analysis. *Procedia Engineering, 91*, 298-303. https://doi.org/10.1016/j.proeng.2014.12.064

Magomedov, U. B. (1998). Thermal conductivity of binary and multicomponent aqueous solutions of inorganic substances. *High temperature, 36*(1), 44-50. https://doi.org/10.1023/A:1017518731726

Mahamaya, M., & Das, S. K. (2020). Characterization of ferrochrome slag as a controlled low-strength structural fill material. *International Journal of Geotechnical Engineering, 14*(3), 312-321. https://doi.org/10.1080/19386362.2018.1448527

Marquardt, D. W. (1963). An algorithm for least-squares estimation of nonlinear parameters. *Journal of the society for Industrial and Applied Mathematics, 11*(2), 431-441. https://doi.org/10.1137/0111030

Man, A., Martino, J., Kim, C. S., & Priyanto, D. (2011). *Characterizing and improving the thermal conductivity of engineered clay barriers for sealing a deep geological repository* (No. AECL-CW--508640-CONF-002). Atomic Energy of Canada Limited. https://inis.iaea.org/collection/NCLCollectionStore/_Public/49/101/49101595.pdf

METER Group, Inc., *TEMPOS Thermal Analyzer Manuel*, Meter Group (2018).

Metwally, I. A., Al-Badi, A. H., & Al Farsi, A. S. (2013). Factors influencing ampacity and temperature of underground power cables. *Electrical Engineering, 95*, 383-392. https://doi.org/10.1007/s00202-012-0271-5

Miller, C. J., & Rifai, S. (2004). Fiber reinforcement for waste containment soil liners. *Journal of Environmental Engineering, 130*(8), 891-895. https://doi.org/10.1061/(ASCE)0733-9372(2004)130:8(891)

Mitchell, J. K., & Kao, T. C. (1978). Measurement of soil thermal resistivity. *Journal of the Geotechnical Engineering Division, 104*(10), 1307-1320. https://doi.org/10.1061/AJGEB6.0000706

Nikoosokhan, S., Nowamooz, H., & Chazallon, C. (2016). Effect of dry density, soil texture and time-spatial variable water content on the soil thermal conductivity. *Geomechanics and Geoengineering, 11*(2), 149-158 https://doi.org/10.1080/17486025.2015.1048313

Ocłoń, P., Bittelli, M., Cisek, P., Kroener, E., Pilarczyk, M., Taler, D., ... & Vallati, A. (2016). The performance analysis of a new thermal backfill material for underground power cable system. *Applied Thermal Engineering, 108*, 233-250. https://doi.org/10.1016/j.applthermaleng.2016.07.102

Ogacho, A. A., Aduda, B. O., & Nyongesa, F. W. (2003). Thermal conductivity of a kaolinite refractory: effect of a plant-derived organic binder. *Journal of materials science, 38*, 2293-2297. https://doi.org/10.1023/A:1023916009846

Olphen, H. V. (1977). *An introduction to clay colloid chemistry, for clay technologists, geologists, and soil scientists* (No. 2nd edition). https://doi.org/10.1097/00010694-196404000-00013

Palomino, A. M., & Santamarina, J. C. (2005). Fabric map for kaolinite: effects of pH and ionic concentration on behavior. *Clays and Clay minerals, 53*(3), 211-223. https://doi.org/10.1346/CCMN.2005.0530302

Pahud, D. (2002). Geothermal energy and heat storage. *Cannobio: SUPSI DCT LEEE. Scuola Universitaria Professionale della Svizzera Italiana*.

Park, J., & Santamarina, J. C. (2017). Revised soil classification system for coarse-fine mixtures. *Journal of Geotechnical and Geoenvironmental Engineering, 143*(8), 04017039. https://doi.org/10.1061/(ASCE)GT.1943-5606.0001705

Patel, S., Shahu, J. T., & Senapati, A. (2012). Feasibility of copper slag-fly ash mix as a road construction material. *International Journal on Transportation and Urban Development, 2*(1), 11. https://doi.org/01.IJTUD.02.01.33

Péron, H., Knellwolf, C., & Laloui, L. (2011). A method for the geotechnical design of heat exchanger piles. In *Geo-Frontiers 2011: Advances in Geotechnical Engineering* (pp. 470-479). https://doi.org/10.1061/41165(397)49

Pinson, D., Zou, R. P., Yu, A. B., Zulli, P., & McCarthy, M. J. (1998). Coordination number of binary mixtures of spheres. *Journal of Physics D: Applied Physics, 31*(4), 457. https://doi.org/10.1088/0022-3727/31/4/016

Puppala, A. J., & Musenda, C. (2000). Effects of fiber reinforcement on strength and volume change in expansive soils. *Transportation Research Record, 1736*(1), 134-140. https://doi.org/10.3141/1736-17

Rabab'ah, S., Al Hattamleh, O., Aldeeky, H., & Alfoul, B. A. (2021). Effect of glass fiber on the properties of expansive soil and its utilization as subgrade reinforcement in pavement applications. *Case Studies in Construction Materials, 14*, e00485. https://doi.org/10.1016/j.cscm.2020.e00485

Roshankhah, S., Garcia, A. V., & Carlos Santamarina, J. J. J. O. G. (2021). Thermal conductivity of sand–silt mixtures. *Journal of Geotechnical and Geoenvironmental Engineering, 147*(2), 06020031. https://doi.org/10.1061/(ASCE)GT.1943-5606.0002425

Sanghamitra, B., & Reddy, C. N. V. S. (2017). Potential of Ferro chrome slag as construction material. *Indian Highway, 45*(6), 11-17. Retrieved https://www.researchgate.net/profile/Cnv-Reddy/publication/317692010_Potential_of_Ferro_Chrome_Slag_as_Construction_Material/links/5b439c7daca2728a0d688aca/Potential-of-Ferro-Chrome-Slag-as-Construction-Material.pdf

Sharqawy, M. H. (2013). New correlations for seawater and pure water thermal conductivity at different temperatures and salinities. *Desalination, 313,* 97-104. https://doi.org/10.1016/j.desal.2012.12.010

Song, X., Fan, H., Liu, J., & Yang, X. (2020). An improved thermal conductivity model for unsaturated clay. *KSCE Journal of Civil Engineering, 24,* 2364-2371. https://doi.org/10.1007/s12205-020-1812-5

Sun, Q., & Lü, C. (2019). Semiempirical correlation between thermal conductivity and electrical resistivity for silt and silty clay soils. *Geophysics, 84*(3), MR99-MR105. https://doi.org/10.1190/geo2018-0549.1

Sundberg, J. (2016). Evaluation of thermal transfer processes and back-fill material around buried high voltage power cables. *Report/Department of Civil and Environmental Engineering, Chalmers University of Technology, Report*, *5*.

Tandel, Y. & Patel, J.B. (2009) Review of utilisation of copper slag in highway construction. *Australian Geomechanics, 44*, 71-80.

Tang, A. M., Cui, Y. J., & Barnel, N. (2008). Thermo-mechanical behaviour of a compacted swelling clay. *Géotechnique, 58*(1), 45-54. https://doi.org/10.1680/geot.2008.58.1.45

Tarnawski, V. R., & Leong, W. H. (2016). Advanced geometric mean model for predicting thermal conductivity of unsaturated soils. *International Journal of Thermophysics, 37*, 1-42. https://doi.org/10.1007/s10765-015-2024-y

Tenmak. (Jan, 2023). *Bor Elementi.* Tenmak Boren. https://boren.tenmak.gov.tr/tr/calisma-alanlari/bor-elementi.html

Tien, Y. M., Chu, C. A., & Chuang, W. S. (2005). The prediction model of thermal conductivity of sand-bentonite based buffer material. *France Clays in Natural & Engineered Barriers for Radioactive Waste Confinement*, 657.

Uysal, F. F., & Bahar, S. (2018). Cüruf Çeşitleri ve Kullanim Alanlari. *Trakya Üniversitesi Mühendislik Bilimleri Dergisi*, *19*(1), 37-52. Retrieved from https://dergipark.org.tr/en/pub/tujes/issue/32912/398010

Valipour, M., Shourijeh, P. T., & Mohammadinia, A. (2021). Application of recycled tire polymer fibers and glass fibers for clay reinforcement. *Transportation geotechnics, 27*, 100474. https://doi.org/10.1016/j.trgeo.2020.100474

Vapur, H., Soner, T. O. P., Teymen, A., & Türkmenoğlu, M. (2013). Elazığ Ferrokrom Tesisi Cüruflarının Agrega Özelliklerinin Arastırılması. *Çukurova Üniversitesi Mühendislik-Mimarlık Fakültesi Dergisi, 28*(1), 77-88. Retrieved from https://dergipark.org.tr/en/pub/cukurovaummfd/issue/22759/242928

Villar, M. V. (2004). Thermo-Hydro Mechanical Characteristics and Processes in the Clay Barrier of a High Level Radioactive Waste Repository. State of the Art Report.

Wallen, B. M., Smits, K. M., Sakaki, T., Howington, S. E., & Deepagoda TKK, C. (2016). Thermal conductivity of binary sand mixtures evaluated through full water

content range. *Soil Science Society of America Journal, 80*(3), 592-603. https://doi.org/10.2136/sssaj2015.11.0408

Wallenberger, F. T., Watson, J. C., & Li, H. (2001). PPG Industries, Inc. Glass Fibers. Available online: https://www. asminternational. org/documents/10192/1849770/06781g_p27-34. pdf (accessed on 26 March 2022).

Wang, M., Chen, Y. F., Zhou, S., Hu, R., & Zhou, C. B. (2015). A homogenization-based model for the effective thermal conductivity of bentonite–sand-based buffer material. *International Communications in Heat and Mass Transfer, 68*, 43-49. https://doi.org/10.1016/j.icheatmasstransfer.2015.08.007

Wiener, O. (1912). Abhandl. math.-phys. *Kl. Königl. Sachsischen Gesell*, 32, 509.

Xiao, Y., Liu, H., Nan, B., & McCartney, J. S. (2018). Gradation-dependent thermal conductivity of sands. *Journal of Geotechnical and Geoenvironmental Engineering*, *144*(9), 06018010. https://doi.org/10.1061/(ASCE)GT.1943-5606.0001943

Xu, X., Zhang, W., Fan, C., & Li, G. (2020). Effects of temperature, dry density and water content on the thermal conductivity of Genhe silty clay. R*esults in Physics, 16*, 102830. https://doi.org/10.1016/j.rinp.2019.102830

Xu, X. Z., Wang, J. C., & Zhang, L. X. (2001). Frozen soil physics. *Beijing Science and Technology Press, Beijing.*

Xu, Y., Zeng, Z., & Lv, H. (2019). Effect of temperature on thermal conductivity of lateritic clays over a wide temperature range. *International Journal of Heat and Mass Transfer, 138*, 562-570. https://doi.org/10.1016/j.ijheatmasstransfer.2019.04.077

Yadav, M. R., & Saxena, G. S. (1973). Effect of compaction and moisture content on specific heat and thermal capacity of soils. *Journal of the Indian Society of Soil Science, 21*(2), 129-132.

Yadav, S., Veer, J., Gupta, R., & Yadav, P. (2018). Review on utilisation on flyash, copper slag and zinc slag in road construction and embankment. *International Journal of Advance Research in Science and Engineering, 7*(10), 101-109.

Yan, X., Duan, Z., & Sun, Q. (2021). Influences of water and salt contents on the thermal conductivity of loess. *Environmental Earth Sciences, 80*, 1-14. https://doi.org/10.1007/s12665-020-09335-2

Yılmaz, A., & Karaşahin, M. (2010). Mechanical properties of ferrochromium slag in granular layers of flexible pavements. *Materials and structures, 43*, 309-317. https://doi.org/10.1617/s11527-009-9490-2

Yılmaz, A., & Sütaş, İ. (2008). Ferrokrom cürufunun yol temel malzemesi olarak kullanımı. *Teknik Dergi, 19*(93), 4455-4470. Retrieved from https://dergipark.org.tr/en/pub/tekderg/issue/12765/155261

Yılmaz, A., & Yıldız, A. H. (2015). Cüruf atıklarının yol inşaatında kullanılması durumunda çevresel etkileri. *Uluslararası Burdur Deprem ve Çevre Sempozyumu, 267*, 279.

Yigitbasoglu, H. (2004). An Important Ore for Turkey: Boron. *Coğrafi Bilimler Dergisi*, 2(2), 13–25.

Yoon, S., Cho, W., Lee, C., & Kim, G. Y. (2018). Thermal conductivity of Korean compacted bentonite buffer materials for a nuclear waste repository. *Energies, 11*(9), 2269. https://doi.org/10.3390/en11092269

Yoon, S., Kim, M. J., Lee, S. R., & Kim, G. Y. (2018). Thermal conductivity estimation of compacted bentonite buffer materials for a high-level radioactive waste repository. *Nuclear Technology, 204*(2), 213-226. https://doi.org/10.1080/00295450.2018.1471909

Yoon, S., Lee, G. J., Park, T. J., Lee, C., & Cho, D. K. (2022). Thermal conductivity evaluation for bentonite buffer materials under elevated temperature conditions. *Case Studies in Thermal Engineering, 30*, 101792. https://doi.org/10.1016/j.csite.2022.101792

Yun, T. S., & Santamarina, J. C. (2008). Fundamental study of thermal conduction in dry soils. *Granular matter, 10*, 197-207. https://doi.org/10.1007/s10035-007-0051-5

Zhang, N., & Wang, Z. (2017). Review of soil thermal conductivity and predictive models. *International Journal of Thermal Sciences, 117*, 172-183. https://doi.org/10.1016/j.ijthermalsci.2017.03.013

Zhang, N., Yu, X., Pradhan, A., & Puppala, A. J. (2015). Effects of particle size and fines content on thermal conductivity of quartz sands. *Transportation Research Record, 2510*(1), 36-43. http://doi.org/10.3141/2510-05